The role of the periplasmic Cu metallochaperone AccA in metalating the Cu-dependent nitrite reductase AniA in Neisseria gonorrhoea

FIRTH, SAMANTHA,JADE

The role of the periplasmic Cu metallochaperone AccA in metalating the Cu-dependent nitrite reductase AniA in *Neisseria gonorrhoeae*

Samantha Jade Firth

A thesis presented for the degree of Doctor of Philosophy

Durham University Department of Biosciences

March 2023

Abstract

Neisseria gonorrhoeae (the gonococcus) respires nitrite (NO_2^-). This process requires the nitrite reductase, AniA, which contains T1- and T2Cu in its active sites. We have characterised AccA, a PCu_AC homologue with an extended His- and Met-rich C-terminal domain, as a likely periplasmic Cu-binding metallochaperone that metalates AniA.

In this study, biochemical examination of purified AccA and site-directed variants confirms that it binds one Cu(I) atom with femtomolar affinity in the conserved 2 His, 2 Met binding site. The C-terminal domain binds Cu(II) with picomolar affinity, although precise ligands remain unknown. Gonococcal strains lacking AccA or any conserved His and Met residue in AccA fail to grow and reduce NO_2^-. This phenotype is reversed when Cu(II) salts are supplemented in the growth medium. These results suggest that, in the absence of AccA, AniA is expressed as an *apo*-enzyme, but is re-metalated if the periplasmic buffered Cu pool increases. Interestingly, gonococcal strains lacking the C-terminal domain of AccA show reduced growth and NO_2^- consumption only in the presence of the Cu(I) chelator BCS, suggesting a role during Cu starvation.

Cu-transfer experiments using purified proteins confirmed AccA metalates both Cu sites in AniA with metal coordinated by both the Cu primary and C-terminal Cu binding sites. However, the C-terminal tail was required for metalation of the T2-site. AniA is expressed as a monomer and Cu binding induces protein trimerisation. This may offer an alternative role of why AccA is required to metalate AniA *in vitro.*

This work raises questions regarding the thermodynamics and kinetics of how metalloproteins acquire Cu from the buffered cellular pool via metallochaperones.

Table of Contents

List of Figures

List of Tables

List of abbreviations

AccA	AniA Copper Chaperone A
BCA	Bicinchoninic acid
BCS	Bathocuproine disulfonic acid
CV	Column volume
Cys	Cysteine
DP-2	Dansyl peptide 2
DP-3	Dansyl peptide 3
EDTA	Ethylenediaminetetraacetic acid
Fz	Ferrozine
GCBL	Gonococcal base medium liquid
His	Histidine
ICP-MS	Inductively coupled plasma mass spectrometry
IPTG	Isopropyl β-D-1-thiogalactopyranoside
K_D	Dissociation constant
LB	Luria broth
Met	Methionine
MOPS	3-(N-morpholino)propanesulfonic acid
NirK	Cu-containing nitrite reductase
NO_2^-	Nitrite
OD	Optical density
PAR	4-(2'-Pyridylazo)resorcinol
PBS	Phosphate-buffered saline
PCR	Polymerase chain reaction
PES	Polyethersulfone
ROS	Reactive oxygen species
specR	Spectinomycin resistance cassette
T1Cu	Type-1 Cu binding site
T2Cu	Type-2 Cu binding site

Declaration

I conform that this thesis was composed by myself, that the work contained herein is my own except where explicitly stated otherwise in the text, and that this work has not been submitted for any other degree or professional qualification except as specified.

Statement of copyright

Acknowledgements

PhD is never easy, especially a PhD during covid, but I am so thankful for the amazing people who inspired me to keep going through this process and to the BBSRC who funded this PhD.

To Dr Karrera Djoko, I know this was a learning experience for the both of us, with me being your first PhD student as a PI. I consider myself so incredibly lucky to have such a strong, dedicated woman as my mentor for the last four and a half years. I will cherish this time in your lab, and the lessons you have taught me, for a long time to come.

To Dr Kevin Waldron and Dr Emma Tarrant, thank you for blossoming my love of science back when I was a small third year student at Newcastle. I really wouldn't be here without your guidance and encouragement that kept my love of metals in biology alive.

To Dr Peter Chivers, thank you for your guidance and advice during group meetings. They really id wonders for my confidence and made me a better scientist.

To the best colleagues, and friends, I could have made at Durham: Will, Cian, Jack, Louisa, Tessa, Sophie, Josh, Joy, Matthew, Charlotte, Andrew, and Deenah. Thank you for all the discussions that kept me sane throughout this time, I really couldn't have done this without any of you.

To the students who helped me with this work: Jin, Lotte, John, and Daniel. Thanks for the hard work you put in for. You really show just how incredible students at Durham University can be.

To the Blower lab, especially Tom, thank you for your guidance on how to use the AKTA and analytical column, I'm still terrified of getting air in it to this day.

To my family, I know you don't really get what I spent the last couple of years doing but thank you for supporting me and my love of science since I was just a small child annoying you with random facts.

To the best support system, I could ever wish for: Jamie, Meg, Iqra, Errol, Liz, and Jay. My chosen family. I would be so lost without you, thank you for listening to me rant about my love of copper, for always being there for me, for listening to me when I had doubts, for your endless support. I will forever be grateful that you are all in my life and that I get the privilege of calling you friends.

And thank you to Monster Energy drinks, you really managed to get me through those long days in the lab and through writing this thesis.

Chapter 1: Introduction

1.1 The role of metals in biology

Approximately a third of proteins and a half of enzymes require metal ions to function.[1] Metal binding to proteins can help stabilise protein structure, such as Zn in Zn finger motif proteins, where the co-ordination of Zn by Cys and His residues within a hydrophobic core promotes the formation of the recognisable helical structure of the protein.[2,3] Metal ions can also act as enzyme co-factors for catalysis. These reactions typically rely on the ability of metal ions to cycle between two redox states under physiological conditions to serve as electron donors or acceptors,[4] for example Fe in iron-sulfur (Fe-S) clusters in respiratory enzymes.[5] Some metals are able to act as Lewis acid catalysts, such as Zn in many Zn-dependent hydrolases.[6,7]

The attachment of metals to proteins relies on binding to sulfur, nitrogen, or oxygen atoms in the side chain or backbone of amino acid residues.[8,9,10] Key amino acids that participate in metal-binding include the thiol of Cys, the thioester of Met, and the imidazole group of His residues.[11,12,13,14] Furthermore, the carboxylate of charged amino acids such as Asp and Glu and the carbonyl of the amide bond in the peptide backbone can also bind to positively metal ions *via* the electrostatic and polar interactions.[15,16] The affinity of these amino acid ligands for metal ions generally follows the Irving-Williams series (Figure 1.1), with Cu forming the most stable or high-affinity complexes.[17]

$$Mg^{2+} < Mn^{2+} < Fe^{2+} < Co^{2+} < Cu^{2+} \text{ (or } Cu^{1+}) > Zn^{2+}$$

Figure 1.1: Irving-Williams series.

1.1.1 Copper in biology

The use of Cu in cells is thought to have evolved following the shift in the Earth's atmosphere to become more O_2-rich.[18] By utilising Cu, enzymes such as oxidases were able to reduce O_2 and remove it from the cell. This adaptation enabled life to survive the rise in atmospheric O_2 and over time, Cu-dependent enzymes became more common across species.[19]

Cu ions in proteins can be classified into three types of Cu centres, based on their coordination chemistry. Type-1 Cu (T1Cu) centres, which exhibit a distinctive blue colour in solution, are

mononuclear Cu centres.[20,21,22] Type-2 Cu (T2Cu) centres are also mononuclear,[23] while Type-3 Cu (T3Cu) centres are dinuclear.[24] Different Cu centres can work together in enzymes. For example, T2Cu and T3Cu centres form a trinuclear catalytic site in multicopper oxidases, which also contain a T1Cu centre.[25] Another example is Cu-dependent nitrite reductases, which require both T1Cu and T2Cu for function.[26,27] Some notable exceptions to the Cu centre classification system above are the dinuclear Cu_A centre such as those found in respiratory oxidases,[28] and the tetranuclear Cu-S cluster or Cu_Z centre in nitrous oxide reductases.[29,30]

1.2 Copper toxicity in bacteria

Despite the important role that Cu plays as a micronutrient within cells, for example in cytochrome *c* oxidases that are involved in cellular respiration and electron transport,[31] intracellular Cu availability must be tightly controlled due to the potential toxic effects of the metal ion. This principle is true for all micronutrient metals – although they are essential, an excess is cytotoxic.

The potential toxic effects of Cu are multifaceted. Due to its redox reactivity, Cu can react with hydrogen peroxide *via* Fenton-like chemistry to form hydroxyl radicals (Equation 1).[32,33] These reactive oxygen species (ROS) can go on to oxidise other biomolecules, such as amino acid residues (aromatic such as Tyr or sulfur-containing such as Met and Cys), DNA, lipids, and even metalloenzyme centres such as those containing (Fe-S) clusters, leading to oxidative stress.[34,35,36] Oxidation of amino acid side chains can result in damage to the protein structure or cleavage of the polypeptide chain.[34,37] Similarly, DNA damage can cause strand breaks and DNA-protein crosslinks, which are often poorly repaired and can lead to cell death.[38,39] In the case of ROS-mediated Fe-S cluster damage, it can not only result in the loss of enzyme function, but also cause the release of Fe into the cell and increase Fe availability. This excess Fe can undergo Fenton chemistry to increase the ROS present in the cell.[40,33,41] This process does not explain why Cu is more toxic to cells under anaerobic conditions in which ROS cannot be produced.[42] However, it has been identified that in these reducing conditions, Cu(I) interacts non-specifically with proteins which results in ROS-independent protein aggregation, and ultimately cell death.[43,44]

$$Cu(I) + H_2O_2 \rightarrow Cu(II) + {}^{\bullet}OH + {}^{-}OH \qquad \text{(eq. 1)}$$

Given its position at the top of the Irving-Williams series, excess Cu in cells can displace metal ions present in proteins that are lower on the Irving-Williams series.[45,46,47,17] Furthermore, excess Cu can also bind non-specifically to amino acid residues in proteins that scarcely bind metals. Both scenarios are known as 'mis-metalation' and they can cause inactivation of protein and enzyme function. One key example is the favoured binding of Cu over Mn in the periplasmic Mn-dependent oxalate decarboxylase MncA. Cu binds MncA with an affinity of 10^4 over Mn which renders the protein inactive.[46,48] Cu ions can also displace Fe present in Fe-S clusters, one such example being the inactivation of fumarase A in *Escherichia coli* by excess Cu.[35]

1.3 Bacterial copper homeostasis

Due to the toxic effect of Cu previously described, it is crucial that Cu, and all other metals', availability inside cells is kept low. In the current paradigm, metal ions in cells are not present in their 'free' aqueous form.[49] Instead, metals are bound and buffered by components of the crowded cellular milieu, such that metal availability is the inverse of the Irving-Williams series.[50] As such, Cu, which is the most competitive metal in the series, is maintained at lower availability in the cell compared to other transition metals such as Zn and Mn. This prevents mis-metalation as a result of the high binding affinity of Cu to proteins.[50] The precise composition of the intracellular metal buffer is still poorly understood. This buffer likely consists of ligands such as free amino acids (*e.g.* free His or Cys), small peptides (*e.g.* glutathione), non-specific sites on proteins, and small metabolites.[51,52]

The buffered pool of metal in cells not only prevents metal toxicity but it also serves as the source of nutrient metals for metal-dependent enzymes. In this model, the bound metal in the buffer is kinetically labile. This allows facile exchange of metals from the buffer to specific metal-binding sites in proteins and enzymes.[50,53] This transfer of metals typically follows a favourable thermodynamic gradient, *i.e.* from high energy (low affinity or weak binding) to low energy (high affinity or tight binding) sites.[54] The final destination sites of the metal are likely the lowest energy (highest affinity) sites in the cell. This prevents the reverse transfer of metal out of that site back into the buffer which is thermodynamically unfavourable. Alternatively, once bound to its target protein, the metal becomes

kinetically trapped in that site, making the energy barrier for the reverse transfer of metal back into the buffer too great.[55]

Metal availability inside cells is maintained by metallosensors.[50] These are metal-sensing transcriptional regulators that can sense the levels of metal loading in the intracellular buffer and regulate the expression of metal homeostasis proteins (exporters, importers, metallochaperones, and metal storage) accordingly.[56] The roles of these different proteins are briefly summarised below. A generic schematic of the different Cu homeostasis proteins in Gram-negative bacteria is shown in Figure 1.2, but it is important to note that not all proteins are present in all Gram-negative bacteria.

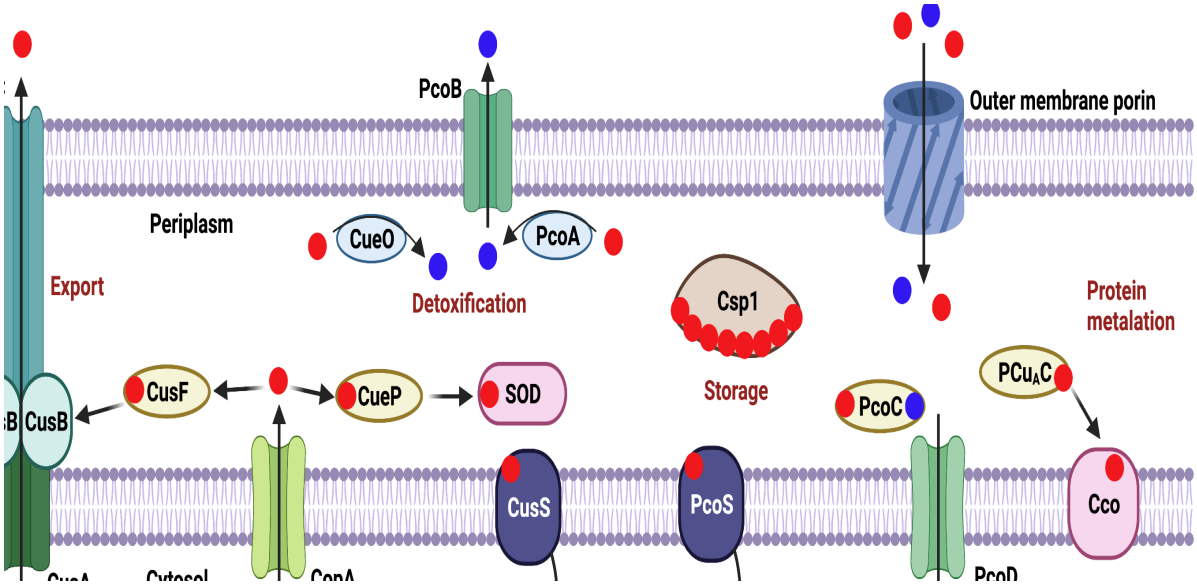

Figure 1.2: An overview of Cu homeostasis in Gram-negative bacteria. Red circles = Cu(I), blue circles = Cu(II), pale blue = multicopper oxidases, yellow = metallochaperones, pink = cuproprotein, dark purple = transcriptional regulators, dark blue = periplasmic copper sensor in two-component system.

1.3.1 Metal sensors

Metallosensors are required to maintain the intracellular buffered concentration of their cognate metal ion.[50] The metal-binding affinity of each metallosensor to the cognate metal is tuned to the buffered availability of that metal.[50] Therefore, if the availability of the buffered metal increases, the metal would flow down the thermodynamic gradient from the buffer to the metallosensor.[54] Conversely, if the availability of the buffered metal decreases, the metal would flow down the thermodynamic gradient from the metallosensor to the buffer.[54] The binding or unbinding of the metal to the metallosensor

induces a conformational change that alters DNA binding and allows for transcriptional control of genes involved in the metal homeostatic pathway.[57]

The best characterised bacterial cupro-metallosensor is perhaps CueR, foud in Gram-negative bacteria. This metallosensor is a MerR family transcriptional activator.[58] Under normal buffered availability of Cu in the cell, CueR exists as an *apo*-protein. The conformation of this *apo*-protein promotes binding to the target promoter DNA sequence but prevents RNA polymerase from binding.[59] However, as the intracellular buffered copper availability increases, CueR binds Cu with high affinity ($\log K_D$ of approx. 21 M^{-1}) and induces a conformational change in the protein that twists the promoter DNA, which allows RNA polymerase to bind and transcribe the target gene.[60,59]

Additional Cu sensing transcription regulators have been identified in bacteria. For example, the two-component system CusRS in Gram-negative bacteria regulates periplasmic Cu(I) availability, likely in anaerobic conditions.[61,62] Furthermore, the two-component PcoRS system has been identified to maintain the buffered availability of Cu in strains of bacteria that are hyper-resistant to copper.[63,63] Gram-positive bacteria possess other cytosolic Cu sensors, including the transcriptional derepressor CopY from many streptococci and CsoR from actinobacteria.[64,65,66]

1.3.2 Metal transporters

The central mechanism in bacterial Cu homeostatic pathways seems to rely on the export of Cu(I) ions out of the cytosol.[67] The P_{1B}-type ATPase Cu(I) exporter CopA is ubiquitous in Gram-negative and Gram-positive bacteria and is present even in bacteria that do not contain the other Cu homeostasis proteins.[68] In fact, bacteria do not seem to have evolved a requirement for Cu inside the cytosol, with all known cuproenzymes being located in the bacterial envelope.[69] The underlying reason for this is unknown.

Expression of CopA is transcriptionally upregulated under conditions of high intracellular Cu availability.[68] Export of Cu(I) by this enzyme is achieved *via* a soluble Cu(I)-binding domain present on the cytosolic side, which captures Cu(I) from the cytosolic buffer and loads the transmembrane domain of the transporter with the metal. Efflux of Cu from the cytosol is driven by ATP hydrolysis, which induces a conformational change in the transporter, allowing Cu to move in a unidirectional

fashion from the cytosol into the periplasm.[70,67] Two closely related CopA transporters have been identified within bacteria: the CopA transporter that exports excess Cu as previously described (usually named CopA1), and a less well-characterised CopA2 transporter that is believed to deliver micronutrient Cu to cytochrome *c* oxidase.[71,72] The cellular function of the two transporters is not interchangeable,[73] although the precise mechanisms that distinguish them is unclear.

Some Gram-negative bacteria contain a second Cu efflux transporter, CusABC, a member of the RND family of transporters.[74] This transporter spans the entire periplasm and directly transports Cu from the cytosol to the extracellular milieu.[69] The CusABC transporter system is the target for the periplasmic Cu chaperone CusF and therefore, can efflux Cu from both the cytosol and the periplasm, controlling the buffered availability of Cu in both these spaces.[75] Furthermore, the periplasmic Cu availability is maintained *via* the periplasmic Cu efflux pump PcoB in some strains of bacteria that are hyper-resistant to Cu.[76]

Whilst Cu efflux systems that prevent accumulation of excess intracellular Cu ions are relatively well understood, how bacteria acquire micronutrient Cu is not clear. Unlike other micronutrient metal ions such as Zn or Fe, a dedicated Cu import system is exceedingly rare, with the exception of chalkophores and chalkophore importers such as those that are present in methanobacteria[77]. It is generally assumed that Cu may either passively diffuse across the outer membrane of Gram-negative bacteria *via* porins or become accidentally taken up by non-specific metal importers in the inner membrane as the 'free' Cu ion or as Cu bound non-specifically to a metallophore such as siderophores.[78,79,80]

1.3.3 Metal detoxification and storage

The maintenance of an appropriate intracellular buffered Cu availability *via* metal transporters is a key element of bacterial Cu homeostasis. In the periplasmic space of Gram-negative bacteria, additional mechanisms are present to counteract potential Cu toxicity. Periplasmic multi-copper oxidases such as CueO and PcoA can oxidise Cu(I) to Cu(II).[81,82] Cu(II) is generally considered the less toxic redox species for cells. However, this mechanism to detoxify Cu is only used in aerobic conditions, because molecular O_2 is needed as the oxidant.

A new family of Cu-binding proteins has also been identified, known as copper storage proteins (Csp). This family of proteins were discovered to bind multiple molecules of Cu(I) ions.[83] Csp proteins are localised to either the cytoplasm (Csp3) and the periplasm (Csp1). They are thought to play a dual role in copper homeostasis. Csp proteins may sequester excess Cu(I) to protect against toxicity. However, they may also store nutrient Cu(I) in a readily-available pool for use when intracellular Cu(I) concentrations drop thus acting as a intracellular Cu buffer.[83,84] These Csp proteins, in addition to the complex homeostatic mechanisms described, ensure that the intracellular Cu concertation is tightly regulated to protect against the detrimental toxic effect of excess Cu.

1.4 Metallochaperones

Metallochaperones are used by cells to facilitate intracellular metal transfer from the buffer to target metalloproteins.[54,85] As previously established, metals are thought to transfer down a thermodynamic gradient until they ultimately bind the correct metalloprotein.[54] Metallochaperones are theorised to aid in this process in two ways. First, the metallochaperones may introduce metal selectivity and reduce mismetalation of metalloproteins by metals at the top of the Irving-Williams series such as Cu or Zn.[17,46] A metallochaperone is thought to acquire its cognate metal from the buffer and transfer the metal to a target protein *via* specific protein-protein interactions and stepwise ligand exchange.[69] This may prevent mismetalation of the target protein by other metals. Secondly, the specific protein-protein interactions between a metallochaperone and a target protein may contribute to lowering the energy barrier for metal transfer from the buffer to the target protein.[54] In this manner, a metallochaperone may be considered to act as an 'insertase'.[86] Because metal transfer between a metallochaperone and the target metalloprotein is thought to require protein-protein contacts, each metallochaperone-metalloprotein pair is thought to be unique.[86]

Several Cu metallochaperone-metalloprotein pairs have been identified within Gram-negative bacteria. Of interest in this project is the metallochaperone PCu_AC, which is required to metalate the Cu_A site of cytochrome *c* oxidase.[87,88] Here, PCu_AC coordinates Cu in a tetrahedral conformation *via* two Met and two His residues in a conserved $HX_nMX_{21/22}HXM$ motif.[89,90] It was previously thought that the PCu_AC and the Cu binding protein Sco1 both acted as metallochaperones to metalate cytochrome c oxidase.[91] However, recent research suggests that the role of Sco1 is to reduce the Cys residues of cytochrome *c* oxidase and PCu_AC is the source of Cu.[92,93]

Whilst PCu_AC and Sco1 were originally thought to only metalate the Cu_A site of cytochrome c oxidases, homologues of these proteins (PccA and SenC respectively) have been identified that metalate the Cu_B site of cytochrome *cbb*$_3$ oxidases which lack a Cu_A sites in *Rhodobacter capsulatus.*[94] Interestingly, the P_{1B}-type ATPase Cu(I) transporter CcoI, a CopA homologue, is required to fully metalate the Cu_B site.[71] This implies that PccA and SenC may acquire Cu directly from CcoI, which relies on the cytoplasmic store of Cu as previously described. Similarly, the Cu metallochaperone CueP has been identified to interact and acquire Cu from CopA in *Salmonella enterica* and ultimately metalates a Cu,Zn-superoxide dismutase which detoxifies ROS generated *via* Cu toxicity.[95] This mechanism linking Cu metallochaperone metalation to high affinity Cu transporters offers more control of the metalation of metalloproteins *via* Cu chaperones, by limiting mismetalation of proteins.

Cu metallochaperones are also used in Cu homeostasis in response to high intracellular Cu. One such example is the cytosolic Cu metallochaperone CopZ which has been extensively studied in Gram-positive bacteria. CopZ traffics Cu from the cytosolic buffer to the metallosensor CopY as well as the Cu efflux pump CopA.[96,97] Recent studies have identified CopZ in Gram-negative bacteria such as *E. coli* where it is produced *via* ribosomal frameshifting from the *copA* mRNA.[98] The role of CopZ is similar in Gram-negative bacteria to that of Gram-positive bacteria. Binding of Cu from the cytosolic buffer induces homodimerisation of CopZ, which stabilises Cu binding in a tetra-nuclear Cu complex.[99] Interaction with CopA weakens the homodimer of CopZ and leads to the formation of a heterodimer of CopZ/CopA where sequential ligand exchange ensures that the transfer from CopZ to CopA is unidirectional and thermodynamically favourable.[100] Additionally, the metallochaperone CusF binds Cu in the periplasm and interacts with CusB where Cu is exported from the cell *via* the CusABC transporter.[101,102] These examples have demonstrated the importance of metallochaperones in directing the movement of Cu and maintaining the buffered concentration within the cell.

1.5 Copper demand in *Neisseria gonorrhoeae*

The obligate human pathogen *Neisseria gonorrhoeae* (the gonococcus) colonises the genitourinary tract and often encounters increased Cu during infection.[103] However, *N. gonorrhoeae* employs an unusual pathway for Cu homeostasis. Many of the Cu homeostatic proteins previously identified in Gram-negative bacteria are lacking in the *N. gonorrhoeae* genome. There is no known Cu sensor in

N. gonorrhoeae as the genome lacks a *cueR* or any other known transcriptional regulator that responds to Cu.[103,104] Despite this, the *copA* genes are still present within the gonococcus genome and are believed to be constituently expressed.[103] The CopA1 protein has been confirmed to confer Cu tolerance, with mutations in the gene resulting in an increase in Cu sensitivity.[103] The CopA2 protein is less well defined, but it is believed to traffic Cu to cytochrome cbb_3 oxidase.[71] Furthermore, a periplasmic Csp1 protein has been identified in *N. Gonorrhoeae* which may play a role in sequestering excess periplasmic Cu when the buffered availably increases, however, its role in gonococcal physiology is yet to be determined.[84]

Despite the notable absence of a recognisable Cu homeostasis system, *N. gonorrhoeae,* rather paradoxically, has a high apparent requirement for nutrient Cu (Figure 1.3). A cytochrome cbb_3 oxidase is located in the inner membrane, acting as a terminal electron acceptor in the reduction of O_2 to H_2O in aerobic conditions.[105,106] The CcoN subunit of cytochrome cbb_3 oxidase contains a dinuclear heme centre comprising of heme *b* and heme b_3 magnetically coupled to a Cu_B centre.[107] Furthermore, the gonococcus contains a homologue to Sco1 which is implicated in metalation of cytochrome c oxidases. However, the role of Sco in *N. gonorrhoeae* is involved in oxidative stress response due to structural similarity to peroxiredoxin and thiol:disulfide oxidoreductases.[108] The outer-membrane-linked protein Laz contains a T1Cu centre which is believed to be an electron donor for cytochrome *c* peroxidase.[109]

N. gonorrhoeae often encounters limited oxygen during colonisation of the genitourinary tract and during biofilm formation.[110] Under these O_2-limited conditions, *N. gonorrhoeae* uses nitrite (NO_2^-) instead of O_2 as a terminal electron acceptor during respiration in a process known as denitrification to generate an electron gradient to drive ATP synthesis.[111] The gonococcus employs a truncated denitrification pathway lacking the first (nitrate reductase) and last (nitrous oxide reductase) enzymes in the typical denitrification pathway.[112] Therefore, in *N. gonorrhoeae* the process relies on the reduction of NO_2^- *via* the Cu-containing nitrite reductase (NirK) to nitric oxide ($NO\cdot$) which is in turn reduced to nitrous oxide *via* nitric oxide reductase (NorB).

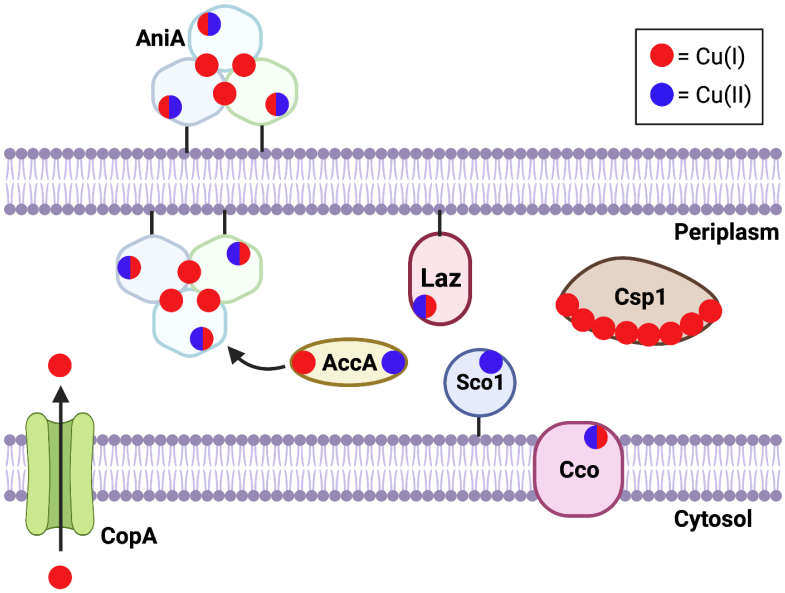

Figure 1.3: Overview of Cu homeostasis and demand by Cu proteins in the Gram-negative bacterium *N. gonorrhoeae.*

1.6 Cu-containing nitrite reductase AniA

AniA is an anaerobically inducible Cu-containing nitrite reductase (NirK) involved in the denitrification pathway in *N. gonorrhoeae.*[113] AniA is a homotrimer in which each monomer of AniA binds two Cu atoms at a T1- and T2Cu centre (Figure 1.4a). The T1Cu centre coordinates Cu by two His, a Cys, and Met residue from the same subunit in a tetrahedral geometry with a short Met-Cu bond resulting in a distinct blue colouring.[114] The T2Cu centre resides at the monomer interface *via* three His residues; two from one monomer whilst the second monomer provides the third (Figure 1.4b).[114] The gonococcal cytochrome c_2 and CcoP and CcoQ subunits of the cytochrome cbb_3 oxidase act as electron donors to the T1Cu centre of AniA, which subsequently donates electrons *via* a Cys-His bridge to the T2Cu centre.[115,116,117,] The active site of AniA consists of the T2Cu centre and a conserved Asp residue which coordinates NO_2^- and upon electron transfer from the T1 results in reduction of NO_2^- to NO·.[114,118]

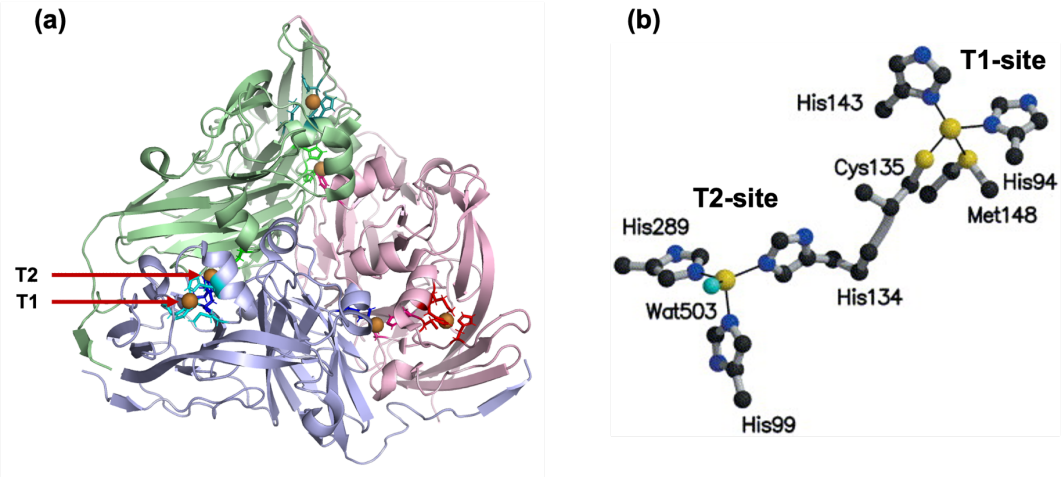

Figure 1.4: Structure of AniA. (a) Crystal structure of the *N. gonorrhoeae* AniA protein. Each monomer coloured separately; Cu centres highlighted. PDB 1KBW. **(b)** Close up of T1- and T2Cu binding sites of AniA, Image adapted from Boulanger and Murphy, 2002.[114]

A unique feature of AniA is that it is tethered to the outer-membrane in *N. gonorrhoeae* and is glycosylated in the C-terminal.[113,119] Antibodies against AniA are raised during infection implying that AniA is located both facing the periplasm and extracellularly.[118] Therefore, as *N. gonorrhoeae* infections are becoming increasingly multi-drug resistant, AniA shows potential as a target for novel antimicrobials, or as a vaccine candidate.[118] Due to its unique extracellular location, questions have been raised regarding how AniA acquires nutrient Cu.

1.7 AccA

Studies by Jen *et al.* (2015) have identified a suspected periplasmic Cu metallochaperone in *N. gonorrhoeae* that is believed to metalate AniA.[120] This protein was identified using a lethal genetic screen in a *norB* gene knockout strain in the genetically similar microorganism *Neisseria meningitidis.* The *norB* knockout strain is unable to reduce the reactive nitrogen species NO·, thus leading to cellular death.[121] A random mutagenesis screen was conducted and colonies that survived during growth under anaerobic conditions were analysed. Survival was indicative of a loss of AniA function as NO_2^- would not be reduced to NO· in these strains. The gene *nmb1557* which encoded a hypothetical periplasmic binding protein was identified in this screen and corresponded to the open reading frame NGO1215 in the gonococcal genome.[120] Further experimentation by Jen *et al* (2015) identified the AniA protein of *N. meningitidis* lacking the gene *nmb1557* existed in an *apo*-form.[120] It

was therefore, suggested that NMB1557, and NGO1215, was involved in the metalation of AniA and thus named AccA (AniA Cu Chaperone A).[120]

Bioinformatical analysis of the *accA* gene identified it as a homologue to the PCu_AC protein, TTHA1943, that delivers Cu to the Cu_A site of cytochrome ba_3 oxidase in *T. thermophilus.*[120,122] This homology has identified a potential Cu(I) binding site motif in AccA of $HX_{10}MX_{22}HXM$ comprising of the amino acid residues His69, Met80, His103, and Met105. Additionally, a draft structure of the AccA protein (unpublished thesis, D. Thaqi) shows similarity with the overall tertiary structure and the potential Cu(I) site of AccA (Figure 1.5). These similarities between AccA and the *T. thermophilus* PCu_AC protein led to suggestions that AccA may also be involved in metalation, and assembly, of the Cu_B site of cytochrome cbb_3 oxidase within *N. gonorrhoeae*. However, an *accA* knockout strain only resulted in a small decrease in cytochrome cbb_3 oxidase activity suggesting that a role in Cu_B site assembly is not essential.[120]

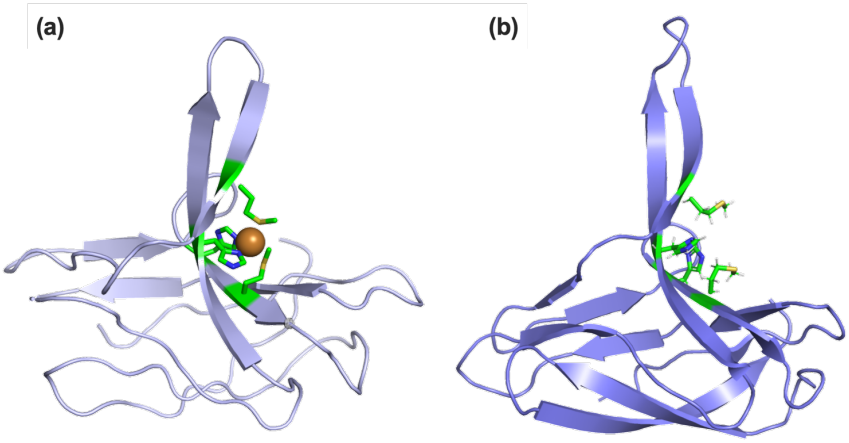

Figure 1.5: Structure of AccA and homology to PCu_AC. Protein structures of **(a)** *N. gonorrhoeae* AccA (draft structure, X-ray crystallography) and **(b)** *T. thermophilus* PCu_AC (PDB: 2K6W, solution NMR) show similarity in Cu(I) binding site, highlighted in green.

In addition to the characteristic Cu(I) binding site from PCu_AC, AccA also contains a C-terminal extension rich in Met and His residues: MPAMNHGHHHGEAHQH. Initial experimentation from Jen *et al*. (2015) identified two Cu binding sites within AccA, a Cu(I) and a Cu(II) binding site.[120] It is predicted that the Cu(II) binding site of AccA is located in the C-terminal extension due to the presence of multiple Met and His residues that are known to bind Cu. However, this binding could not be confirmed *via* crystallography as the C-terminal extension of AccA was disordered (unpublished

thesis, D. Thaqi). The PCu_AC, and AccA, homologue protein PmoF1 has recently been identified in methane-oxidising bacteria. Whilst PmoF1 lacks the typical Cu(I) binding motif of PCu_AC homologue protein it possesses a C-terminal extension which contains a cluster of His residues identified to bind Cu(II).[123] This C-terminal extension does not align with that present within AccA and its role is unknown however, it highlights the diversity of PCu_AC homologue proteins within bacteria.

Whilst predicted Cu(I) and Cu(II) binding sites have been identified within the AccA protein sequence, these sites have not been experimentally confirmed and their exact Cu-binding affinities have not been reported. Furthermore, whilst Jen *et al*. (2015) confirmed that AccA and AniA interact *in vitro via* surface-plasmon resonance, it still remains unknown whether AccA is able to metalate AniA both *in vitro* and *in vivo*.[120]

1.8 Project Aims

This project aimed to examine and confirm the Cu binding properties of the Cu(I) and C-terminal extension of the periplasmic Cu metallochaperone AccA and its role in metalating the Cu-dependent nitrite reductase, AniA, in the pathogenic *Neisseria* species *N. gonorrhoeae*. In order to accomplish this, four main aims of this project were identified:

1. Bioinformatically characterise AccA and AniA and the spread of the genes within bacteria.
2. Identify Cu-binding residues of AccA and determine Cu-binding affinities of WT and mutant proteins *in vitro.*
3. Determine whether AccA is required to metalate AniA, and whether mutants weakening Cu-binding affinity impact AniA metalation *in vivo*.
4. Identify whether AccA can directly transfer Cu to AniA *in vitro.*

Chapter 2: Materials and Methods

All reagents were supplied by Sigma-Aldrich using analytical grade unless stated otherwise. All experiments involving bacterial cultures were repeated in three independent biological replicates unless stated otherwise. Experiments using purified proteins were repeated in duplicate unless stated otherwise.

2.1 Bioinformatical analysis of genes

2.1.1 Analysis of nonsynonymous SNPs

BLAST searches of key gonococcal genes (*accA, aniA etc)* were performed by using BLASTN (version 2.9.0) from the NCBI website. Complete gene sequences were collected for all *N. gonorrhoeae* strains. Genes were translated to amino acid sequences to detect nonsynonymous SNPs. Nonsynonymous SNPs were visualised on protein structures (sourced from the PDB) using PyMOL.

2.1.2 Generation of phylogenetic trees

BLAST searches of key gonococcal genes (*accA* and *aniA*) were performed by using nucleotide BLAST (version 2.9.0) from the NCBI website. Complete gene sequences were collected for the reference strains of either all *Neisseria* species or all Betaproteobacteria. Genes were translated to amino acid sequences using MEGA11. Protein sequences were aligned using MAFFT online version. Protein sequences were analysed in MEGA11 and any sequence lacking conserved Cu binding sites were removed. Phylogenetic trees were generated in the software MEGA11 using the maximum-likelihood method and the Jones-Taylor-Thornton (JTT) model.

2.2 Bacterial strains and growth conditions

All bacteria strains were stocked in broth + 20% glycerol and stored at -80°C.

Table 2.1: Reagents for bacterial growth.

Reagent	Concentration
***N. gonorrhoeae* culture reagent**	
Kellogg's I	100 X
Kellogg's II	1000 X
Sodium bicarbonate	100 X
Antibiotic	
Ampicillin	100 µg/mL
Chloramphenicol	30 µg/mL
Kanamycin	100 µg/mL
Spectinomycin	100 µg/mL

2.2.1 *N. gonorrhoea*

Neisseria gonorrhoeae strain 1291 was used in this study. *N. gonorrhoeae* was propagated from glycerol stocks on GC agar (Oxoid) supplemented with Kellogg's supplements I and II, as described in Dillard (2015).[124] Bacteria were incubated for 16-24 hours at 37°C in an air-tight container in the presence of 5-9% atmospheric CO_2 (generated by CO_2 Gas Generator Sachets, Oxoid).

N. gonorrhoeae microaerobic liquid cultures (30 mL broth in 50 mL screw-cap tubes) were prepared to a starting OD_{600} value of 0.1 in a GC broth (GCBL) as described in Dillard (2015).[124] Kellogg's supplements I, II, and 5% (vol/vol) sodium bicarbonate were added to the broth immediately before use. Broth was always pre-warmed to 37°C before inoculation. Liquid cultures were incubated for 8 or 10 hours at 37°C without shaking. Sodium nitrite was supplemented to a final concentration of 2 mM at time = 0, 5, 7, 8, and 9 hours. OD_{600} values were measured at t = 0, 4, 5, 6, 7, 8 hours. After 8 or 10 hours, bacteria were centrifuged at 5000 rpm for 5 minutes and resuspended into 1 mL of GCBL medium containing 20% (vol/vol) glycerol. The suspensions were split into two 0.5 mL aliquots and stored at -80°C for subsequent biochemical assays.

N. gonorrhoeae aerobic liquid cultures (50 mL broth in 250 mL flask) were prepared as previously described. Liquid cultures were incubated for 8 hours at 37°C shaking at 180 rpm. Sodium nitrite was supplemented to a final concentration of 2 mM at time = 0, 5, and 7 hours. OD_{600} values were measured in 1-hourly intervals during growth.

2.2.2 *E. coli*

Escherichia coli was used in this study for sub-cloning of all *N. gonorrhoeae* genetic constructs and overexpression of AccA and AniA proteins. *E. coli* strains were propagated from glycerol stocks on LB agar (Melford) containing the appropriate antibiotic (see Table 2.1). Bacteria were incubated overnight at 37°C. *E. coli* DH5α strain was used for plasmid propagation. *E. coli* BL21 strains were used for overexpression of AccA and AniA proteins. For sub-strains of *E. coli* BL2, see Table 3.

2.3 Cloning and generation of constructs

The sequence of the *accA* and *aniA* genes were obtained from the genome sequence of *Neisseria gonorrhoeae* FA 1090 (GenBank: AE004969.1). The sequences of all constructs were confirmed *via* Sanger sequencing at Durham University Genomics facility.

2.3.1 Generation of Golden Gate Assembly constructs in *N. gonorrhoeae*

All *N. gonorrhoeae* mutant strains were generated by homologous recombination of the genetic constructs into the WT strain of *N. gonorrhoeae* 1291, which is naturally competent. Golden Gate Assembly (New England Biolabs) was used to generate all genetic constructs for transformation into *N. gonorrhoeae*. The assembled components were: 1000 bp of the 5'-upstream flanking sequence of the *accA* gene, the *accA* gene itself, a *specR* cassette encoding spectinomycin resistance (amplified from pCTS32 plasmid), and a 1000 bp of the 3'- downstream flanking sequence of *accA*. All four pieces were amplified by PCR using the Q5 enzyme (New England Biolabs) and primers that carried BsaI cleavage sites and the appropriate overhangs (Table 2.2). All pieces were individually subcloned into the SmaI site of pTRB479. This plasmid is a modified pUC19 plasmid that lacks BsaI cleavage sites. The resulting plasmids were transformed into chemically competent *E. coli* DH5α cells.

The four pieces of DNA were subsequently assembled using The NEB® Golden Gate Assembly Kit (BsaI-HF®v2) following manufacturer's guidelines. The final assembly was in the following orientation: 5' upstream→*accA*→*specR*→3' downstream (Figure 2.1). The assembly was subcloned into the HincII site of pUC19, then transformed into chemically competent *E. coli* DH5α cells and confirmed by Sanger sequencing.

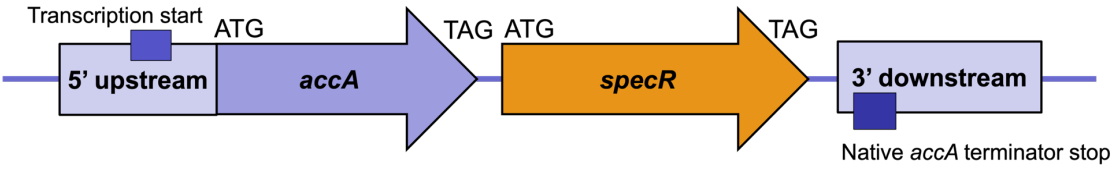

Figure 2.1: Design of Golden Gate construct for homologous transformation in native gene site in *N. gonorrhoeae.*

To transform into *N. gonorrhoeae*, the assembled construct was linearised by PCR using primers *accA*→*specR* linearisation-F and *accA*→*specR* linearisation-R (Table 2.2). Transformation followed the procedure described in Dillard 2015[124]. Briefly, 8 single, opaque (piliated) colonies of *N. gonorrhoeae* were gently streaked through 10 µL of a total of 1 µg of linearised DNA on GC agar plates. The plates were incubated for 7 hours and then sub-streaked onto fresh GC agar containing spectinomycin. Plates were incubated at 36°C for 16 hours and colonies identified as successful transformants by PCR and sequencing.

The genetic constructs for generating site-directed mutants of the *accA* gene were made following the same approach as described above, except that the DNA piece containing the *accA* gene was replaced with the various mutant genes. The Δ*accA* mutant gene was generated using the NEB Q5® site-directed mutagenesis kit per manufacturer's guidelines, primers Δ*accA*-F and Δ*accA*-R (Table 2.2), and the *accA* Golden Gate construct as the template. The H69A-*accA,* M105A-*accA,* H103A/M105A-*accA,* and ΔC-terminal-*accA* mutant constructs were generated by splice overlap extension PCR (see Table 2.2 for primers) using the *accA* Golden Gate construct as the template. The M80A-*accA*, H103A-*accA*, H69A/M80A-*accA*, ΔCu primary-*accA*, and ΔCu tract-*accA* constructs were synthesised commercially by IDT as gBlock® gene fragments.

2.3.2 Generation of overexpression constructs in *E. coli*

Overexpression constructs for AccA were generated using the *accA* mutant genes previously generated. Constructs were generated *via* PCR using primers with 5' extensions containing NdeI (FP) and BamHI (RP) cleavage sites. The gene constructs were subcloned into pET11b cleaved by NdeI and BamHI. The overexpression construct for the ΔC-terminal AccA protein was generated. Overhangs were attached to the gene using primers. The gene was amplified for LIC cloning into pSATL vector using StuI. The gene was inserted following a His_6-SUMO tag for protein purification.

The overexpression construct for WT AniA was generated using *aniA* gene from *N. gonorrhoeae* FA 1090. The ΔT1- and ΔT2-AniA gene inserts were synthesised by IDT as gBlock® gene fragments. Constructs were generated *via* PCR using primers with 5' extensions containing NcoI (FP) and XhoI (RP) cleavage sites. The RP also contained a thrombin cleavage site as described in Boulanger *et al*[114]**.** The constructs were subcloned into a pET29a vector cleaved by NcoI and XhoI. The gene was inserted directly before a His_6-tag. The designed constructs lacked the N-terminus signal sequence and C-terminal glycosylation site to generate soluble AniA protein as previously described in Boulanger *et al*.[114]

Table 2.2: List of primers used in this study. Underlined sequences indicate site of intended mutation.

Construct name	Primer name	Sequence (5'→3')	Template
***accA N. gonorrhoeae* constructs**			
accA→*spec*	5' upstream-F	CAGTTGGGTCTCCGGAGGACAAACGCATCTTGATTATCG	*N. gonorrhoeae* genome
	5' upstream-R	CAGTTGGGTCTCCATCTTCCTGCTCCTTTAATATCAG	
	accA-F	CAGTTGGGTCTCCAGATGAAAAAATTATTGGCAGCCG	*N. gonorrhoeae* genome
	accA-R	CAGTTGGGTCTCCTTAGTGCTGATGCGCTTC	
	specR-F	CAGTTGGGTCTCCCTAAAATAGGTACTAATGAAAATAGTGAGG	pCTS32
	specR-R	CAGTTGGGTCTCCGAAAGGTGTTTCCACCATTTTT	
	3' downstream-F	CAGTTGGGTCTCGTTTCTGCTGGAAATATTTGAAATGC	*N. gonorrhoeae* genome
	3' downstream-R	CAGTTGGGTCTCGATGGCGTGAAACTCAAATCGTTCA	
	accA GG-F	GCATTTTTTTGGGTTTCCGAAA	

	accA GG-R	CAAACCTTTGAGCAGGTAATG	*accA*→*spec* Golden Gate reaction
	accA→*specR* linearisation-F	GAGCAGATTGTACTGAGAGTGC	pUC19::*accA*→*spec*
	accA→*specR* linearisation-R	GAGCGCAGCGAGTCAGTGAG	
Δ*accA*→*spec*	Δ*accA*-F	AATAGGTACTAATGAAAATAGTGAGG	pUC19::*accA*→*spec*
	Δ*accA*-R	CTTCCTGCTCCTTTAATATC	
Splice overlap extension PCR external	SOE-F	GCTGCAAGGCGATTAAGTTGGGTAACGC	pUC19::*accA*→*spec* or *accA* mutants
	SOE-R	GAGGAAGCGGAAGAGCGCCCAATAC	
H69A-*accA*	H69A SOE-F	GCGTCGAAGTG**GCA**ACCCACATCAAC	pUC19::*accA*→*spec*
	H69A SOE-R	GTTGATGTGGGT**TGC**CACTTCGACGC	
M105A-*accA*	M105A SOE-F	CAGCTATCACGTG**GCA**TTTATGGGTTTGA	pUC19::*accA*→*spec*
	M105A SOE-R	TCAAACCCATAAA**TGC**CACGTGATAGCTG	
H103A/M105A-*accA*	M103A/M105A SOE-F	ACCCGGCAGCTAT**GCA**GTG**GCA**TTTATGGGTTTGA	pUC19::*accA*→*spec*
	H103A/M105A SOE-R	TCAAACCCATAAA**TGC**CAC**TGC**ATAGCTGCCGGGT	
ΔC-terminal-*accA*	ΔC-terminal SOE-F	AACCGCGCCGTAAAATAGGTACTAATGAAAATAGTGAGGAGGATATATTTGAATACATAC	pUC19::*accA*→*spec*
	ΔC-terminal SOE-R	ACCTATTTTACGGCGCGGTTTTGACTTCCA	
Protein overexpression			
accA protein	AccA O/E-F	CATGAGCATATGAAAAAATTATTGGCAGCCGTG	pUC19::*accA*→*spec* constructs
	AccA O/E-R	CATGAGGGATCCTTAGTGCTGATGCGC	
ΔC-terminal-*accA* protein	ΔC-terminal AccA O/E-F	CAACAGCAGACGGGAGGTGCCGGAGTCCATGTCGAGGACG	pUC19::ΔC-terminal-*accA*→*spec*
	ΔC-terminal AccA O/E-R	GCGAGAACCAAGGAAAGGTTATTACGGCGCGGTTTTGACTTCCAGTTG	
aniA protein	AniA O/E-F	CAGCAGCATATGGCCGCACAAGCTACC	*N. gonorrhoeae* genome or GenScript synthesised DNA
	AniA O/E-R	CATCTCGAGGCTGCCGCGCGGTACGGCGTAAGCGGTATC	

Table 2.3: List of plasmids used and generated in this study.

Plasmid name	Description	Source	Strain stocked
Vectors			
pCTS32	Source of *specR* cassette for gonococcal transformation	M. Apicella Lab (Iowa)	*E. coli* DH5α
pET11b	Tagless expression vector	Novagen	*E. coli* DH5α

pET29a	His_6 tagged expression vector	N. Robinson Lab (Durham)	*E. coli* DH5α
pSATL	His6-SUMO tagged expression vector	T. Blower Lab (Durham)	*E. coli* DH5α
pTRB479	pUC19 plasmid with BsaI sites removed for Golden Gate cloning	T. Blower Lab (Durham)	*E. coli* DH5α
pUC19	Cloning vector	NEB	*E. coli* DH5α
Cloning			
pUC19::*accA*→*specR*	Plasmid to complement *accA* gene into *N. gonorrhoeae*	This work	*E. coli* DH5α
pUC19::H69A-*accA*→*specR*	Plasmid to complement H69A-*accA* mutant gene into *N. gonorrhoeae*	This work	*E. coli* DH5α
pUC19::M80A-*accA*→*specR*	Plasmid to complement M80A-*accA* mutant gene into *N. gonorrhoeae*	This work	*E. coli* DH5α
pUC19::H103A-*accA*→*specR*	Plasmid to complement H103A-*accA* mutant gene into *N. gonorrhoeae*	This work	*E. coli* DH5α
pUC19::M105A-*accA*→*specR*	Plasmid to complement M105A-*accA* mutant gene into *N. gonorrhoeae*	This work	*E. coli* DH5α
pUC19::H69A/M80A-*accA*→*specR*	Plasmid to complement H69A/M80A-*accA* mutant gene into *N. gonorrhoeae*	This work	*E. coli* DH5α
pUC19::H103A/M105-*accA*→*specR*	Plasmid to complement H103A/M105-*accA* mutant gene into *N. gonorrhoeae*	This work	*E. coli* DH5α
pUC19::ΔCu primary-*accA*→*specR*	Plasmid to complement ΔCu primary-*accA* mutant gene into *N. gonorrhoeae*	This work	*E. coli* DH5α
pUC19::ΔCu tract-*accA*→*specR*	Plasmid to complement ΔCu tract-*accA* mutant gene into *N. gonorrhoeae*	This work	*E. coli* DH5α
pUC19::ΔC-terminal-*accA*→*specR*	Plasmid to complement ΔC-terminal-*accA* mutant gene into *N. gonorrhoeae*	This work	*E. coli* DH5α
Overexpression			
pET11b::*accA*	Plasmid for overexpression of WT AccA. The *accA* gene was subcloned between the T7 promoter and terminator	This work	*E. coli* BL21 pLysS
pET11b::H69A-*accA*	Plasmid for overexpression of H69A AccA. The *accA* gene was subcloned between the T7 promoter and terminator	This work	*E. coli* BL21 pLysS
pET11b::H69A-*accA*	Plasmid for overexpression of H69A AccA. The *accA* gene was subcloned between the T7 promoter and terminator	This work	*E. coli* BL21 pLysS
pET11b::M80A-*accA*	Plasmid for overexpression of M80A AccA. The *accA* gene was subcloned between the T7 promoter and terminator	This work	*E. coli* BL21 pLysS

pET11b::H103A-*accA*	Plasmid for overexpression of H103A AccA. The *accA* gene was subcloned between the T7 promoter and terminator	This work	*E. coli* BL21 pLysS
pET11b::M105A-*accA*	Plasmid for overexpression of M105A AccA. The *accA* gene was subcloned between the T7 promoter and terminator	This work	*E. coli* BL21 pLysS
pET11b::ΔCu primary-*accA*	Plasmid for overexpression of ΔCu primary AccA. The *accA* gene was subcloned between the T7 promoter and terminator	This work	*E. coli* BL21 Rosetta 2
pET11b::ΔCu tract-*accA*	Plasmid for overexpression of ΔCu tract AccA. The *accA* gene was subcloned between the T7 promoter and terminator	This work	*E. coli* BL21 Rosetta 2
pSATL::ΔC-terminal-*accA*	Plasmid for overexpression of ΔC-terminal AccA. The *accA* gene was subcloned between the His_6-SUMO and T7 terminator	This work	*E. coli* BL21 Rosetta 2
pET29a::*aniA*	Plasmid for overexpression of AniA. The *accA* gene was subcloned between T7 promoter and directly before the His_6 tag	This work	*E. coli* BL21 Rosetta 2
pET29a::ΔT1-*aniA*	Plasmid for overexpression of ΔT1-AniA. The *accA* gene was subcloned between T7 promoter and directly before the His_6 tag	This work	*E. coli* BL21 Rosetta 2
pET29a::ΔT2-*aniA*	Plasmid for overexpression of ΔT2-AniA. The *accA* gene was subcloned between T7 promoter and directly before the His_6 tag	This work	*E. coli* BL21 Rosetta 2

2.4 Protein overexpression and purification

Table 2.4: Recipes of buffers used in protein purification.

Buffer	Recipe
Resuspension buffer A	50 mM Tris-HCl pH 8.0, 150 mM NaCl, 5 mM imidazole, 15% glycerol
Resuspension buffer B	50 mM Tris-HCl pH 8.0, 150 mM NaCl, 25 mM imidazole, 15% glycerol
His-Trap A1	50 mM Tris-HCl pH 8.0, 150 mM NaCl, 5 mM imidazole
His-Trap A2	50 mM Tris-HCl pH 8.0, 150 mM NaCl, 25 mM imidazole
His-Trap A3	50 mM Tris-HCl pH 8.0, 25 mM imidazole
His-Trap B1	50 mM Tris-HCl pH 8.0, 150 mM NaCl, 250 mM imidazole
His-Trap B2	50 mM Tris-HCl pH 8.0, 150 mM NaCl, 250 mM imidazole
Q-Column A1	50 mM Tris-HCl pH 8.0
Q-Column A2	50 mM Tris-HCl pH 7.0
Q-Column B1	50 mM Tris-HCl pH 8.0, 250 mM NaCl
Q-Column B2	50 mM Tris-HCl pH 7.0, 250 mM NaCl, 15% glycerol
SP-Column A	50 mM MOPs pH 6.5
SP-Column B	50 mM MOPs pH 7.2, 150 mM NaCl, 15% glycerol
2x PBS	2.74 mM NaCl, 5.4 mM KCl, 20 mM Na_2HPO_4, and 3.6 mM KH_2PO_4

2.4.1 Overexpression and purification of AccA proteins

All AccA proteins except the ΔC-terminal mutant were purified using the same method.

BL21 transformants were plated on LB agar containing ampicillin and chloramphenicol and incubated overnight at 37°C. Cells from the agar plates were harvested and resuspended in 10 mL of PBS and used to inoculate 1 L of LB broth in a 2 L flask containing ampicillin and chloramphenicol to a starting OD_{600} value of 0.01. Cultures were incubated at 37°C with shaking at 180 rpm until an OD_{600} of 0.6 was reached (approx. 3-4 hours). Protein expression was induced by adding isopropyl β-D-1-thiogalactopyranoside (IPTG) to a final concentration of 0.1 mM and ampicillin was also supplemented to the cultures. Cultures were then cooled to 22°C and shaken for a further 16 hours.

Bacteria were harvested by centrifugation (6000 rpm, 4°C, 15 minutes) using an Avanti J26-XP centrifuge with a JLA-16.250 rotor. The pellets were resuspended in resuspension buffer A (Table 2.4), apart from pellets of bacteria expressing the ΔC-terminal AccA protein, which were resuspended in resuspension buffer B (Table 2.4). Bacteria were lysed by sonication (40 kPsi) using a Q700CA sonicator and clarified by centrifugation (21000 rpm, 4°C, 15 minutes) using an Avanti J26-XP centrifuge with a JA-25:50 rotor. Any remaining insoluble debris or aggregates were removed by filtration through a 0.45 µm polyethersulfone (PES) filter (Starlab).

Soluble cell lysates were loaded onto a HisTrap™ HP 5 mL column (Cytiva). The column was then washed with 20 column volumes (CV) of buffer His-Trap A1 (Table 2.4). AccA proteins were eluted with 3 CV of buffer His-Trap B1 (Table 2.4). The sample was then diluted with buffer Q-column A1 to a salt concentration of less than 50 mM. Ethylenediaminetetraacetic acid (EDTA) was also added to the protein to a final concentration of 1 mM to remove any potential metal contaminants. The sample was then loaded onto a HiTrap™ Q HP 5 mL (Cytiva) column to remove any contaminant proteins.

The ΔC-terminal AccA protein was loaded onto a HisTrap™ HP 5 mL column. The column was then washed with 20 CV of buffer His-Trap A2 (Table 2.4) and the protein was eluted with 3 CV of buffer His-Trap B1 (Table 2.4). The eluted protein was immediately loaded onto a HiTrap™ Q HP 5 mL. This time, the protein was bound to the column. The column was washed with 10 CV of buffer Q-Column A1 and eluted with 3 CV of buffer Q-Column B1 (Table 2.4). A final concentration of 15% vol/vol

glycerol was added to the sample. The sample was then incubated overnight with hSENP2 SUMO protease (generously donated by the Blower Lab, Durham University) at 4°C with gentle shaking at 50 rpm to cleave the His_6-SUMO tag. To remove the cleaved tag, the sample was reloaded on a HisTrap™ HP 5 mL column. The cleaved ΔC-terminal AccA protein was found in the flow-through, which was collected. The column was also washed with 20 CV of buffer His-Trap A1 (Table 2.4) to elute any weakly bound ΔC-terminal AccA protein. All fractions were pooled and then loaded onto a HiTrap™ Q HP 5 mL column to remove any contaminant proteins. The ΔC-terminal AccA protein was found in the flow-through, which was collected. The pH of the flow-through was lowered to 6.5 using solid MOPS. The sample was loaded onto a HiTrap™ SP HP 1 mL column (Cytiva), washed with 10 CV of buffer SP-Column A, and finally eluted in 1 mL fractions using buffer SP-Column B (Table 2.4).

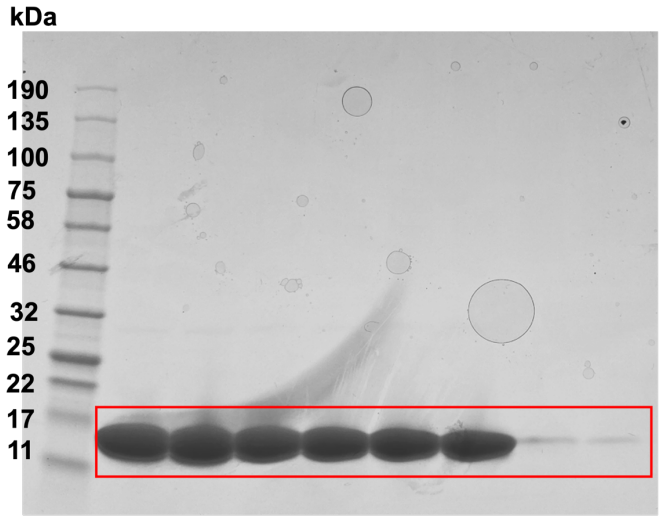

Figure 2.2: Protein purification of AccA. SDS-PAGE from final purification stage of AniA. Each lane represents a single 1 mL fraction eluted from a 1 mL SP column.

2.4.2 Overexpression and purification of AniA proteins

BL21 transformants were plated on LB agar containing ampicillin and chloramphenicol and incubated overnight at 37°C. Cells from the agar were resuspended in 10 mL of PBS, and used to inoculate 1 L of LB broth in a 2 L flask containing kanamycin and chloramphenicol to a starting OD_{600} of 0.01.

Cultures were shaken at 180 rpm and 37°C until an OD_{600} of 0.6 was reached. Protein expression was induced by adding IPTG to a final concentration of 0.1 mM and the cultures were supplemented with kanamycin. Cultures were cooled to 22°C and shaken for a further 4 hours. Cells were harvested by

centrifugation, resuspended in resuspension buffer B (Table 2.4), lysed, and clarified as previously described for the purification of AccA proteins.

The cell lysates containing AniA proteins were loaded onto a HisTrap™ HP 5 mL column. The column was then washed with 20 CV of buffer His-Trap A2 (Table 2.4) followed by 5 CV of His-Trap A3 to remove any salt. AniA proteins were eluted using 4 CV of buffer His-Trap B2 (Table 2.4) directly into a HiTrap™ Q HP 5 mL column, which was attached to HisTrap column. The HisTrap column was removed and the Q column was washed with 10 CV of buffer Q-Column A2 (Table 2.4) and the protein was eluted with 3 CV of 2x PBS. The sample was diluted with water so that the concentration of PBS was 1x. Thrombin (500 units; Cytiva) was added to the AniA proteins, and the mixture was incubated overnight at 22°C with gentle shaking at 50 rpm to cleave the His_6 tag. The mixture was then re-loaded on a HisTrap HP 5 mL column. The cleaved protein lacking the His_6 tag was found in the flow-through, which was collected. The column was washed further with 10 CV of buffer His-Column A1 (Table 2.4) to elute weakly-bound, cleaved AniA proteins. The flow-through and wash fractions were combined and diluted with water to a salt concentration of less than 50 mM, then loaded on a HiTrap Q HP 5 mL column. The column was washed with 10 CV of buffer Q-Column A2 (Table 2.4) and the protein was eluted finally in 1 mL fractions with buffer Q-Column B2 (Table 2.4).

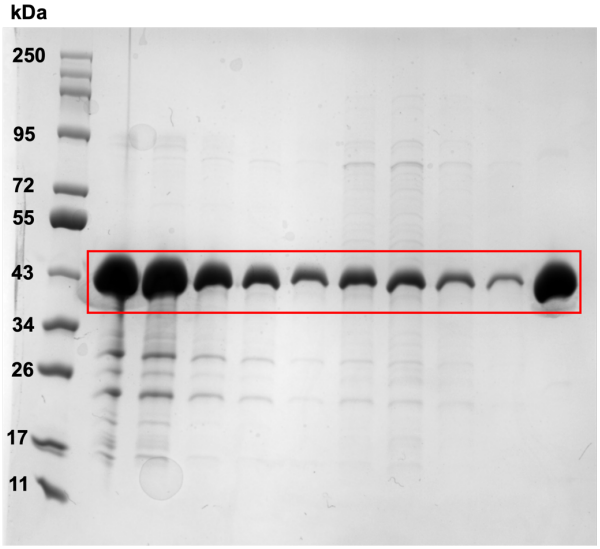

Figure 2.3: Protein purification of AniA. SDS-PAGE from final purification stage of AniA. Each lane represents a single 1 mL fraction eluted from a 5 mL Q column.

2.4.3 Confirmation of protein by Mass Spectrometry

The molecular weights of all purified proteins were confirmed via native Electrospray Ionisation Mass Spectrometry at the Mass Spectrometry Facility, Department of Chemistry (Table 2.5). All proteins were confirmed to be metal-free by ICP-MS.

Table 2.5: Theoretical and actual mass of proteins purified in this study.

Protein	Theoretical Mass (kDa)	Actual Mass (kDa)
WT AccA	15.166	15.166
H69A-AccA	15.100	15.100
M80A-AccA	15.106	15.106
H103A-AccA	15.100	15.100
M105A-AccA	15.106	15.106
ΔCu primary-AccA	14.914	14.914
ΔCu tract-AccA	14.920	14.920
ΔC-terminal-AccA	13.356	13.356
WT-AniA	35.014	35.013
ΔT1-AniA	34.789	34.788
ΔT2-AniA	34.815	34.814

2.5 Characterisation and calibration of stock solutions

2.5.1 Metal and probe calibrations

Concentrations of stock solutions of $CuCl_2$ were estimated using excess bathocuproine disulfonic acid (BCS) as a colourimetric reporter for Cu. A master stock solution was prepared in 50 mM MOPS buffer pH 7.2 containing excess BCS (>1 mM) and 2 mM sodium ascorbate. This master stock was added to different serial dilutions of an unknown concentration of $CuCl_2$. The UV-visible absorbance at 483 nm was obtained and the concentration of $[Cu^{I}(BCS)_2]^{3-}$, which reported the concentration of CuCl2, was determined using the Beer-Lambert (eq. 3) law and the extinction coefficient ε_{483} = 13000 cm^{-1} M^{-1}.

$$2\ BCS + Cu(I) \rightleftharpoons Cu^{I}(BCS)_2 \qquad \text{(eq. 2)}$$

$$A = \varepsilon cl \qquad \text{(eq. 3)}$$

The concentrations of colourimetric probes, namely BCS, bicinchoninic acid (BCA), and ferrozine (Fz) were estimated using the stock of $CuCl_2$ of known concentration. A master stock of each probe was prepared in 50 mM MOPS pH 7.2 containing 2 mM sodium ascorbate. A serial dilution of the $CuCl_2$ stock was prepared in deionised water and added to the previously prepared master stock of each probe. The optical spectrum of each sample was recorded from 300 to 800 nm, and the peak absorbance for each *holo*-probe (λ_{max} reported in Table 2.6) was plotted against the Cu concentration. The software DynaFit (BioKin Ltd) was used to fit the curves to an equation describing the equilibrium of Cu binding. Each curve showed a sharp endpoint corresponding to the Cu concentration that saturated the probe. This endpoint was used to determine the concentration of the probe using the appropriate Cu:probe ratios as in Table 2.6.

Table 2.6: Properties of colourimetric and fluorescence probes used in this study. *F* fluorescence, λ_{ex} = 350 nm, λ_{em} = 550 nm.

Probe	Complex	Binding constant		λ_{max} (nm)		ε (cm^{-1} M^{-1})
		β_2 (M^{-2})	K_A (M^{-1})	*holo*	*Apo*	
BCS	$[Cu^{I}(BCS)_2]^{3-}$	6.3×10^{19}	-	483	-	1300
BCA	$[Cu^{I}(BCA)_2]^{3-}$	1.6×10^{17}	-	562	-	7900
Fz	$[Cu^{I}(Fz)_2]^{3-}$	1.3×10^{15}	-	470	-	4320
DP-2	Cu^{II} (DP2)	-	1.3×10^{10}	-	*F*	4500
DP-3	Cu^{II}(DP3)	-	2.0×10^{12}	-	*F*	4500

The concentrations of the fluorescent dansyl peptide probes DP-2 and DP-3 were estimated as above but in the absence of ascorbate. Instead of recording optical absorbances, the fluorescence emission at 550 nm following excitation at 350 nm was recorded. Fluorescence emission values were plotted against Cu concentrations. The data were fitted with DynaFit as described above and the endpoints were used to determine the probe concentrations.

2.5.2 Protein concentrations

The extinction coefficients of *apo*-AccA and *apo*-AniA proteins were predicted using the ExPASy ProtParam tool using the amino acid sequences. The predicted extinction coefficient (ε) of AccA was 6990 cm^{-1} M^{-1} at 280 nm. The predicted extinction coefficient (ε) of AniA was 24870 cm^{-1} M^{-1} at 280 nm.

Due to interference in the spectrum at 280 nm the concentration of *holo*-AccA was determined by stoichiometry. Unbound Cu was removed via a PD-10 desalting column (Cytiva). *Holo*-AccA was denatured in 50 mM MOPS pH 7.2 containing 6 M guanidine hydrochloride and the concentration of Cu in the sample was measured using excess BCS as previously described. As the stoichiometry of Cu in AccA is known to be 2:1 Cu:AccA, the concentration of AccA in the sample was therefore half of the Cu concentration.

2.6 Determining metal stoichiometry of AccA proteins

Apo-proteins were incubated with an excess of metal (> 3 molar equivalents of Cu(I), Cu(II), Co, Fe, Mn, Ni, in 50 mM MOPS pH 7.2 for 15 minutes at ambient temperature, followed by passage through a PD-10 desalting column (Cytiva) in the same buffer to remove any unbound metal ions. Where a reducing environment was required, for example to load the with Cu(I), 2 mM sodium ascorbate was added to the sample. Protein collected in 0.5 mL fractions. The protein was denatured in a 50 mM MOPS buffer, pH 7.2 containing 6 M guanidine hydrochloride buffer. The concentration of Co, Fe, Ni, and Zn in each sample was measured using an excess of the colourimetric probe 4-(2'-Pyridylazo)resorcinol (PAR, 20 mM) and the following extinction coefficients: Co-PAR ε_{514} = 50000 cm^{-1} M^{-1}, Fe-PAR ε_{705} = 18600 cm^{-1} M^{-1}, Ni-PAR ε_{500} = 52000 cm^{-1} M^{-1}, Zn-PAR ε_{514} = 66000 cm^{-1} M^{-1}. The concentration of Mn was measured using the colourimetric probe MagFura2 and ε_{369} = 29900 cm^{-1} M^{-1}. The concentration of Cu was determined using the colourimetric probe BCS as previously described. Metal concentration of AccA protein incubated with Cu(I) was measured in the presence and absence of ascorbate to determine whether Cu(I) was bound to the protein and the final metal stoichiometry.

2.7 Estimation of metal binding affinity via ligand competition

2.7.1 Principles of equilibration competition reactions to estimate K_D

The unknown metal binding affinities of proteins can be determined using metal binding probes with known affinities using mass balance equations. The competition at equilibrium can be described as follows.

$$P + ML \rightleftharpoons MP + L \quad \text{(eq. 4)}$$

or

$$P + ML_2 \rightleftharpoons MP + 2L \quad \text{(eq. 5)}$$

where P = Protein, M = Metal, and L = Ligand/Probe

The exchange constants (K_{ex}) for the above equations can be expressed as:

$$K_{ex} = \frac{[ML][P]}{[L][MP]} = \frac{K_{D(P)}}{K_{D(L)}} \quad \text{(eq. 6)}$$

or

$$K_{ex} = \frac{[ML_2][P]}{[L]^2[MP]} = K_{D(P)}\beta_2 \quad \text{(eq. 7)}$$

Where K_D = dissociation constant, β_2 = conditional accumulated formation constant for ML_2, at a specific pH

$$K_{D(L)} = \frac{[M_{aq}][L]}{[ML]} \quad \text{(eq. 8)}$$

or

$$\beta_2 = \frac{[ML_2]}{[M_{aq}]\,[L]^2} \quad \text{(eq. 9)}$$

K_{ex} can be calculated as the colourimetric probes used in this study report [ML] or $[ML_2]$.

The following can be assumed within the competition assay:

$$[L] = [L]_{total} - [ML] \quad \text{(eq. 10)}$$

$$[MP] = [M]_{total} - [ML] \quad \text{(eq. 11)}$$

$$[P] = [P]_{total} - [MP] \quad \text{(eq. 12)}$$

or

$$[L] = [L]_{total} - [ML_2] \quad \text{(eq. 13)}$$

$$[MP] = [M]_{total} - [ML_2] \quad \text{(eq. 14)}$$

$$[P] = [P]_{total} - [MP] \quad \text{(eq. 15)}$$

Therefore, the $K_{D(P)}$ can be calculated using the K_{ex} equation rearranged as:

$$K_{D(P)} = K_{D(L)}K_{ex} \quad \text{(eq. 16)}$$

or

$$K_{D(P)} = K_{D(L)}\beta_2 \quad \text{(eq. 17)}$$

The total and the equilibrium concentrations of protein, probe, and metal can be determined in a competition assay reaction by measuring the solution absorbance or fluorescence. If the K_A of a probe is known, then the K_A or K_D of a protein with unknown metal binding affinity can be calculated. All calculations were performed using DynaFit.

2.7.2 Estimation of Cu K_D using ligand competition

The Cu(I) dissociation constant was estimated for each AccA protein (WT AccA, H69A-AccA, M80A-AccA, H103A-AccA, M105A-AccA, ΔCu primary-AccA, ΔCu tract-AccA, and ΔC-terminal AccA) by competition with colourimetric probes of known affinities to Cu(I) (BCS, BCA, Fz; Table 2.6). A master stock containing 160 μM probe (or 80 μM BCS), 30 μM protein, and 2 mM sodium ascorbate was prepared in 50 mM MOPS pH 7.2. The master stock (135 μL) was added to a known $CuCl_2$ (15 μL) concentration in 150 μL UVette™ cuvettes (Eppendorf). The optical spectrum of the sample was collected from 400 to 800 nm. The absorbance values at the relevant λ_{max} were plotted against total Cu concentrations (Table 2.6). The data were fitted to an equation describing the relevant equilibrium using DynaFit software to obtain the K_D values for the protein. All competition experiments were performed in duplicate.

The Cu(II) dissociation constant was estimated for WT AccA, ΔCu primary-AccA, ΔCu tract-AccA, and ΔC-terminal-AccA proteins by competition with fluorescent probes of known affinities to Cu(II) (DP2,

DP3). A master stock of 4 μM probe and 4 μM protein was prepared in 50 mM MOPS pH 7.2. The master stock (180 μM) was added to a known $CuCl_2$ (20 μL) concentration in 200 μL black μClear® microplates (Greiner). The fluorescence emission intensity at 550 nm following excitation at 350 nm was recorded and plotted against Cu concentrations. The data were again fitted to an equation describing the relevant equilibrium using DynaFit software. These competition experiments were also performed in duplicate.

2.8 Calculating rate of nitrite consumption of *N. gonorrhoeae* cells

2.8.1 Calculating nitrite consumption

Nitrite consumption by *N. gonorrhoeae* was measured by Griess assay. Frozen pellets were thawed on ice, resuspended in 0.5 mL of complete GCLB and separated into two 0.25 mL aliquots. The first aliquot was set aside for quantification of total protein content as described below. The second aliquot was immediately incubated at 37°C for 10 minutes, followed by the addition of 1 mM sodium nitrite to initiate nitrite consumption. The reaction mixture was sampled at t = 0 min and every 1 minute thereafter for a total of 7 minutes, immediately diluted 20-fold into deionised water, and finally mixed 1:1 with Griess reagent to a total volume of 200 μL. The Griess reagent turns pink and absorbs light at 545 nm in the presence of nitrite. The concentration of nitrite remaining at each time point was determined by comparing the absorbance value of the sample at 545 nm against a standard curve of known nitrite concentrations (160, 80, 40, 20, 10, 5, 2.5, and 0 μM).

2.8.2 Measurements of protein concentration in cells

Total amounts of proteins in *N. gonorrhoeae* cells were determined using the QuantiPro™ BCA Assay Kit following manufacturer's guidelines. Briefly, the first 0.25 mL aliquot of *N. gonorrhoeae* cells from section 2.2.1 was centrifuged at 13000 rpm for 1 minute and resuspended in 0.25 mL of PBS to remove background GCBL medium. This suspension was serially diluted by 2.5, 5, 10, 20, and 40-fold in PBS. Each serial dilution was then added to the QuantiPro BCA reagent in a 96-well microtitre plate and incubated at 50°C for 1 h. The absorbance value of each sample at 562 nm was recorded and compared to a standard curve of known concentrations of bovine serum albumin (BSA) (300, 250, 200, 150, 100, 50, 25, and 0 μg/mL) to determine the protein concentration in each sample.

2.8.3 Calculating percentage rate of nitrite consumption vs WT control

Nitrite concentrations were plotted on a scatter graph and a linear regression used to calculate the slope of the graph in order to determine the NO_2^- consumption per minute. This was divided by protein concentration calculated in each sample to calculate the rate of NO_2^- consumption per mg protein per minute. The calculated rates were converted to percentage rate of NO_2^- consumption vs WT control. This allowed comparison between biological replicates.

2.9 Measuring Cu loading of AniA proteins

All Cu loading experiments were performed in 50 mM Tris pH 7.5 unless stated otherwise. A known concentration of $CuCl_2$, Cu(I)Cu(II)-AccA, or Cu(II)Cu(II)-AccA was added to 70 μM of *apo*-AniA, *apo*-T1-AniA, or *apo*-T2-AniA in a final volume of 200 μL in a UV-Star® 96-well microplate (Greiner). The solution spectrum of each mixture was recorded between 400 to 1000 nm every 15 minutes for a total of 180 minutes using a SPECTROstar nano plate reader (BGM Labtech) There were small variations in the background absorbances of the different wells in the microtitre plate. These variations were removed by collecting the spectrum of each well containing only 200 μL of 50 mM Tris pH 7.5 (no protein of Cu) prior to the Cu loading experiments. This blank spectrum was subtracted from the spectrum of each protein sample. To allow for comparison between wells, the spectrum at 90 minutes when 0 μM Cu, or AccA, was added to AniA was removed from all other spectrums. Spectral data obtained from microtitre plates were noisy, particularly when compared with spectra data obtained from quartz cuvettes. Since Cu loading results in an isosbestic point at 420 nm when measured using a quartz cuvette, the collected spectra from the same sample over the entire time series were further corrected to ensure so that their absorbance values at 420 nm were identical (at exactly the average of the absorbance values at this wavelength). This approach allowed removal of noise and monitoring of the time-dependent changes in each spectrum. All Cu loading experiments were performed in duplicate.

2.10 Determining protein size *via* analytical size exclusion chromatography and mass photometry

2.10.1 Size exclusion chromatography

Protein samples were diluted to a final concentration of 30 µM in 20 mM Tris-HCl, 150 mM NaCl pH 7.9. A 100 µL aliquot of each sample was injected onto a Superose 6, 10/300 GL column (Cytiva), which had been equilibrated with the same buffer. The protein was eluted with 1 CV of buffer at a flow rate of 0.5 mL/min and 4°C. Protein elution was monitored by measuring the absorbance (mAU) *via* the built-in UV-Vis detector in an ÄKTA Pure system. Absorbance values were plotted against the elution volume to generate the chromatogram and determine peaks of protein elution. The size of proteins in solution was predicted by comparing the elution volume of the protein against those of protein standards provided by the Blower Lab (Durham University). Experiments were repeated in duplicate.

2.10.2 Mass photometry

A 100 nM stock of each protein was used for mass photometry using the Refeyn OneMP mass photometer (Refeyn), which estimates the size of a protein based on light scattering. The mass photometer was pre-calibrated against commercial protein standards. The instrument was blanked with 50 mM MOPS pH 7.2 buffer. A coverslip containing 18 µL of the same buffer and 2 µL of the 100 nM protein stock was subsequently inserted into the photometer. Light scattering images were recorded for 1 minute. The contrast signals for each sample were then compared with the calibration curve and total signal counts plotted against the predicted protein mass in kDa. Access to the mass photometer was limited and therefore the experiment was only performed once.

Chapter 3: Investigating the conservation of *accA* and *aniA* genes within Betaproteobacteria

Previous research has established that the PCu_AC homologue protein, AccA, may act as a Cu metallochaperone to the nitrite reductase, AniA, in *Neisseria gonorrhoeae*.[120] We are therefore, interested in the conservation of these two proteins amongst different *N. gonorrhoeae* isolates, *Neisseria* species, and amongst Betaproteobacteria. In particular, we are also interested in whether PCu_AC homologue proteins always co-exist with Cu-containing nitrite reductases.

3.1 Analysis of amino acid substitutions within AccA and AniA proteins in *N. gonorrhoeae* strains

3.1.1 Amino acid substitutions in AccA are located away from Cu-binding ligands

All 49 *N. gonorrhoeae* isolated analysed in this study contain AccA. The amino acid sequence of AccA was highly conserved across all strains of *N. gonorrhoeae* analysed (Figure 3.1). In this study, only three amino acid substitutions were found within the AccA protein sequences, resulting in an overall sequence conservation of 98% across all the *N. gonorrhoeae* strains. Only a small subset of strains possessed these amino acid substitutions. AccA is a PCu_AC homologue which therefore contains the predicted $HX_nMX_{21/22}HXM$ Cu(I)-binding motif, as shown in the unpublished draft structure (Figure 3.1a). The residues predicted to be located in this motif, namely His69, Met80, His103, and Met105, were absolutely conserved in *N. gonorrhoeae*. The three variations in the AccA sequence were found in the unstructured regions of the protein, distant from the predicted primary Cu(I)-binding site and the Met/His-rich C-terminal tail. Of the 47 strains analysed in this study, only two strains, 1291 and FA 1090, had a mutation in amino acid 46, from a His to a Pro residue. These same two strains were also the only strains to have a mutation in amino acid 57, from a Gly to a Val residue. Although strains 1291 and FA 1090 originate from clinical samples, both strains have been the predominant laboratory strains for nearly five decades. Therefore, these mutations might have arisen through repeated handling in the laboratory and unrelated to any particular clinical feature of the gonococcal disease. The C-terminus of AccA contains a Met/His-rich region predicted to bind Cu(II) however, this region was not solved in the crystal structure. This region was largely conserved, with only one variation in amino acid sequence found at position 145, which resulted in a Pro to Ser

mutation in five gonococcal strains, including 1291 and FA 1090. Based on the positions of these amino acids within the AccA protein structure, they are not likely to impact Cu binding to the protein.

(a)

```
1291        MKKLLAAVMMAGLAGAVSAAGVHVEDGWARTTVEGMKMGGAFMKIPNDEAKQDFLLVGSS  60
FA19        MKKLLAAVMMAGLAGAVSAAGVHVEDGWARTTVEGMKMGGAFMKIHNDEAKQDFLLGGSS  60
            ************************************************** *********** ***

1291        PVADRVEVHTHINDNGVMRMREVKGGVPLEAKSVTELKPGSYHVMFMGLKKQLKEGDKIP  120
FA19        PVADRVEVHTHINDNGVMRMREVKGGVPLEAKSVTELKPGSYHVMFMGLKKQLKEGDKIP  120
            ************************************************************

1291        VTLKFKNAKAQTVQLEVKTAPMSAMNHGHHHGEAHQH*        157
FA19        VTLKFKNAKAQTVQLEVKTAPMPAMNHGHHHGEAHQH*        157
            ********************* ***************
```

(b)

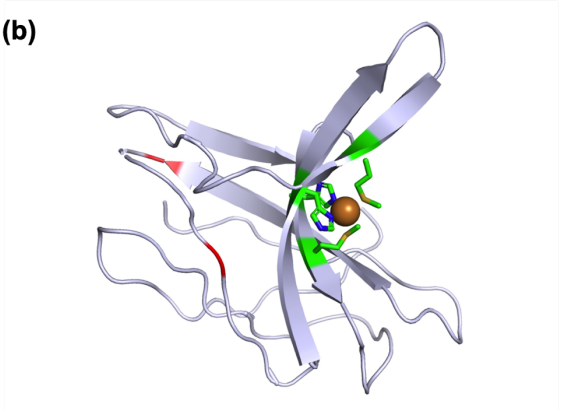

Figure 3.1: Amino acid substitutions of AccA are located outside of from Cu-binding sites. (a) CLUSTAL O sequence alignment of AccA protein sequence in *N. gonorrhoeae* strains (1291 and FA19). Amino acid substitutions are highlighted by red box. **(b)** A visualisation of the AccA protein in *N. gonorrhoeae.* Cu atoms are shown as brown spheres. The amino acid sequences were compared for all known strains of *N. gonorrhoeae*. DNA sequences located via BLAST search from the NCBI website were translated. Amino acid substitutions are highlighted in red. Cu-binding residues are highlighted in green with side chains displayed. AccA draft structure produced by D. Thaqi (unpublished thesis).

3.1.2 Amino acid substitutions in AniA are located away from Cu-binding ligands

All 49 *N. gonorrhoeae* isolates analysed in this study contain AniA. The amino acid sequences of AniA are generally conserved. Single amino acid substitutions among *N. gonorrhoeae* strains occurred outside of the Cu binding sites in the nitrite reductase AniA (Figure 3.2). In this study, six amino acid substitutions were found within the AniA protein sequence, resulting in an overall sequence conservation of 98.5% amongst the *N. gonorrhoeae* strains. The amino acid residues that coordinate the T1Cu centre (His134, His183, Cys175, and Met188) and the T2Cu centre (His139, His174, His329) are absolutely conserved. Of 49 strains analysed in this study, only one strain had a

substitution for amino acid in position 18, which was an Ala to Thr mutation. In contrast, 22 of the strains had a Glu to Pro substitution in amino acid 23. These substitutions were located in the N-terminal signal peptide. This peptide is cleaved upon secretion of AniA into the periplasmic space, and therefore would not be present in the final protein structure. The other remaining substitutions were located in flexible, unstructured regions of the protein, predominantly at the C-terminus. The only amino acid that was substituted in a structured region of the protein was residue 323 where, in 30% of the strains, a Ser to Asn substitution occurred. The final 29 amino acid residues of AniA contain the glycosylation sites.[119] These residues were conserved in all strains of *N. gonorrhoeae* except one that contained an insertion of 5 amino acid residues before the terminal 6 residues. Based on the positions of the variable amino acids within the AniA protein structure, they are not likely to impact Cu binding to the protein. Based on amino acid sequence analyses, the various mutations in AniA do not appear to be co-selected with specific mutations in AccA. Therefore, we do not think that the mutations in AniA will impact the potential interactions with AccA.

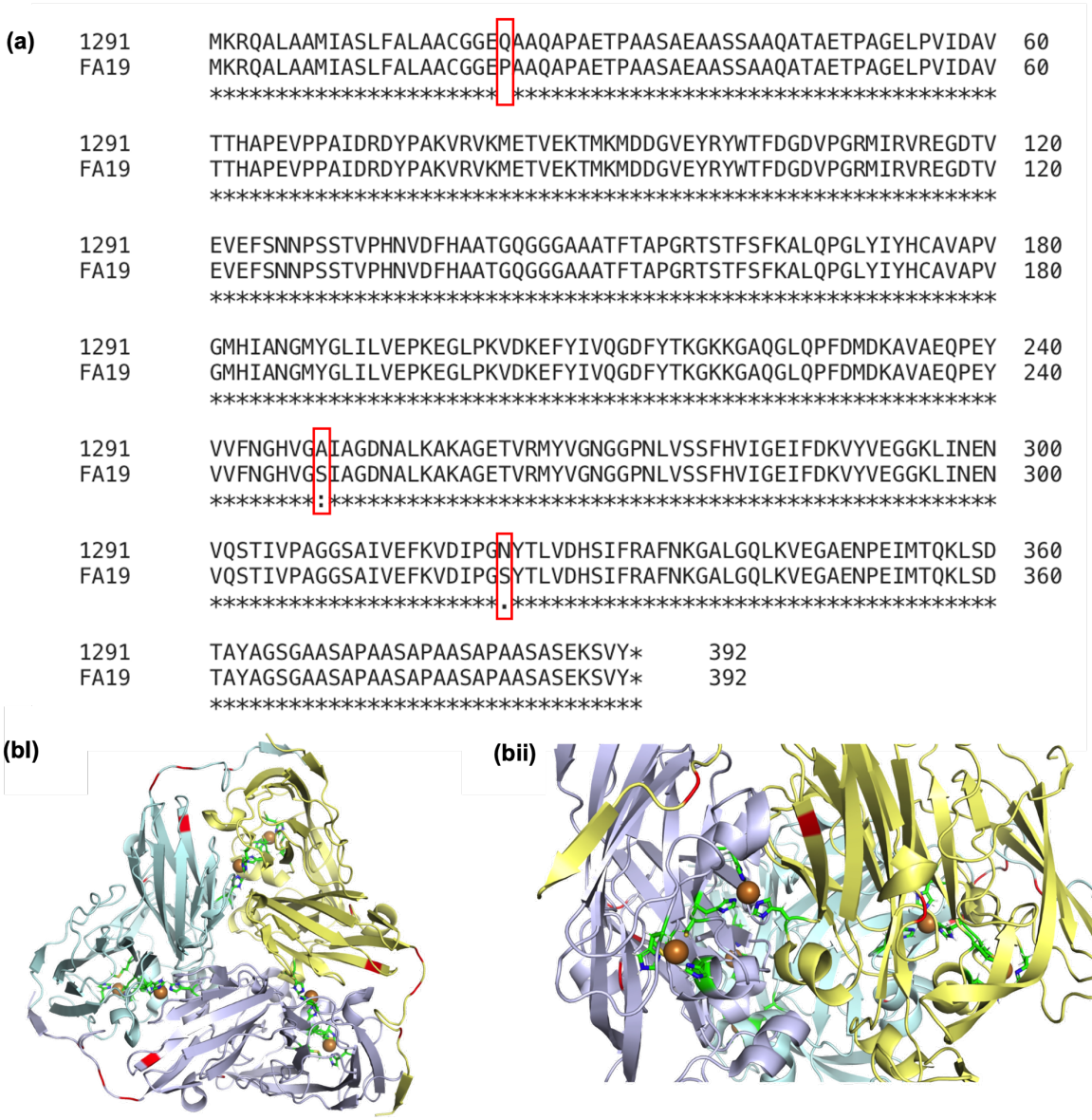

Figure 3.2: Amino acid substitutions of AniA are located outside of from Cu-binding sites. (a) CLUSTAL O sequence alignment of AniA protein sequence in *N. gonorrhoeae* strains (1291 and FA19). Amino acid substitutions are highlighted by red box. **(bi-ii)** A visualisation of the AniA protein in *N. gonorrhoeae.* Cu atoms are shown as brown spheres. The amino acid sequences were compared for all known strains of *N. gonorrhoeae*. DNA sequences located via BLAST search from the NCBI website were translated. Amino acid substitutions are highlighted in red. Cu-binding residues are highlighted in green with side chains displayed. AniA monomers are coloured blue, green, and yellow. AniA structure PDB 1KBW.

3.2 *Neisseria* species that contain AccA homologues do not always contain AniA homologues

A phylogenetic tree of AccA proteins was created , and the presence of AniA highlighted, to determine cooccurrence of AniA and AccA homologues in other *Neisseria* species. Of the species analysed in this study only four of them did not contain an AniA homologue protein but did contain an AccA homologue (Figure 3.3). Furthermore, AccA homologue proteins with an extended Met/His-rich C-terminal tail did not cluster in the phylogenetic tree. This suggests that AccA and AniA homologues did not co-occur in *Neisseria* species, implying a varied role of AccA homologues between species.

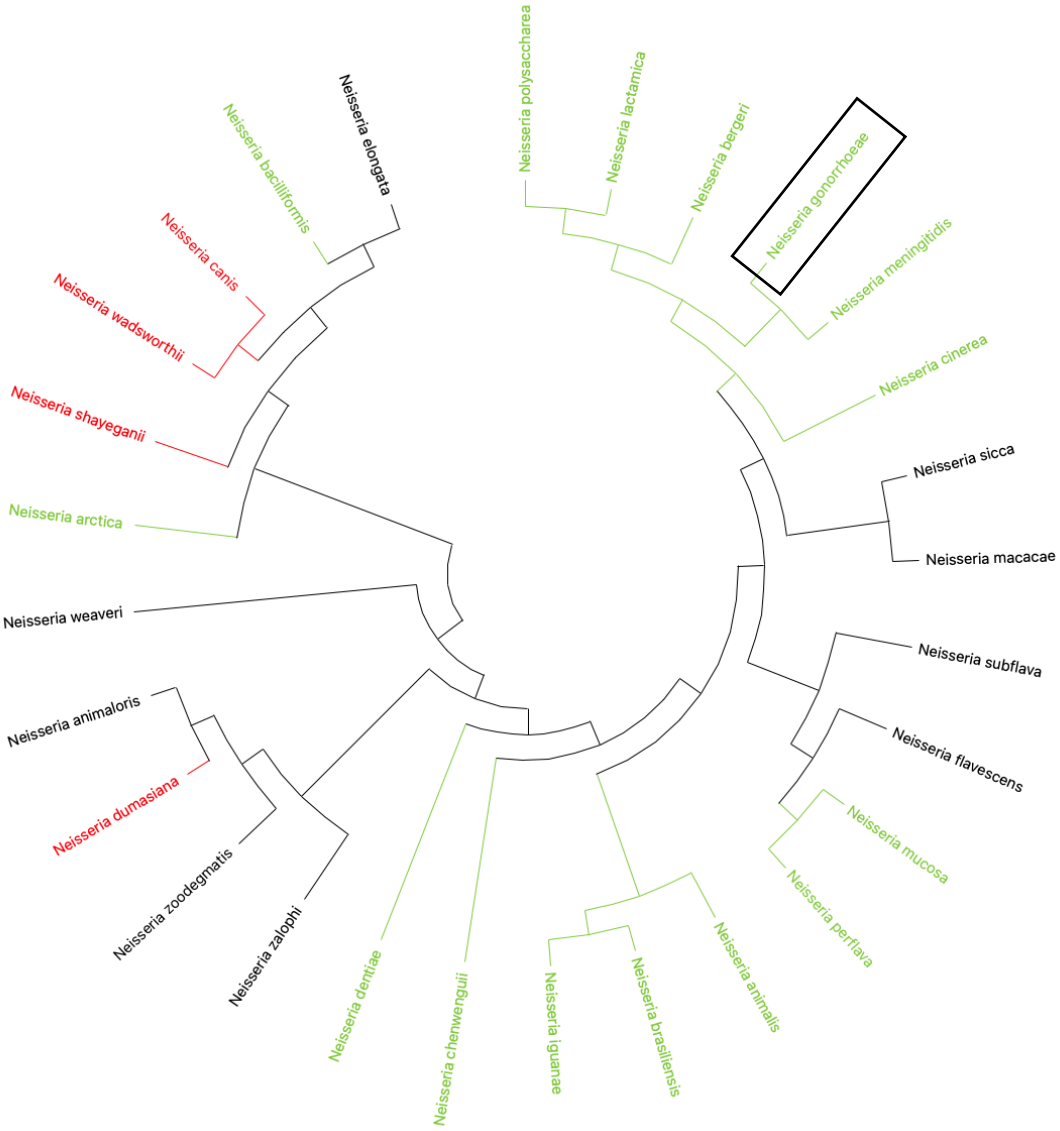

Figure 3.3: AccA does not coexist with AniA in all *Neisseria* species. Phylogenetic tree of AccA protein from reference strains in species of *Neisseria.* DNA sequences located via BLAST search from the NCBI website were translated. Amino acid sequences were then aligned with MAFFT and a phylogenetic tree was generated in MEGA. Species that do not contain a AniA homologue are coloured in red, and AccA protein with an extended Met/His-rich C-terminal tail coloured in green.

3.3 AccA homologues are absolutely conserved in *Neisseria* species

To further investigate the conservation of AccA in *Neisseria* species and its importance in Cu homeostasis and trafficking to target proteins, the conservation of known Cu proteins was studied in reference genomes (Table 3.1). All analysed species contain an AccA homologue protein, but not all of them contain an AniA homologue protein (Table 3.1). The two species, *Neisseria shayegnanii* and *Neisseria wasdsworthii,* lacking an AniA homologue do not contain NorB and NosZ, the enzymes involved in the downstream steps in the denitrification pathway. This implies that these two species do not have a requirement for denitrification. These species do, however, contain homologues to AccA. This implies that AccA homologues in these species may be involved in a different role than metalating AniA. Interestingly, the only cuproproteins that are absolutely conserved across all *Neisseria* species are AccA, an azurin of unknown function Laz, the Cu efflux transporter CopA1, and the aerobic respiration proteins Sco and cytochrome *cbb*$_3$ oxidase. These analyses underscore the importance of aerobic respiration in *Neisseria*, although clearly many species are able to also respire in the absence of O_2 by using the denitrification pathway.

.

Table 3.1: AccA is conserved amongst all species of *Neisseria* but NirK/AniA is not. Conservation of proteins involved in denitrification and Cu-binding proteins in *Neisseria* species. Proteins that are present in the species are depicted with a Y and coloured green. Proteins that are not present are depicted with an N and coloured red. Asterisks denote the following: * protein not present in reference strain but present in all other strains. ** AccA homologue does not contain Met/His-rich C-terminal tail. *** species does not contain protein but contains accessory proteins.

Species	Protein										
	Nar	NirK	AccA	NorB	NosZ	CopA1	Csp	Laz	Sco	Cyt *cbb*$_3$	CueR
N. gonorhoeae	N	Y	Y	Y	Y	Y	Y	Y	Y	Y	N
N. meningitidis	N	Y	Y	Y	N***	Y	N	Y	Y	Y	N
N. elongata	Y	Y	Y*	Y	N	Y	Y	Y	Y	Y	Y
N. bacilliformis	Y	Y	Y	Y	N	Y	Y	Y	Y	Y	N
N. shayeganii	N	N	Y**	N	N	Y	N	Y	Y	Y	N
N. wadsworthii	Y	N	Y**	N	N	Y	N	Y	Y	Y	Y
N. macacae	N	Y	Y**	Y	Y	Y	Y	Y	Y	Y	N
N. mucosa	N	Y	Y	Y	Y	Y	Y	Y	Y	Y	Y*
N. flavescens	N	Y	Y**	Y	Y	Y	Y	Y	Y	Y	N
N. subflava	N	Y	Y	Y	Y	Y	Y	Y	Y	Y	Y
N. lactamica	N	Y	Y	Y	Y	Y	Y	Y	Y	Y	N
N. polysaccharea	N	Y	Y	Y	Y	Y	Y	Y	Y	Y	N
N. cinerea	N	Y	Y	Y	Y	Y	Y	Y	Y	Y	Y

3.4 Betaproteobacteria species that contain AniA homologues do not always contain AccA homologues

AniA (NirK) protein sequences from Betaproteobacteria were examined. Phylogenetic analysis of these AniA (NirK) proteins confirms that the proteins from *Neisseria* species are clustered together, consistent with high sequence conservation as previously identified earlier (Figure 3.4). Furthermore, AniA (NirK) proteins from bacteria genera that are closely related to *Neisseria* in the *Neisseriaceae* family, such as *Kingella,* also cluster with *Neisseria.* In this *Neisseria* cluster, the species also contain AccA.

A distinct cluster of AniA (NirK) proteins is found in species of *Achromobacter*, *Alcaligenes*, and *Nitrosomonas*. Many of these species do not also contain an AccA homologue. In particular, only one out of the ten *Nitrosomonas* species contains both NirK/AniA and AccA homologues, suggesting that either the metallochaperone is not required for loading of Cu into the nitrite reductase, or an unidentified metallochaperone plays this role. This *Nitrosomonas* species, namely *Nitrosomonas eutropha*, was clustered with two other *Nitrosomonas* species in a different branch from the vast majority of NirK/AniA homologues from *Nitrosomonas* species, suggesting a different evolutionary pathway for this protein.

Additional species that contain only NirK/AniA but not AccA are those belonging to the *Burkholderia* genus. None of these species also contain AccA homologue proteins, despite many species possessing more than one copy of a NirK/AniA protein. The presence of multiple copies of NirK/AniA in these species may highlight the importance of denitrification for bacterial metabolism. The processes underlying Cu acquisition from the buffer in these NirK/AniA species remains to be determined.

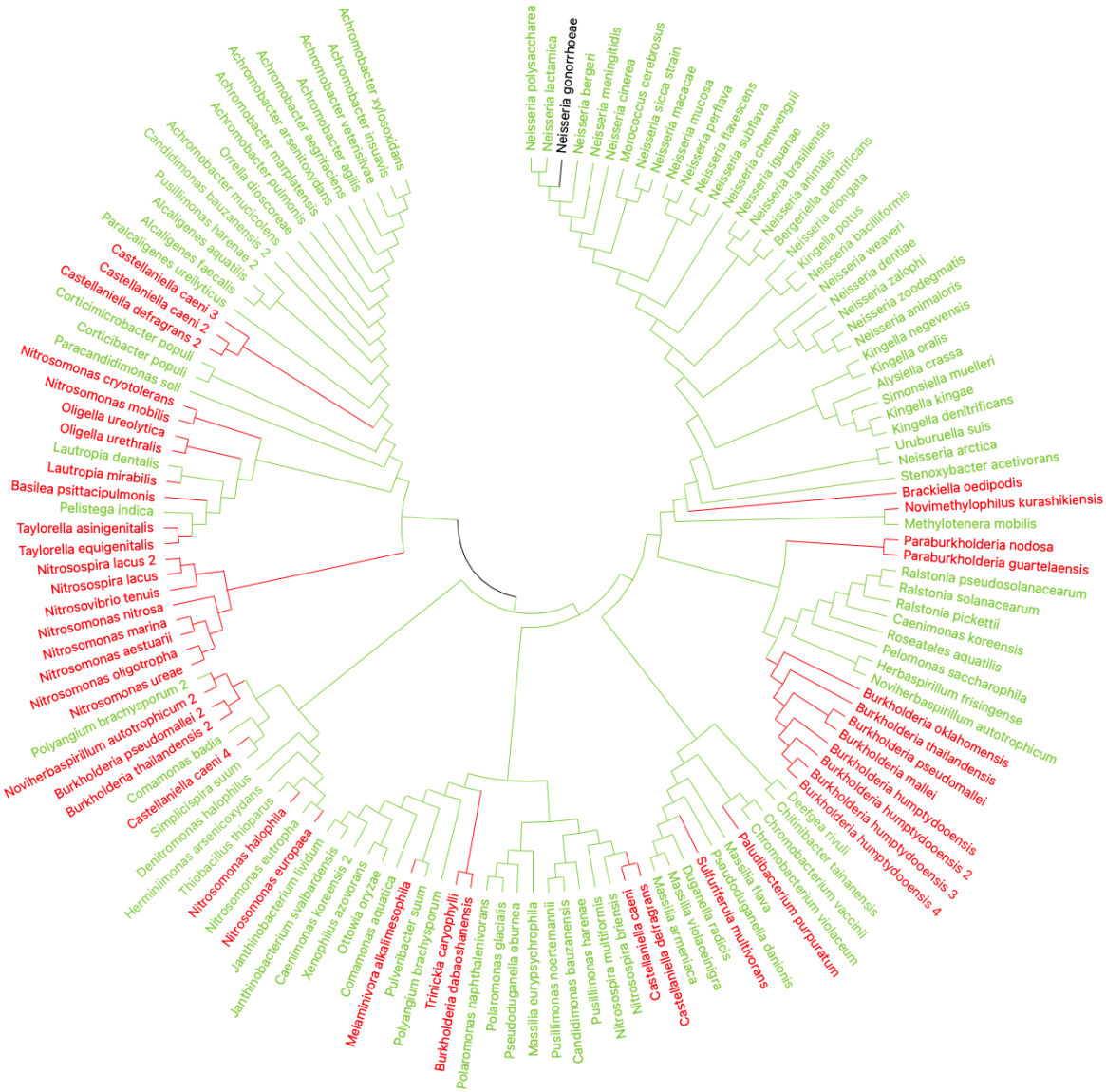

Figure 3.4: AniA homologues do not coexist with AccA homologues in all Betaproteobacteria species. Phylogenetic tree of AniA homologue protein from reference strains in species of Betaproteobacteria. DNA sequences located via BLAST search from the NCBI website were translated. Amino acid sequences were then aligned with MAFFT and a phylogenetic tree was generated in MEGA. Species that contain a AccA homologue are coloured in green. Species that do not contain a AccA homologue are coloured in red. *Neisseria gonorrhoeae* are coloured in black.

3.5 AccA homologue proteins in Betaproteobacteria that also contain AniA homologue proteins do not cluster, except for in *Neisseria* species

Analyses of the AccA protein sequences in Betaproteobacteria reveal that many more species contain an AccA (Figure 3.5) than those that contain AniA (Figure 3.4). The phylogenetic tree indicates that the AccA homologue proteins from species in the *Neisseria* genus and other genus in the *Neisseriaceae* family are clustered together. Most of these species contain AniA in addition to AccA

(Figure 3.4). Outside this cluster, the distribution of species that contain both AccA and NirK/AniA seems to be undefined, with no clearly identifiable grouping or clustering. These analyses suggest that in the majority of Betaproteobacteria species, AccA homologues are not involved in metalating nitrite reductases and instead serve alternative roles, such as PCu_AC which metalates cytochrome *c* oxidases.[93]

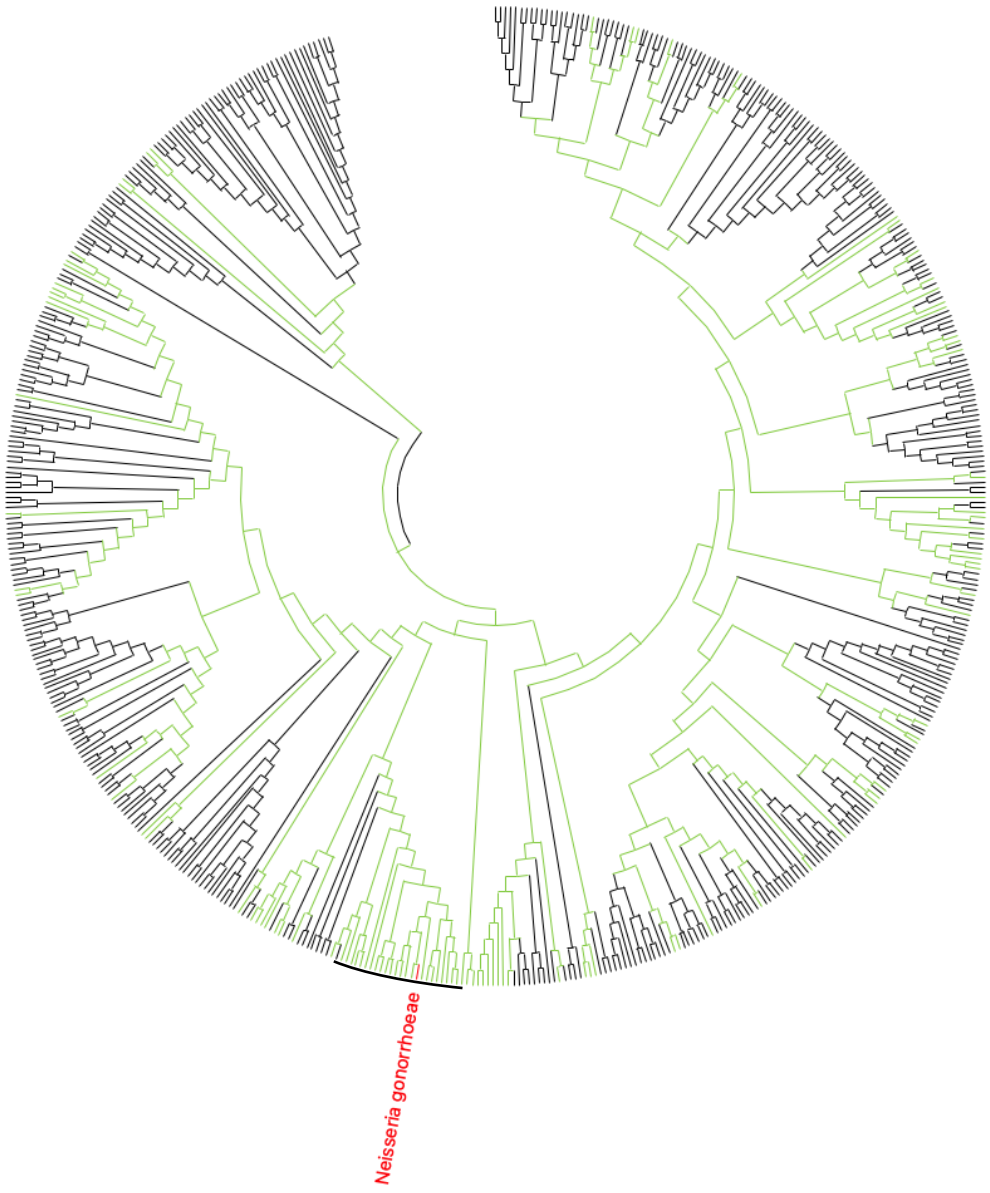

Figure 3.5: AccA homologues of species of Betaproteobacteria that also contain AniA homologues do not cluster together in a phylogenetic tree. Phylogenetic tree of AccA homologue proteins from reference strains in species of Betaproteobacteria. DNA sequences located via BLAST search from the NCBI website were translated. Amino acid sequences were then aligned with MAFFT and a phylogenetic tree was generated in MEGA. Species that contain an AniA homologue are coloured in green. *Neisseria gonorrhoeae* are coloured in red. A black line on outside of tree represents bacteria from the *Neisseriaceae* family.

3.6 Discussion

3.6.1 Single amino acid substitutions of AccA and AniA occurred away from Cu-binding sites within *N. gonorrhoeae*

The importance of AniA in *N. gonorrhoeae* pathogenesis has long been recognised.[113] As the T1Cu and T2Cu centres of AniA are required for enzyme activity, the absolute conservation of the amino acid residues that act as ligands to coordinate Cu is not surprising. Furthermore, the few amino acid substitutions present in *N. gonorrhoeae* strains occurred in flexible regions of the protein which are unlikely to impact enzyme structure or Cu binding.

3.6.2 The C-terminal extension of AccA is not conserved in all *Neisseria* species

We have established that both AccA and AniA are absolutely conserved in *N. gonorrhoeae,* however, many *Neisseria* species contain a truncated AccA protein that lacks the Met/His-rich C-terminal tail extension. The presence of a C-terminal extension has also been identified in a subset of PCu_AC proteins.[123,125] Studies of these PCu_AC proteins and initial studies of AccA indicate that the extended Met/His-rich C-terminal extension binds Cu(II) in addition to the Cu(I) in the $HX_nMX_{21/22}HXM$ Cu(I)-binding motif.[123,125] As AniA contains two Cu-sites, the ability of AccA to bind two Cu atoms may aid in efficient metalation. However, this does not explain why a large subset of AccA homologue proteins in *Neisseria* species do not contain this extension.

Interestingly, apart from *N. gonorrhoeae,* the remaining *Neisseria* species exclusively colonise the O_2-rich upper respiratory tract.[126] Therefore, these species would not rely heavily on denitrification or AniA function for pathogenesis, at least not to the same the extent as *N. gonorrhoeae*, which is known to encounter O_2 limitation in the genitourinary tract.[110] Indeed, the AniA protein is often missing or mutated in strains of *N. meningitidis*, which colonises the upper airway and the brain.[127] Furthermore, two species of *Neisseria* that contained AccA homologue proteins did not contain a homologue to AniA, or any downstream enzymes involved in the denitrification pathway.

The *accA* gene in *N. gonorrhoeae* is thought to be upregulated in response to low O_2 on account of an FNR binding motif found upstream of the transcriptional start site.[128] This idea seems to complement the requirement of AccA to metalate AniA during growth in low O_2 environment. Whether the other

AccA homologue proteins in other *Neisseria* species are also transcriptionally controlled by FNR is unknown. Nevertheless, we have established that AccA homologues are conserved in all *Neisseria* species, suggesting that AccA plays an important role in *Neisseria* physiology, presumably by loading the Cu_B site of cytochrome *cbb*$_3$ oxidase. In this regard, an *accA*-knockout mutant of *N. gonorrhoeae* does display a slight defect in cytochrome *cbb*$_3$ oxidase activity, suggesting that AccA may contribute to activation of the oxidase.[120] However, aerobic respiration clearly does not rely solely on AccA, because this *accA*- knockout mutant strain does not display any growth defect during aerobic growth (see Chapter 5).

3.6.3 AccA and AniA proteins from the family *Neisseriaceae* cluster suggesting a similar function to *N. gonorrhoeae*

Our analyses of AccA sequences found only one major cluster of species that contains *both* AccA and AniA proteins. This cluster consists exclusively of the *Neisseriaceae* family of bacteria, including *Neisseria, Kingella, Alysiella,* and *Simosiella.* This suggests that the AccA present in all *Neisseriaceae* bacteria are similar and perhaps have the same function in loading the AniA nitrite reductase with Cu. AccA proteins outside of this cluster may have a different role such as PCu_AC in loading cytochrome *cbb*$_3$.

In contrast, our analyses of AniA sequences found several clusters of species that also contain AccA homologues. One is from the family *Neisseriaceae* as above. The AniA proteins in these species all contain the N-terminal lipoprotein signal sequences (data not shown). This signal sequence is cleaved *via* the Sec lipoprotein signal peptidase and allows subsequent lipidation and insertion of the protein into the outer membrane.[129] It is tempting to suggest that this linkage of AniA to the outer membrane explains why these species also contain an AccA, but precisely when AniA is loaded with Cu, whether before or after becoming embedded in the outer membrane, is unclear. It is possible that the sequestration of AniA to the membrane physically limits its access to Cu in the periplasmic Cu buffer, necessitating the presence of a metallochaperone, AccA, to deliver this Cu to AniA. In other species, AniA is freely soluble in the periplasm and may be able to access the periplasmic Cu buffer more readily, and thus rendering AccA non-essential. This is similar to how the cytochrome *c* oxidase enzyme is embedded in the inner membrane, and PCu_AC is required to metalate the Cu_A site of cytochrome c oxidase in many bacteria.[28,88]

Interestingly, the cytochrome *cbb*$_3$ oxidase present in *N. gonorrhoeae* and other bacteria from the family *Neisseriaceae* does not contain a Cu_A site, instead containing a Cu_B site only.[106] Whilst there are examples of PCu_AC metalating the Cu_B site in Gram-negative bacteria, initials studies suggest that AccA is not essential for cytochrome c oxidase activity in *N. gonorrhoeae* as previously discussed.[120] Ultimately, phylogenetic analysis of the coexistence of AccA and AniA within Betaproteobacteria may have provided an insight to similar roles of AccA identified by Jen *et al* (2015) in species of the *Neisseriaceae* family of bacteria.[120]

Chapter 4: Characterisation of Cu(I) and Cu(II) binding in native and mutant forms of AccA

The bioinformatic search in Chapter 3, and previous research by Jen *et al*. (2015) has identified that AccA metalates AniA and is a homologue to the periplasmic Cu chaperone PCu_AC family of proteins.[120] PCu_AC proteins typically bind Cu(I) by two His and two Met residues in a $HX_nMX_{21/22}HXM$ motif. Bioinformatical analysis of the AccA protein predicted residues His69, His103, Met80, and Met105 to be the Cu(I)-binding ligands. An unpublished draft structure of AccA (D. Thaqi) shows these predicted amino acid residue sidechains coordinating the Cu(I) atom (Figure 4.1). These resides form the Cu primary site. However, structures elucidated through X-ray crystallography are limited, in that they provide only a snapshot of the protein. To understand the more dynamic role of these residues comprising the Cu primary site, further biochemical determination of Cu binding affinity is required. Analysis of the draft structure identified three Met (36, 78, 107) and a His (71) residue surrounding the Cu primary site that may act as a tract for Cu-transfer from either the periplasmic buffer to AccA, or from AccA to AniA (Figure 4.1). We are therefore interested in whether a mutant protein of AccA lacking this tract impacts AccA Cu binding stoichiometry or affinity. Unlike the majority of PCu_AC family proteins, AccA possesses an extended C-terminal tail domain that is rich in additional His (six) and Met (two) residues that could not be identified in the draft structure due to disorder. Initial experimentation by Jen *et al.* (2015) identified that binds Cu(II) in addition to Cu(I). We predict that this Cu(II) binding site is located in the C-terminal tail of AccA.[120]

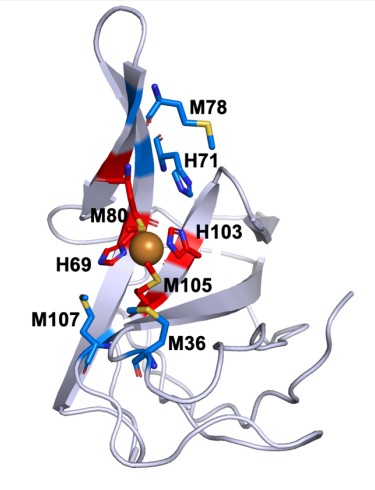

Figure 4.1: AccA draft structure with Cu primary binding site. Cu binding sites are highlighted (red) and predicted Cu tract (blue) displayed.

Mutations of the two predicted Cu binding sites, as well as the possible Cu tract were created (Figure 4.2, Table 4.1). Metal stoichiometry and binding affinities were measured for both Cu(I) and Cu(II). We hope that understanding Cu binding of AccA will elucidate its role in metalating the nitrite reductase AniA.

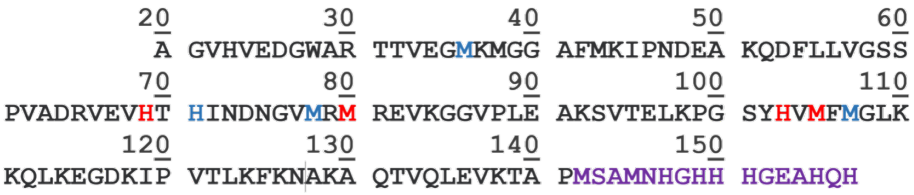

Figure 4.2: The protein sequence of AccA with possible Cu binding sites highlighted. Cu primary site (red), C-terminal tail (purple), Cu tract (blue).

Table 4.1: List of amino acid residues comprising predicted Cu binding sites.

Binding site	Predicted amino acid residues
Cu primary	H69, M80, H103, M105
C-terminal tail	M142 to H157
Cu tract	M36, H71, M78, M107

4.1 Metal binding stoichiometry and selectivity of AccA and mutant proteins

4.1.1 AccA can bind Cu, Ni, and Zn

Previous work by Jen *et al*. (2015) determined the metal binding stoichiometry of the *N. meningitidis* AccA.[120] In this work, AccA was shown to bind two Cu atoms, a single Ni atom, or a single Zn atom. To confirm that the *N. gonorrhoeae* protein behaves as the *N. meningitidis* protein, these experiments were repeated.

To determine the metal binding stoichiometry of AccA the protein was loaded with excess metal and then desalted to remove any excess unbound metal. To determine Cu(I) binding stoichiometry of AccA the protein was incubated with excess metal and ascorbate to create a reducing environment. AccA bound both Cu(I) and Cu(II), consistent with its role as a Cu metallochaperone (Table 4.2). AccA was shown to bind two equivalents of Cu(II) when incubated with Cu in an oxidative environment. AccA incubated with Cu(I) was shown to bind one equivalent of Cu(I) and one

equivalent of Cu(II) (Table 4.2). This suggests that the Cu(I) atom in one site is protected from oxidation however, the second Cu binding site resulted in oxidation to Cu(II). These data support the results of Jen *et al.* (2015) which identified one Cu(I)- and one Cu(II)-binding site in the *N. meningitidis* AccA protein.[120]

AccA also bound two equivalents of Ni and one equivalent of Zn (Table 4.2). AccA did not bind Co or Mn (Table 4.2). After AccA was incubated with Fe the Fe precipitated, preventing measurement of stoichiometry. However, as metal binding is predicted to be immediate, we assume that AccA does not bind Fe. This shows AccA is selective in binding metal ions at the top of the Irving-Williams series.

Table 4.2: AccA binds Cu, Ni, and Zi. Stoichiometry of transition metals when AccA was incubated with excess metal for 15 minutes then desalted. Metal concentration was determined with the colourimetric probe PAR.

Metal	[M]/[AccA]
Cu(I)	0.93 (±0.03)
Cu(II)	2.1 (±0.1)
Co	0.37 (±0.1)
Fe	N/A
Mn	0.33 (±0.2)
Ni	2.1 (±0.06)
Zn	1.2 (±0.09)

4.1.2 AccA binds Cu(I) at the Cu primary site and Cu(II) at the C-terminal tail

To further investigate the role AccA has in binding Cu, stoichiometry of Cu(I) and Cu(II) was measured in key mutants of the predicted Cu binding sites (see Table 4.1). These results are summarised in Section 4.10 (Figure 4.16, and 4.18).

As previously discussed, WT AccA bound one equivalent of Cu(I) and two equivalents of Cu(II). It must be noted that when AccA is incubated with Cu(I), the protein has a mixed stoichiometry of one equivalent Cu(I) plus one equivalent Cu(II), therefore, the protein is saturated with two equivalents of Cu (Table 4.3). When the Cu primary site was deleted, AccA could not bind Cu(I), suggesting that this

is the location of the Cu(I) binding sites (Table 4.3). Single mutants of the Cu primary site (H69A, M80A, H103A, and M105) had no defect in Cu(I) stoichiometry, except for the M80A protein which bound 0.75 equivalents of Cu. Further inspection of raw data revealed that M80A bound a mixed species of either 0.5 or 1 equivalent of Cu(I) suggesting that this amino acid is important in Cu(I) binding in the primary site (Table 4.3). Deletion of the C-terminal tail of AccA resulted in a loss of Cu(II) binding when the protein was incubated with Cu(I) (Table 4.3). This suggests that the second Cu binding site in AccA occurs at the C-terminal tail and that this site coordinates Cu(II).

Table 4.3: AccA binds Cu(I) at the Cu primary site and Cu(II) at the C-terminal tail. Stoichiometry of Cu when AccA was incubated with excess Cu(I) or Cu(II) for 15 minutes and then desalted. Metal concentration was determined with the colourimetric probe BCS.

Mutant	Stoichiometry when incubated with Cu(I)		Stoichiometry when incubated with Cu(II)	
	[Cu(I)]/[AccA]	[Cu(II)]/[AccA]	[Cu(I)]/[AccA]	[Cu(II)]/[AccA]
WT	0.93 (±0.03)	1.0 (±0.09)	0.20 (±0.02)	1.9 (±0.1)
H69A	0.89 (±0.04)	1.2 (±0.1)	0.19 (±0.2)	2.1 (±0.2)
M80A	0.73 (±0.2)	1.3 (±0.1)	0.29 (±0.06)	1.9 (±0.1)
H103A	0.97 (±0.07)	1.3 (±0.2)	0.22 (±0.05)	1.8 (±0.2)
M105A	0.94 (±0.1)	1.3 (±0.07)	0.03 (±0.03)	2.1 (±0.2)
ΔCu primary	0.31 (±0.06)	1.3 (±0.1)	0.26 (±0.08)	1.7 (±0.6)
ΔCu tract	0.88 (±0.01)	0.94 (±0.3)	0.23 (±0.02)	1.7 (±0.05)
ΔC-terminal	1.3 (±0.2)	0.15 (±0.2)	0.26 (±0.04)	0.83 (±0.07)

4.2 AccA binds Cu(I) with femtomolar affinity

Colourimetric probes with known affinities for Cu(I) were used to determine the Cu(I) binding affinity of AccA (Table 2.6). The colourimetric probe ferrozine (Fz) was the weakest Cu(I) binding probe used in these experiments. Fz forms a 2:1 complex with Cu(I) with a reported β_2 value of 1.3×10^{15} M^{-2}.[130] A titration of Cu into a solution of 160 μM Fz, in the presence of excess ascorbate as a reductant, resulted in a spectrum in which absorbance increased with Cu concentration with clear peaks at 470 and 600 nm (Figure 4.3ai). When the absorbance at 470 nm was plotted against Cu concentration, it resulted in a clear linear increase, until 80 μM Cu was titrated into Fz and the line plateaued. As only

160 μM of Fz was used in these experiments, and Fz forms a 2:1 complex with Cu(I), this plateau was a result of the Fz becoming saturated with Cu.

When Cu was titrated into a mix of Fz and 30 μM AccA, the spectra showed an increase in absorbance with Cu concentration and a peak at 470 nm. However, the peak at 600 nm was not as pronounced and overall there was a slight blue-shift (to the left) to the spectra compared to the Fz only control. This may have been caused by the formation of a tertiary complex between AccA, Fz, and Cu (Figure 4.3aii). When the absorbance at 470 nm was plotted against Cu concentration, there was no increase in absorbance until 30 μM of Cu was added to the titration mix of 160 μM Fz and 30 μM AccA (Figure 4.3aiii). This result is consistent with the presence of one high-affinity or tight Cu(I) binding site in AccA. After the high-affinity Cu(I) binding site of AccA was saturated, the gradient of the titration curve was shallower compared to the Fz only control. This result suggests that one or more additional Cu(I) binding sites in AccA competes effectively with Fz. Interestingly, the titration curve did not plateau until a total of 160 μM of Cu(I), *i.e.* an excess over AccA, was added to the reaction. These data suggest that there are multiple weaker Cu(I) binding sites in AccA which compete with Fz for Cu (Figure 4.3aiii). Fitting the data to an equilibrium model, using the software DynaFit, modelled a total of three possible Cu(I) binding sites (Figure 4.3aiv). This suggests that AccA binds three atoms of Cu(I). AccA binds one atom of Cu(I) in a tight, high-affinity, binding site most likely comprising of the Cu primary site. Furthermore, AccA binds Cu(I) in at least two additional weak binding sites. The Cu(I) binding affinities of these weak sites were calculated in the picomolar and nanomolar range at K_D 9.8 x 10^{-13} M and 1.3 x 10^{-11} M or a logK_D of -12 M (± 0.2) and -10.9 M (± 0.3) respectively. However, these weak binding sites may be non-specific Cu binding to the protein or a complex of AccA-Cu-Fz as indicated by the shift in the spectra when Cu is titrated with AccA and Fz compared to Fz alone.

$$2Fz + Cu^{I} \rightleftharpoons Cu^{I}(Fz)_2 \quad \text{(eq. 17)}$$

$$AccA + Cu^{I} \rightleftharpoons Cu^{I}AccA \quad \text{(eq. 18)}$$

$$Cu^{I}AccA + Cu^{I} \rightleftharpoons (Cu^{I})_2AccA \quad \text{(eq. 19)}$$

$$(Cu^{I})_2AccA + Cu^{I} \rightleftharpoons (Cu^{I})_3AccA \quad \text{(eq. 20)}$$

Because the high-affinity AccA Cu(I) binding site outcompeted Fz for Cu(I), it was not possible to use Fz to determine the affinity AccA has for Cu(I) in this site. We, therefore, used a colourimetric probe with a higher affinity for Cu(I), namely bicinchoninic acid (BCA). BCA forms a 2:1 complex with Cu(I) and has a reported β_2 value of 1.6 x 10^{17} M^{-2}.[130] Similar to Fz, when Cu(I) was titrated into a solution of BCA the spectra showed an increase of absorbance with a peak at 562 nm (Figure 4.3bi). When the absorbance at 562 nm was plotted against Cu concentration it resulted in a clear linear increase, until 80 μM Cu was titrated into BCA and the line plateaued (Figure 4.3biii). As only 160 μM of BCA was used in these experiments, and BCA forms a 2:1 complex with Cu(I), this plateau was a result of the BCA becoming saturated with Cu.

When Cu was titrated into a mix of BCA and 30 μM AccA, the spectra showed an increase in absorbance with Cu concentration with a peak at 562 nm. There was no change in the spectra when Cu(I) was titrated into a mixture of BCA and AccA compared to BCA alone (Figure 4.3bii). This suggests that an AccA-Cu(I)-BCA complex does not form in these conditions. Similar to the Fz titration, when Cu(I) was titrated into a mix of 160 μM BCA and 30 μM AccA there was no increase in absorbance, until after 30 μM of Cu(I) was added to the reaction mix. This corresponded to saturation of the high-affinity Cu primary binding site of AccA (Figure 4.3biii). After saturation of the Cu primary site of AccA, the absorbance at 562 nm increased until 110 μM Cu was added to the reaction mix suggesting that only one Cu(I) binding site was detected in AccA when Cu(I) was titrated in a mixture of AccA and BCA. When the data were fitted to an equilibrium model using the software DynaFit only one Cu(I) binding site, corresponding to the tight Cu primary site, was identified. Therefore, the weaker Cu(I) binding sites of AccA detected with Fz are outcompeted by BCA.

$$2BCA + Cu^{I} \rightleftharpoons Cu^{I}(BCA)_2 \qquad \text{(eq. 21)}$$

$$AccA + Cu^{I} \rightleftharpoons Cu^{I}AccA \qquad \text{(eq. 22)}$$

Because the high-affinity Cu primary site of AccA also outcompeted BCA for Cu(I), we could not use this data to determine the Cu(I) affinity of this site. We therefore used the colourimetric probe bathocuproine disulfonate (BCS) which forms a 2:1 complex with Cu(I) and has a reported β_2 value of 6.3 x 10^{19} M^{-2}.[130] A titration of increasing Cu(I) concentrations into a solution of BCS resulted in an

increased absorbance in the spectra, and a peak at 482 nm was observed (Figure 4.3ci). Plotting the peak at 482 nm resulted in a linear increase of absorbance until 40 μM of Cu(I) was titrated into BCS, at which point the line plateaued (Figure 4.3cii). As only 80 μM of BCS was used in these experiments, and as BCS forms a 2:1 complex with Cu(I), this plateau was a result of the BCS becoming saturated with Cu.

When Cu(I) was titrated into a mixture of BCS and 20 μM AccA, the peak at 483 nm when BCS was saturated was reduced compared to the BCS only control the overall spectra remained the same (Figure 4.3cii). However, unlike the curves when Cu(I) was titrated into a mixture of AccA and Fz or BCA, there was an increase of absorbance at all Cu concentrations until 50 μM of Cu was added to the titration mix where the absorbance plateaued (Figure 4.3cii). This indicates that the high-affinity Cu(I) Cu primary binding site of AccA does not outcompete, but instead competes with BCS for Cu. To determine Cu(I) affinity, the absorbance at 483 nm was plotted on a graph. When the data were fitted to an equilibrium model with the software DynaFit, only one Cu(I) binding site was identified in AccA. This binding site had a Cu(I) affinity in the femtomolar range at K_D of 2.0 x 10^{-17} M or a logK_D of -16.7 (± 0.3) M. Curve fits using affinities that were calculated to be 10x weaker (2.0 x 10^{-16}) or 10x tighter (2.0 x 10^{-18}) than the measured affinity value were simulated (Figure 4.3ciii). As our model curve fits within the 10x weaker and 10x tighter curves, we can be confident that the calculated affinity of AccA for Cu(I) is within the correct range.

$$2BCS + Cu^{I} \rightleftharpoons Cu^{I}(BCS)_2 \qquad \text{(eq. 23)}$$

$$AccA + Cu^{I} \rightleftharpoons Cu^{I}AccA \qquad \text{(eq. 24)}$$

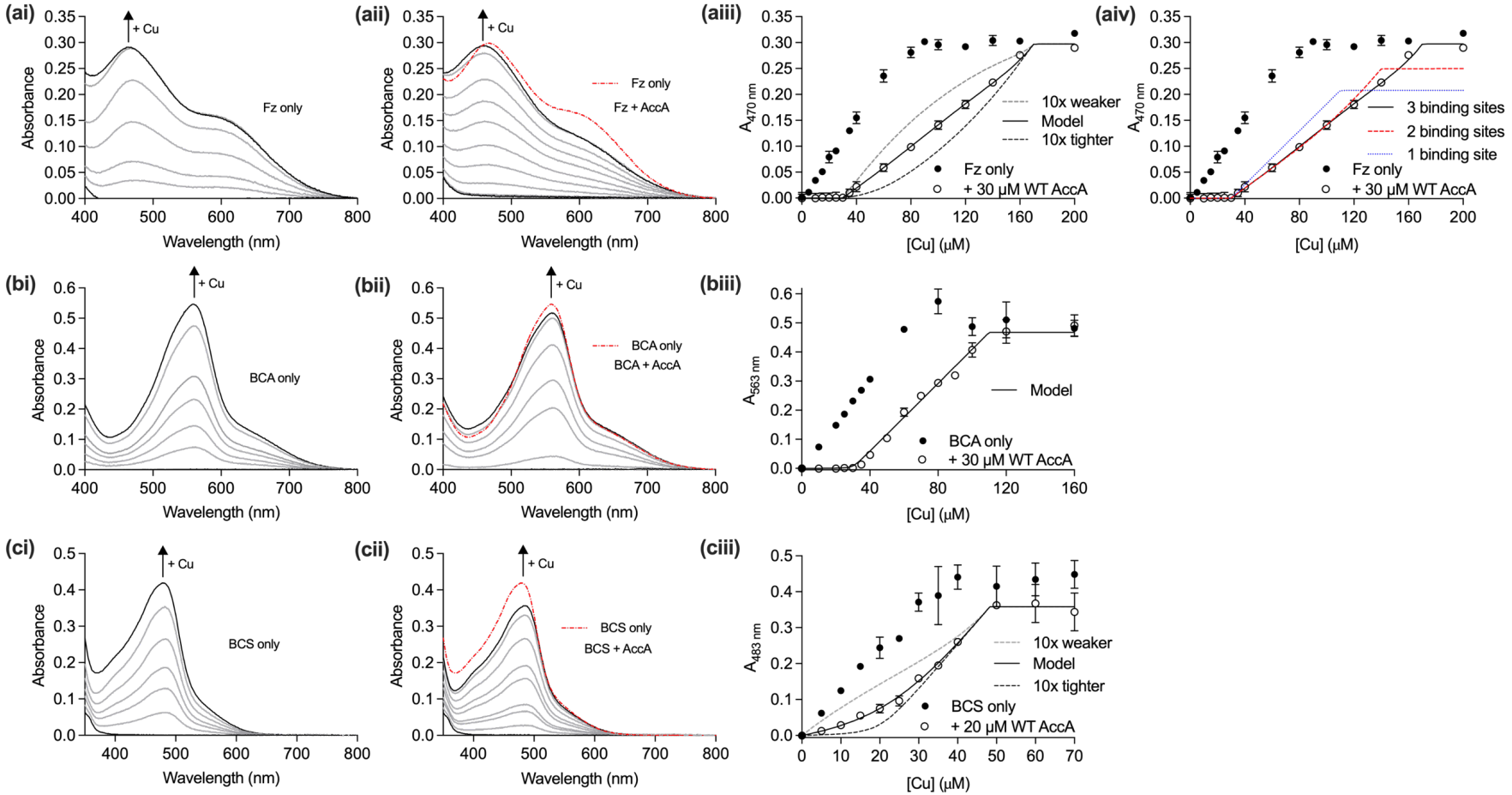

Figure 4.3: WT AccA competes with BCS only for Cu(I). WT AccA competition against the Cu(I)-specific colourimetric probe **(a)** ferrozine (Fz), **(b)** bicinchoninic acid (BCA), **(c)** bathocuproine disulfonate (BCS). **(xi)** UV-VIS spectra of a reducing **(ai)** Fz, **(bi)** BCA, and **(ci)** BCS solution from 400-800 nm when Cu(I) was titrated against probe. Excess ascorbate was used to reduce Cu(II). A black line represents *apo*-probe and *holo*-probe. **(xii)** UV-VIS solution of a reducing solution when Cu(I) was titrated against a solution of AccA and **(aii)** Fz, **(bii)** BCA, and **(cii)** BCS from 400-800 nm. Excess ascorbate was used in solution to reduce Cu(II). Black lines represent *apo*-probe and *holo*-probe. A red dotted line represents saturated probe when no AccA was present. **(xiii)** Titration of Cu in probe solution; absorbance at **(aiii)** 470 nm, **(biii)** 562 nm, and **(ciii)** 483 nm were plotted against Cu(I) concentration in the presence of probe (black circles) or in the presence of probe and AccA (open circles). The model fit to the data (black line), and 10-fold weaker and stronger models (dashed lines) are shown.. **(aiv)** Data from **aiii** with models for 1 (blue dotted line), 2 (red dashed line), and 3 (black line) Cu binding sites in the protein. Data points represent the mean of n = 2. Error bars represent standard deviation

4.3 Investigating Cu(I) binding at the Cu primary site

4.3.1 A ΔCu primary AccA mutant binds Cu(I) with low picomolar affinity

Previous stoichiometry experiments (Table 4.3) identified that AccA binds Cu(I) at the Cu primary site consisting of H69, M80, H103, and M105. We have also calculated the Cu(I) binding affinity of the WT protein at a logK_D of -16.7 M (Figure 4.3ciii). We hypothesise that mutation of one or more of the residues that comprise the Cu primary site would weaken the affinity of the site for Cu(I). To achieve this, we generated a mutant protein of AccA lacking the Cu primary site in its entirety, H69A/M80A/H103A/M105A. From this point on this mutant will be referred to as ΔCu primary AccA.

In contrast to the WT protein, the ΔCu primary mutant now competes with Fz for Cu(I) (Figure 4.4ai). This suggests that the affinity of the protein is reduced by at least 10,000-fold as the WT protein competed with BCS which has a β_2 for Cu(I) of 6.3 x 10^{19} M^{-2} whereas Fz has a for Cu(I) of 1.3 x 10^{15} M^{-2}. The data was modelled in the software DynaFit. Interestingly, the modelling software detected four Cu(I) binding sites in the ΔCu primary mutant when the titration curves for the WT AccA protein were best fit using a three binding site model. The affinity of the ΔCu primary mutant for Cu(I) was estimated to be in the picomolar range, with a K_D of 1.8 x 10^{-12} M or a logK_D of -11.8 M (± 0.1) this was a factor of 10,000 lower than the WT protein. The remaining three Cu(I) binding sites in the ΔCu primary AccA mutant had affinities in the nanomolar range with a logK_D of -11 M (± 0.1), -10.1 M (± 0.2), and -9.3 M (± 0.5) calculated respectively. The logK_D affinities of Cu(I) binding sites outside the Cu primary site of WT AccA were previously calculated at -12 M and -10.9 M which corresponds to the two tightest binding sites in the ΔCu primary AccA protein at -11.8 and -11 respectively. Fz proved to be the optimal probe to use to determine Cu(I) affinity for the ΔCu primary AccA protein as there was no competition between BCA and the protein (Figure 4.4b).

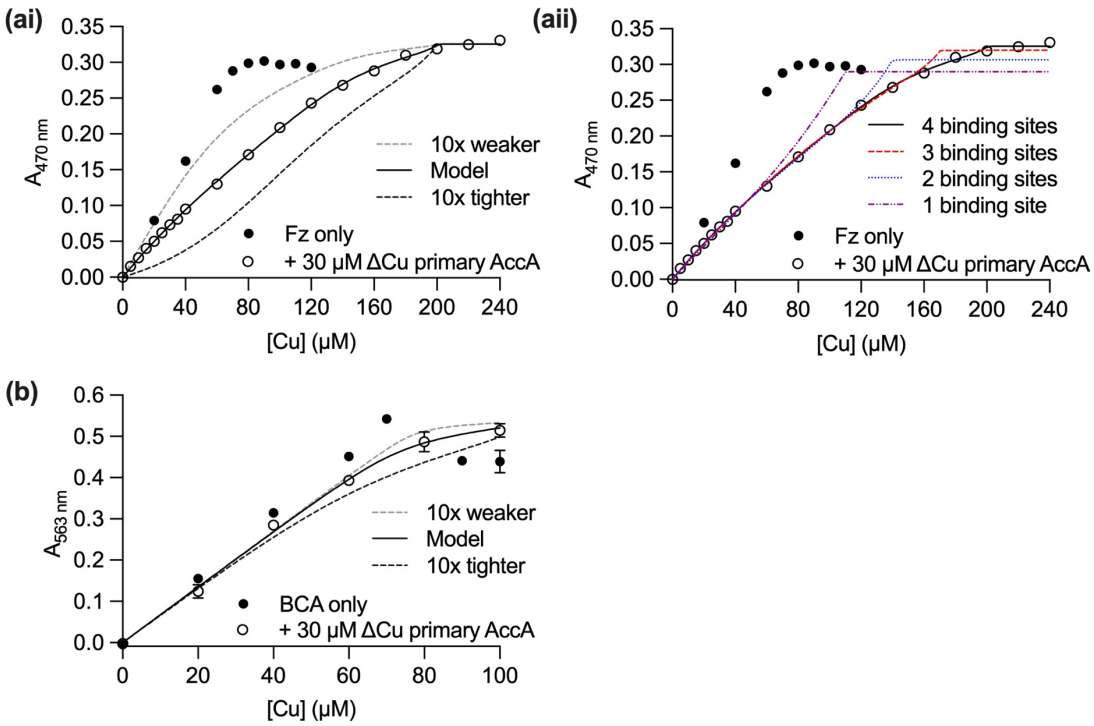

Figure 4.4: ΔCu primary AccA competes with only Fz for Cu(I). ΔCu primary AccA competition against the Cu(I) specific colourimetric probe **(a)** ferrozine (Fz) and **(b)** bicinchoninic acid (BCA). Titration of Cu in probe solution. Absorbance at **(ai)** 470 nm, and **(b)** 562 nm were plotted against Cu(I) concentration in the presence of a probe (black circles) or in the presence of a probe and AccA (open circles). The model fit to the data (black line) and 10-fold weaker and stronger models (dashed lines) are shown. **(aii)** Data from **ai** with models for 1 (purple dotted and dashed line), 2 (blue dotted line), 3 (red dashed line), and 4 (black line) Cu binding sites in the protein. Data points represent the mean of n = 2. Error bars represent standard deviation.

4.3.2 A H69A primary site mutant binds Cu(I) with picomolar affinity

We have established that Cu(I) binds tightly to the Cu primary site of AccA. However, it is unknown whether the four amino acid residues in this site contribute equally to Cu(I) binding. It was hypothesised that individual site directed mutagenesis of the amino acid residues that coordinate Cu in the primary site would weaken the Cu(I) binding affinity. We, therefore, used site-directed mutagenesis of single amino acids to determine their impact on Cu(I) binding.

The H69A mutant competed with Fz (Figure 4.5ai). The data was modelled with the software DynaFit which detected four Cu(I) binding sites (Figure 4.5aii). Three of the four binding sites had affinities in the nanomolar range K_D of 9.2 x 10^{-12} M, 2.2 x 10^{-11} M, and 4.8 x 10^{-10} M or a logK_D of -11 M (± 0.1), -10.7 M (± 0.2), and -9.3 M (± 0.4). Additionally, the remaining binding site's affinity lay in the picomolar

range K_D 2.3 x 10^{-13} M or a logK_D of -12.6 M (± 0.1). These affinities align with the those in the sites previously calculated for the WT and ΔCu primary AccA proteins.

The H69A AccA protein additionally competed with BCA (Figure 17b). The titration of Cu(I) added to a solution of 160 μM BCA and 30 μM H69A AccA plateaued after 110 μM of Cu was added to the reaction. This suggests that only one site could compete with BCA. The software DynaFit was used to model the data and detected one Cu(I) binding site with a picomolar K_D of 2.8 x 10^{-14} M or a logK_D of -13.5 M (± 0.2).

The decrease in absorbance in the BCA only standard curve is a result of the probes saturating and forming a 1:1 complex with Cu(I) over time rather than a 2:1 complex (Figure 4.5b). The H69A mutant did not compete with BCS (Figure 17c). As BCA was the strongest probe that the H69A AccA competed with, the affinity of -13.5 M was used for the Cu primary binding site.

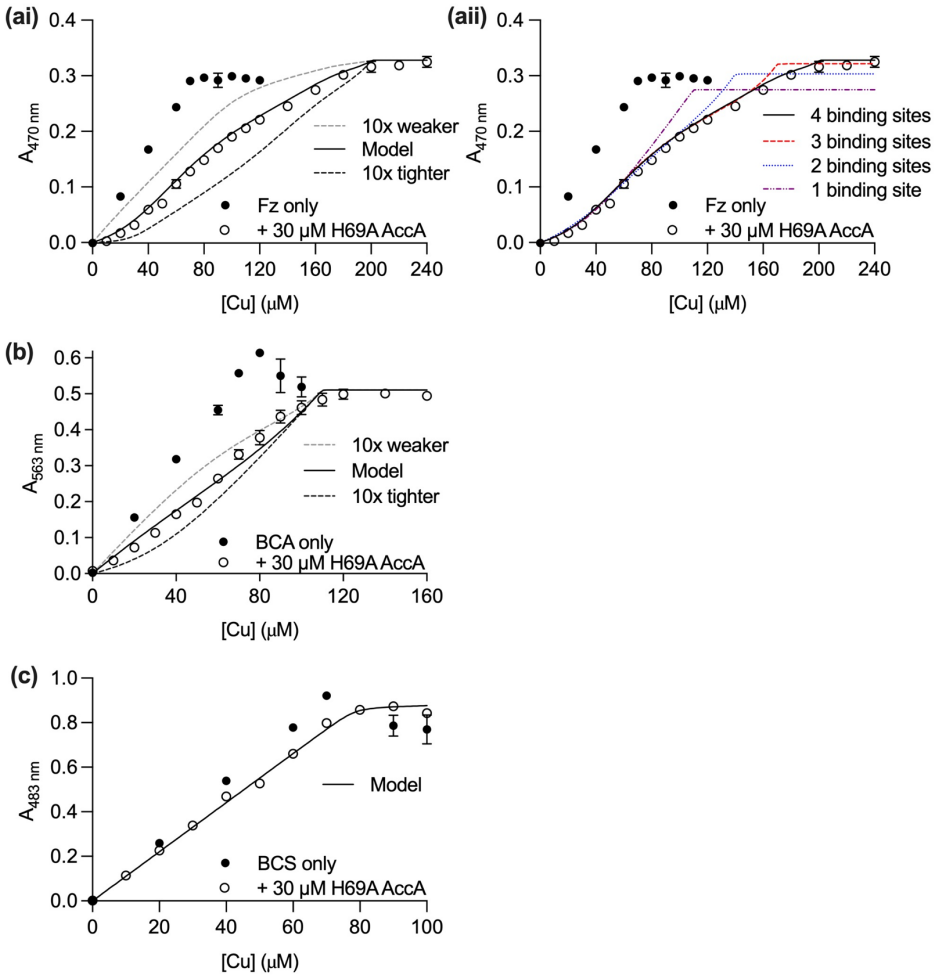

Figure 4.5: H69A AccA competes with BCA for Cu(I). H69A AccA competition against the Cu(I) specific colourimetric probe **(a)** ferrozine (Fz), **(b)** bicinchoninic acid (BCA), and **(c)** bathocuproine disulfonate (BCS). Titration of Cu in probe solution. Absorbance at **(ai)** 470 nm, **(b)** 562 nm, and **(c)** 483 nm were plotted against Cu(I) concentration in the presence of probe (black circles) or in the presence of probe and AccA (open circles). The model fit to the data (black line) and 10-fold weaker and stronger models (dashed lines) are shown. **(aii)** Data from **ai** with models for 1 (purple dotted and dashed line), 2 (blue dotted line), 3 (red dashed line), and 4 (black line) Cu binding sites in the protein. Data points represent the mean of n = 2. Error bars represent standard deviation.

4.3.3 A M80A primary site mutant binds Cu(I) with picomolar affinity

Similar to the H69A, the M80A AccA mutant protein competed with Fz (Figure 4.6ai). The software DynaFit was used to model the data and detected four Cu(I) binding sites (Figure 4.6aii). Three of these binding sites had an affinity in the nanomolar range with a calculated K_D of 6.1 x 10^{-12} M, and 5.2 x 10^{-11} M or a logK_D of -11.2 M (± 0.3), and -10.2 M (± 0.4). The remaining weak binding site had an affinity in the picomolar range K_D = 9.3 x 10^{-13} M or a logK_D of -12 M (± 0.3). These Cu(II) binding affinities align with the those in sites previously calculated for the WT and ΔCu primary AccA proteins.

Additionally, there was one binding site in the picomolar range K_D 2.3 x 10^{-13} M or a logK_D of -13.2 M (± 0.4).

The M80A AccA protein also competed with BCA (Figure 4.6b). Only one Cu(I) binding site was detected when the data was modelled with DynaFit, suggesting that three weaker binding sites detected by competition with Fz are outcompeted by BCA. This Cu(I) binding site had a picomolar K_D of 1.3 x 10^{-14} M or a logK_D of -13.9 M (± 0.1). The M80A mutant did not compete with BCS (Figure 4.6c). The decrease in absorbance in the BCA and BCS only standard curves is a result of the probes saturating and forming a 1:1 complex with Cu(I) over time rather than a 2:1 complex. As BCA was the strongest probe that the M80A AccA competed with, the affinity of -13.9 M was used for the Cu primary binding site.

Interestingly, the M80A had previously shown mixed 0.5 to 1 equivalent of Cu(I) bound in stoichiometry experiments, whereas the other single Cu primary mutants all bound 1 equivalent of Cu(I) (Table 4.3). However, the calculated affinity does not differ from that of the H69A AccA protein. These data suggest that the affinity of the M80A protein is not related to the difference in stoichiometry.

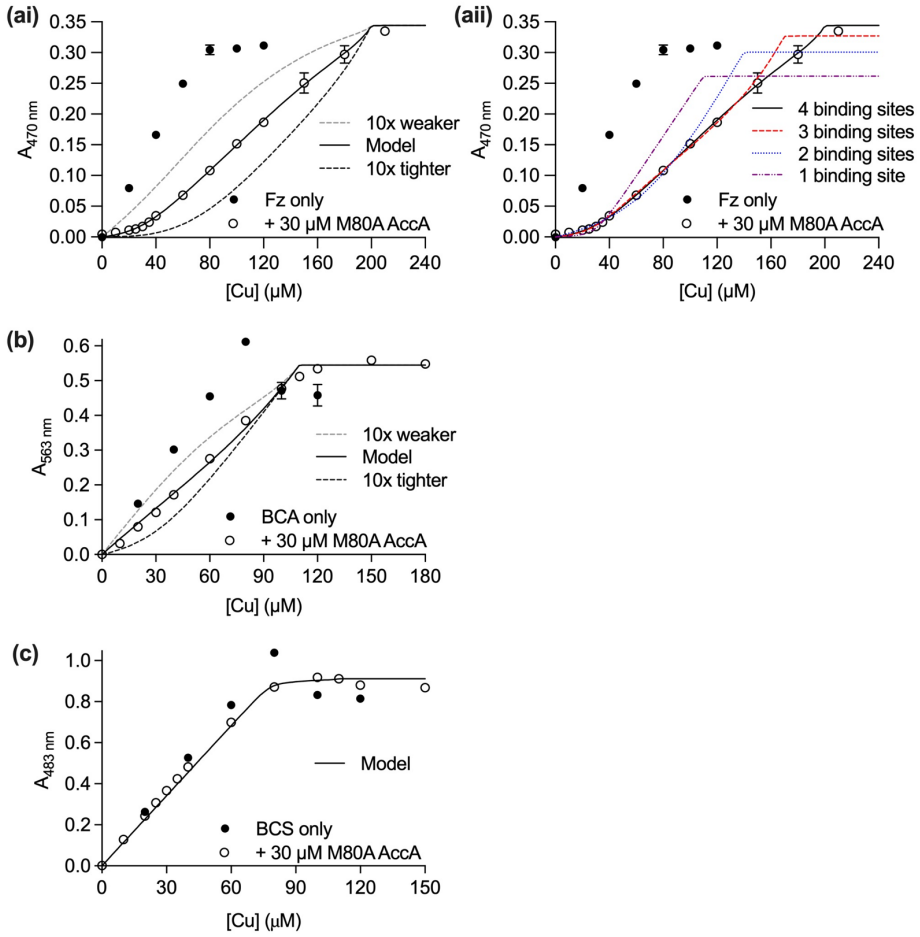

Figure 4.6: M80A AccA competes with BCA for Cu(I). M80A AccA competition against the Cu(I) specific colourimetric probe **(a)** ferrozine (Fz), **(b)** bicinchoninic acid (BCA), and **(c)** bathocuproine disulfonate (BCS). Titration of Cu in probe solution. Absorbance at **(ai)** 470 nm, **(b)** 562 nm, and **(c)** 483 nm were plotted against Cu(I) concentration in the presence of probe (black circles) or in the presence of probe and AccA (open circles). The model fit to the data (black line) and 10-fold weaker and stronger models (dashed lines) are shown. **(aii)** Data from **ai** with models for 1 (purple dotted and dashed line), 2 (blue dotted line), 3 (red dashed line), and 4 (black line) Cu binding sites in the protein. Data points represent the mean of n = 2. Error bars represent standard deviation.

4.3.4 A H103A primary site mutant binds Cu(I) with picomolar affinity

The H103A AccA protein also competed with Fz for Cu(I) (Figure 4.7ai). The software DynaFit detected four Cu(I) binding sites when the data was modelled (Figure 4.7aii). Like the H69A and M80A AccA proteins, three of the four binding sites had affinities in the nanomolar range K_D of 3.3 x 10^{-12} M, 1.2 x 10^{-11} M, and 1.1 x 10^{-10} M or a logK_D of -11.4 M (± 0.2), -10.9 M (± 0.2), and -10.0 M (± 0.02) respectively which align with those in the sites previously calculated for the WT and ΔCu primary AccA proteins. Additionally, there was one binding site in the picomolar range K_D 4.8 x 10^{-13} M or a logK_D of -12.3 M (± 0.1).

The H103A AccA protein additionally competed with BCA for Cu(I) (Figure 4.7bi). Only one Cu(I) binding site was detected when the data was modelled with DynaFit, suggesting that three weaker binding sites detected by competition with Fz are outcompeted by BCA. The Cu(I) binding site was calculated to have a picomolar K_D of 1.2 x 10^{-14} M or a logK_D of -13.9 M (± 0.1). The H103A AccA protein did not compete with BCS for Cu(I) (Figure 4.7c). As BCA was the strongest probe that the H103A AccA protein competed with the affinity of -13.9 M was used for the Cu primary binding site.

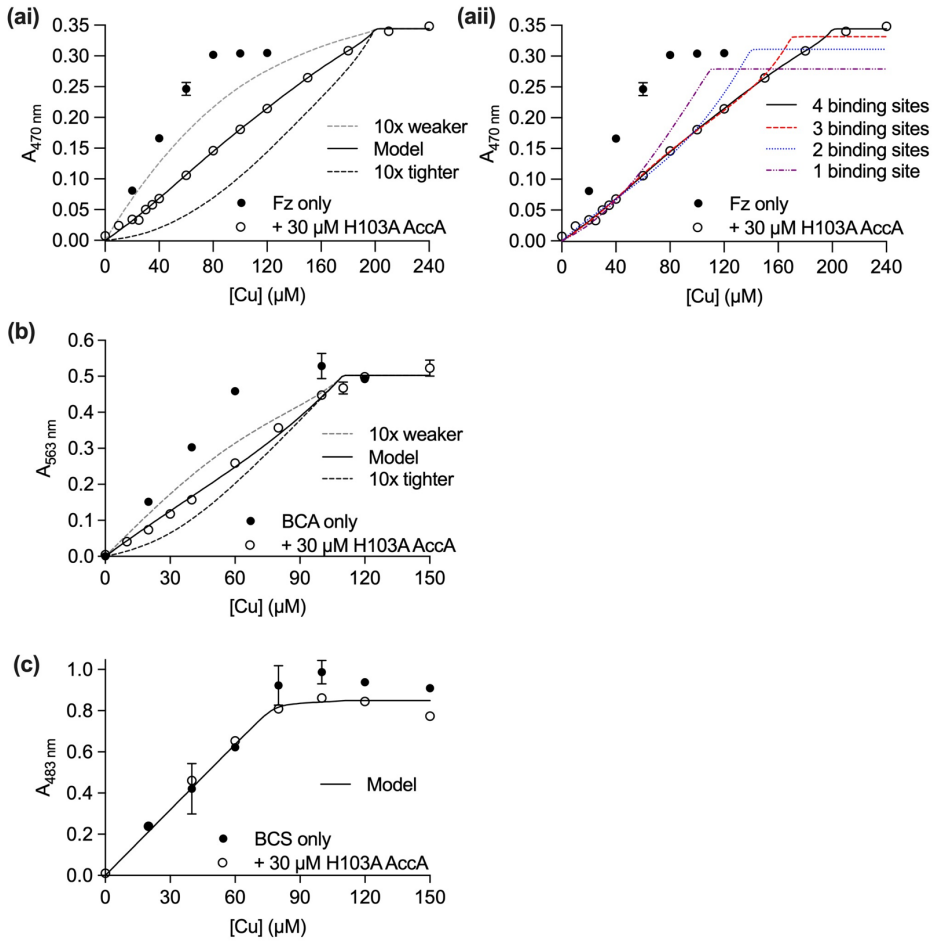

Figure 4.7: H103A AccA competes with BCA for Cu(I). H103A AccA competition against the Cu(I) specific colourimetric probe **(a)** ferrozine (Fz), **(b)** bicinchoninic acid (BCA), and **(c)** bathocuproine disulfonate (BCS). Titration of Cu in probe solution. Absorbance at **(ai)** 470 nm, **(b)** 562 nm, and **(c)** 483 nm were plotted against Cu(I) concentration in the presence of probe (black circles) or in the presence of probe and AccA (open circles). The model fit to the data (black line) and 10-fold weaker and stronger models (dashed lines) are shown. **(aii)** Data from **ai** with models for 1 (purple dotted and dashed line), 2 (blue dotted line), 3 (red dashed line), and 4 (black line) Cu binding sites in the protein**.** Data points represent the mean of n = 2. Error bars represent standard deviation.

4.3.5 A M105A primary site mutant binds Cu(I) with picomolar affinity

The final single Cu primary site mutant tested was the M105A AccA protein. The M105A AccA protein competed with Fz for Cu (Figure 4.8ai). Data analysis with the software DynaFit detected four Cu(I) binding residues when the curve was modelled (Figure 4.8aii). Three of the four binding sites had affinities in the nanomolar range K_D of 1.5 x 10^{-12} M, 1.3 x 10^{-11} M, and 4.0 x 10^{-10} M or a logK_D of -11.8 M (± 0.01), -10.9 M (± 0.02), and -9.4 M (± 0.5). The remaining weak binding site had an affinity in the picomolar range K_D = 1.5 x 10^{-12} M or a logK_D of -11.8 M (± 0.01). These Cu(II) binding affinities align with those in the sites previously calculated for the WT and ΔCu primary AccA proteins. Additionally, there was one binding site in the picomolar range K_D 4.6 x 10^{-14} M or a logK_D of -13.3 M, although error could not be calculated for this binding site.

Like the previous single Cu primary mutants, the M105A AccA protein competed with BCA for Cu. Data modelling with the software DynaFit identified one Cu(I) binding site, suggesting that three weaker binding sites detected by competition with Fz are outcompeted by BCA (Figure 4.8b). The Cu(I) binding site was calculated to have a picomolar affinity with a K_D of 3.1 x 10^{-14} M or a logK_D of -13.5 M (± 0.1). The M105A AccA protein did not compete with BCS for Cu(I) (Figure 4.8c). As BCA was the strongest probe that the M105A AccA protein competed with, the affinity of -13.5 was used for the Cu primary binding site.

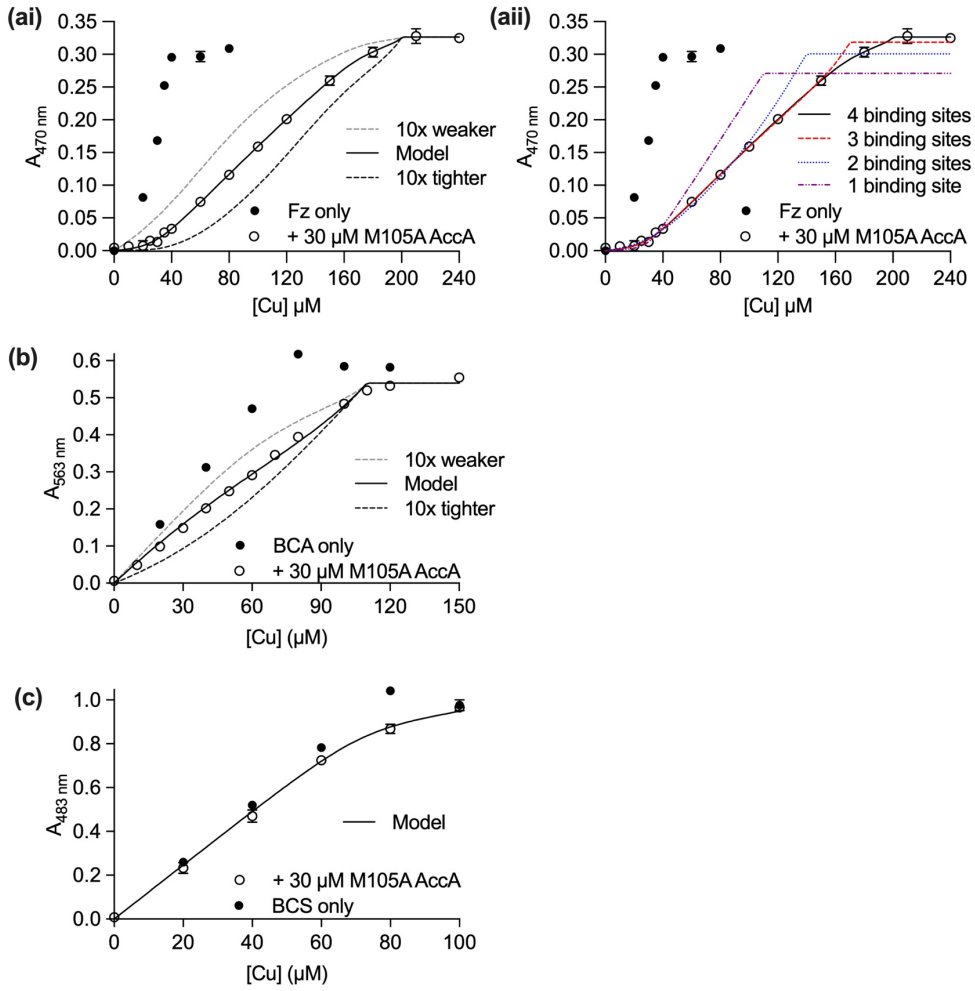

Figure 4.8: M105A AccA competes with BCA for Cu(I). M105A AccA competition against the Cu(I) specific colourimetric probe **(a)** ferrozine (Fz), **(b)** bicinchoninic acid (BCA), and **(c)** bathocuproine disulfonate (BCS). Titration of Cu in probe solution. Absorbance at **(ai)** 470 nm, **(b)** 562 nm, and **(c)** 483 nm were plotted against Cu(I) concentration in the presence of probe (black circles) or in the presence of probe and AccA (open circles). The model fit to the data (black line) and 10-fold weaker and stronger models (dashed lines) are shown. **(aii)** Data from **ai** with models for 1 (purple dotted and dashed line), 2 (blue dotted line), 3 (red dashed line), and 4 (black line) Cu binding sites in the protein**.** Data points represent the mean of n = 2. Error bars represent standard deviation.

4.4 The predicted Cu tract has a role in stabilising Cu(I) bound to the primary site

The predicted Cu tract is comprised of His and Met residues surrounding the Cu primary site. We hypothesise that the Cu tract may be involved in Cu binding or transfer to AniA. We are therefore, interested in whether a mutant AccA protein lacking these residues (M36, H71, M78, M107) has a reduced affinity for Cu(I) in the weaker binding sites and not the Cu primary site.

Like the WT AccA protein, the ΔCu tract AccA protein outcompeted Fz for Cu until it was saturated. This suggests that the Cu primary site is intact (Figure 4.9ai). Interestingly, when the data was

modelled by DynaFit, only two Cu(I) binding sites were found (Figure 4.9ai). This is in contrast with the WT AccA protein which had three Cu(I) binding sites (Figure 4.3ai). These data suggest that the Cu tract may be coordinating Cu in these weaker Cu(I) binding sites when the protein is titrated against Fz. The single weak Cu binding site in the ΔCu tract AccA mutant protein had a high nanomolar affinity of K_D 4.5 x 10^{-12} M or a logK_D of -11.3 M (± -0.4). This weak binding site is comparable the weakest binding site identified in the WT AccA protein, which had an affinity of -10.9 M (± 0.3)

When Cu was titrated into a mixture of BCA and the ΔCu tract AccA protein, the gradient of the curve showed that there was little competition between BCA and the ΔCu tract AccA protein for Cu as there was only a small increase in absorbance (Figure 4.9b). Therefore, much of the Cu bound the ΔCu tract AccA protein until it was saturated. Thus the ΔCu tract AccA protein almost outcompeted BCA for Cu. This suggests that the ΔCu tract AccA protein has an intermediate affinity between the WT AccA protein that outcompetes BCA and the single ΔCu primary mutant proteins that compete with BCA.

To further determine the affinity of Cu(I) binding in the ΔCu tract AccA protein, a competition assay for Cu(I) against BCS was performed. There was almost no competition between BCS and the ΔCu tract AccA at very low concentrations of Cu, indicated by little change in absorbance compared to the BCS only control. However, as the Cu concentration increased, the ΔCu tract AccA competed with BCS (Figure 4.9c).

The software DynaFit was used to model both BCA and BCS competition curves and resulted in a calculated K_D for Cu(I) of 7.0 x 10^{-16} M and 8.6 x 10^{-15} M, or a logK_D of -15.2 M (±0.8) and -14.1 M (±0.9) respectively. This suggests that the affinity of the ΔCu tract AccA protein for Cu(I) lies between what can be detected from BCA and BCS. We, therefore, averaged the two calculated Cu(I) affinities to give a final K_D of ΔCu tract AccA for Cu(I) at 4.6 x 10^{-15} or a logK_D of -14.3 (±0.7). Future experiments that maintaining a constant Cu concentration but varying the concentration of ΔCu tract AccA could more accurately predict the Cu(I) binding affinity of this mutant.

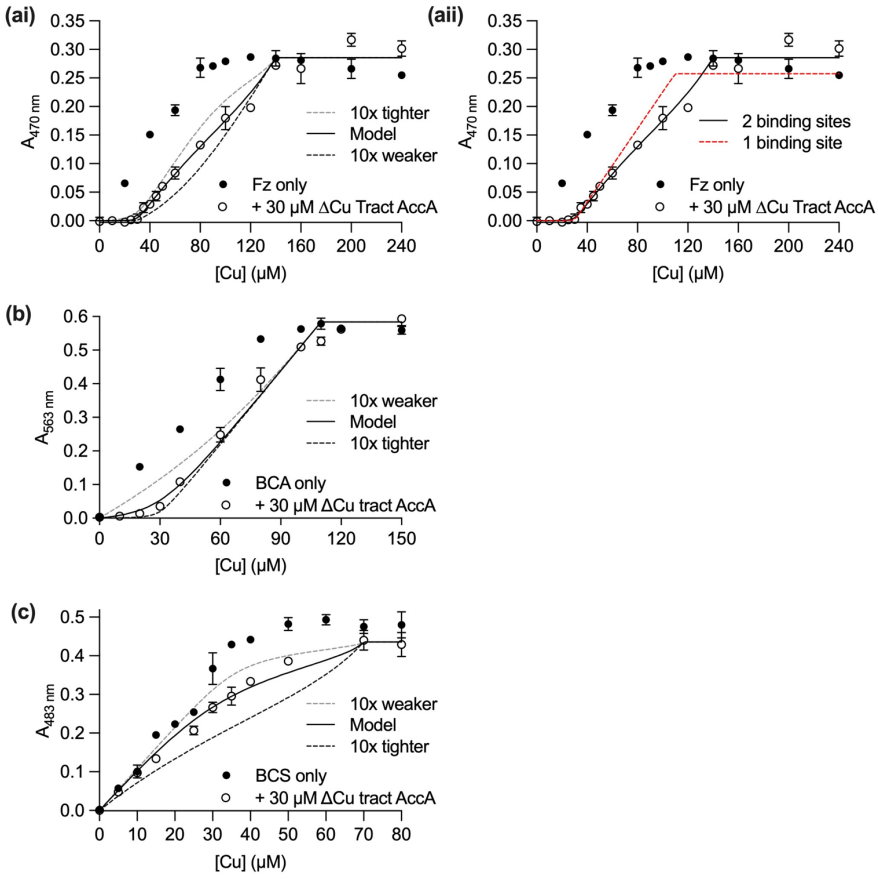

Figure 4.9: ΔCu tract AccA competes with BCA and BCS for Cu(I). ΔCu tract AccA competition against the Cu(I) specific colourimetric probe **(a)** ferrozine (Fz), **(b)** bicinchoninic acid (BCA), and bathocuproine disulfonate (BCS). Titration of Cu in probe solution. Absorbance at **(ai)** 470 nm, **(b)** 562 nm, and **(c)** 483 nm were plotted against Cu(I) concentration in the presence of probe (black circles) or in the presence of probe and AccA (open circles). The model fit to the data (black line) and 10-fold weaker and stronger models (dashed lines) are shown. **(aii)** Data from **ai** with models for 1 (red dashed line), and 2 (black line) Cu binding sites in the protein**.** Data points represent the mean of n = 2. Error bars represent standard deviation.

4.5 The C-terminal tail of AccA is not involved in high-affinity Cu(I) binding

The main Cu(I) binding site in AccA has been identified in the Cu primary site which makes up the $HX_nMX_{21/22}HXM$ binding motif. However, the C-terminal tail of AccA contains six His and two Met residues that are hypothesised to bind Cu(II). We are therefore interested in whether the C-terminal tail also binds Cu(I). To investigate this, a mutant AccA protein lacking the terminal 16 amino acids was constructed; this mutant is henceforth referred to as ΔC-terminal AccA.

The ΔC-terminal AccA protein outcompetes Fz for Cu(I) (Figure 4.10ai). When DynaFit was used to model the data, two Cu(I) binding sites were detected in contrast to the three Cu(I) binding sites calculated in equivalent studies on the WT AccA protein (Figure 4.10aii). The tight Cu(I) site was most

likely the Cu primary site. Loss of one of the weaker Cu(I) binding sites suggests that the C-terminal tail can bind Cu(I) though at a weaker affinity than the Cu primary site. The weak binding site, most likely within the Cu tract, had a picomolar affinity for Cu(I) of K_D 9.1 x 10^{-13} M or logK_D of -12.1 M (± 0.7) which corresponds to the weak WT AccA affinity of -12 M (± 0.2).

The ΔC-terminal tail AccA protein outcompetes BCA, however, the weaker binding sites do not compete with BCA (Figure 4.10b). As the ΔC-terminal tail AccA protein outcompetes both Fz and BCA for Cu(I) in the tight binding site, a competition assay with BCS was performed. Like the WT AccA protein, the ΔC-terminal tail competed with BCS and only one Cu binding site was detected when the data was modelled with DynaFit (Figure 4.10c). The Cu(I) binding site was calculated to have a femtomolar affinity with a K_D of 2.2 x 10^{-17} or a logK_D of -16.7 (± 0.2). This calculated K_D corresponds with the tight primary Cu(I) binding site calculated using the WT protein.

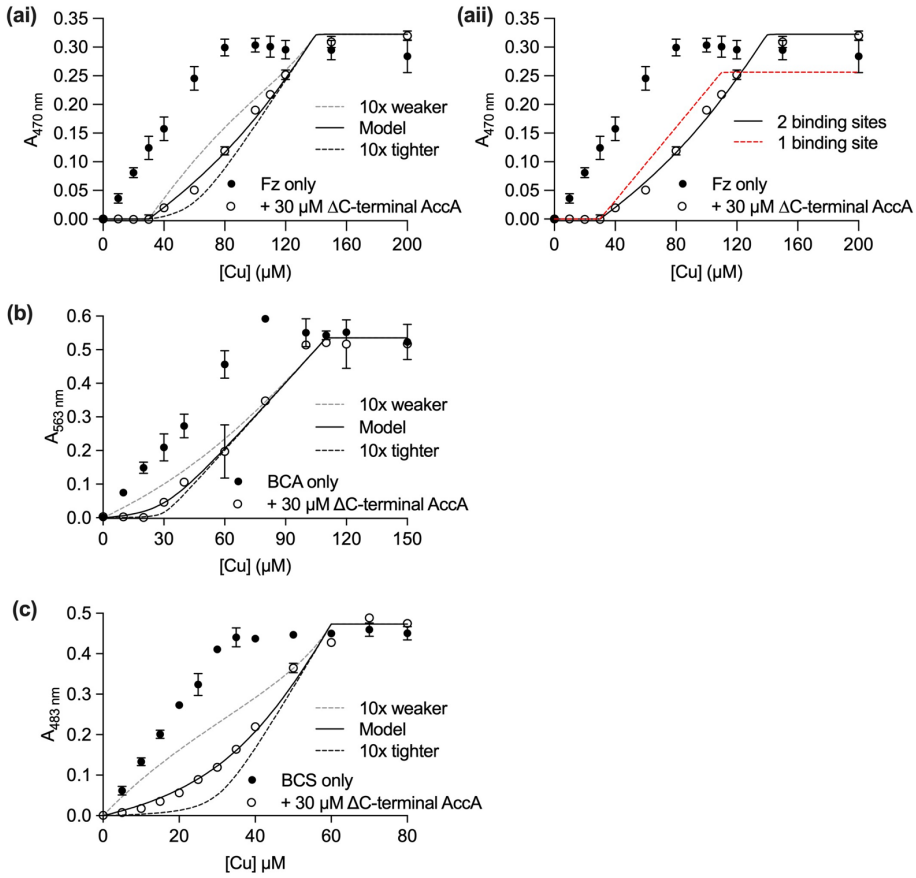

Figure 4.10: The C-terminal tail is not required to bind Cu(I) with tight affinity. ΔC-terminal AccA competition against the Cu(I) specific colourimetric probe **(a)** ferrozine (Fz), **(b)** bicinchoninic acid (BCA), and **(c)** bathocuproine disulfonate (BCS). Titration of Cu in probe solution. Absorbance at **(ai)** 470 nm, **(b)** 562 nm, and **(c)** 483 nm were plotted against Cu(I) concentration in the presence of probe (black circles) or in the presence of probe and AccA (open circles). The model fit to the data (black line) and 10-fold weaker and stronger models (dashed lines) are shown. **(aii)** Data from **ai** with models for 1 (red dashed line), and 2 (black line) Cu binding sites in the protein**.** Data points represent the mean of n = 2. Error bars represent standard deviation.

4.6 WT AccA binds Cu(II) at two binding sites with picomolar and nanomolar affinity

Previous work by Jen *et al*. (2015) and stoichiometry data in this thesis (Table 4.3) identified that AccA stably binds Cu(II) in addition to Cu(I).[120] We hypothesise tight Cu(II) binding to be located in the C-terminal tail of AccA. We are therefore interested in determining the Cu(II) binding affinity of AccA and AccA mutant proteins.

Fluorescent peptide probes with known affinities for Cu(II) were used to determine the Cu(II) binding affinity of AccA. The fluorescent probe DP-2 (dansyl peptide 2) was the weakest Cu(II) binding probe used in these experiments with a reported K_D value of 7.9 x 10^{-11} M.[130,131] *Apo*-DP-2 has a distinct

peak of fluorescence at 550 nm when excited at 350 nm, which is quenched when increasing concentrations of Cu(II) are added (Figure 4.11ai). Plotting the peak in fluorescence at 550 nm resulted in a linear decrease in fluorescence until 4 μM of Cu(II) was titrated into DP-2 and the curve plateaued (Figure 4.11aiii). As 4 μM of DP-2 was used in these experiments and DP-2 binds Cu(II) in a 1:1 stoichiometry, this corresponds to saturated DP-2. When WT AccA protein was introduced to the reaction mix, the initial fluorescence was slightly quenched compared to the DP-2 spectrum alone (data not shown). Therefore, the quenching of fluorescence at 550 nm was normalised by calculating *apo*-DP-2/total DP-2 to allow for comparisons to be drawn.

WT AccA outcompeted DP-2 for Cu(II) until the protein is saturated at 4 μM Cu(II) (Figure 4.11aii). Following AccA saturation, the gradient was shallower than the DP-2 only control and the probe was not saturated until 12 μM of Cu(II) was added to the reaction mix. These data suggest there was a weaker Cu(II) binding site in AccA (Figure 4.11aii). Modelling the data with the software DynaFit identified two Cu(II) binding sites within AccA. The affinity of the tight binding site could not be determined as AccA outcompeted DP-2. The weaker binding site had an affinity in the nanomolar range with an affinity K_D of 7.2 x 10^{-11} M or a logK_D of -10.1 M (± 0.2). These data further confirm the stoichiometry data in Table 4.3, where AccA was discovered to have a stoichiometry of two Cu(II) atoms when incubated with Cu(II).

$$DP\text{-}2 + Cu^{II} \rightleftharpoons Cu^{II}DP\text{-}2 \qquad \text{(eq. 25)}$$

$$AccA + Cu^{II} \rightleftharpoons Cu^{II}AccA \qquad \text{(eq. 26)}$$

$$Cu^{II}AccA + Cu^{II} \rightleftharpoons (Cu^{II})_2AccA \qquad \text{(eq. 27)}$$

Because AccA outcompeted DP-2 for Cu(II), we could not use this probe to determine the affinity of the tight Cu(II) binding site of AccA. We therefore, used a fluorescent probe with a tighter affinity for Cu(II), DP-3 (dansyl peptide 2). DP-3 has a reported K_D of 5.0 x 10^{-13}M.[130] Like DP-2, *apo*-DP-3 has a peak of fluorescence at 550 nm when excited at 350 nm. This fluorescence is quenched when increasing concentrations of Cu(II) are added (Figure 4.11bi). Similarly, when AccA was introduced to the reaction mix, the initial fluorescence was slightly quenched compared to the DP-3 spectrum alone

(data not shown). Therefore, the quenching of fluorescence at 550 nm was normalised by calculating *apo*-DP-3/total DP-3 to allow for comparisons to be drawn.

WT AccA competed with DP-3 for Cu(II) (Figure 4.11bii). Fluorescence at 550 nm was quenched when increasing concentrations of Cu(II) were titrated into a mixture of 4 μM DP-2 and 4 μM AccA. After 4 μM of Cu was added to the titration mix there was a shift in the gradient resulting in a shallower gradient until fluorescence was quenched when 12 μM Cu(II) was added to the experiment. Modelling of the data using DynaFit identified two Cu(II) binding sites (Figure 4.11biii). The tight Cu(II) binding site was calculated to have a K_D of 1.02 x 10^{-12} M or a logK_D of -12.0 (± 0.2). Furthermore, the weak Cu(II) binding site was calculated to have a K_D of 2.9 x 10^{-12} M or a logK_D of -11.5 M (± 0.2). The predicted logK_D of this weaker Cu(II) binding site was previously calculated at -10.1 M when these experiments were performed with the weaker probe DP-2. While these values do vary, they both show this weaker site to be in the nanomolar range.

$$DP\text{-}3 + Cu^{II} \rightleftharpoons Cu^{II}DP\text{-}3 \qquad \text{(eq. 28)}$$

$$AccA + Cu^{II} \rightleftharpoons Cu^{II}AccA \qquad \text{(eq. 29)}$$

$$Cu^{II}AccA + Cu^{II} \rightleftharpoons (Cu^{II})AccA \qquad \text{(eq. 30)}$$

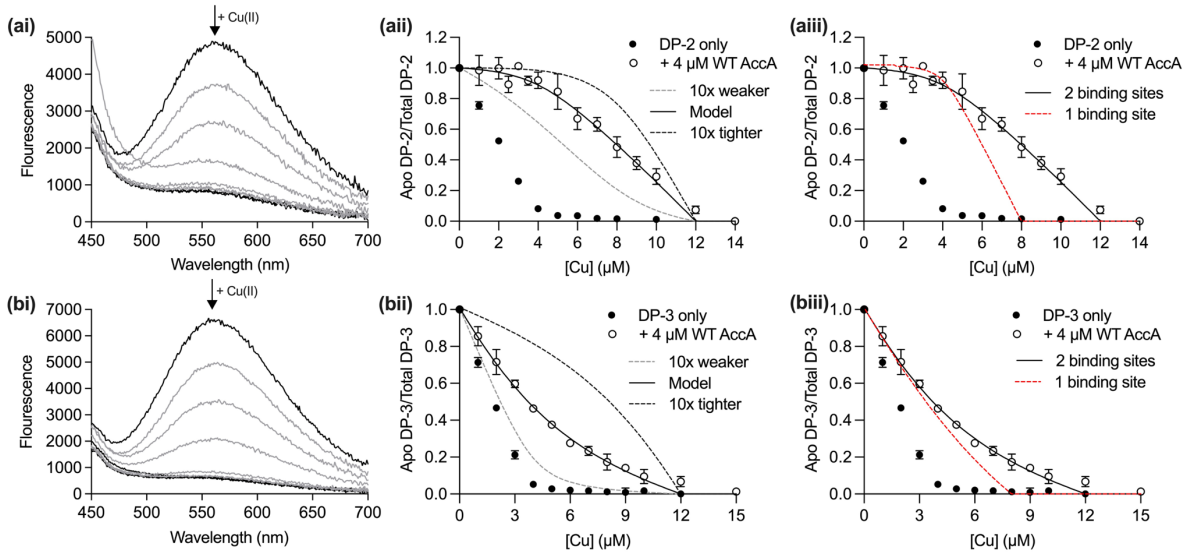

Figure 4.11: WT AccA competes with DP-3 only for Cu(II). WT AccA competition against the Cu(II) specific fluorescent probe **(a)** DP-2 and **(b)** DP-3. **(xi)** Quenching of fluorescence spectra of **(ai)** DP-2, and **(bi)** DP-3 solution upon excitation at 350 nm from 450 – 700 nm with increasing concentrations of Cu(II) added to the reaction mix. A black line represents *apo*-probe and *holo*-probe. **(xii)** Titration of Cu(II) in **(ai)** DP-2 and **(bi)** DP-3 solution. Fluorescence was measured at 550 nm upon excitation at 350 nm in the presence of 4 μM probe only (black circles) or in the presence of 4 μM probe and 4 μM AccA (open circles). Fluorescence was normalised relative to *apo*-probe. The model fit to the data (black line) and 10-fold weaker and stronger models (dashed lines) are shown. **(xiii)** Data from **xii** with models for 1 (red dashed line), and 2 (black line) Cu binding sites in the protein. Data points represent the mean of n = 2. Error bars represent standard deviation.

4.7 ΔCu primary AccA binds Cu(II) with picomolar affinity

Analysis of Cu(II) binding affinity identified two binding sites with nanomolar affinity in WT AccA protein. We hypothesise that one of these sites is located within the C-terminal tail of the protein and the remaining site resides in the Cu primary site or within the Cu tract. To confirm these hypotheses, Cu(II) binding affinity was determined for the ΔCu primary AccA mutant.

Similar to the WT AccA protein, the ΔCu primary AccA protein outcompeted DP-2 for Cu(II) until it was saturated at 4 μM Cu(II) (Figure 4.12ai). This suggests that the tighter Cu(II) binding site identified in the WT protein remains intact in the ΔCu primary AccA mutant. When the data was modelled using DynaFit, two Cu(II) binding sites were identified (Figure 4.12aii). As the tight Cu(II) binding site outcompeted DP-2, this could not be used to measure Cu(II) binding affinity. The weaker Cu(II) binding site had a calculated affinity K_D of 6.9 x 10^{-11} M or a logK_D of -10.2 M (± 0.2).

To accurately measure the affinity of the tight Cu(II) binding site, the ΔCu primary AccA protein was titrated against DP-3. The ΔCu primary AccA protein competed with DP-3 for Cu (Figure 4.12b). When this data was modelled using the software DynaFit, only one Cu(II) binding site was identified. This contrasts with the data generated *via* competition of Cu(II) with DP-2 that identified two Cu(II) binding sites. This suggests that the weak Cu(II) binding sites identified via DP-2 may be non-specific Cu binding to AccA or this site is outcompeted by DP-3. However, as the calculated affinity for the weak Cu(II) binding site by DP-2 competition was -10.2 M in the ΔCu primary mutant and -10.1 in the WT protein, which competed with DP-3 in a weak site, DP-3 outcompeting the ΔCu primary mutant at the weak site seems unlikely. This, therefore, suggests that the Cu primary site of AccA is involved in coordinating Cu in the weak Cu(II) binding site. Nevertheless, the tight Cu(II) binding site remained present in the ΔCu primary mutant with a calculated affinity for Cu(II) in the picomolar range at a K_D of 2.09 x 10^{-12} M or a logK_D of -11.7 M (± 0.1).

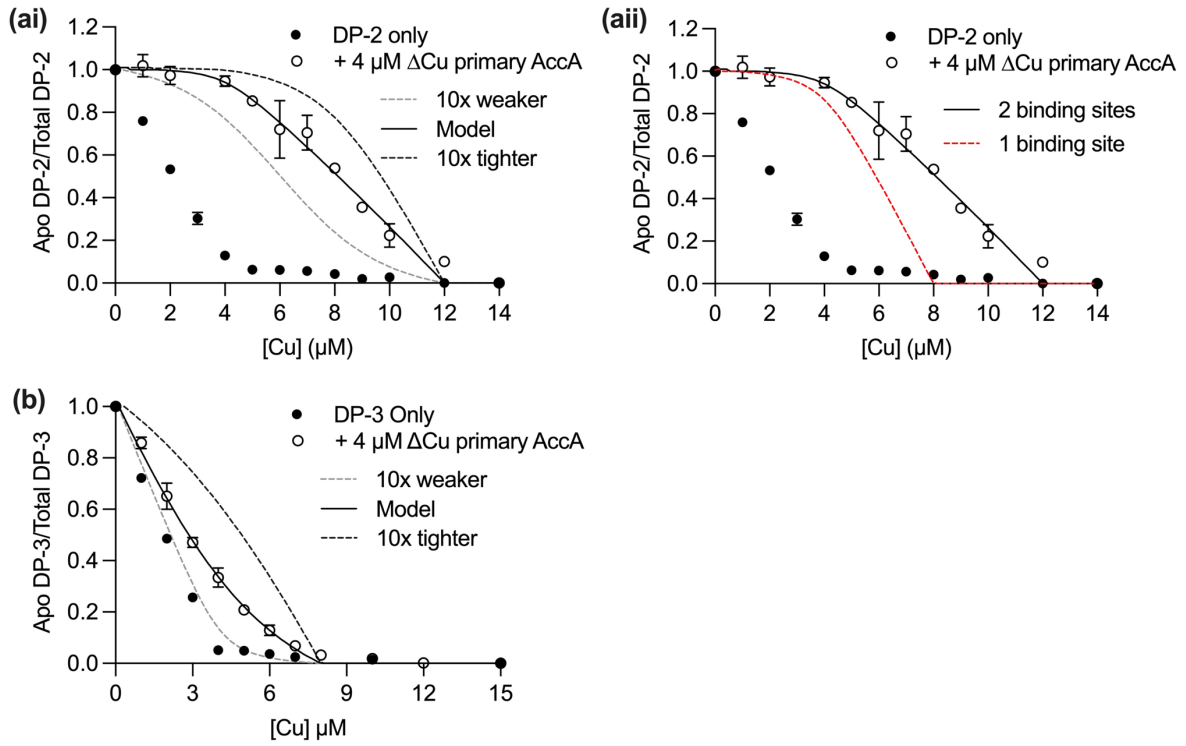

Figure 4.12: ΔCu primary AccA competes with DP-3 only for Cu(II). ΔCu primary AccA competition against the Cu(II) specific fluorescent probes **(a)** DP-2 and **(b)** DP-3. Titration of Cu(II) in **(ai)** DP-2 and **(b)** DP-3 solution. Fluorescence was measured at 550 nm upon excitation at 350 nm in the presence of 4 μM probe only (black circles) or in the presence of 4 μM probe and 4 μM ΔCu primary AccA (open circles). Fluorescence was normalised relative to *apo*-probe. The model fit to the data (black line) and 10-fold weaker and stronger models (dashed lines) are shown. **(aii)** Data from **ai** with models for 1 (red dashed line), and 2 (black line) Cu binding sites in the protein. Data points represent the mean of n = 2. Error bars represent standard deviation.

4.8 ΔCu tract AccA binds Cu(II) with picomolar affinity

To confirm whether the predicted Cu tract has a role in binding, Cu(II) was titrated into a mixture of 4 μM DP-2 and 4 μM ΔCu tract AccA protein. The ΔCu tract AccA protein outcompeted DP-2 for Cu(II) (Figure 4.13ai). However, once the ΔCu tract AccA protein was saturated by the addition of 4 μM of Cu(II) to the titration mix, fluorescence was quenched. The resulting curve had a shallower gradient than the DP-2 only control, suggesting a second Cu(II) binding site is present within the protein. This was confirmed when data was modelled using DynaFit, as two Cu(II) binding sites were identified (Figure 4.13aii). As the tight binding site outcompeted DP-2, we could not calculate the affinity of this site. The affinity of the weaker binding site was in the nanomolar range with a calculated K_D of 6.0 x 10^{-11} M or a logK_D of -10.2 M (± 0.2).

As the ΔCu tract AccA protein outcompeted DP-2 for Cu(II) in the tight Cu(II) binding site, the titration was repeated using DP-3. The ΔCu tract AccA protein competed with DP-3 for Cu(II) (Figure 4.13b). Like the ΔCu primary AccA protein, data modelling using DynaFit identified one Cu(II) binding site (Figure 4.13b). As the WT AccA protein had two Cu(II) binding sites, this suggests that Cu(II) in the weak binding site may be coordinated by amino acid residues in both the Cu tract and Cu primary bindings sites. DynaFit calculated the affinity of the ΔCu tract AccA protein for Cu(II) to be in the picomolar range. The K_D was calculated as 9.8 x 10^{-13} M and the logK_D was calculated as -12.0 M (± 0.1).

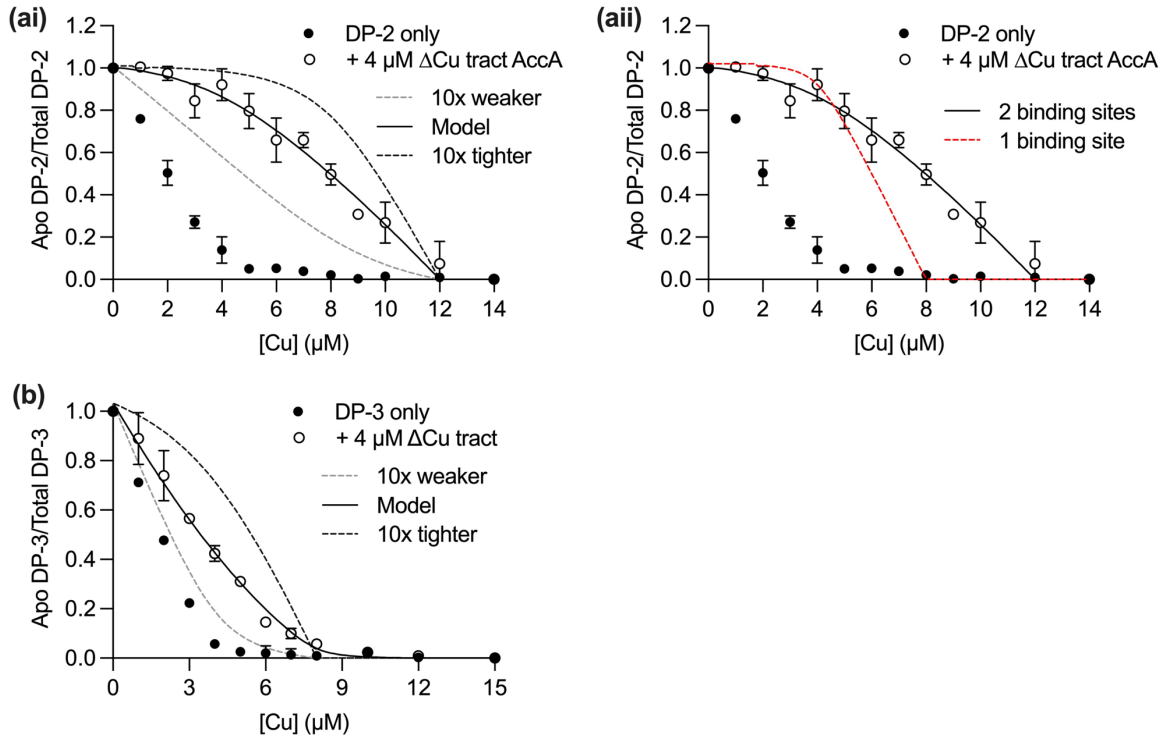

Figure 4.13: ΔCu tract AccA competes with only DP-3 for Cu(II). ΔCu tract AccA competition against the Cu(II) specific fluorescent probe **(a)** DP-2 and **(b)** DP-3. Titration of Cu(II) in **(ai)** DP-2 and **(b)** DP-3 solution. Fluorescence was measured at 550 nm upon excitation at 350 nm in the presence of 4 μM probe only (black circles) or in the presence of 4 μM probe and 4 μM ΔCu primary AccA (open circles). Fluorescence was normalised relative to *apo*-probe. The model fit to the data (black line) and 10-fold weaker and stronger models (dashed lines) are shown. **(aii)** Data from **ai** with models for 1 (red dashed line), and 2 (black line) Cu binding sites in the protein. Data points represent the mean of n = 2. Error bars represent standard deviation.

4.9 Investigating the role of the C-terminal tail of AccA in Cu(II) binding

4.9.1 A ΔC-terminal AccA protein loses tight binding of Cu(II)

Cu(II) affinity experiments on WT AccA protein identified two Cu(II) binding sites. Analysis of Cu(II) binding of the ΔCu primary and ΔCu tract AccA proteins identified that these mutants lose the weak Cu(II) binding sites but retain the tight Cu(II) binding site. We hypothesise that this tight binding site is located within the C-terminal tail of AccA.

To further probe the role of the C-terminal tail of AccA, the affinity for Cu(II) was measured. The ΔC-terminal tail AccA protein competed with DP-2 (Figure 4.14a). Unlike the WT, ΔCu primary, and ΔCu tract proteins which outcompeted DP-2 for Cu(II) until the protein was saturated, the ΔC-terminal mutant competed with DP-2. This suggests that the tight Cu(II) binding site was lost in this mutant.

Analysis using the software DynaFit identified one Cu(II) binding site with a calculated affinity in the nanomolar range at 4.8 x 10^{-10} M or a logK_D of -9.3 M (± 0.2). The weak Cu(II) binding site in the WT protein was calculated to have an affinity of -10.1 (± 0.2), therefore, the binding site present within the ΔC-terminal AccA protein corresponds to the weak binding site. The ΔC-terminal tail AccA protein was competed with DP-3 for Cu(II), but the protein did not compete with DP-3 (Figure 4.14b). This confirmed that the tight binding site was lost in the ΔC-terminal AccA mutant.

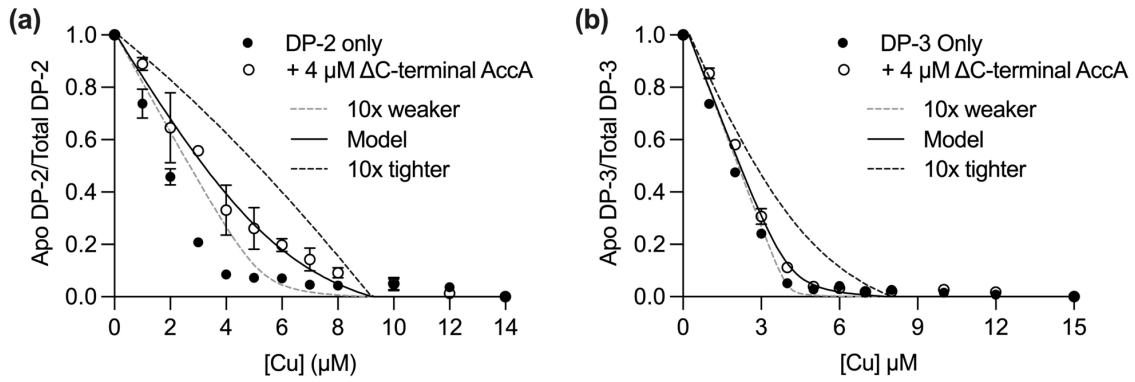

Figure 4.14: ΔC-terminal AccA competes with DP-2 for Cu(II). ΔC-terminal AccA competition against the Cu(II) specific fluorescent probe **(a)** DP-2 and **(b)** DP-3. Titration of Cu(II) in **(ai)** DP-2 and **(b)** DP-3 solution. Fluorescence was measured at 550 nm upon excitation at 350 nm in the presence of 4 μM probe only (black circles) or in the presence of 4 μM probe and 4 μM ΔCu primary AccA (open circles). Fluorescence was normalised relative to *apo*-probe. The model fit to the data (black line) and 10-fold weaker and stronger models (dashed lines) are shown. Data points represent the mean of n = 2. Error bars represent standard deviation.

4.9.2 A C-terminal peptide of AccA binds Cu(II) with high nanomolar affinity

We have identified that Cu(II) binds the C-terminal tail of AccA with picomolar affinity (Figure 4.14a,b). We hypothesise that an artificial C-terminal tail peptide (CTP) would bind Cu(II) with similar affinity to the tight Cu(II) binding site in the WT AccA protein.

The CTP competed against DP-3 (Figure 4.15). When the data was modelled with DynaFit one Cu(II) binding site was identified a high nanomolar affinity. The affinity was calculated to be K_D of 3.5 x10^{-12} M or a logK_D of -11.5 M (± 0.1). This is comparable to the Cu(II) binding affinities calculated at the tight Cu(II) binding site in the WT (-12.0 M), ΔCu primary (-11.7 M), and ΔCu tract AccA (-12.0 M) proteins.

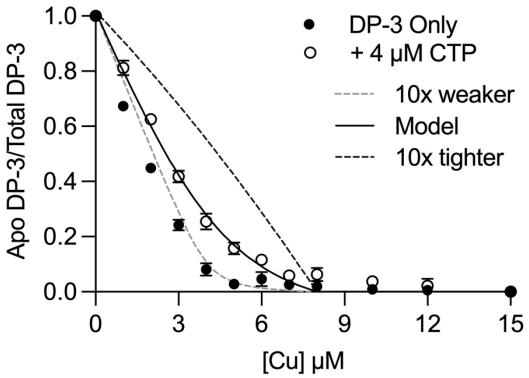

Figure 4.15: A C-terminal peptide of AccA competes with DP-3 for Cu(II). C-terminal peptide (CTP) competition against the Cu(II) specific fluorescent probe DP-3. Titration of Cu(II) in DP-3 solution. Fluorescence was measured at 550 nm upon excitation at 350 nm in the presence of 4 μM probe only (black circles) or in the presence of 4 μM probe and 4 μM ΔCu primary AccA (open circles). Fluorescence was normalised relative to *apo*-probe. The model fit to the data (black line) and 10-fold weaker and stronger models (dashed lines) are shown. Data points represent the mean of n = 2. Error bars represent standard deviation.

4.10 Discussion

Previous work by Jen *et* al. (2015) identified that a possible metallochaperone to the gonococcal nitrite reductase AniA, AccA, is a homologue of the periplasmic Cu chaperone PCu_AC.[120] PCu_AC binds Cu at a central binding site with a $HX_nMX_{21/22}HXM$ motif that is present in AccA.[89] Interestingly, unlike most PCu_AC family proteins, AccA has an extended C-terminal tail rich in Met and His residues. We were therefore interested in understanding the Cu stoichiometry and affinity of AccA to increase our understanding of how AccA binds Cu.

4.10.1 AccA binds Cu(I) with femtomolar affinity at the Cu primary site

A bar graph was used to directly compare calculated Cu(I) affinities in the tightest binding site for each protein (Figure 4.16). The WT AccA and ΔC-terminal AccA proteins both bound Cu(I) with femtomolar affinity, calculated logK_D of -16.7 M. The ΔCu primary AccA protein bound Cu(I) with picomolar affinity and had the weakest affinity for Cu(I), calculated logK_D of -11.8 M. The single ΔCu primary amino acid substitutions (H69A, M80A, H103A, M105A) had an intermediate affinity between the WT and ΔCu primary AccA proteins and bound Cu(I) with a picomolar affinity, calculated logK_D of -13.5 M to -13.9 M. The ΔCu tract AccA had a picomolar affinity, calculated logK_D -14.3 M.

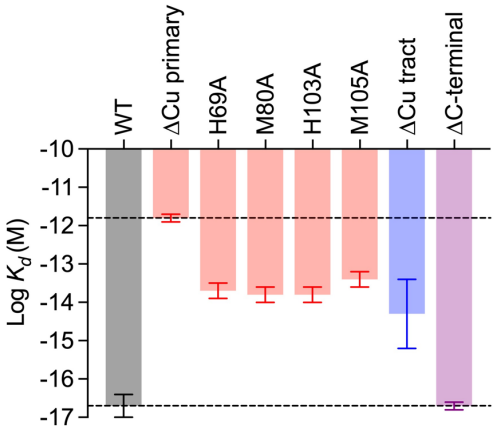

Figure 4.16: Visualisation of all affinities calculated for AccA and mutant proteins for Cu(I). The logK_D for Cu(I) of WT (black), ΔCu primary (red), ΔCu tract (blue), and ΔC-terminal tail (purple) AccA proteins. Dotted line at -16.7 M and -11.8 M represent maximum and minimum affinities calculated. Data represents a mean of n = 2. Error bars represent standard deviation.

An $HX_nMX_{21/22}HXM$ motif was identified in AccA based on bioinformatical searches and protein homology. These residues were identified as H69, M80, H103, and M105. In this chapter we identified that these amino acids are required for AccA to coordinate one Cu(I) atom with femtomolar affinity (K_D 2.0 x 10^{-17} M). Studies of Cu(I) binding affinities of PCu_AC homologues have reported affinities in the high picomolar range. The PCu_AC homologue in *Rhodobacter capsulatus*, PccA, has a reported affinity of 8.0 x 10^{-16} M, whereas the *Thermus thermophilus* PCu_AC protein binds Cu(I) with a reported affinity of 2.2 x 10^{-13} M.[89] It must be noted that metal binding affinity is dependent upon environmental conditions, particularly the pH and the buffer used.[132] All affinity experiments described in this thesis were performed in 50 mM MOPS pH 7.2 and therefore the Cu(I) binding affinity may only be directly compared under identical conditions.

Additionally, the affinity of a metallochaperone for its cognate metal is dependent on the intracellular buffered concentration of metal within the cell. The affinity of the metallochaperone must be higher than the affinity of the buffer to acquire metal. Some cells may buffer Cu to lower concentrations than others. As *N. gonorrhoeae* does not have a typical Cu homeostasis pathway, and no sensor to detect intracellular Cu concentrations, Cu may be buffered to lower concentrations in the gonococcus compared to bacteria which employ a more typical homeostatic pathway.[104,50] This may explain the tighter metal binding affinity. It is therefore hypothesised that mutants of AccA where the primary site has a reduced affinity for Cu may not acquire Cu from the periplasmic buffered pool.

4.10.2 The Cu primary site of AccA is stabilised by the predicted Cu tract

Analysis of Cu(I) affinity of a ΔCu tract AccA mutant, in which amino acid residues surrounding the Cu primary site of AccA (Met36, His71, Met78, Met107) were mutated, resulted in a decrease of affinity from femtomolar -16.7 M (± 0.3) to picomolar -14.3 M (± 0.7). These data suggest that amino acids in the Cu tract may act to stabilise the binding of Cu(I) in the primary site. As single mutants of the Cu tract were not generated for this study, it is unknown whether all or only some of the amino acid residues are involved in stabilising the Cu(I) binding site. Furthermore, the draft crystal structure does not show coordination of Cu to any of these amino acids. However, analysis of the crystal structure shows that His71 is 5.6 Å and Met107 is 6.5 Å away from the Cu(I) atom coordinated by the Cu primary site (Figure 4.17a,b). It would not, therefore, be surprising that these two residues could bind Cu through either direct or second sphere coordination to stabilise Cu(I) bonding at the primary site.[133] Future work may benefit from the generation of a crystal structure of the ΔCu tract mutant which may elucidate how residues in the Cu tract may stabilise Cu binding in the primary site.

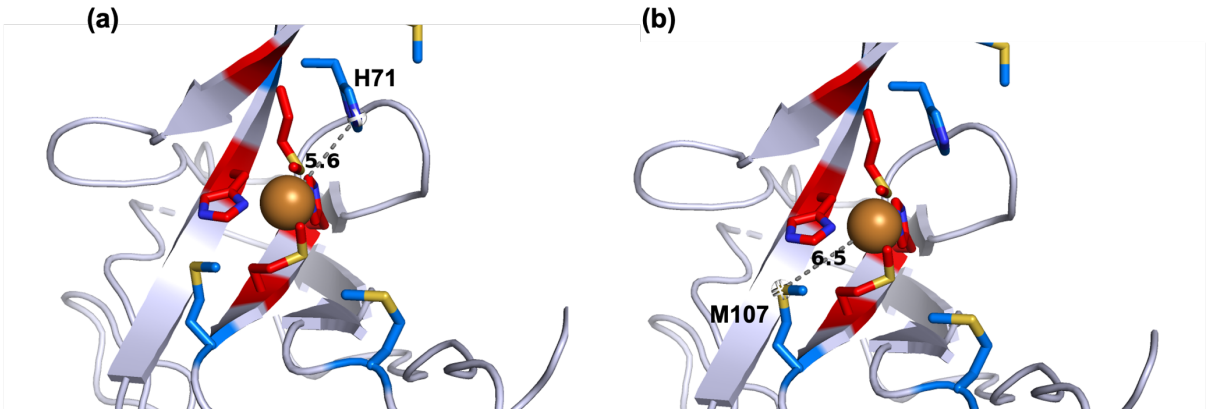

Figure 4.17: Close up of Cu primary site of AccA showing distance between Cu tract residues. **(a)** His71, and **(b)** Met107 to the Cu atom.

4.10.3 AccA contains weak binding sites that bind Cu(I) with picomolar and nanomolar affinity

Investigation of Cu(I) binding of WT AccA identified two weak binding sites which bound Cu with picomolar and nanomolar affinity respectively with calculated logK_D of -12 M (± 0.2) and -10.9 M (± 0.3). These weak binding sites are most likely made up of amino acid residues in both the Cu tract and in the C-terminal tail, as proteins lacking these sites lost the picomolar binding site (ΔCu tract) and the nanomolar (ΔC-terminal) binding site. These weak binding sites may be involved in a series of

transfer reactions of Cu from the periplasmic buffer to the Cu primary site of AccA, where Cu(I) is bound at higher affinity. This may render transfer from the buffer to AccA more thermodynamically favourable by offering a stepwise transfer from high energy (weak binding) to low energy (tight binding) Cu binding sites. Additionally, these weak sites themselves may be acting as a periplasmic buffer. Under O_2-limited conditions, expression of *accA* is upregulated by FNR.[128] In these conditions, Cu would be found as Cu(I) in the periplasm and the presence of stable Cu(I) binding sites in the picomolar and high nanomolar range could preferentially bind Cu over the periplasmic buffer. Nevertheless, *in vivo* research in *N. gonorrhoeae* of ΔCu tract and ΔC-terminal mutant proteins is required to further elucidate the role of these weaker Cu(I) binding sites in Cu-acquisition of AccA.

4.10.4 AccA binds Cu(II) with picomolar affinity at the C-terminal tail

A bar graph was used to visually compare calculated Cu(II) affinities in the tightest binding site for each protein (Figure 4.18). The WT AccA, ΔCu primary AccA, and ΔCu tract proteins all bound Cu(II) with high nanomolar to picomolar affinity, calculated logK_D -12 M, -11.5 M. The ΔC-terminal tail AccA protein bound Cu(II) with low nanomolar affinity and had the weakest affinity for Cu(II), calculated logK_D -9.3 M. The role of the C-terminal tail of AccA in binding Cu(II) was further investigated using a C-terminal peptide. The affinity of the CTP for Cu(II) was in the high nanomolar range, similar to the WT protein, confirming the C-terminal tail as the location of Cu(II) binding.

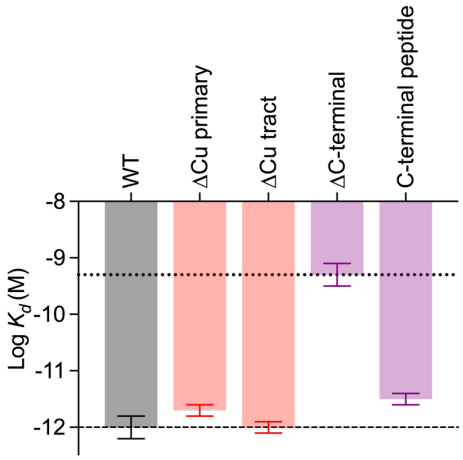

Figure 4.18: Visualisation of all affinities calculated for AccA and mutant proteins for Cu(II). The logK_D for Cu(II) of WT (black), ΔCu primary (red), ΔCu tract (blue), ΔC-terminal tail (purple), and CTP (purple) AccA proteins. Dotted lines at -12 M and -9.3 M represent maximum and minimum affinities calculated. Data represents a replicate of n = 2. Error bars represent standard deviation.

The role of the extended His and Met rich C-terminal tail of AccA in binding Cu was further investigated in this chapter using mutant protein lacking this tail, or a peptide of the tail. We identified that the C-terminal tail binds Cu(II) with picomolar affinity. This extended C-terminal tail is not unique to AccA and *N. gonorrhoeae*. PCu_AC homologues from *Bradyrhizobium diazoefficiens*, *Bradyrhizobium japonicum,* and *Methylosinus trichosporium* all have an extended unstructured His and Met rich C-terminal tail.[123,134] Furthermore, these C-terminal extensions bind Cu(II). Interestingly, the C-terminal tail of the PCu_AC protein in *B. japonicum* is required to form the Cu_A centre in the aa_3-cytochrome C oxidase. Direct Cu loading experiments to AniA from AccA would be necessary to determine whether the C-terminal tail of AccA is required to metalate AniA. However, as upregulation of both *aniA* and *accA* genes is dependent on O_2-limitation by FNR, it is unlikely that Cu located within the periplasm is in the oxidised Cu(II) form.[128] It is, therefore, unlikely that AccA would encounter Cu(II) within the cell without the aid of an oxidising agent or electron transfer. As discussed in 4.10.3 the C-terminal tail binds Cu(I) with high nanomolar affinity which may play a role in Cu buffering or transfer to the low-energy Cu primary site. Ultimately the role of the C-terminal extension of PCu_AC homologues is still unclear and further research is required to elucidate this.

Chapter 5: Characterising AniA activity *in vivo* by monitoring microaerobic growth and nitrite consumption in *N. gonorrhoeae*

While the Cu binding and affinity experiments using purified AccA as described in Chapter 4 have provided insights into which amino acid side chains in AccA contribute to binding Cu *in vitro*, it is still not known whether these amino acids are important in the function of AccA in activating AniA *in vivo*. Previous studies have indicated the importance of AniA in gonococcal growth during O_2 limitation in the presence of nitrite.[115,112,] As AccA is the metallochaperone predicted to provide periplasmic Cu to AniA, our hypothesis is that deletion of the *accA* gene would lead to defects in both microaerobic growth and nitrite consumption. We, therefore, created site-directed mutant strains of gonococci, in which key His and Met amino acid residues in AccA identified in Cu binding affinity experiments are mutated to Ala (Table 5.1).

Biochemical experiments using purified AccA protein identified two main Cu binding sites: a Cu primary site and a C-terminal tail site. Furthermore, a possible Cu tract surrounding the Cu primary site was identified to be important to maintain tight binding of the primary site. Thus, the mutants generated for *in vivo* studies were designed to further examine the importance of these binding sites in delivering Cu to AniA.

Table 5.1: List of gene mutations generated.

Mutation	Modification
Δ*aniA*	*aniA* gene deleted and replaced with a *kanR* cassette.
accA$^+$	As the WT strain, but *specR* cassette added between gene and terminator stem loop
Δ*accA*	Gene deleted. *specR* cassette added between gene and terminator stem loop
H69A	His69 mutated to Ala. *specR* cassette between gene and terminator stem loop
M80A	Met80 mutated to Ala. *specR* cassette added between gene and terminator stem loop
H103A	His103 mutated to Ala. *specR* cassette added between gene and terminator stem loop
M105A	Met105 mutated to Ala. *specR* cassette added between gene and terminator stem loop

H69A/M80A	His69, Met80 mutated to Ala. *specR* cassette added between gene and terminator stem loop
H103A/M105A	His103, Met105 mutated to Ala. *specR* cassette added between gene and terminator stem loop
ΔCu primary	His69, Met80, His103, Met105 mutated to Ala. *specR* cassette added between gene and terminator stem loop
ΔCu tract	Met36, His71, Met78, Met107 mutated to Ala. *specR* cassette added between gene and terminator stem loop
ΔC-terminal	Terminal 16 amino acids (His- and Met-rich region) deleted. *specR* cassette between gene and terminator stem loop

5.1 The role of AniA in microaerobic growth and NO_2^- consumption

As described in Chapter 1, *N. gonorrhoeae* employs a truncated denitrification pathway to respire in O_2-limiting environments.[112] The first step of this pathway relies on the reduction of NO_2^- to NO· by the Cu-dependent nitrite reductase AniA. To first verify the role of the *aniA* gene in *N. gonorrhoeae* 1291, a series of growth and NO_2^- consumption assay experiments were performed using the Δ*aniA* knockout mutant strain. This mutation did not result in a reduced growth phenotype compared to the WT strain in aerobic growth conditions (Figure 5.1). This result confirms that AniA is not required for growth and respiration when O_2 is abundant in the growth environment.

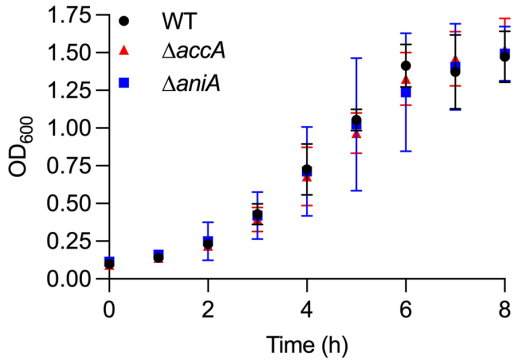

Figure 5.1: AniA and AccA are not required during aerobic growth of *N. gonorrhoeae*. Growth curves of WT (black closed circle), Δ*accA* (red triangle), and Δ*aniA* (blue square) strains of *N. gonorrhoeae* 1291 over 8 h in aerobic conditions (shaking 50 mL cultures). Nitrite (2 mM $NaNO_2$) was supplemented at t = 0, 5, and 7 h. Data points represent the mean of n = 3. Error bars represent standard deviation.

Next, to confirm that NO_2^- is required for microaerobic growth of *N. gonorrhoeae*, growth of the WT 1291 strain in static cultures was monitored in the presence or absence of supplemental NO_2^-. A steady increase in optical density, indicating bacterial growth, was observed over a period of 8 hours when cultures were grown in the presence of NO_2^- (Figure 5.2). In contrast, cultures lacking supplemental NO_2^- failed to grow (Figure 5.2), consistent with the established requirement for NO_2^- during microaerobic growth conditions.

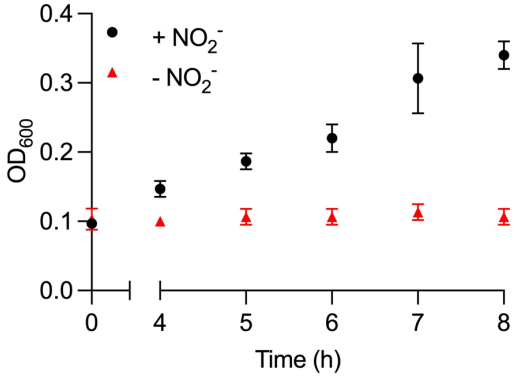

Figure 5.2: NO_2^- is required for microaerobic growth of *N. gonorrhoeae*. Growth curves of *N. gonorrhoeae* 1291 in the absence (red triangles) and presence (black circles) of nitrite (NO_2^-). Cultures were incubated for 8 h in microaerobic conditions (static 30 mL cultures). NO_2^- (2 mM $NaNO_2$) was supplemented at t = 0, 5, and 7 h (red square). Data points represent the mean of n = 3. Error bars represent standard deviation.

As anticipated following prior investigations of *aniA* knockout strains, the Δ*aniA* strain did not grow microaerobically in the presence of NO_2^- (Figure 5.3a). In addition, supplemental Cu in the media did not promote growth of this mutant (Figure 5.3a). These results are consistent with the established role of AniA as the sole nitrite reductase in *N. gonorrhoeae*.

It was noted that growth in the presence of 10 μM Cu led to a slight growth defect in microaerobic WT cultures (Figure 5.3a), likely due to the potential toxic effects of Cu alone or the combined toxicity of Cu and NO_2^- against this organism.[135]

To verify that NO_2^- was consumed during microaerobic growth, the concentrations of NO_2^- remaining in the spent media were measured (Figure 5.3b). In this experiment, cultures were supplemented with 2 mM NO_2^- at t = 0 and 5 h. The NO_2^- concentrations in the media decreased steadily in WT cultures during growth between 5 and 8 h, consistent with NO_2^- consumption (Figure 5.3b). In contrast, the concentrations of NO_2^- in the growth media did not change in Δ*aniA* strain cultures (Figure 5.3b), which did not grow, suggesting that bacterial growth promoted the consumption of NO_2^-. It was noted that a higher concentration of NO_2^- was present in the WT culture after 8 hours in those supplemented with 10 μM, compared to the 0 or 1 μM supplemented cultures (Figure 5.3b). This can be accounted for by the toxic effects of Cu, which led to reduced growth and subsequently a reduced capacity to consume NO_2^-.

A spontaneous, AniA-independent, reaction between Cu ions and reactive nitrogen species has previously been identified.[103] However, the results generated in this work indicate that Cu and NO_2^- do not spontaneously react in the media. The concentrations of NO_2^- remaining in the Δ*aniA* cultures did not decrease over time, even in the presence of supplemental Cu (Figure 5.3b). Furthermore, the Griess reaction is specific in detecting NO_2^- concentration and not other nitrogen oxides that may be present in the culture such as NO•.[136] Therefore, loss of NO_2^- from the culture media reliably represents AniA activity in *N. gonorrhoeae.*

The rate of NO_2^- consumption of the cells was measured to estimate the specific activity of AniA. Here, NO_2^- was added to a concentrated sample of cells and the concentration of NO_2^- was measured every minute for 7 minutes. The slope of the graph was used to calculate the rate of NO_2^- consumption. The rate was then normalised to the total protein content in the sample, to yield the

specific activity of AniA as nmol of NO_2^- consumed per min per mg of protein. These experiments confirmed that the WT cells consumed NO_2^- while the Δ*aniA* mutant strain did not (Figure 5.3c). In addition, growth in the presence of supplemental Cu did not influence NO_2^- consumption (and therefore, AniA activity) in either strain. Taken together, these results are all consistent with AniA being the only enzyme in *N. gonorrhoeae* that consumes NO_2^-.

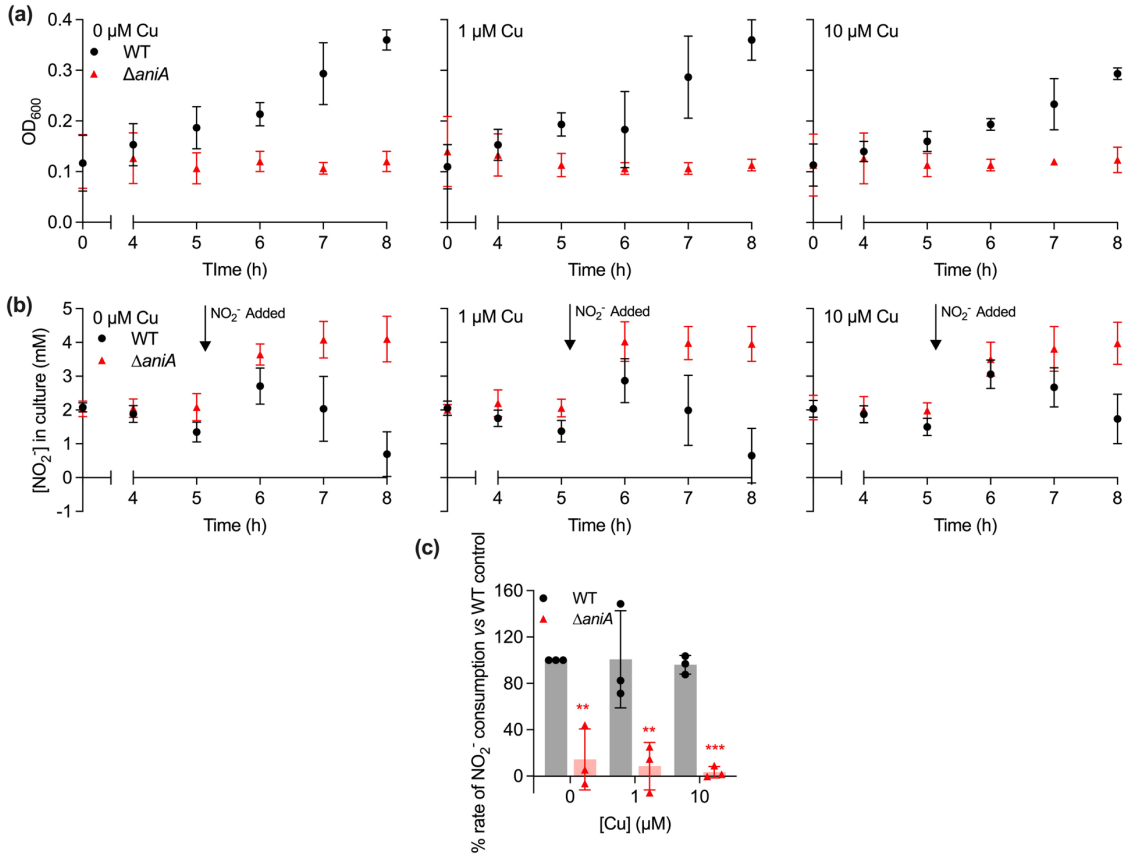

Figure 5.3: AniA is required for microaerobic growth and NO_2^- consumption. (a) Growth curves of WT (black circles) and Δ*aniA* (red triangles) strains of *N. gonorrhoeae* 1291. Cultures were incubated for 8 h in microaerobic conditions (static 30 mL cultures). NO_2^- (2 mM $NaNO_2$) was supplemented at t = 0 and 5 h. Cells were grown in the presence of 0, 1, and 10 μM $CuSO_4$. Data points represent the mean of n = 3. Error bars represent standard deviation. Two-way ANOVA analysis of all growth curves resulted in statistical significance at t = 8 h between WT and Δ*aniA* strains (P <0.0001). **(b)** NO_2^- concentrations remaining in the supernatant of the cultures after each time point. Nitrite supplementation at 5 h is depicted by arrow on graph. Data points represent the mean of n = 3. Error bars represent standard deviation. Two-way ANOVA analysis of all graphs resulted in statistical significance at t = 8 h between WT and Δ*aniA* strains (P <0.0001). **(c)** Percentage rate of nitrite consumption (nmol/min/mg of protein), standardised against the WT control (no Cu supplemented) of WT and Δ*aniA* strains of *N. gonorrhoeae* 1291 after 8 h of microaerobic growth. Individual data points are displayed. Error bars represent standard deviation. ** = 0.0025, 0.0014, *** = 0.0009. P-values were generated by two-way ANOVA multiple comparison against the mean of the 0 μM Cu WT control.

5.2 Investigating the role of AccA as a metallochaperone to AniA

5.2.1 Genetic strategy to construct the *accA* mutants

We have established in Chapter 4 that AccA binds Cu with femtomolar affinity. However, the role of AccA as a metallochaperone that delivered Cu to AniA has not been confirmed. We, therefore, generated a series of *accA* deletion and site-directed mutant strains of *N. gonorrhoeae* to investigate the role of AccA *in vivo.*

Traditional methods of generating site-directed mutants in *N. gonorrhoeae* use gene deletion and subsequent complementation of the WT, or mutated, gene *in trans* into a secondary site in the genome. This secondary site typically encodes a pseudogene such as *proB* or *difA*.[124] This approach fails to consider transcriptional control of a gene in the original loci. Both the *accA* and *aniA* genes in *N. gonorrhoeae* are under FNR transcriptional regulation in response to low cellular O_2.[128] This transcriptional regulation is lost when a gene is inserted into a pseudogene and therefore, its role in physiology may be altered compared to the WT protein. Therefore, the genetic strategy employed in this work introduced the mutations into the original *accA* loci of *N. gonorrhoeae.* This strategy ensured that transcriptional control of the *accA* gene was retained.

The genetic construct was created *via* Golden Gate Assembly consisting of the *accA* gene, 5' and 3' flanking regions, and a *specR* cassette encoding spectinomycin resistance (Figure 5.4a). The *specR* cassette does not have its own promoter, therefore, transcription of *specR* was controlled by the native transcriptional control of *accA.* Additionally, the *specR* cassette was positioned between the *accA* gene and the native terminator stop of *accA,* ensuring that the two genes were co-transcribed and co-translated into proteins. The 5'-upstream and 3'-downstream flanking regions of the *accA* gene ensured that the construct could be recombined into the native loci of the *N. gonorrhoeae* genome. Successful transformants were positively selected via spectinomycin resistance.

The *accA*→*specR* complement strain (*accA*$^+$) behaved as a WT *N. gonorrhoeae* strain. There was no difference in microaerobic growth (Figure 5.4b) or NO_2^- consumption (Figure 5.4c) in the *accA*$^+$ strain compared to the WT strain. As mutant strains of the *accA* gene contained the *specR* cassette, from

this point onwards, *accA*$^{+}$ was used as the control in experiments. Advantages of this included retention of the *specR* cassette, and its isogeneity to various *accA* mutant strains.

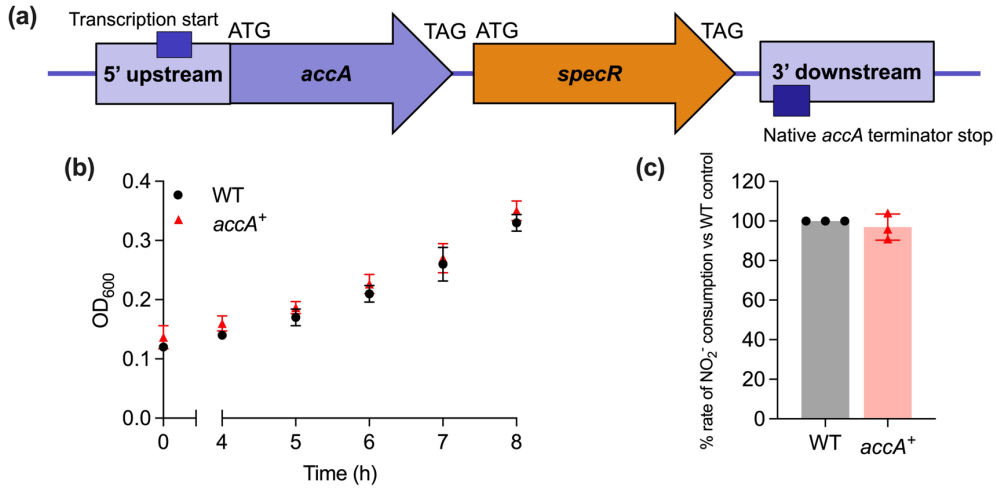

Figure 5.4: An *accA→specR* strain acts as WT *N. gonorrhoeae.* (a) A visualisation of the construct created via Golden Gate Assembly to insert the WT copy of the *accA* gene into *N. gonorrhoeae* 1291. A *spectinomycin* cassette immediately follows the *accA* gene. The upstream and downstream regions immediately flanking the *accA→specR* fusion allows for transcription, translation, and homologous recombination into the original locus in *N. gonorrhoeae.* **(b)** Growth curves of WT (black circles) and *accA→specR* (*accA*$^{+}$) complement (red triangles) strains of *N. gonorrhoeae.* Strains were incubated for 8 h in microaerobic conditions (static 30 mL cultures) with NO_2^- (2 mM $NaNO_2$) supplemented at t = 0, 5, and 7 h. Data points represent the mean of n = 3. Error bars represent standard deviation. **(c)** Percentage rate of NO_2^- consumption (nmol/min/mg of protein) compared to the WT control. The presence of the *specR* cassette immediately following the *accA* gene did not affect nitrite consumption by *N. gonorrhoeae* cells. Individual data points are displayed. Error bars represent standard deviation.

5.2.2 AccA is required for microaerobic growth and NO_2^- consumption of *N. gonorrhoeae*

As there was no defect in aerobic growth (Figure 5.1), the role of AccA to metalate and activate AniA *in vivo* was determined by monitoring growth and NO_2^- consumption in microaerobic conditions in a Δ*accA* knockout strain. We hypothesise that the AniA in this strain would remain in its *apo*-enzyme state due to the lack of metallochaperone.

As expected, the Δ*accA* strain did not grow in microaerobic conditions (Figure 5.5a). This phenotype is consistent with an inactive AniA. Interestingly, supplementation of Cu(II) salts restored growth to *accA*$^{+}$ levels, suggesting that AniA is once again active. These results suggest that in the Δ*accA* strain, AniA is produced as an *apo*-enzyme, consistent with the role of AccA in metalating AniA.

However, when the Cu supply to cells is increased, then AccA is not required to metalate AniA. Therefore, AccA is required to metalate AniA when Cu is not in excess or when it is limited.

Monitoring the rate of NO_2^- consumption (and thus specific AniA activity) by the Δ*accA* strain confirmed that the Δ*accA* strain did not consume NO_2^-. However, Cu supplementation during growth restored NO_2^- consumption to *accA*$^+$ levels (Figure 5.5b). These data confirm that AccA is required to metalate AniA.

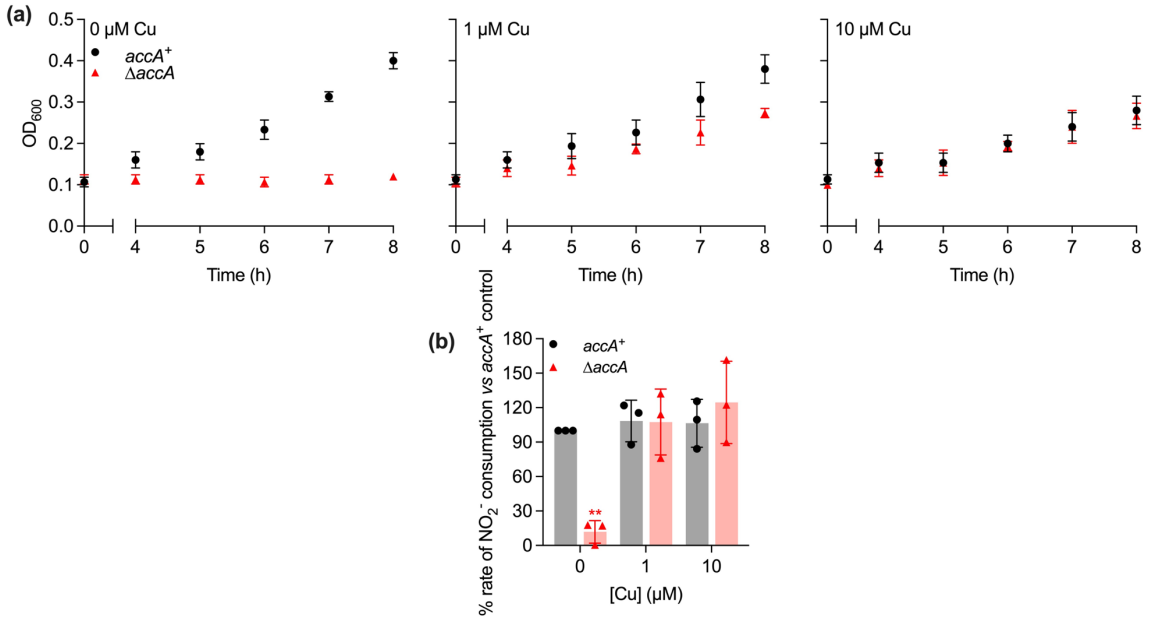

Figure 5.5: An Δ*accA* knockout acts like an Δ*aniA* knockout, but addition of Cu restores growth and NO_2^- consumption. (a) Growth curves of WT (black circles) and Δ*accA* (red triangles) strains of *N. gonorrhoeae* 1291. Cultures were incubated for 8 h in microaerobic conditions (static 30 mL cultures). Nitrite (2 mM $NaNO_2$) was supplemented at t = 0, 5, and 7 h. Cells were grown in the presence of 0, 1, and 10 µM $CuSO_4$. Data points represent the mean of n = 3. Error bars represent standard deviation. Two-way ANOVA analysis of growth curves resulted in statistical significance at t = 8 h between *accA*$^+$ and Δ*accA* strains in 0 and 1 µM Cu growth curves only (P = <0.0001, and 0.0002 respectively). **(b)** Percentage rate of nitrite consumption (nmol/min/mg of protein) standardised against the WT control (no Cu supplemented) of WT and Δ*accA* strains of *N. gonorrhoeae* 1291 after 8 h of microaerobic growth. Individual data points are displayed. Error bars represent standard deviation. ** = 0.002. P-value generated by two-way ANOVA multiple comparison against the mean of the 0 µM Cu WT control.

5.3 The role of the Cu primary site of AccA in metalating AniA *in vivo*

5.3.1 Cu primary site single mutants have a growth and NO_2^- defect

Previously in Chapter 4, single site-directed H69A, M80A, H103A, and M105A mutants of the Cu primary site in AccA displayed reduced (from femtomolar to picomolar affinities) affinities for Cu(I). In this chapter, we are therefore interested in whether this weakened affinity for Cu leads to a defect in microaerobic growth and NO_2^- consumption *in vivo.*

The H69A-*accA* mutant has a reduced growth phenotype compared to the control *accA*$^+$ strain (Figure 5.6a). After 8 hours of growth, the final OD_{600} in the *accA*$^+$ culture was 0.35, whereas the H69A-*accA* strain had a final OD_{600} was 0.17 (Figure 5.6a). Growth of the H69A-*accA* strain was higher than that of the Δ*accA* knockout mutant strain (Figure 5.6a). As shown previously for the Δ*accA* knockout mutant strain (Figure 5.5a), addition of Cu to the growth media restored growth of the H69A-*accA* back to the same level as the control *accA*$^+$ strain. Furthermore, the rate of NO_2^- consumption by the H69A-*accA* was reduced compared to the *accA*$^+$ strain (Figure 5.6b). However, this rate was reproducibly higher than that of the Δ*accA* strain. Again, this defect in NO_2^- consumption was restored when Cu was supplemented into the growth media (Figure 5.6b).

These data suggest that the weakened affinity of the H69A-*accA* mutant for Cu suppresses metalation of AniA, either as a result of impaired Cu acquisition by AccA or impaired Cu-transfer from AccA to AniA, leading to an intermediate phenotype between the *accA*$^+$ and Δ*accA* knockout strains.

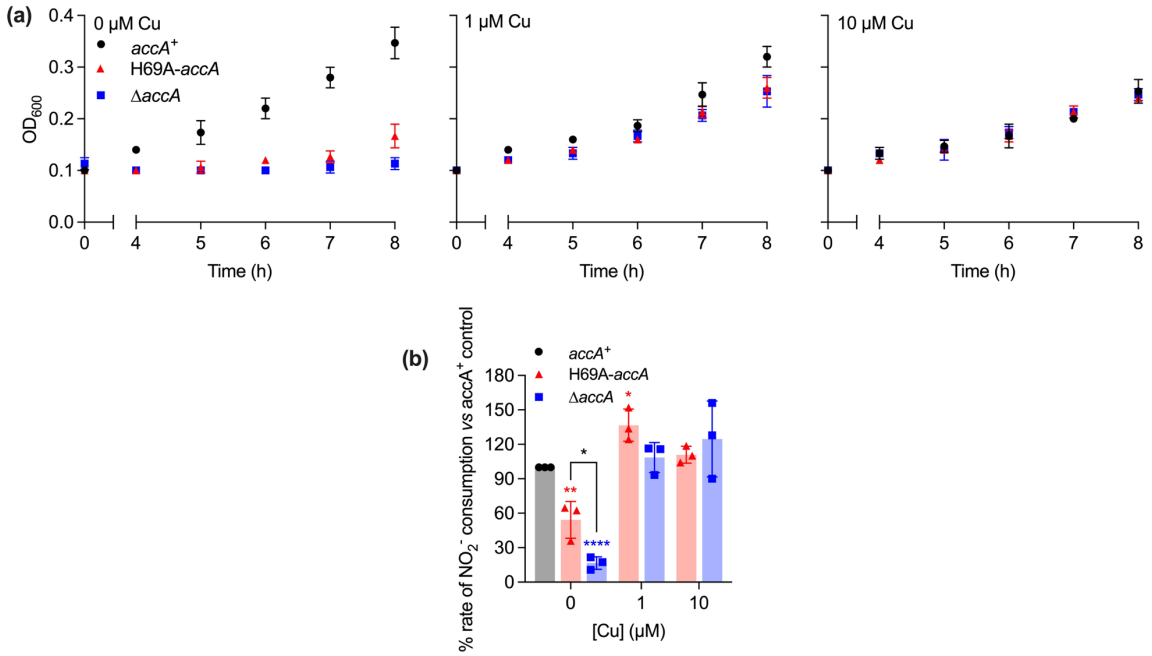

Figure 5.6: The H69A-*accA* mutant has a reduced growth and NO_2^- consumption phenotype, confirming the role of the Cu primary binding site. (a) Growth curves of complemented WT, *accA*$^+$ (black circles), H69A-*accA* (red triangles), and Δ*accA* (blue squares) strains of *N. gonorrhoeae* 1291. Strains were incubated for 8 h in microaerobic conditions (static 30 mL cultures) with nitrite (2 mM $NaNO_2$) supplemented at t = 0, 5, and 7 h. Cells were grown in the presence of 0, 1, or 10 µM $CuSO_4$. Data points represent the mean of n = 3. Error bars represent standard deviation. Two-way ANOVA analysis of growth curves resulted in statistical significance at t = 8 h between the *accA*+ and H69A-*accA* strains in 0 and 1 µM Cu growth curves only (P = <0.0001). Two-way ANOVA analysis of growth curves resulted in statistical significance at t = 8 h between the *accA*$^+$ and Δ*accA* strains in 0 and 1 µM Cu growth curves only (P = <0.0001). Two-way ANOVA analysis of growth curves resulted in statistical significance at t = 8 h between the H69A-*accA* and Δ*accA* strains in 0 µM Cu growth curve only (P = 0.001). **(b)** Percentage rate of nitrite consumption (nmol/min/mg of protein) standardised against the *accA*$^+$ control (no Cu supplemented) of *accA*$^+$, H69A-*accA*, and Δ*accA* strains of *N. gonorrhoeae* 1291 after 8 h of microaerobic growth. Individual data points are displayed. Error bars represent standard deviation. Two-way ANOVA multiple comparison against the mean of the 0 µM Cu *accA*$^+$ control resulted in statistical significance in H69A-*accA* 0 and 1 µM Cu (P = ** 0.006, * 0.0309), and Δ*accA* 0 Cu (P = **** < 0.0001). An unpaired t-test between H69A-*accA* and Δ*accA* 0 µM Cu strains resulted in a statistical significance (P = * 0.0181).

The growth M80A-*accA* strain of *N. gonorrhoeae* phenocopies the H69A-*accA* strain: it was reduced compared to the *accA*$^+$ strain but increased compared to the Δ*accA* strain (Figure 5.7a). This growth defect is again restored when Cu is supplemented to the media during growth. Similarly, the M80A-*accA* strain displayed a reduced rate of NO_2^- consumption compared to the *accA*$^+$ strain. Interestingly, unlike the H69A-*accA* strain, the rate of NO_2^- consumption by the M80A-*accA* strain was not distinguishable from the ΔaccA knockout strain (Figure 5.7b). This observation may indicate that the thioether side-chain of Met80 plays a more important role than the imidazole side-chain of His69 in metalating and activating AniA.

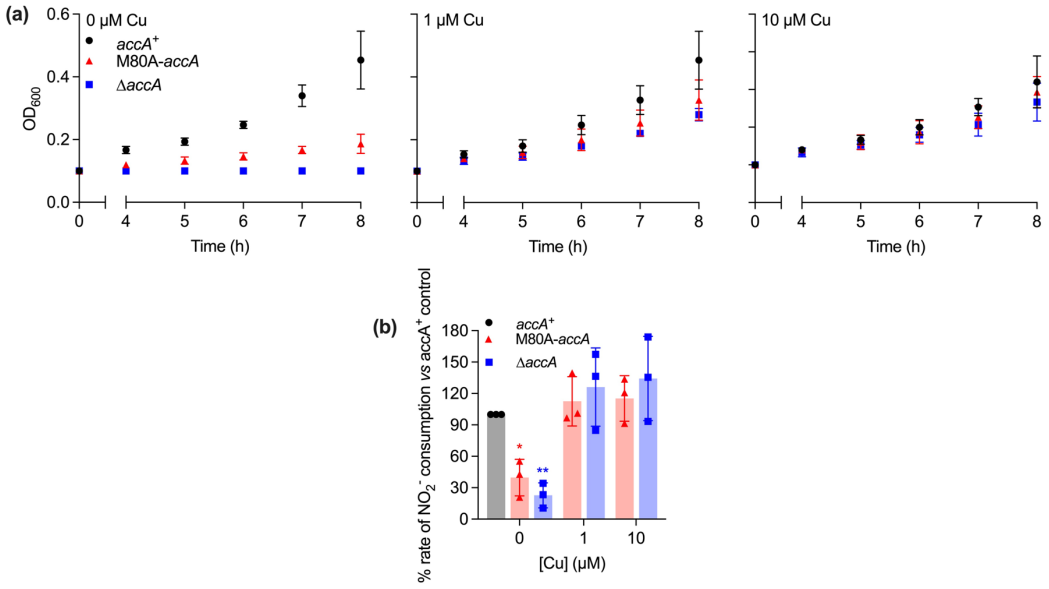

Figure 5.7: The M80A-*accA* strain phenocopies the H69A mutant, confirming the role of the Cu primary binding site. (a) Growth curves of complemented WT, *accA*$^+$ (black circles), M80A-*accA* (red triangles), and Δ*accA* (blue squares) strains of *N. gonorrhoeae* 1291. Strains were incubated for 8 h in microaerobic conditions (static 30 mL cultures) with nitrite (2 mM $NaNO_2$) supplemented at t = 0, 5,and 7 h. Cells were grown in the presence of 0, 1, or 10 µM $CuSO_4$. Data points represent the mean of n = 3. Error bars represent standard deviation. Two-way ANOVA analysis of growth curves resulted in statistical significance at t = 8 h between the *accA*$^+$ and M80A-*accA* strains in 0 and 1 µM Cu growth curves only (P = <0.0001 and 0.0001 respectively). Two-way ANOVA analysis of growth curves resulted in statistical significance at t = 8 h between the *accA*$^+$ and Δ*accA* strains in 0 and 1 µM Cu growth curves only (P = < 0.0001). Two-way ANOVA analysis of growth curves resulted in statistical significance at t = 8 h between the M80A-*accA* and Δ*accA* strains in 0 µM Cu growth only (P = 0.0005). **(b)** Percentage rate of nitrite consumption (nmol/min/mg of protein) standardised against the *accA*$^+$ control (no Cu supplemented) of *accA*$^+$, M80A-*accA*, and Δ*accA* strains of *N. gonorrhoeae* 1291 after 8 h of microaerobic growth. Individual data points are displayed. Error bars represent standard deviation. Two-way ANOVA multiple comparison against the mean of the 0 µM Cu *accA*$^+$ control resulted in statistical significance in M80A-*accA* 0 µM Cu (P = * 0.0234) and Δ*accA* 0 µM Cu (P = ** 0.0032) samples. An unpaired t-test did not detect any statistical significance between the M80A-*accA* and Δ*accA* 0 µM Cu samples.

The H103A-*accA* strain, like the H69A-*accA* and M80A-*accA* strains described earlier, showed a reduced growth phenotype compared to the *accA*$^+$ strain (Figure 5.8a), which restored upon Cu supplementation of the growth media. Interestingly, despite the reduced growth, the H103A-*accA* strain did not show a reduced NO_2^- consumption (Figure 5.8b). This result suggests that AniA in this strain is fully active. However, further experimentation showed a slight defect to NO_2^- consumption in the H103A-*accA* strain which will be followed up in a later section (Figure 5.14).

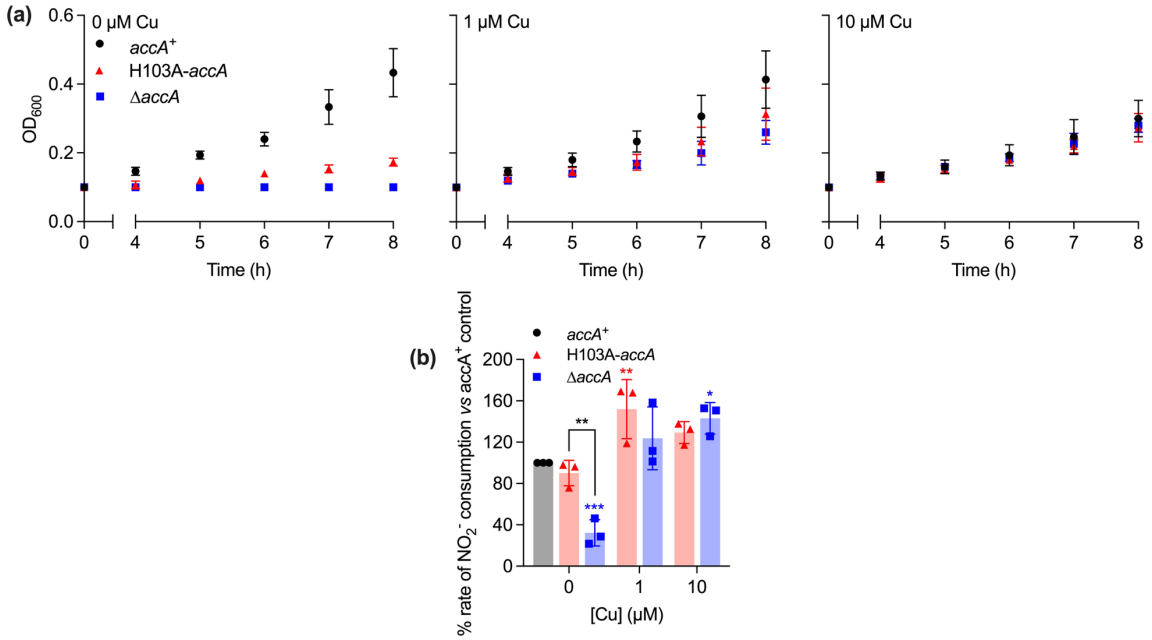

Figure 5.8: The H103A-*accA* strain has a reduced growth phenotype but not a reduced nitrite consumption. (a) Growth curves of complemented WT, *accA*$^+$ (black circles), H103A-*accA* (red triangles), and Δ*accA* (blue squares) strains of *N. gonorrhoeae* 1291. Strains were incubated for 8 h in microaerobic conditions (static 30 mL cultures) with nitrite (2 mM $NaNO_2$) supplemented at t = 0, 5, and 7 h. Cells were grown in the presence of 0, 1, or 10 µM $CuSO_4$. Data points represent the mean of n = 3. Error bars represent standard deviation. Two-way ANOVA analysis of growth curves resulted in statistical significance at t = 8 h between the *accA*$^+$ and H103A-*accA* strains in 0 and 1 µM Cu growth curves only (P = < 0.0001 and 0.0042 respectively). Two-way ANOVA analysis of growth curves resulted in statistical significance at t = 8 h between the *accA*$^+$ and Δ*accA* strains in 0 and 1 µM Cu growth curves only (P = <0.0001). Two-way ANOVA analysis of growth curves resulted in statistical significance at t = 8 h between the H103A-*accA* and Δ*accA* strains in 0 µM Cu growth curves only (P = 0.0132). **(b)** Percentage rate of nitrite consumption (nmol/min/mg of protein) standardised against the *accA*$^+$ control (0 µM Cu supplemented) of *accA*$^+$, H103A-*accA*, and Δ*accA* strains of *N. gonorrhoeae* 1291 after 8 h of microaerobic growth. Individual data points are displayed. Error bars represent standard deviation. Two-way ANOVA multiple comparison against the mean of 0 µM Cu *accA*$^+$ resulted in statistical significance in H103A-*accA* 1 µM Cu (P = ** 0.0066), 0 and 10 µM Cu Δ*accA* (P = *** 0.0005, * 0.0269) samples. An unpaired t-test between H103A-*accA* and Δ*accA* 0 µM Cu samples resulted in a statistical significance (P = ** 0.0047).

The final single Cu primary site mutant, M105A-*accA,* also showed a reduced growth phenotype that was restored upon Cu supplementation of the growth media (Figure 5.9a). Interestingly, the final OD_{600} was lower in the M105A-*accA* than the previous single mutant strains with a final OD_{600} of 0.15. Like the H69A-*accA* strain, the M105A-*accA* strain has a reduced NO_2^- consumption compared to the *accA*$^+$ strain, but is increased compared to the Δ*accA* strain (Figure 5.9b).

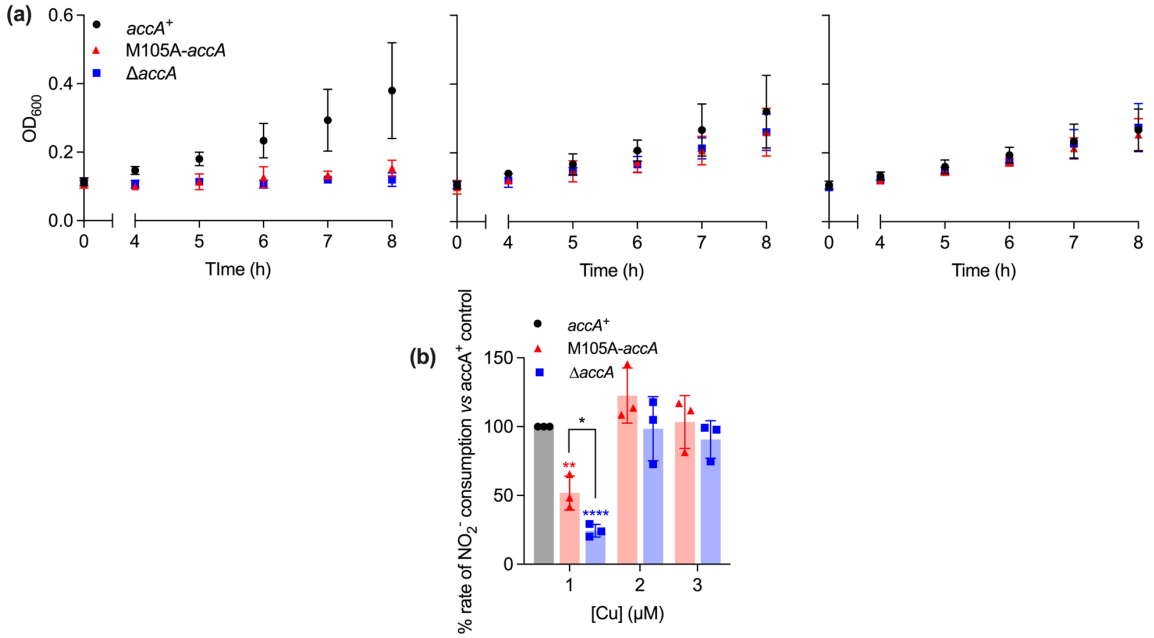

Figure 5.9: The M105A-*accA* strain phenocopies the H69A-*accA* and M80A-*accA* strains, confirming the role of the Cu primary binding site. (a) Growth curves of complemented WT, *accA*$^+$ (black circles), M105A-*accA* (red triangles), and Δ*accA* (blue squares) strains of *N. gonorrhoeae* 1291. Strains were incubated for 8 h in microaerobic conditions (static 30 mL cultures) with nitrite (2 mM $NaNO_2$) supplemented at t = 0, 5, and 5 h. Cells were grown in the presence of 0, 1, or 10 μm $CuSO_4$. Data points represent the mean of n = 3. Error bars represent standard deviation. Two-way ANOVA analysis of growth curves resulted in statistical significance at t = 8 h between the *accA*$^+$ and M105A-*accA* strains in the 0 μM Cu growth curve only (P = <0.0001). Two-way ANOVA analysis of growth curves resulted in statistical significance at t = 8 h between the *accA*$^+$ and Δ*accA* strains In the 0 μM Cu growth curve only (P = <0.0001). Two-way ANOVA analysis of growth curves did not result in any statistical significance between M105A-*accA* and Δ*accA* strains at t = 8 h. **(b)** Percentage rate of nitrite consumption (nmol/min/mg of protein) standardised against the *accA*$^+$ control (0 μM Cu supplemented) of *accA*$^+$, M105A-*accA*, and Δ*accA* strains of *N. gonorrhoeae* 1291 after 8 h of microaerobic growth. Individual data points are displayed. Error bars represent standard deviation. Two-way ANOVA multiple comparison against the mean of 0 μM *accA*$^+$ resulted in statistical significance in M105A-*accA* 0 μM Cu (P = ** 0.0026) and 0 μM Cu Δ*accA* (P = **** <0.0001) samples. An unpaired t-test between M105A-*accA* and Δ*accA* 0 μM Cu samples resulted in statistical significance (P= * 0.0226).

Taken together, these data confirm the role of His69, Met80, His103, and Met105 in the Cu primary site of AccA in metalating AniA *in vivo.* Mutation in any of these residues result in a drastic decrease in microaerobic growth. Interestingly, NO_2^- consumption in these mutants are not equally impacted. This suggests that despite all of the single mutant proteins displaying the same affinity for Cu(I) *in vitro*. Therefore, whilst each of the residues in the primary site contributes similarly to binding Cu(I) *in vitro*, some may be more important than others in metalating AniA *in vivo*.

5.3.2 Double Cu primary site mutants act as a Δ*accA* knockout strain

To further investigate the importance of the Cu primary site of AccA in metalating AniA, double mutants were created. The H69A/M80A-*accA* (Figure 5.10) and the H103/M105-*accA* (Figure 5.11) mutant strains of *N. gonorrhoeae* each phenocopied the Δ*accA* strain, in that each strain did not grow in microaerobic conditions or consume NO_2^- (Figure 5.10-11). This growth defect was restored when Cu was supplemented into the growth media.

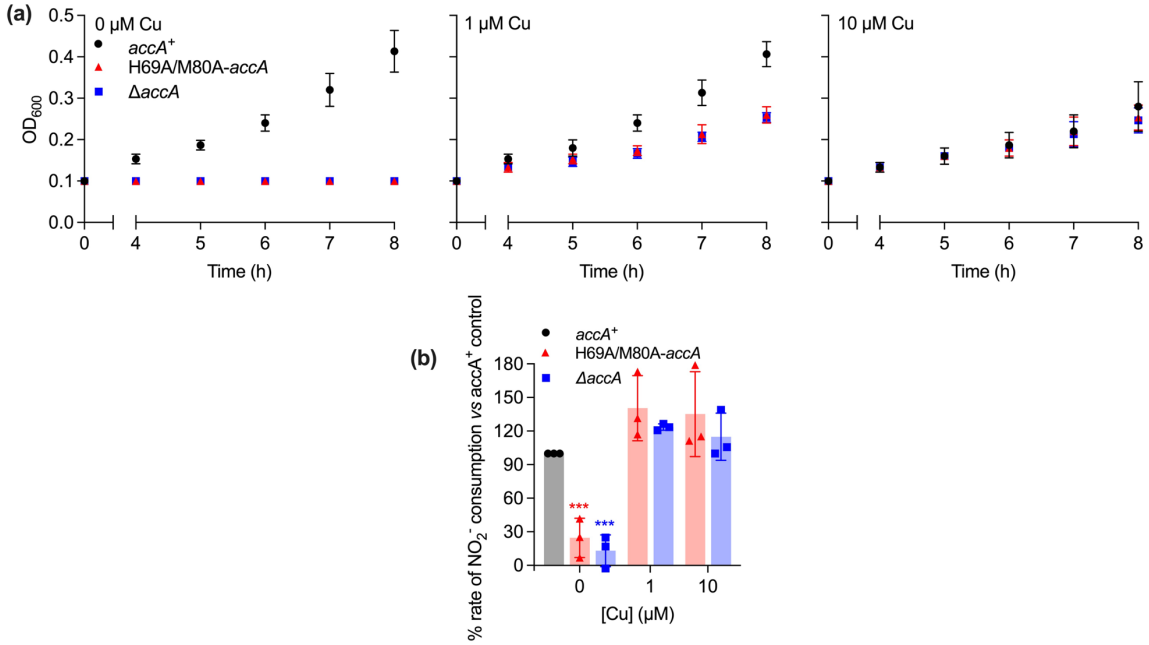

Figure 5.10: The H69A/M80A-*accA* double mutant strain phenocopies a Δ*accA* knockout strain, confirming the role of the Cu primary site of AccA in activating AniA. (a) Growth curves of complemented WT, *accA*$^+$ (black circles), H69A/M80A-*accA* (red triangles), and Δ*accA* (blue squares) strains of *N. gonorrhoeae* 1291. Strains were incubated for 8 h in microaerobic conditions (static 30 mL cultures) with nitrite (2 mM $NaNO_2$) supplemented at t = 0, 5, and 7 h. Cells were grown in the presence of 0, 1, or 10 μM $CuSO_4$. Data points represent the mean of n = 3. Error bars represent standard deviation. Two-way ANOVA analysis of growth curves resulted in statistical significance at t = 8 h between *accA*$^+$ and H69A/M80A-*accA* strains in the 0, and 1 μM Cu growth curves only (P = <0.0001). Two-way ANOVA analysis of growth curves resulted in statistical significance at t = 8 h between the *accA*$^+$ and Δ*accA* strains in the 0, and 1 μM Cu growth curves only (P = <0.0001). **(b)** Percentage rate of nitrite consumption (nmol/min/mg of protein) standardised against the *accA*$^+$ control (0 μM Cu supplemented) of *accA*$^+$, H60A/M80A-*accA*, and Δ*accA* strains of *N. gonorrhoeae* 1291 after 8 h of microaerobic growth. Individual data points are displayed. Error bars represent standard deviation. Two-way ANOVA multiple comparison against the mean of 0 μM *accA*$^+$ resulted in statistical significance in H69A/M80A-*accA* 0 μM Cu (P = *** 0.0008) and 0 μM Cu Δ*accA* (P = *** 0.0002) samples.

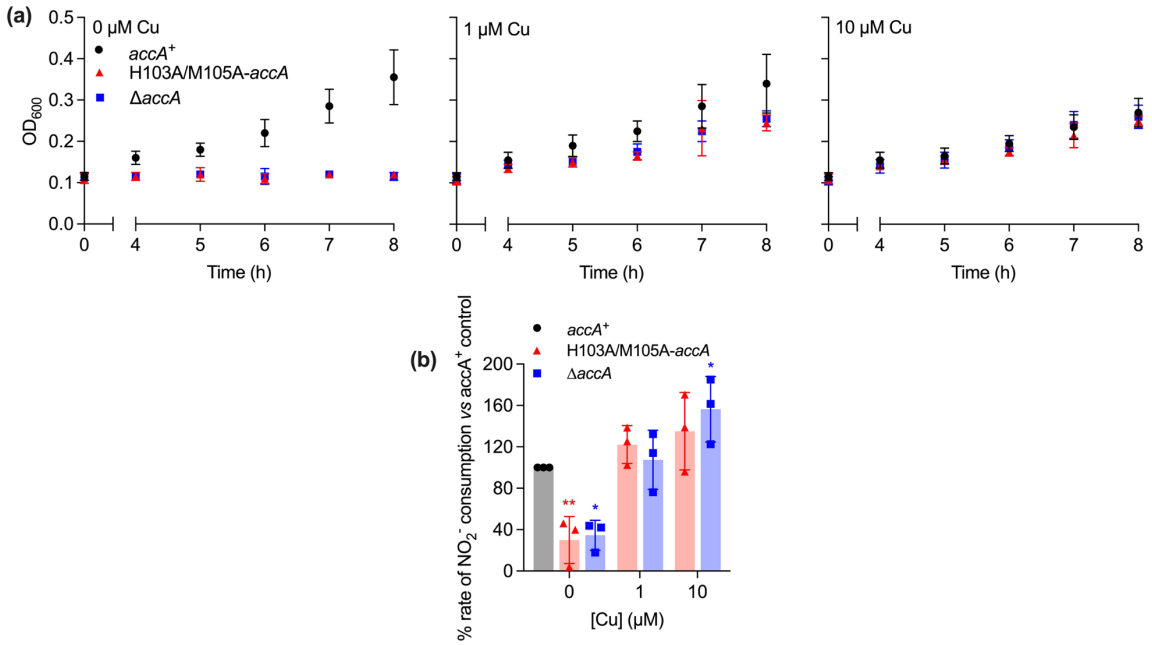

Figure 5.11: The H103A/M105A-*accA* double mutant strain phenocopies a Δ*accA* knockout strain, confirming the role of the Cu primary site of AccA in activating AniA. (a) Growth curves of complemented WT, *accA*$^+$ (black circles), H103A/M105A-*accA* (red triangles), and Δ*accA* (blue squares) strains of *N. gonorrhoeae* 1291. Strains were incubated for 8 h in microaerobic conditions (static 30 mL cultures) with nitrite (2 mM $NaNO_2$) supplemented at t = 0, 5, and 7 h. Cells were grown in the presence of 0, 1, or 10 μM $CuSO_4$. Data points represent the mean of n = 3. Error bars represent standard deviation. Two-way ANOVA analysis of growth curves resulted in statistical significance at t = 8 h between *accA*$^+$ and H69A/M80A-*accA* strains in the 0, and 1 μM Cu growth curves only (P = <0.0001 and 0.0001 respectively). Two-way ANOVA analysis of growth curves resulted in statistical significance at t = 8 h between the *accA*$^+$ and Δ*accA* strains in the 0, and 1 μM Cu growth curves only (P = <0.0001 and 0.0006 respectively). **(b)** Percentage rate of nitrite consumption (nmol/min/mg of protein) standardised against the *accA*$^+$ control (0 μM Cu supplemented) of *accA*$^+$, H103A/M105A-*accA*, and Δ*accA* strains of *N. gonorrhoeae* 1291 after 8 h of microaerobic growth. Individual data points are displayed. Error bars represent standard deviation. Two-way ANOVA multiple comparison against the mean of 0 μM *accA*$^+$ resulted in statistical significance in H103A/M105A-*accA* 0 and 10 μM Cu (P = ** 0.0062) and 0 μM Cu Δ*accA* (P = * 0.0108 and 0.0302 respectively) samples.

5.3.3 The Cu primary site is required to activate AniA *in vivo*

A total deletion of all four residues in the Cu primary site (H69A/M80A/H103A/M105A) was used to further examine the importance of the Cu primary site in metalating AniA *in vivo.* This strain was named ΔCu primary-*accA.* This mutant failed to grow in microaerobic conditions, consistent with a Δ*accA* strain (Figure 5.12a). Addition of Cu to the growth media restored growth to *accA*$^+$ levels. Furthermore, the ΔCu primary-*accA* strain did not consume NO_2^- (Figure 5.12b). This defect was also restored when cells were grown in the presence of Cu. These data reinforce the previous conclusion that the Cu primary site of AccA is required for activation of AniA *in vivo*.

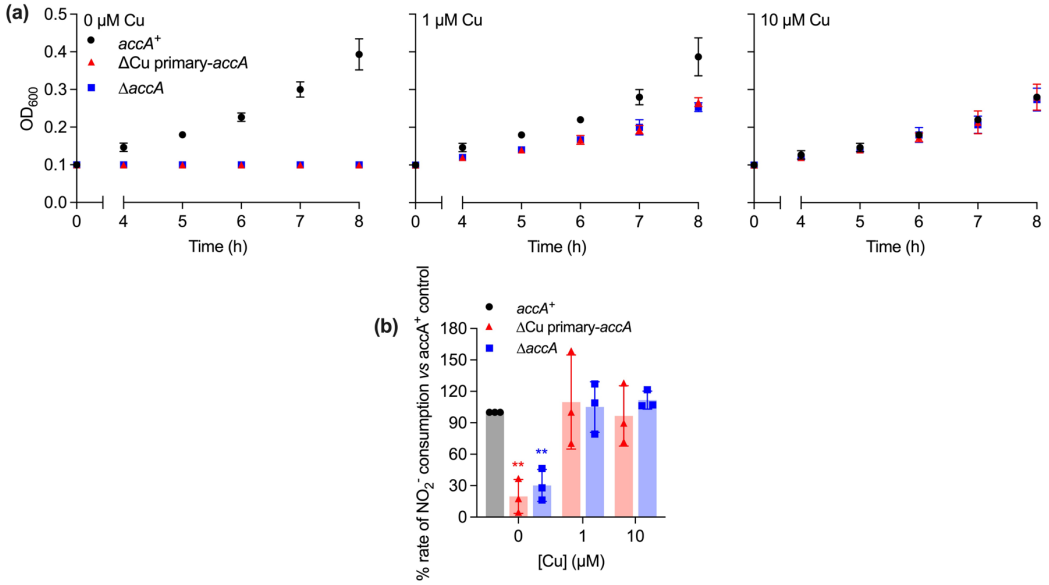

Figure 5.12: The ΔCu primary-*accA* mutant strain phenocopies a Δ*accA* knockout strain, confirming the role of the Cu primary site of AccA in activating AniA. (a) Growth curves of complemented WT, *accA*$^+$ (black circles), ΔCu primary-*accA* (red triangles), and Δ*accA* (blue squares) strains of *N. gonorrhoeae* 1291. Strains were incubated for 8 h in microaerobic conditions (static 30 mL cultures) with nitrite (2 mM $NaNO_2$) supplemented at t = 0, 5, and 7 h. Cells were grown in the presence of 0, 1, or 10 µM $CuSO_4$. Data points represent the mean of n = 3. Error bars represent standard deviation. Two-way ANOVA analysis of growth curves resulted in statistical significance at t = 8 h between *accA*$^+$ and ΔCu primary-*accA* strains in the 0, and 1 µM Cu growth curves only (P = <0.0001). Two-way ANOVA analysis of growth curves resulted in statistical significance at t = 8 h between the *accA*$^+$ and Δ*accA* strains in the 0, and 1 µM Cu growth curves only (P = <0.0001). **(b)** Percentage rate of nitrite consumption (nmol/min/mg of protein) standardised against the *accA*$^+$ control (0 µM Cu supplemented) of *accA*$^+$, ΔCu primary-*accA*, and Δ*accA* strains of *N. gonorrhoeae* 1291 after 8 h of microaerobic growth. Individual data points are displayed. Error bars represent standard deviation. Two-way ANOVA multiple comparison against the mean of 0 µM *accA*$^+$ resulted in statistical significance in H103A/M105A-*accA* 0 and 10 µM Cu (P = ** 0.0013) and 0 µM Cu Δ*accA* (P = ** 0.0047) samples.

5.3.4 The ΔCu tract-*accA* strain has a reduced growth phenotype suggesting a role in metalating AniA

Biochemical experiments described in Chapter 4 demonstrated that deleting the possible Cu tract residues in AccA led to a weakening of the affinity of the Cu primary site to Cu(I) from a $logK_D$ of -16.7 M to -14.3 M. As previously discussed, the Met side-chains from the Cu tract may stabilise Cu binding in AccA by direct coordination or second sphere coordination with Cu. We, therefore, were interested in whether a ΔCu tract-*accA* strain showed any phenotype.

The ΔCu tract-*accA* strain showed a reduced growth phenotype (Figure 5.13). However, this reduction in growth was relatively minor when compared with the reduction caused by single site mutations of

the Cu primary site (Figure 5.6-9). Despite the decrease in microaerobic growth, there was no difference in the rate of NO_2^- consumption by the ΔCu tract-*accA* strain compared to the control *accA*$^+$ strain. As NO_2^- consumption was only monitored using cells at the end of growth, it is possible that by this time AniA was already fully metalated. However, if samples were collected earlier during growth a defect in NO_2^- compared to the *accA*$^+$ could have been observed.

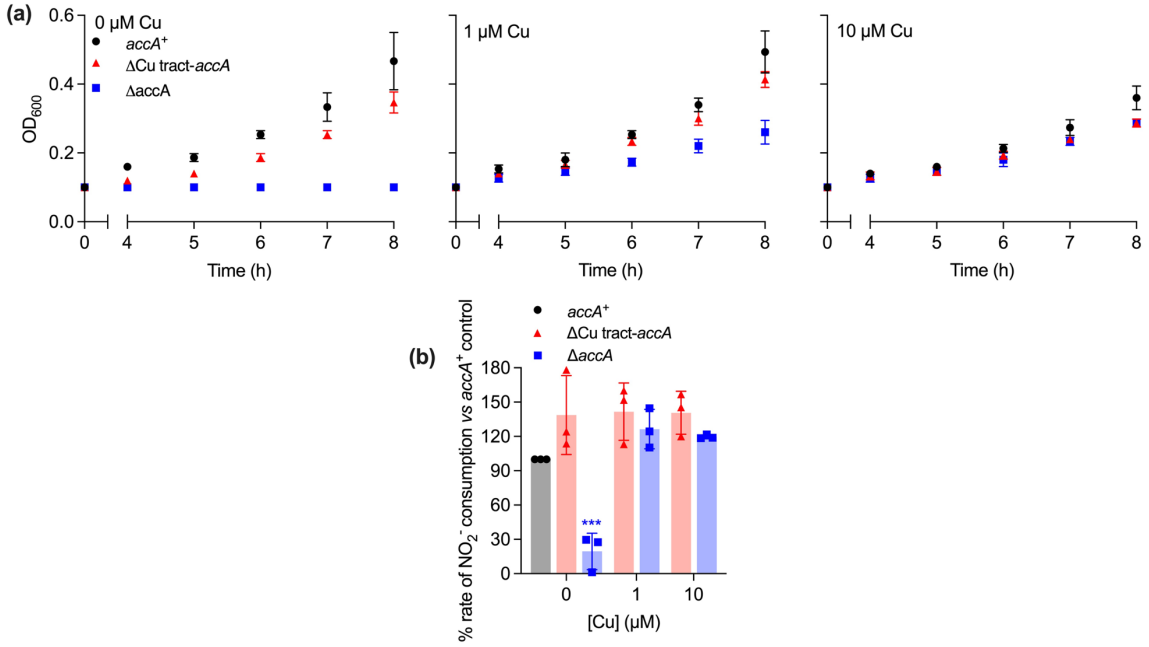

Figure 5.13: The ΔCu tract-*accA* mutant has a reduced growth phenotype indicating a role in activating AniA. (a) Growth curves of complemented WT, *accA*$^+$ (black circles), ΔCu tract-*accA* (red triangles), and Δ*accA* (blue squares) strains of *N. gonorrhoeae* 1291. Strains were incubated for 8 h in microaerobic conditions (static 30 mL cultures) with nitrite (2 mM $NaNO_2$) supplemented at t = 0, 5, and 7 h. Cells were grown in the presence of 0, 1, or 10 μM $CuSO_4$. Data points represent the mean of n = 3. Error bars represent standard deviation. Two-way ANOVA analysis of growth curves resulted in statistical significance at t = 8 h between *accA*$^+$ and ΔCu tract-*accA* strains in the 0, 1, and 10 μM Cu growth curves (P = <0.0001, 0.0001, and <0.0001 respectively). Two-way ANOVA analysis of growth curves resulted in statistical significance at t = 8 h between the *accA*$^+$ and Δ*accA* strains in the 0, 1, and 10 μM Cu growth curves (P = <0.0001). Two-way ANOVA analysis of growth curves resulted in statistical significance at t = 8 h between ΔCu tract-*accA* and Δ*accA* strains in the 0, and 1 μM Cu growth curves only (P = <0.0001). **(b)** Percentage rate of nitrite consumption (nmol/min/mg of protein) standardised against the *accA*$^+$ control (0 μM Cu supplemented) of *accA*$^+$, ΔCu tract-*accA*, and Δ*accA* strains of *N. gonorrhoeae* 1291 after 8 h of microaerobic growth. Individual data points are displayed. Error bars represent standard deviation. Two-way ANOVA multiple comparison against the mean of 0 μM *accA*$^+$ resulted in statistical significance in and 0 μM Cu Δ*accA* (P = *** 0.0002) sample.

5.3.5 Reduced NO_2^- consumption in single Cu primary mutants is restored after 10 hours of growth

The examination of the different Cu(I) primary site mutants revealed potentially interesting differences between the mutants. However, in the previous experiments, the mutants were grown separately and could only be directly compared to the *accA*$^+$ and Δ*accA* controls. It is possible that the differences between the mutants were a result of slight variations in growth conditions. Therefore, the only way to determine whether these differences are real was to grow and assay them in parallel.

The resulting microaerobic growth curves supported what was previously observed (Figures 5.6-13). The ΔCu tract mutant showed a slight growth defect. Single Cu primary site mutants showed a more drastic growth defect, although they all grew above the background Δ*accA* knockout mutant strain. It is of note that the M80A-*accA* strain showed reduced growth compared to the remaining three single mutants in this experiment. This contrasts with previous experimentation in which the single mutants were grown separately, as the M105A-*accA* showed a reduced growth compared to the remaining single mutants. The double Cu primary site, ΔCu primary, and Δ*accA* mutants all failed to grow (Figure 5.14a).

The rate of NO_2^- consumption was measured after cells were grown for 8 hours. Overall, this data confirmed what was previously observed when the mutant strains were grown and assayed separately. The double mutant strains (H69A/M80A-*accA* and H103A/M105A-*accA*), the ΔCu primary-*accA* strain, and the Δ*accA* knockout strain did not consume NO_2^-. The ΔCu tract-*accA* strain had no defect in NO_2^- consumption compared to the *accA*$^+$ strain. The single mutant strains all had a reduced NO_2^- consumption phenotype compared to the *accA*$^+$ strain. However, when the strains were investigated separately, the H103A-*accA* did not show a reduced NO_2^- consumption phenotype compared to the *accA*$^+$ strain (Figure 5.14b). This highlights the importance of growing and assaying the strains in parallel.

The NO_2^- consumption of the strains was measured again after 10 hours of growth. There was no change in rate of the NO_2^- consumption in the *accA*$^+$, double mutant strains, ΔCu primary-*accA* strain, or the ΔCu tract-*accA* strain. Interestingly, three of the four single mutants showed an increase in NO_2^- consumption, to *accA*$^+$ levels. However, the M80A-*accA* strain did not show this restoration of NO_2^-

consumption. This may suggest that whilst there is no change in Cu(I) binding affinity compared to the remaining single mutant protein, M80 may be important in Cu acquisition from the buffer or its transfer to AniA. This improvement of the rate of NO_2^- consumption in the single mutants may be explained by the weakened affinity for Cu(I) these mutants have. The single mutants may take longer to acquire Cu, therefore, extending the growth time allowed more AccA to acquire and transfer Cu to AniA, resulting in more active protein.

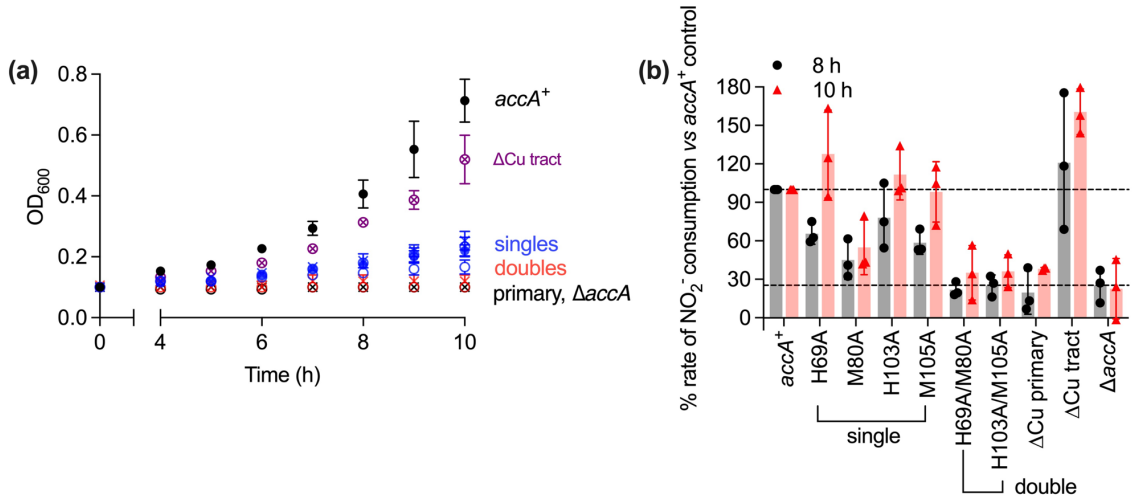

Figure 5.14: The single Cu primary mutants, H69A, H103A, and M105A, have an improved NO_2^- consumption at 10 h of growth compared to 9 h of growth, indicating inefficiency in AniA activation. (a) Growth curves of: complemented WT, *accA*$^+$ (black circles); ΔCu tract-*accA* (purple circle with cross); single Cu primary mutants, H69A (blue cross), M80A (blue open circles), H103A (blue circle with cross), and M105A (blue closed circle); double Cu primary mutants, H69A/M80A (red open circle), H103A/M105A (red cross); ΔCu primary (black cross); and Δ*accA* (black open circle) strains of *N. gonorrhoeae* 1291. Strains were incubated for 10 h in microaerobic conditions (static 30 mL cultures) with nitrite (2 mM $NaNO_2$) supplemented at t = 0, 5, 7, 8, and 9 h. Data points represent the mean of n = 3. Error bars represent standard deviation. **(b)** Percentage rate of nitrite consumption (nmol/min/mg of protein) standardised against the *accA*$^+$ control of *accA*$^+$; ΔCu tract-*accA*; single Cu primary mutants, H69A, M80A, H103A, and M105A; double Cu primary mutants, H69A/M80A, and H103A/M105A; ΔCu primary; and Δ*accA* of *N. gonorrhoeae* 1291 after 8 (black circle) and 10 (red triangle) h of microaerobic growth. Individual data points are displayed. Error bars represent standard deviation. A dotted line at 25.3% represents inactive AniA, and a dotted line at 100% represents fully active AniA.

5.4 Investigating the role of AccA during Cu starvation.

The growth medium used in these studies was clearly Cu-sufficient, assured by its support of maximal growth under microaerobic growth conditions. Furthermore, addition of Cu into the medium did not improve growth. In fact, only 10 μM of Cu was needed to achieve toxicity through Cu excess. The single, double, and quadruple Cu primary site mutant strains showed a clear growth defect in the medium used for experimentation, but the ΔCu tract-*accA* strain only showed a minor defect. We,

therefore, wondered whether this defect could be enhanced if the Cu in the medium was reduced to mimic Cu starvation.

5.4.1 The ΔCu tract mutant did not grow or consume NO_2^- during Cu starvation

We established that the ΔCu tract-*accA* strain has a reduced growth phenotype in microaerobic conditions compared to the *accA*$^+$ strain (Section 5.3.4).

To promote Cu starvation, the cell-impermeable, high-affinity, Cu(I)-specific chelator BCS was added to the culture medium. Addition of BCS suppressed growth of control *accA*$^+$ strain (Figure 5.15a) when compared to the untreated control, consistent with Cu starvation. Interestingly, growth was not recovered to untreated control levels when $CuBCS_2$ was supplemented into the media (Figure 5.15a). This suggests that even under these conditions, entry of Cu into the cell may remain restricted. Addition of BCS abolished growth of the ΔCu tract-*accA* strain (Figure 5.15a). Supplementation with $CuBCS_2$ restored growth of this mutant strain back to the control *accA*$^+$ levels under these condition (Figure 5.15a).

The impact of BCS on the activity of AniA was clearly observed upon measuring the rates of NO_2^- consumption. Despite the reduced growth phenotype observed in the *accA*$^+$ upon treatment with BCS alone or $CuBCS_2$, there was no defect in the rate of NO_2^- consumption. This suggests that AniA is still metalated, and active, in these conditions. As previously demonstrated the rate of NO_2^- consumption can be restored with longer growth (Section 5.3.5). Therefore, measuring the rate of NO_2^- consumption after 8 hours of growth rather than 10 would provide an insight into whether metalation of AniA took longer in these conditions. This may explain the reduced growth phenotype, or whether AniA metalation was not impaired and the metalation of a different Cu-dependent enzyme such as cytochrome cbb_3 was impacted under these conditions. BCS reduced the rates of NO_2^- consumption in the ΔCu tract-*accA* strain, but re-addition of Cu into the culture medium restored these rates back to the control levels (Figure 5.15b). Assessing these results in parallel suggests that the ΔCu tract AccA protein does not acquire Cu or transfer Cu to AniA effectively *in vivo*. Therefore, the Cu tract residues may play a key role in the function of AccA as a metallochaperone.

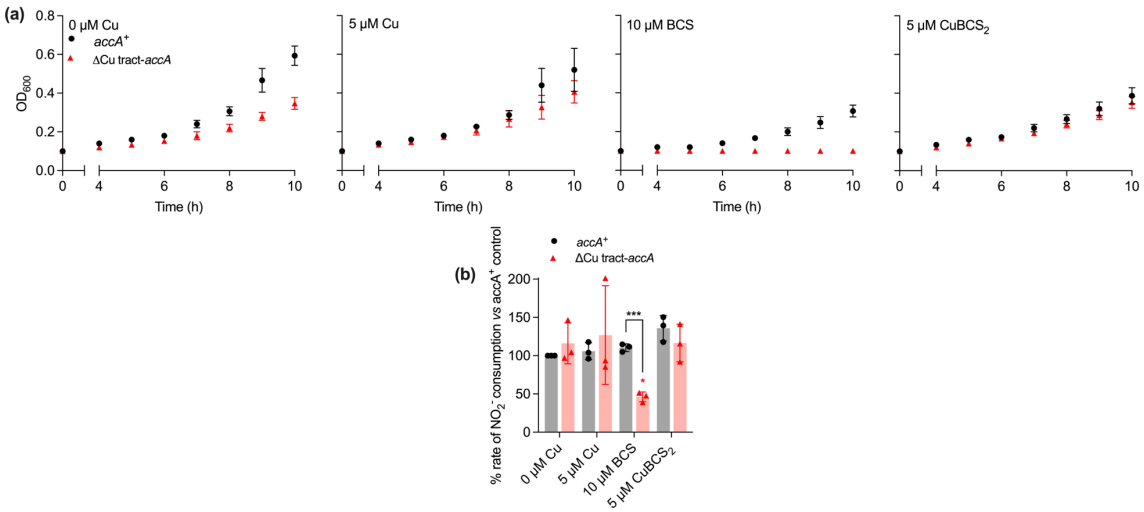

Figure 5.15: The ΔCu tract-*accA* mutant did not grow or consume NO_2^- under Cu starvation conditions. (a) Growth curves of complemented WT, *accA*$^+$ (black circles) and ΔCu tract-*accA* (red triangles) strains of *N. gonorrhoeae* 1291. Strains were incubated for 10 h in microaerobic conditions (static 30 mL cultures) with nitrite (2 mM $NaNO_2$) supplemented at t = 0, 5, 7, 8, and 9 h. Cells were grown in the presence of 0 µM Cu/BCS, 5 µM $CuSO_4$, 10 µM BCS_2, and 5 µM $CuBCS_2$. Data points represent the mean of n = 3. Error bars represent standard deviation. Two-way ANOVA analysis of growth curves resulted in statistical significance at t = 10 h between *accA*$^+$ and ΔCu tract-*accA* strains in the 0 µM Cu/BCS, 5 µM Cu, and 10 µM BCS growth curves (P = <0.0001, 0.0255, and <0.0001 respectively). **(b)** Percentage rate of nitrite consumption (nmol/min/mg of protein) standardised against the *accA*$^+$ control (0 µM Cu supplemented) of *accA*$^+$ and ΔCu tract-*accA* strains of *N. gonorrhoeae* 1291 after 10 h of microaerobic growth. Individual data points are displayed. Error bars represent standard deviation. Two-way ANOVA multiple comparison against the mean of 0 µM *accA*$^+$ resulted in statistical significance in 10 µM BCS ΔCu tract-*accA* (P = * 0.0418) sample. An unpaired t-test between *accA*$^+$ and ΔCu tract-*accA* 10 µM BCS samples resulted in statistical significance (P = *** 0.0002).

5.4.2 The C-terminal tail of AccA may have a role during Cu starvation

In Chapter 4, the C-terminal tail of AccA was shown to bind Cu(II) strongly with picomolar affinity, but not Cu(I). As described in Chapter 1, this C-terminal tail is unique to AccA and is absent from other PCuAC homologues that have been characterised. We are therefore interested in whether deletion of the C-terminal tail of AccA affects the function of AccA in activating AniA *in vivo*.

The ΔC-terminal-*accA* strain did not have a reduced growth phenotype in control conditions (Figure 5.16a). This implies that under these conditions, the C-terminal tail of AccA is not involved in metalating AniA. Supplementation of Cu into the growth media did not result in a phenotype. However, implementing artificial Cu starvation by addition of BCS during growth resulted in a reduced growth phenotype in the ΔC-terminal-*accA* strain compared to the *accA*$^+$ strain. This growth defect was restored to *accA*$^+$ levels when the ΔC-terminal-*accA* strain was grown in the presence of

$CuBCS_2$. These data imply that the C-terminal tail of AccA is required to metalate AniA *in vivo* only during Cu starvation.

The NO_2^- consumption of the ΔC-terminal-*accA* strain was reduced in the 10 μM BCS sample compared to the *accA*$^+$ 10 μM BCS sample (Figure 5.16b). However, both the defect in microaerobic growth and NO_2^- consumption are relatively minor compared to the other effects previously observed in other mutant strains. While these results allude to a possible role of the C-terminal tail in the functions of AccA *in vivo*, this tail is certainly not as important as the primary Cu site or the Cu tract in metalating AniA. As previously observed during microaerobic growth, the addition of $CuBCS_2$ restored NO_2^- consumption in the ΔC-terminal-*accA* strain. This further confirms that the C-terminal tail of AccA may only play an important role to metalate, and activate, AniA during Cu starvation.

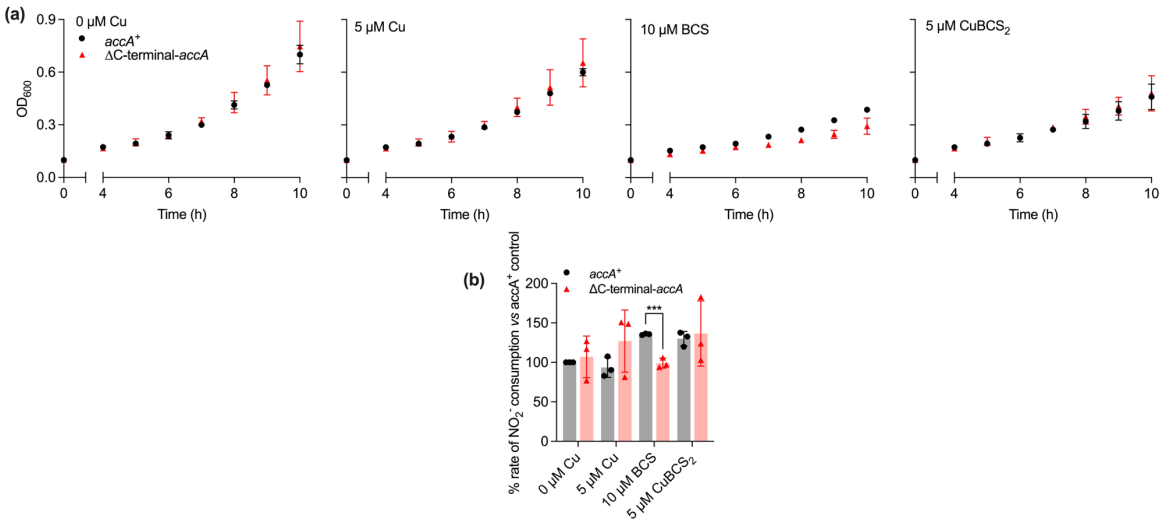

Figure 5.16: The ΔC-terminal-*accA* mutant only has a reduced growth phenotype and NO_2^- consumption in the presence of BCS, suggesting a role during Cu starvation. (a) Growth curves of complemented WT, *accA*$^+$ (black circles) and ΔC-terminal-*accA* (red triangles) strains of *N. gonorrhoeae* 1291. Strains were incubated for 10 h in microaerobic conditions (static 30 mL cultures) with nitrite (2 mM $NaNO_2$) supplemented at t = 0, 5, 7, 8, and 9 h. Cells were grown in the presence of 0 μM Cu/BCS, 5 μM $CuSO_4$, 10 μM BCS_2, and 5 μM $CuBCS_2$. Data points represent the mean of n = 3. Error bars represent standard deviation. Two-way ANOVA analysis of growth curves resulted in statistical significance at t = 10 h between *accA*$^+$ and ΔC-terminal-*accA* strains in the 10 μM BCS growth curve only (P = <0.0001). **(b)** Percentage rate of nitrite consumption (nmol/min/mg of protein) standardised against the *accA*$^+$ control (0 μM Cu supplemented) of *accA*$^+$ and ΔC-terminal-*accA* strains of *N. gonorrhoeae* 1291 after 10 h of microaerobic growth. Individual data points are displayed. Error bars represent standard deviation. An unpaired t-test between *accA*$^+$ and ΔC-terminal-*accA* 10 μM BCS samples resulted in statistical significance (P = *** 0.0006).

5.5 Investigating Cu availability to AniA in a Δ*copA1* knockout strain

CopA is a P-type ATPase that removes toxic Cu from the cytosol of Gram-negative bacteria.[70] The routing of Cu within the cell is still highly debated. Some hypothesise that Cu from the environment can be transported across the outer membrane to the periplasm *via* outer membrane porins, unidentified specific Cu importers, or non-specific metal importers.[64] Once in the periplasm, Cu is captured by the periplasmic buffer and is passed to target Cu-binding proteins directly.[64] Others argue that periplasmic Cu proteins do not acquire Cu directly from the periplasmic buffer. Instead, Cu must be first routed through the cytoplasm and re-exported back out to the periplasm *via* CopA.[64]

The *N. gonorrhoeae* genome encodes two CopA protein named CopA1 and CopA2. CopA proteins sense and coordinate Cu *via* a CXXC motif for transport to the periplasm.[137] The CopA2 protein contains an extended N-terminal region which contains two additional CXXC motifs compared to the CopA1 protein (Figure 5.17). Work to identify whether CopA proteins are involved in Cu acquisition by AccA was only conducted using a Δ*copA1* strain of *N. gonorrhoeae* which was previously generated by the lab. Unfortunately, a Δ*copA2* mutant strain could not be generated, suggesting that CopA2 may be essential in one or more fundamental cellular process.

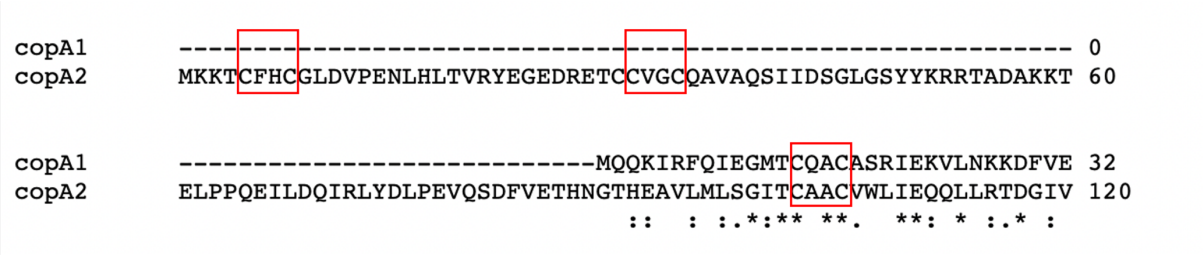

Figure 5.17: The CopA2 protein has an extended N-terminal region with additional CXXC motifs. CLUSTAL O multiple sequence alignment of the N-terminus of *N. gonorrhoeae* CopA1 and CopA2 proteins. CXXC motifs highlighted by red box.

The Δ*copA1* strain of *N. gonorrhoeae* was confirmed to be more sensitive to growth inhibition by added Cu than the WT strain (Figure 5.18a). This has previously been reported by Djoko *et al* (2013(in which supplementation of Cu and NO_2^- were more toxic in a Δ*copA1* strain of *N. gonorrhoeae* compared to the WT strain.[138] This growth defect could have been due to redox cycling between Cu and NO_2^- in the cytoplasm which resulted in the build-up of toxic reactive nitrogen species.[137] However, Cu treatment also led to a reduction in the rates of NO_2^- consumption (Figure 5.18a). This

may suggest that the growth defect in a Δ*copA1* strain of *N. gonorrhoeae* may not be due to redox cycling between Cu and NO_2^- but instead due to a lack of metalation of AniA by AccA.

Previous studies have indicated that excess Cu led to inhibition of heme biosynthesis in the *copA1* mutant strain of *N. gonorrhoeae*. The downstream enzyme in the gonococcal denitrification pathway, NorB, is heme-dependent.[138] To determine whether the defect in growth and NO_2^- consumption was due to inactivation of NorB as a result of inhibited heme biosynthesis, the experiment was repeated in the presence of 1 μM hemin (Figure 5.18b). The addition of hemin alone, without Cu, suppressed growth in both the WT and Δ*copA1* strains of *N. gonorrhoeae.* This suggests that hemin alone has some toxic effect on the cells. However, the rate of NO_2^- consumption of hemin only treated cells did not result in a defect in NO_2^- consumption. This means that the toxicity of hemin and the resulting growth defect was not related to the denitrification pathway.

Supplementation of a combination of Cu and hemin led to further toxicity. However, the growth defect between the WT and Δ*copA1* strain previously observed in Figure 5.18a with the additional of Cu was not observed when hemin was also present in the media (Figure 5.18b). Interestingly, the defect in the rate of NO_2^- consumption in the Δ*copA1* strain of *N. gonorrhoeae* upon Cu supplementation during growth was still present, even when hemin was added to the growth media. This suggests that the loss of NO_2^- consumption in the Cu-treated Δ*copA1* strain was genuine and was not related to heme deficiency or NorB activity.

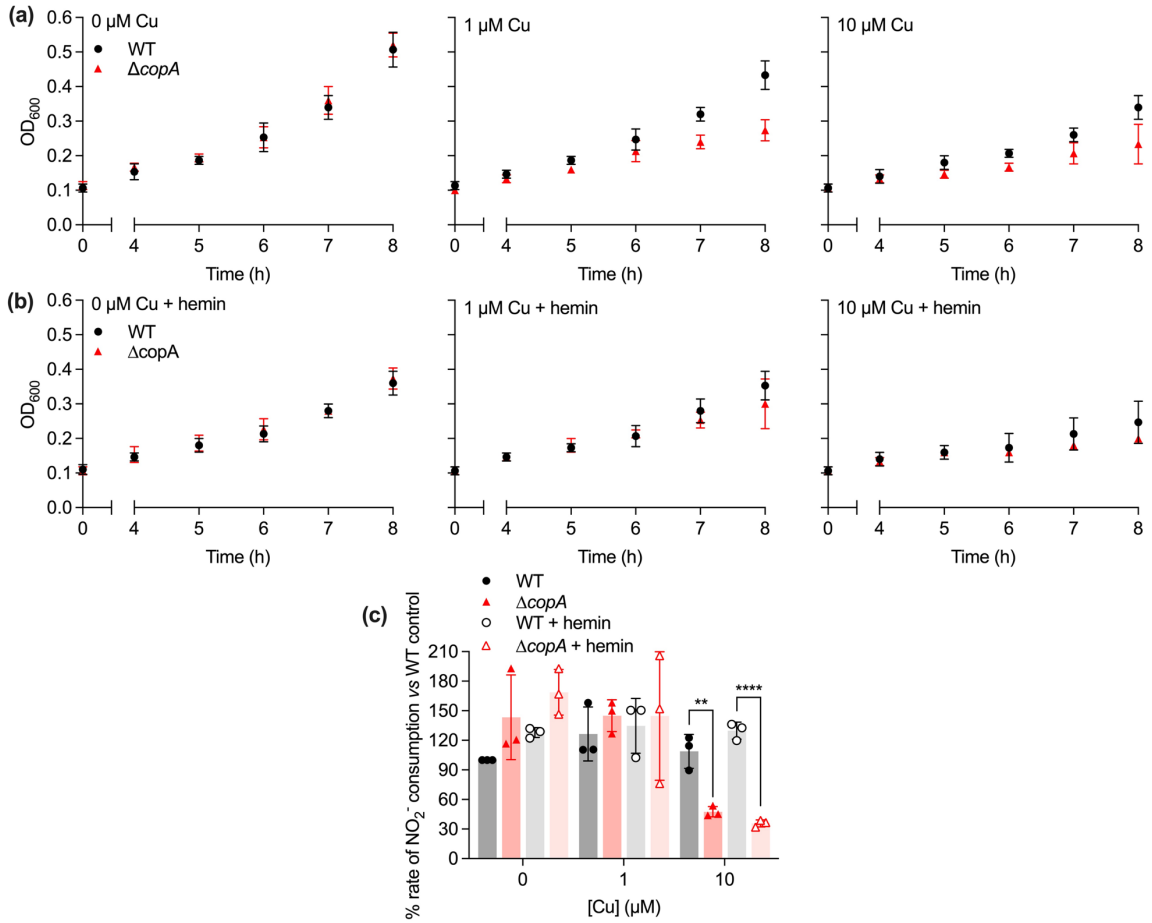

Figure 5.18: A Δ*copA* mutant strain of *N. gonorrhoeae* is more sensitive to Cu than a WT strain. **(a)** Growth curves of WT (black circles) and Δ*copA* (red triangles) strains of *N. gonorrhoeae.* Strains were incubated for 8 h in microaerobic conditions (static 30 mL cultures) with nitrite (2 mM $NaNO_2$) supplemented at t = 0, 5, and 7 h. Cells were grown in the presence of 0, 1, and 10 µM $CuSO_4$. Data points represent the mean of n = 3. Error bars represent standard deviation. Two-way ANOVA analysis of growth curves resulted in statistical significance at t = 8 h between WT and Δ*copA* strains in 1 and 10 µM Cu growth curves (P= <0.0001 and 0.0001 respectively). **(b)** Growth curves of WT (black circles) and Δ*copA* (red triangles) strains of *N. gonorrhoeae.* Strains were incubated for 8 h in microaerobic conditions (static 30 mL cultures) with nitrite (2 mM $NaNO_2$) supplemented at t = 0, 5, and 7 h. Cells were grown in the presence of 1 µM hemin and 0, 1, and 10 µM $CuSO_4$. Data points represent the mean of n = 3. Error bars represent standard deviation. **(c)** Percentage rate of nitrite consumption (nmol/min/mg of protein) standardised against the WT control (0 µM Cu, 0 µM hemin supplemented) of WT and Δ*copA* strains of *N. gonorrhoeae* 1291 after 8 h of microaerobic growth. Individual data points are displayed. Error bars represent standard deviation. An unpaired t-test between Δ*copA* and WT 0 µM Cu, 0 µM hemin samples resulted in a statistical significance (P = ** 0.0041). An unpaired t-test between Δ*copA* and WT 0 µM Cu, 1 µM hemin samples resulted in a statistical significance (P = **** <0.0001).

To further investigate the role of cellular Cu routing in metalating AniA, microaerobic growth and NO_2^- consumption were measured during Cu starvation (BCS treatment) of WT and Δ*copA1* strains of *N. gonorrhoeae* (Figure 5.19a-b). Interestingly, the Δ*copA1* strain had improved microaerobic growth compared to the WT strain. It is important to note that *N. gonorrhoeae* contains two copies of the *copA* gene: *copA1,* and *copA2.* CopA1 acts as previously described; by exporting Cu from the cytosol

to the periplasm. The CopA2 protein is predicted to transport Cu directly to the cytochrome oxidase *cbb*$_3$.[71] This is of note because the CcoP and CcoQ subunits of cytochrome *cbb*$_3$, in conjunction with cytochrome *c*$_2$, are predicted to be electron donors to AniA.[115,116,117,139] It is, therefore, possible that the Δ*copA1* knockout allows CopA2 to transport more Cu to *cbb*$_3$ under Cu starvation than in the WT strain.

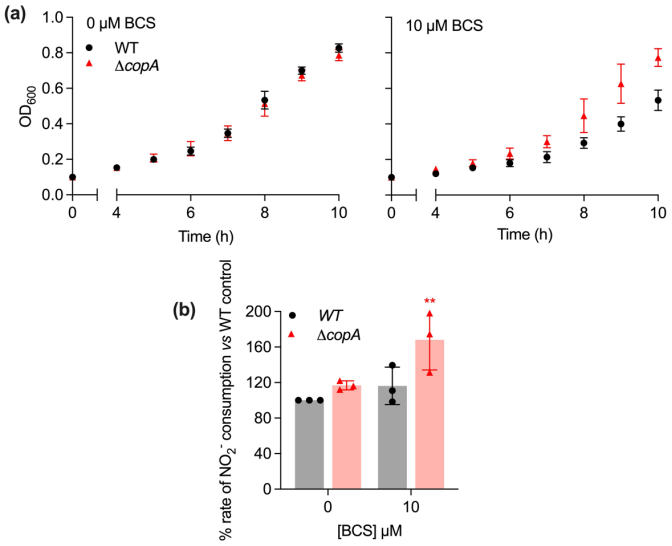

Figure 5.19: A Δ*copA* mutant strain has an improved fitness in Cu starvation conditions compared to WT strains of *N. gonorrhoeae.* (a) Growth curves of WT (black circles) and Δ*copA* (red triangles) strains of *N. gonorrhoeae.* Strains were incubated for 10 h in microaerobic conditions (static 30 mL cultures) with nitrite (2 mM $NaNO_2$) supplemented at t = 0, 5, 7, 8, and 9 h. Data points represent the mean of n = 3. Error bars represent standard deviation. Two-way ANOVA analysis of growth curves resulted in statistical significance at t = 10 h between WT and Δ*copA* strains in 10 μM BCS growth curve (P= <0.0001). **(b)** Percentage rate of nitrite consumption (nmol/min/mg of protein) standardised against the WT control (no BCS supplemented) of WT and Δ*copA* strains of *N. gonorrhoeae* 1291 after 10 h of microaerobic growth. Individual data points are displayed. Error bars represent standard deviation. Two-way ANOVA multiple comparison against the mean of the 0 μM BCS WT control resulted in statistical significance in Δ*copA* 10 μM BCS sample (P = ** 0.0082).

5.6 Discussion

Determining Cu binding affinity and stoichiometry of AccA and mutant proteins has provided an insight into how AccA binds and transfers Cu to AniA *in vivo.* Measuring aerobic growth and calculating the percentage rate of NO_2^- consumption of key AccA mutants in the predicted Cu binding sites (Cu primary and C-terminal tail) as well as the predicted Cu tract, has provided us with an increased insight into how AccA may act as a metallochaperone *in vivo.*

5.6.1 AccA is only required when Cu is not in excess

Throughout this chapter, Δ*accA* knockout strains of *N. gonorrhoeae* did not grow microaerobically or consume NO_2^- unless the media was supplemented with excess Cu. This suggests that AccA, a PCu_AC metallochaperone homologue, is not required to metalate, and thereby activate, AniA *in vivo* when intracellular Cu availability is increased. This mimics previous studies determining the role of PCu_AC in metalation of cytochrome *c* oxidases. The bacterium *Rhodobacter sphaeroides* contains two cytochrome *c* oxidase proteins, an *aa_3-type CcO* and a *cbb_3-type CcO* which contain a Cu_A and a Cu_B site respectively.[94] PCu_AC is required to metalate both proteins. A mutant strain of *Rhodobacter sphaeroides* lacking PCu_AC resulted in a decrease in fully assembled cytochrome *c* oxidase for both types of cytochrome proteins. This defect, as in the case of AniA in a strain lacking AccA in *N. gonorrhoeae,* was restored upon Cu supplementation during growth.[94]

It is well-established that Cu is not freely available within the cell and is instead buffered by unknown small molecules or amino acids.[140] Furthermore, if a cuproprotein's affinity for Cu is higher than the buffer, Cu will ultimately flow down the thermodynamic gradient until the protein is metalated.[54] As noted in Chapter 1, Cu sits at the top of the Irving-Williams series.[17] This means that intracellular Cu concentration must be tightly regulated so to prevent incorporation of Cu into any incorrect protein and toxicity does not occur.[56] Therefore, it is plausible that addition of Cu to the growth media has increased the bioavailable pool of Cu and as such, AniA can now acquire Cu without the need of a dedicated Cu metallochaperone (Figure 5.20b). This is reflected by the restored microaerobic growth and NO_2^- consumption in the Δ*accA* strain of *N. gonorrhoeae* when Cu is supplemented into the growth media. Furthermore, the effects of Cu toxicity can be observed when Cu is supplemented into the cells during growth. This suggests that the bioavailable pool of buffered Cu is saturated in these conditions, resulting in Cu toxicity and decreased growth.[54] This is further confirmed by initial optimisation experiments, in which addition of 100 μM Cu to the growth media resulted in a severe growth defect.

5.6.2 The Cu primary site is required to metalate AniA *in vivo*

This chapter has highlighted the role of the Cu primary binding site in metalating AniA. A complete removal of this site, ΔCu primary-*accA* resulted in the same phenotype as a complete Δ*accA* knockout

strain. Furthermore, it was identified that at least 3 of the 4 amino acids in this site (H69, M80, H103, and M105) were required to maintain Cu binding or transfer to AniA. We have previously established that the WT AccA protein has a Cu(I) affinity in this site in the femtomolar range (log K_d -16.7 M). This affinity is weakened to picomolar affinity in single Cu primary site mutants (H69A -13.5 M, M80A -13.9 M, H103A -13.9 M, M105A -13.9 M), whilst a complete knockout of the Cu primary site resulted in an affinity in the high nanomolar range (-11.8 M). As we have established, AccA must acquire Cu from the bioavailable buffered pool.[54] The weakened affinity in the Cu primary site may result in AccA not competing for Cu in these conditions until the bioavailability of Cu is increased, as seen previously in Δ*accA* strains. Interestingly, investigations using the single Cu primary site mutants resulted in an intermediate growth and NO_2^- consumption phenotype. The picomolar affinity these mutants have for Cu(I) could result in more competition to acquire Cu from the buffered pool which may explain why, in the case of all the mutants but M80A, this reduced NO_2^- consumption phenotype is restored at 10 hours compared to 8 hours of microaerobic growth (Figure 5.20a). This allows us to estimate the affinity of the periplasmic Cu buffer to be in mid-picomolar range, as it must have a tighter affinity than the ΔCu primary mutant of -11.8 M but a similar, if not slightly weaker, affinity to the single mutants at -13.9 M. We hypothesise that this defect is in Cu acquisition from the buffer, as AniA must be thermodynamically downhill to AccA to acquire Cu. This can be confirmed through direct transfer experiments using purified proteins.

The Cu tract had a reduced growth phenotype compared to the *accA*$^+$ strain. Like the single Cu primary site mutants, the ΔCu tract AccA protein had a picomolar affinity for Cu (Log K_d -14.3 M). As previously discussed, the amino acid residues in the Cu tract may stabilise the Cu primary binding site. It is interesting that the Cu tract mutant growth defect is minor in comparison to the single Cu primary site mutants, due to the similar affinities these proteins have for Cu(I). As previously explained in Chapter 4, there are limitations to the calculated affinity for the ΔCu tract AccA protein and further experimentation is required to confirm this.

5.6.3 The role of AccA during Cu starvation

The human Cu storage protein ceruloplasmin is transported to the urinary tract upon bacterial infection.[141] Ceruloplasmin is known to bind Cu(II) at very tight, high-affinity, sites that are not dialysable or exchangeable.[142] As *N. gonorrhoeae* colonises the urinary tract, there is the possibility

that the pathogen faces Cu limitation, through sequestering of Cu by ceruloplasmin, during colonisation. Treatment with BCS was sufficient to generate artificial Cu starvation within the cell, and resulted in a reduced growth phenotype in the *accA*$^{+}$ strain. The weakened affinity for Cu(I) in the ΔCu tract mutant may explain why the ΔCu tract-*accA* strain could not grow or consume NO_2^- under these conditions, as Cu would flow down the thermodynamic gradient to proteins with stronger Cu affinities. We therefore predict that AccA mutant proteins with weaker affinities, such as the single Cu primary site mutants, would not be able to acquire Cu under these starvation conditions.

Unlike other PCu_AC homologue proteins, AccA has an extended His and Met-rich C-terminal tail.[120] We have previously shown that the C-terminal tail of AccA is required to bind Cu(II) with picomolar affinity (log K_d -12.0 M). However, the denitrification pathway would only be active when very little O_2 is present and therefore, Cu would exist as Cu(I).[128] We previously identified in Chapter 4 that Cu(I) binds to the C-terminal tail with a picomolar affinity (logK_D -10.9 M) and is therefore unlikely to acquire Cu(I) *in vivo*. An alternative role for the C-terminal tail may be as an intermediate buffer site that bridges the periplasmic buffer and the AccA primary site. The C-terminal tail is flexible in structure and therefore could potentially be better at stepwise associate transfer of Cu(I) from a periplasmic buffer molecule than the Cu primary site. Cu would in turn flow down a thermodynamic gradient to the low-energy, high-affinity, Cu primary site which would bind Cu stably (Figure 5.20ci-ii). This role of the C-terminal tail as a periplasmic buffer may explain the slight defects observed during Cu starvation.

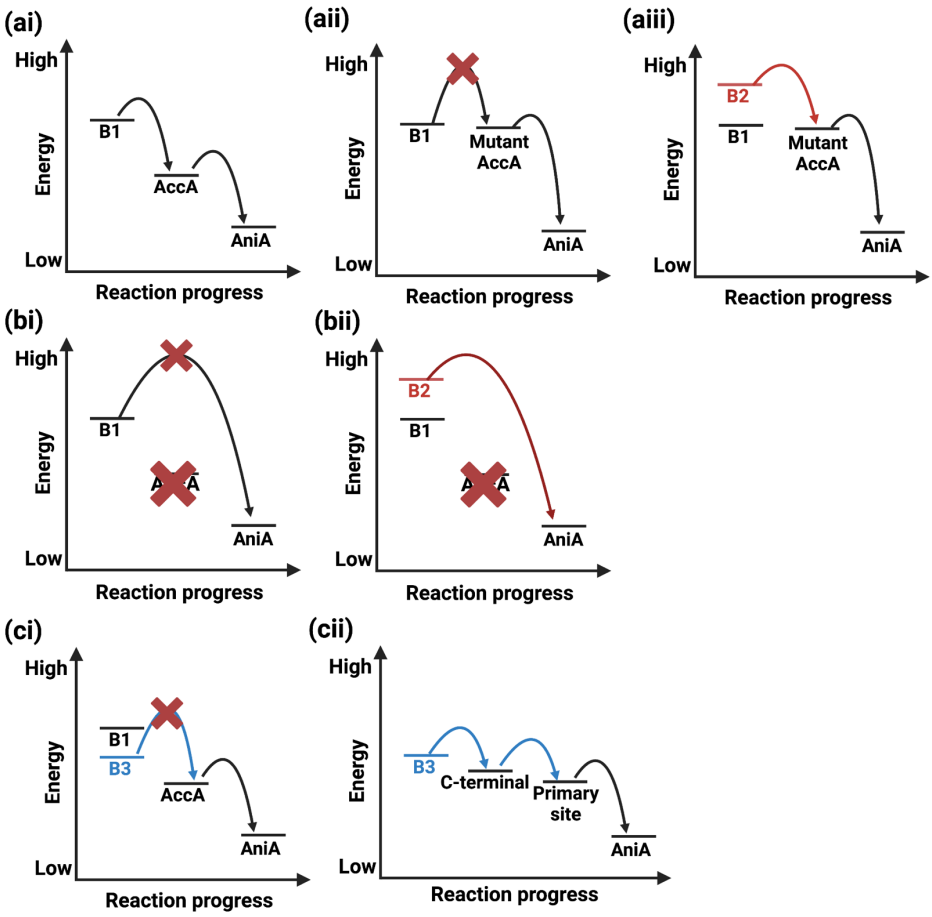

Figure 5.20: Thermodynamic model of Cu-transfer from the periplasmic buffer to AccA and AniA. (a) Transfer of Cu from the periplasmic buffer to AniA. **(ai)** Transfer occurs in a stepwise process from the buffer (B1) to AccA to AniA down a thermodynamic gradient from high energy to low energy sites. **(aii)** Mutant AccA proteins that weaken Cu(I) binding i.e, ΔCu primary are higher energy sites. The energy barrier of transfer of Cu from the buffer (B1) to AccA is too great and AccA, and therefore AniA, is not metalated. **(aiii)** Increasing the bioavailable concentration of Cu (the buffered pool) (B2) increases the energy of the buffer, and the energy barrier of Cu-transfer can be overcome. **(b)** Transfer of Cu from the periplasmic buffer (B1) to AniA when AccA is missing. **(bi)** The energy barrier of Cu-transfer is too high so AniA does not receive Cu. **(bii)** When the periplasmic buffer concentration increases the energy barrier decreases so Cu can be transferred directly from the buffer to AniA. **(c)** Cu-transfer from the periplasmic buffer to AniA during Cu starvation (B3). **(ci)** The energy barrier from the buffer during starvation may be too great to directly metalate the Cu primary site of AccA. **(cii)** A stepwise transfer from the buffer to the C-terminal of AccA to the primary site may be required.

5.6.4 Routing of Cu within the cell

A strain of *N. gonorrhoeae* lacking the *copA1* gene was used to investigate Cu routing within the cell. A Δ*copA1* strain of *N. gonorrhoeae* was more sensitive to Cu as a result of Cu build-up in the cytosol, leading to Cu toxicity. High Cu concentrations supplemented during growth led to a decreased NO_2^- consumption phenotype. However, it is unclear whether a lack of Cu leading to AniA inactivation is the

causative factor, or if this may instead be attributed to redox cycling. The latter may be present due to reaction of excess Cu with NO_2^-, limiting the substrate for AniA to reduce. Measuring the concentration of NO_2^- remaining in the spent media may help determine which of these hypotheses is correct.

During Cu starvation, the Δ*copA1* strain of *N. gonorrhoeae* displayed both an improved growth phenotype and rate of NO_2^- consumption compared to the WT strain. AccA is translocated to the periplasm *via* the Sec secretory pathway. Therefore, AccA folds, and most likely acquires Cu in the periplasm.[143] There is a possibility that the unstructured C-terminal tail could acquire Cu before secretion however it is unlikely that AccA would retain this Cu during secretion. If the periplasmic pool of buffered Cu relied on CopA1 to fill it, then deletion of CopA1 would reduce periplasmic buffered Cu concentration. This would in turn reduce metalation of AccA and ultimately metalation of AniA. This would result in a reduced growth and NO_2^- consumption phenotype, although this was not observed. Instead, the cells demonstrated improved growth and NO_2^- consumption.

We therefore hypothesise that the phenotype observed in the Δ*copA1* strain of *N. gonorrhoeae* was due to cytosolic Cu buffering. A deletion of CopA1 would trap Cu in the cytosol, increasing the cytosolic buffered pool for protein targets.[54] There are no known cytosolic Cu proteins identified in *N. gonorrhoeae,* however, cytochrome cbb_3 oxidase is localised to the inner membrane and requires nutrient Cu provided *via* the P_{1B}-type ATPase CopA2, also known as CcoI.[71] It therefore, may be plausible that the number of fully assembled cytochrome cbb_3 oxidase units is greater in a Δ*copA1* strain of *N. gonorrhoeae* compared to the WT under Cu starvation conditions which increases the cytosolic Cu pool. Studies have shown that the CcoP and CcoQ subunits of cytochrome cbb_3 oxidase are electron donors to AniA and therefore NO_2^- consumption is dependent upon the rate of electron transfer.[115,116,117] Therefore, the improved growth phenotype observed in the Δ*copA1* mutant is most likely not due directly to AniA metalation.

Chapter 6: Characterisation of AniA properties and Cu-transfer from AccA to AniA *in vitro* by monitoring the Type-1 Cu binding site of AniA

Studies detailed in Chapters 4 and 5 have characterised that AccA binds Cu with high affinity and is required to activate AniA *in vivo*. We are interested in AccA's ability to metalate AniA *in vitro.* AniA possesses two Cu binding sites; Type-1 (T1) and Type-2 (T2). The *holo*-T1 binding site displays distinct spectroscopic features that can be monitored, and is the reason why Cu-dependant nitrite reductase proteins are known as blue copper proteins.[21] These features allow us to directly measure Cu binding in the T1 site of AniA following incubation with Cu-loaded AccA. The following experiments were performed with WT, ΔT1, and ΔT2 mutants of soluble AniA proteins, lacking both the signal sequence and the C-terminal glycosylation site (Figure 6.1, Table 6.1).

```
        50         60         70         80         90
 AAQATAETP  AGELPVIDAV  TTHAPEVPPA  IDRDYPAKVR  VKMETVEKTM
       100        110        120        130        140
KMDDGVEYRY  WTFDGDVPGR  MIRVREGDTV  EVEFSNNPSS  TVPHNVDFHA
       150        160        170        180        190
ATGQGGGAAA  TFTAPGRTST  FSFKALQPGL  YIYHCAVAPV  GMHIANGMYG
       200        210        220        230        240
LILVEPKEGL  PKVDKEFYIV  QGDFYTKGKK  GAQGLQPFDM  DKAVAEQPEY
       250        260        270        280        290
VVFNGHVGAI  AGDNALKAKA  GETVRMYVGN  GGPNLVSSFH  VIGEIFDKVY
       300        310        320        330        340
VEGGKLINEN  VQSTIVPAGG  SAIVEFKVDI  PGNYTLVDHS  IFRAFNKGAL
       350        360
GQLKVEGAEN  PEIMTQKLSD  TAYA
```

Figure 6.1: Amino acid sequence of recombinant AniA protein. The Cu binding sites are underlined and coloured differently; Type-1 (red), Type-2 (blue).

Table 6.1: List of modified AniA proteins. For AccA proteins see Table 4.1.

Protein	Modifications
WT-AniA	N-terminal signal sequence and C-terminal glycosylation site removed.
ΔT1-AniA	N-terminal signal sequence and C-terminal glycosylation site removed. H134A, C175A, H183A, M188A.
ΔT2-AniA	N-terminal signal sequence and C-terminal glycosylation site removed. H139A, H174A, H329A.

6.1 Generation of *apo*-AniA and metal loading *via* Cu ions

6.1.1 Generation of *apo*-AniA

Other Cu-NIRs reported in the literature were typically purified in the partially or fully metalated forms. In case of loss of Cu from the enzyme, typically the T2-site, reconstruction of the Cu sites was usually performed by incubating the enzyme for a prolonged period in the presence of excess Cu ions, or by adding Cu ions to protein purification buffers. It was difficult to find any information or examples regarding generation of *apo*-AniA. Experiments investigating direct transfer of Cu from AccA required *apo*-AniA. We, therefore, conducted a purification protocol to generate *apo*-AniA.

Many Cu-NIRs are overexpressed by *E. coli* cells when cultured in growth media supplemented with Cu salts. This ensures that the enzyme acquires Cu during protein expression. To ensure AniA would be metal-free, we overexpressed the protein in *E. coli*, in standard LB broth. Care was taken throughout the protein purification protocol to ensure there was no contamination with Cu ions. Fresh purification columns were used for AniA. ICP-MS analysis of purified AniA confirmed that the protein was metal-free. This was confirmed through ICP-MS analysis (Table 6.2).

Table 6.2: ICP-MS analysis of *apo*-AniA confirming metal-free purification.

Protein	[Cu]/[AniA]
WT-AniA	0.03

6.1.2 AniA can be metalated directly by Cu ions

First, it was determined whether the two Cu sites in the purified *apo*-AniA protein could be reconstituted directly with Cu ions. Following the common approach in the literature, an excess of $CuCl_2$ (6 molar equivalents) was added to a solution of *apo*-AniA. This addition of Cu(II) ions into *apo*-AniA resulted in the appearance of two distinct absorbance peaks at 460 and 600 nm in the optical spectrum of the protein, both of which increased in intensity over time (Figure 6.2a). These features are characteristic of the Type-1 Cu (T1Cu) centre in Cu-NIRs. An isosbestic point was also identified at 420 nm, indicating the presence of only two species in the reaction, namely *apo*-AniA and T1Cu-loaded AniA.

The T2Cu centre in AniA is optically silent. Therefore, to determine whether this site was also loaded with Cu, AniA protein was desalted on a PD-10 column to remove any excess unbound Cu. The eluent was then subjected to ICP-MS analysis, which revealed a final stoichiometry of two Cu per AniA monomer. Taken together with data regarding loading into the T1Cu site, this stoichiometry suggests that both the T1 and T2 sites in AniA are fully metalated when incubated with Cu(II) salts (Figure 6.2a).

The above Cu loading experiment was then repeated in different buffers to determine the optimal buffer to use for further Cu-transfer experiments from AccA to AniA (Figure 6.2b). The end point absorbances after 2 hours of incubation at 460 and 600 nm were plotted. Prior experiments described in Chapter 4, to determine Cu affinity of AccA were conducted in 50 mM MOPS pH 7.2, therefore, this buffer was selected as the starting point for experiments. The other buffers used were: 50 mM MOPS pH 7.5, 50 mM Tris pH 7.5, 50 mM HEPES pH 7.5, and 50 mM KPI pH 7.5 (Figure 6.2b). The T1Cu site of AniA was metalated in all cases, regardless of the buffer used. Both the 50 mM Tris pH 7.5 and 50 mM HEPES pH 7.5 buffers resulted in the highest T1Cu absorbance peaks following 2 hours of incubation (Figure 6.2b). However, the HEPES pH 7.5 buffer produced inconsistencies between experiments (data not shown). Therefore, the Tris pH 7.5 buffer was selected as the optimum buffer for Cu-transfer from solution to AniA.

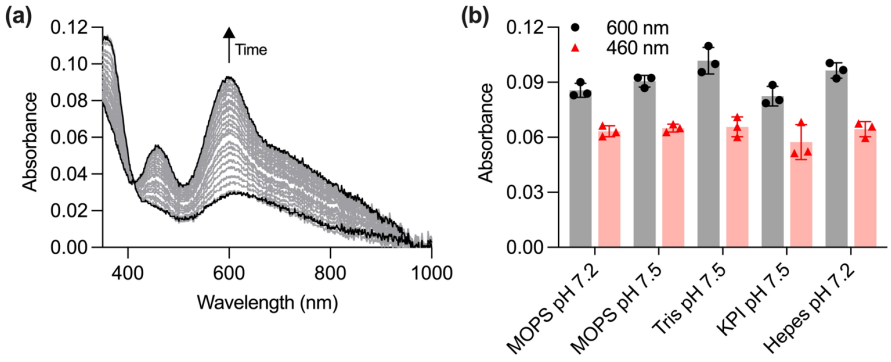

Figure 6.2: The Type-1 Cu site of AniA can be monitored spectroscopically. (a) UV-VIS spectra of AniA during Cu loading over time from 450 – 1000 nm. Data were corrected to a 0 µM Cu control and using an isosbestic point at 420 nm. Black lines represent time = 0 and 125 minutes. Grey lines represent intermediate points. **(b)** End-point of the formation of the T1 Cu site of AniA at 600 (black circles) and 460 nm (red triangles). Absorbance was measured in 5-minute intervals for 120 minutes of 70 µM WT-AniA in the presence of excess $CuCl_2$. Experiments were performed in 50 mM of the following buffers: MOPS pH 7.2, MOPS pH 7.5, Tris pH 7.5, HEPES pH 7.5, and KPI pH 7.5. Data points represent mean of n = 3. Error bars represent standard deviation. Cu-transfer to AniA was determined to be optimal in Tris pH 7.5 and therefore, all subsequent experiments transfer were performed in this buffer.

6.2 The T1Cu site is preferentially metalated over the T2Cu site

There are three ways in which Cu could load into AniA, dependent upon the Cu affinities of the two Cu sites. Cu could load into both sites equally if both sites bind Cu with similar affinities. Cu could load first into the T1Cu site if this site binds Cu more strongly than the T2Cu site. Alternatively, Cu could load first into the T2Cu site if this site binds Cu more strongly than the T1Cu site.

To distinguish between the possibilities, loading into the T1Cu binding site was examined at different Cu:AniA stoichiometries between 0 – 2.0. In parallel, we also examined the loading of two AniA variants: ΔT1-AniA, in which His134, Cys175, His183, and Met188 that form the T1Cu binding site were mutated to Ala, and ΔT2-AniA, in which His139, His174, and His329 that form the T2Cu binding site were mutated to Ala (Table 6.1).

First, we confirmed that there was no change in spectral properties in the solution absorbances at 600 or 460 nm when the ΔT1-AniA protein was used compared to the WT AniA protein. This confirmed that the T1Cu binding site was successfully deleted. Absorbances at 600 and 460 nm, corresponding to the T1Cu centre, increased as expected for both the WT-AniA and the ΔT2-AniA proteins. Both absorbance values increased linearly with Cu concentrations and saturated at 1 molar equivalent of Cu(II) (Figure 6.3a-b). This findings suggest that Cu loads initially into the T1Cu site in AniA. Cu may load into the T2Cu site after the T1Cu site is fully metalated, at 1 molar equivalent of Cu.

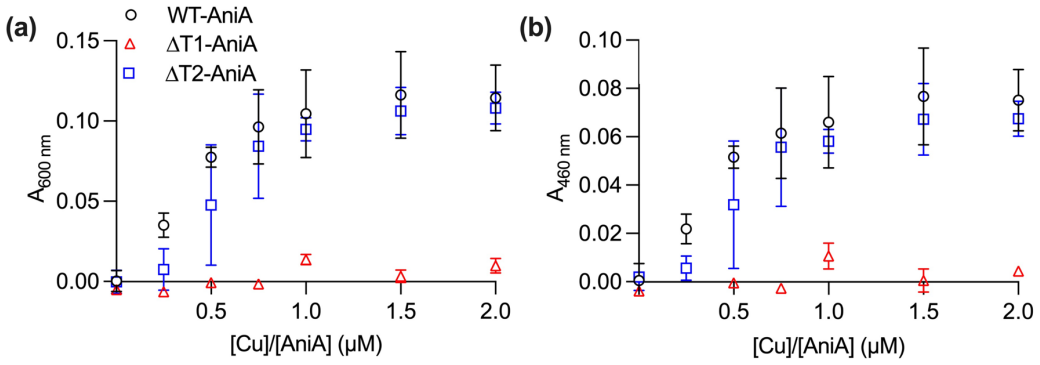

Figure 6.3: Cu-transfer from soluble Cu to AniA saturates the T1 Cu binding site at 1 equivalent of Cu in WT- and ΔT2-AniA proteins. Endpoint of Cu-transfer to the T1 site of AniA proteins at 600 nm at different Cu concentrations. Absorbance was measured at 600 nm **(a)** and 460 nm **(b)** following incubation of 185 minutes of 70 μM WT-AniA (black open circles), ΔT1-AniA (red triangles), and ΔT2-AniA (blue squares) with excess $CuCl_2$ salt. Data points represent the mean of n = 2. Error bars represent standard deviation.

6.3 Cu loading into the T1Cu site is slow

Cu loading into the T1Cu site of WT AniA was slow. The absorbances at 600 (Figure 6.4a) and 460 (Figure 6.4b) nm did not plateau until more than 60 minutes after addition of free Cu(II) in the absence of AccA. Interestingly, Cu loading into the T1Cu site in the ΔT2-AniA mutant protein was much faster (Figure 6.5). The absorbances at 600 and 460 nm in the ΔT2-AniA mutant plateaued after only 10 minutes incubation, compared to 120 minutes for the WT-AniA protein. These results suggest that Cu-binding to the T2-site is a rate-limiting step in metalation of AniA.

6.3.1 Cu loading from AccA to AniA is slower than from free Cu(II) ions

Since we have established that *apo*-AniA can become metalated directly by 'free' Cu(II) ions, we wished to determine whether *apo*-AniA can also be metalated by *holo*-AccA. To prepare *holo*-AccA, we incubated *apo*-AccA with an excess of Cu(I) or Cu(II) and removed any unbound Cu ions on a PD-10 desalting column. Previous experiments described in Chapter 4 consistently showed that incubation of AccA with an excess of Cu(I) led to generation of Cu(I)Cu(II)-AccA, while incubation with an excess of Cu(II) led to generation of Cu(II)Cu(II)-AccA (Table 4.3). In both cases, a stoichiometry of 2:1 total Cu:AccA was obtained.

As each monomer of *apo*-AniA also binds two Cu atoms (T1Cu and T2Cu), theoretically, 1 molecule of *holo*-AccA could fully load 1 molecule of *apo*-AniA with Cu. However, in this experiment, to ensure full metalation of AniA, *holo*-AccA was added always in excess, at three times the concentration (210 μM) of AniA (70 μM). Free Cu(II) in solution was used as a positive control of Cu loading to AniA. To keep the same total Cu:AniA stoichiometry, six times the concentration of soluble Cu(II) (420 μM) was added, relative to AniA (70 μM). This stoichiometry of 6 total Cu per 1 AniA monomer replicates the experiment with 3:1 AccA:AniA.

Like 'free' Cu(II), addition of either Cu(I)Cu(II)-AccA or Cu(II)Cu(II)-AccA to *apo*-AniA led to an increase in the absorbances at 600 and 460 nm of AniA over time, indicating that AccA was indeed able to metalate the T1Cu site of AniA. Interestingly, Cu loading by AccA was slower than loading by 'free' Cu(II) (Figure 6.4). AniA absorbances at 600 and 460 nm did not plateau until after 150 minutes after addition of Cu(II)Cu(II)-AccA (Figure 6.4). These absorbances developed even more slowly after addition of Cu(I)Cu(II)-AccA and no plateau was reached during the course of experimentation (Figure 6.4).

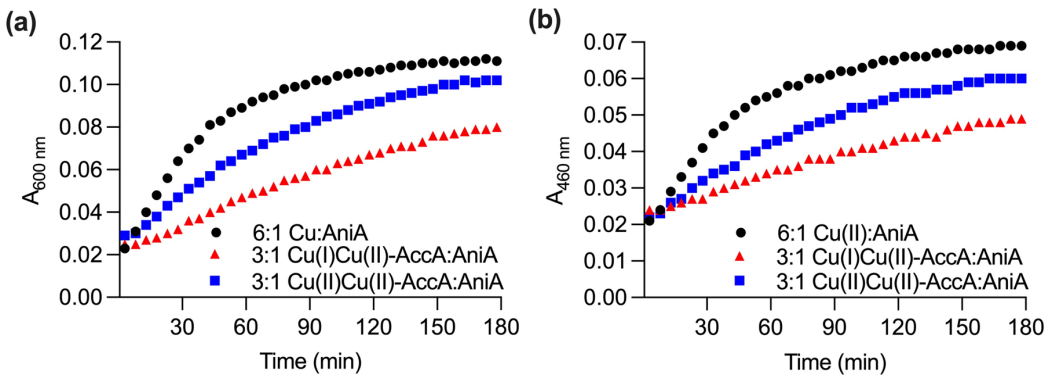

Figure 6.4: AniA can acquire Cu from AccA however, it is slower than directly from the buffer. Monitoring the formation of the T1Cu site of ΔWT-AniA over time. Absorbance was measured at 600 nm **(a)** and 460 nm **(b)** 5-minute intervals over 185 minutes of 70 μM WT-AniA in the presence of excess $CuCl_2$ (black circles), excess Cu(I) loaded AccA (red triangles), and excess Cu(II) loaded AccA (blue squared). Experiments were performed in duplicate with only one replicate shown.

As observed previously with 'free' Cu(II), loading of the T1Cu site in the ΔT2-AniA mutant by either form of Cu-loaded AccA was much faster than loading of the T1Cu site in the WT AniA protein (Figure 6.5). Likewise, the final T1Cu absorbances at 600 and 460 nm in ΔT2-AniA after Cu loading from Cu(I)Cu(II)-AccA were much lower than the after Cu loading from Cu(II)Cu(II)-AccA (Figure 6.5). The optical properties of the T1Cu centre in AniA only appear when the T1 site is loaded with Cu(II). These features disappear when the Cu centre is reduced to Cu(I). Therefore, it is possible that Cu(I)Cu(II)-AccA partially loads the T1Cu site of AniA with Cu(I). To avoid complications arising from mixed redox species, in all subsequent experiments, only Cu(II)Cu(II)-loaded AccA was used.

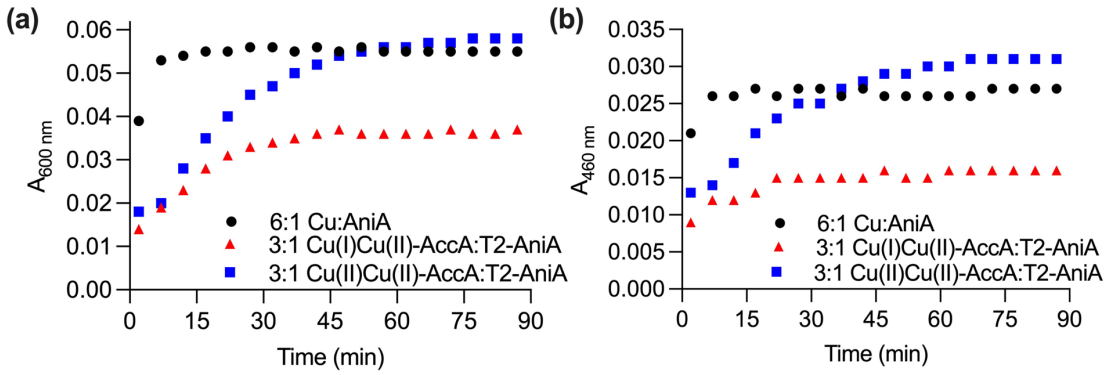

Figure 6.5: A ΔT2-AniA protein acquires Cu quicker than from the WT AniA protein. Monitoring the formation of the T1Cu site of ΔT2-AniA over time. Absorbance was measured at 600 nm **(a)** and 460 nm **(b)** for 5-minute intervals over 185 minutes of 70 μM WT-AniA in the presence of excess $CuCl_2$ (black circles), excess Cu(I) loaded AccA (red triangles), and excess Cu(II) loaded AccA (blue squared). Experiments were performed in duplicate with only one replicate shown.

6.4 Investigation of Cu-transfer from AccA and mutant AccA proteins to AniA

6.4.1 Cu-transfer from Cu(II)-loaded AccA to AniA saturates the T1 site at 1 equivalent of AccA in both WT- and ΔT2-AniA proteins

In the initial experiment, an excess of Cu-loaded AccA was added to *apo*-AniA. To determine the precise stoichiometry of Cu loading into AniA, the formation of the T1Cu centre was monitored upon addition of different molar equivalents of Cu(II)Cu(II)-AccA. Figure 6.6di-ii shows that the final absorbances of WT AniA protein at 600 and 460 nm increased linearly with increasing equivalents of Cu(II)Cu(II)-AccA. A clear end point was observed at 1 molar equivalent of Cu(II)Cu(II)-AccA per WT AniA monomer (Figure 6.6d). Identical titration

curves were obtained with the ΔT2-AniA protein (Figure 6.6d). As expected, no spectral features were observed with the ΔT1-AniA protein (Figure 6.6). The observed stoichiometry of 1:1 Cu(II)Cu(II)-AccA:AniA was interesting, as it suggests that both Cu binding sites of AccA are used to metalate a single AniA monomer.

The absorbance at 600 and 460 nm did not change when increasing concentrations of Cu(II)-loaded AccA were incubated with ΔT1-AniA (Figure 6.6b). The increase in absorbance at 600 and 460 nm was faster in a ΔT2-AniA protein compared to WT-AniA, regardless of concentration of Cu(II)-loaded AccA (Figure 6.6c). The absorbance at 600 and 460 nm saturated after 60 minutes in the ΔT2-AniA protein, compared to 120 minutes in the WT-AniA protein. This further supports the earlier conclusion that the T1Cu site of AniA is metalated faster when the T2 site is missing.

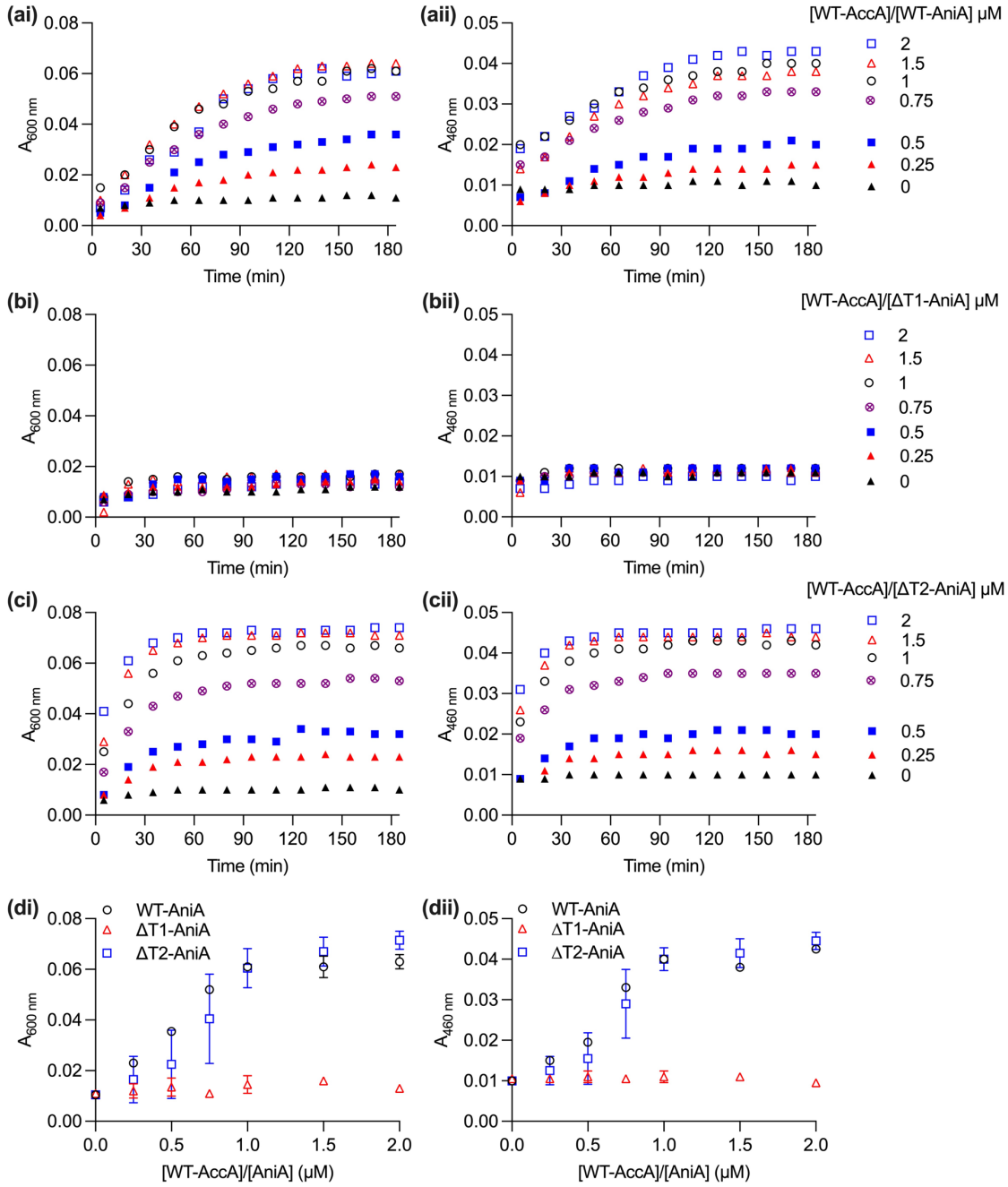

Figure 6.6: Cu-transfer from Cu(II)Cu(II)-WT AccA to AniA saturates the T1 Cu-binding site at 1 equivalent of protein in WT- and ΔT2-AniA proteins. Cu-transfer to the T1Cu site of **(a)** WT-, **(b)** ΔT1-, and **(c)** ΔT2-AniA at different Cu(II)Cu(II)-WT AccA protein concentrations over time. Absorbance was measured at 600 nm **(i)** and 460 **(ii)** in 5-minute intervals over 185 minutes of 70 µM WT-AniA in the presence of 0 (black triangle), 0.25 (red triangle), 0.5 (blue square), 0.75 (purple circle with cross), 1 (black open circle), 1.5 (red open triangle), and 2 (blue open square) equivalents of Cu(II)-loaded AccA. Experiments were performed in duplicate with only one replicate shown. **(d)** Endpoint of Cu-transfer to the T1 site of AniA proteins after incubation with different Cu(II)Cu(II)-AccA concentrations. Absorbance was measured at 600 nm **(di)** and **(dii)** following incubation of 185 minutes of 70 µM WT-AniA (black open circles), ΔT1-AniA (red triangles), and ΔT2-AniA (blue squares) with WT-AccA. Data points represent the mean of n = 2. Error bars represent standard deviation.

The increased rate in T1Cu site loading in a ΔT2-AniA mutant was further investigated by determining the initial rate of absorbance increase at 600 and 460 nm after incubation with Cu(II)Cu(II)-AccA. This was determined by calculating the slope of the curve until the curve plateaued. Both the WT-AniA and ΔT2-AniA proteins showed an increase in the rate of absorbance increase at both wavelengths, which saturated at 1 molar equivalent of AccA per AniA monomer (Figure 6.7). However, the rate of absorbance increase was higher in the ΔT2-AniA mutant regardless of concentration of AccA, compared to WT-AniA. Thus, it appears that the rate of loading for the T1Cu site is limited by the T2Cu site.

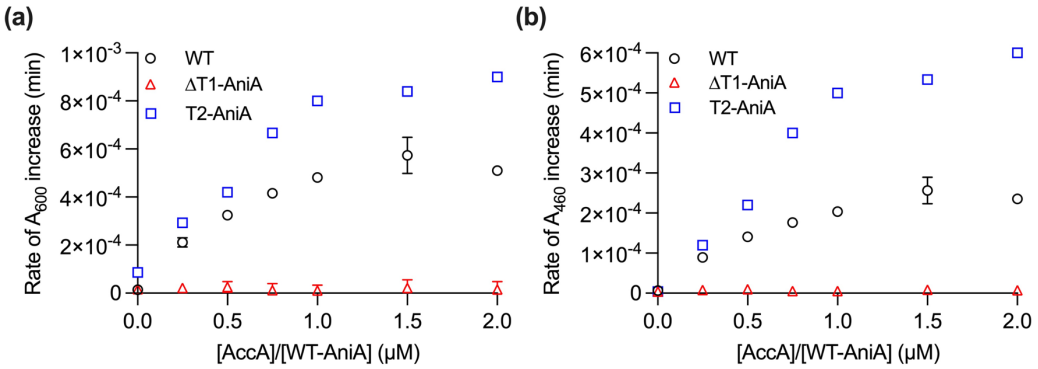

Figure 6.7: The rate of Cu-transfer to AniA and AniA mutant proteins. The rate of Cu-transfer from different concentration of AccA to AniA was determined using the initial linear slope of increasing absorbance at 600 nm **(a)** and 460 **(a)** over 5-minute intervals of 70 μM WT-AniA (black circles), ΔT1-AniA (red triangles), and ΔT2-AniA (blue squares) in the presence of increasing concentrations of WT AccA Data points represent the mean of n = 2 except for the T2 mutant where only one data set is shown. Error bars represent standard deviation.

6.4.2 Cu-transfer from Cu(II)-loaded ΔCu primary AccA to WT-AniA saturates the T1 site at 1 equivalent of AccA

Chapter 5 established that the primary Cu site of AccA is required to activate AniA *in vivo*, as the *N. gonorrhoeae* ΔCu primary-*accA* mutant strain phenocopied the Δ*accA* complete deletion mutant strain and failed to grow in the absence of supplemental Cu. We, therefore, were interested whether a ΔCu primary-AccA protein impacts Cu loading of AniA *in vitro*. The formation of the T1Cu centre in AniA was monitored at 600 and 460 nm ,following addition of different concentrations of Cu(II)-loaded ΔCu primary AccA. It must be noted that previous stoichiometry experiments in Chapter 4 of the ΔCu primary AccA protein identified a mixed species of Cu(II)-AccA and Cu(II)Cu(II)-AccA. Interestingly, the Cu(II)-loaded ΔCu primary

AccA protein was also able to metalate the T1Cu site in AniA with Cu. The stoichiometry of Cu loading was again 1:1 Cu(II)-loaded ΔCu primary AccA:AniA (Figure 6.8). The loading of AniA by the AccA protein *in vitro* is a downhill transfer and relies on AniA binding Cu tighter than AccA. Weakening the affinity of AccA for Cu such as accomplished using the ΔCu primary mutant, creates a more thermodynamically favourable transfer from AccA, as opposed to the WT protein.

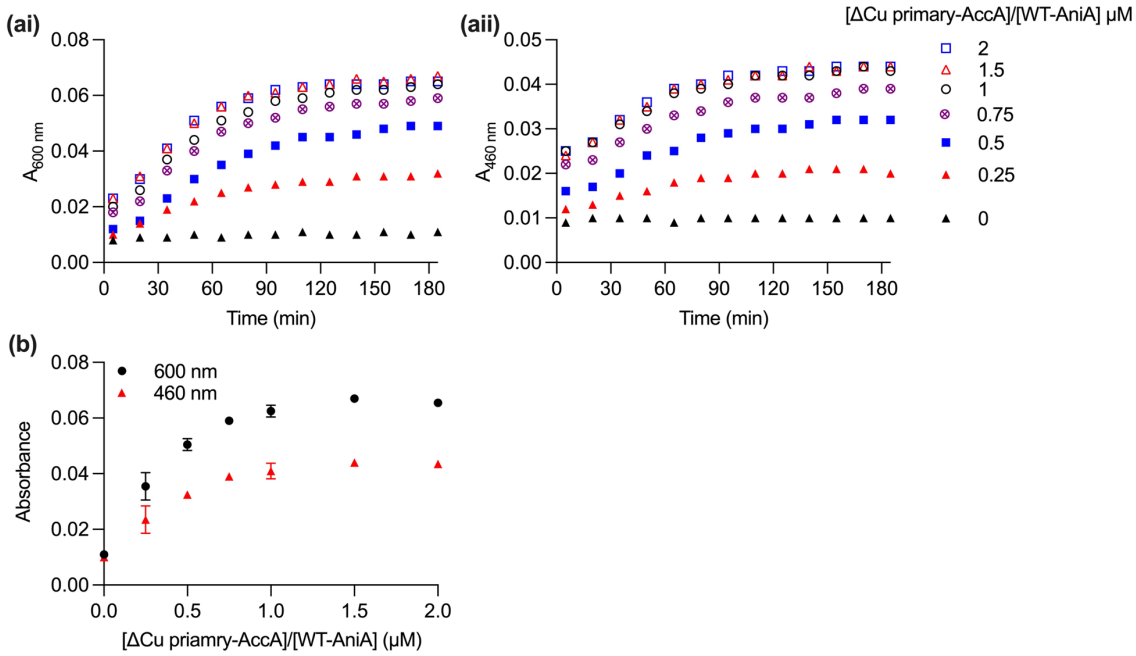

Figure 6.8: Cu-transfer from Cu(II)Cu(II)-ΔCu primary AccA to AniA saturates the T1 Cu-binding site at 1 equivalent of protein in WT-AniA. (a) Cu-transfer to the T1 site of WT-AniA at different Cu(II)Cu(II)-ΔCu primary AccA protein concentrations over time. Absorbance was measured at 600 nm **(ai)** and 460 **(aii)** in 5-minute intervals over 185 minutes of 70 μM WT-AniA in the presence of 0 (black triangle), 0.25 (red triangle), 0.5 (blue square), 0.75 (purple circle with cross), 1 (black open circle), 1.5 (red open triangle), and 2 (blue open square) equivalents of Cu(II)Cu(II)-ΔCu primary AccA. Experiments were performed in duplicate but only one replicate shown. **(b)** Endpoint of Cu-transfer to the T1Cu site of WT AniA after incubation with different Cu(II)Cu(II)-ΔCu primary AccA concentrations. Absorbance was measured at 600 nm (black circles) and 460 nm (red circles). Data points represent the mean of n = 2. Error bars represent standard deviation.

6.4.3 Cu-transfer from Cu(II)-loaded ΔCu tract AccA to WT-AniA saturates the T1 site at 1 equivalent of AccA

Chapter 5 established that the Cu tract of AccA is required to fully activate and, therefore, metalate AniA *in vivo*. The *N. gonorrhoeae* ΔCu tract *accA* mutant strain showed a decreased growth and NO_2^- consumption phenotype. We are therefore interested in the potential impact of a ΔCu tract AccA protein upon Cu-transfer to AniA *in vitro.* The formation of the T1Cu binding site was monitored by plotting the absorbance at 600 and 460 nm, following incubation of WT-AniA with different concentrations of Cu(II)-loaded ΔCu tract AccA. Similar to the ΔCu primary AccA mutant, previous stoichiometry experiments in Chapter 4 identified that the ΔCu tract mutant bound Cu(II) in a mixed stoichiometry of Cu(II)-AccA and Cu(II)Cu(II)-AccA (Table 4.3). The absorbance at 600 and 460 nm increased linearly over the course of 120 minutes and then plateaued following incubation, regardless of the concentration of Cu(II)-loaded ΔCu tract AccA (Figure 6.9a).

The endpoint of absorbance at 600 and 460 nm for each concentration of ΔCu tract AccA was plotted. The absorbance at both 600 and 460 nm increased linearly and plateaued at 1 equivalent of Cu(II)-loaded ΔCu tract AccA (Figure 6.9b). Each ΔCu tract-AccA protein was previously identified to contain two Cu atoms. Therefore, the absorbance plateaued and the T1 site saturated, at two equivalents of Cu(II) atoms per monomer of AniA.

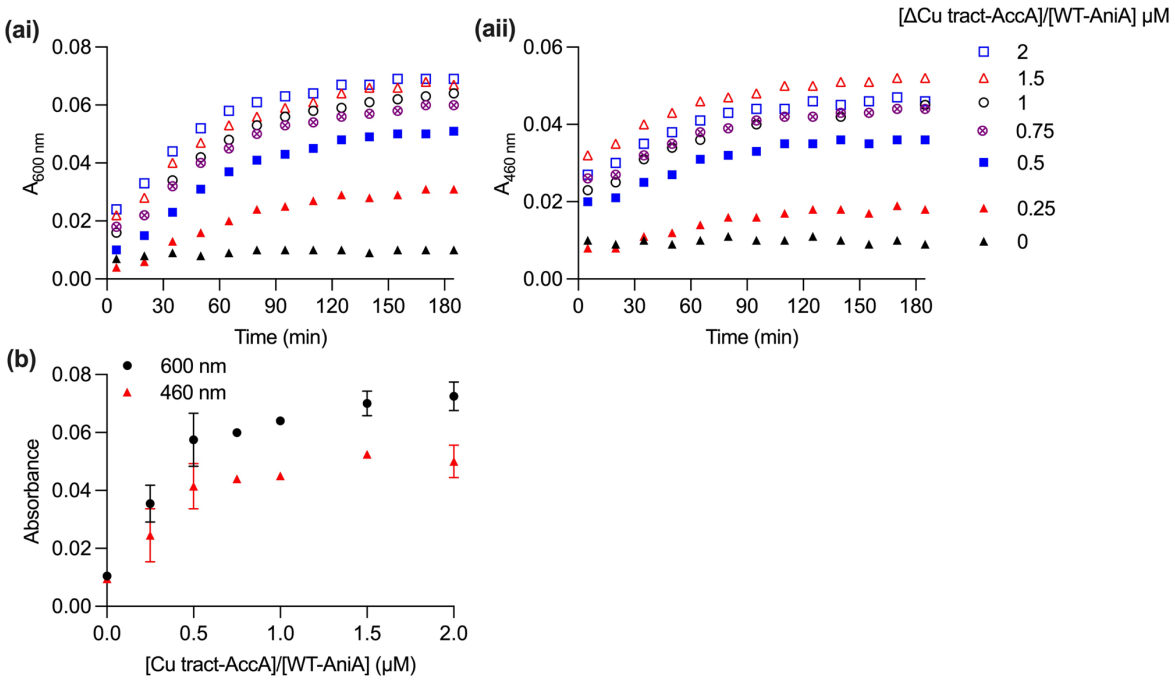

Figure 6.9: Cu-transfer from Cu(II)Cu(II)-ΔCu tract AccA to AniA saturates the T1 Cu-binding site at 1 equivalent of protein in WT-AniA. (a) Cu-transfer to the T1Cu site of WT-AniA at different Cu(II)Cu(II)-Cu tract AccA protein concentrations over time. Absorbance was measured at 600 nm **(ai)** and 460 **(aii)** in 5-minute intervals over 185 minutes of 70 μM WT-AniA in the presence of 0 (black triangle), 0.25 (red triangle), 0.5 (blue square), 0.75 (purple circle with cross), 1 (black open circle), 1.5 (red open triangle), and 2 (blue open square) equivalents of Cu(II)Cu(II)-ΔCu tract AccA. Experiments were performed in duplicate but only one replicate shown. **(b)** Endpoint of Cu-transfer to the T1Cu site of WT AniA after incubation with different Cu(II)Cu(II)-ΔCu tract AccA concentrations. Absorbance was measured at 600 nm (black circles) and 460 nm (red circles). Data points represent the mean of n = 2. Error bars represent standard deviation.

6.4.4 Cu-transfer from Cu(II)-loaded ΔC-terminal AccA to WT-AniA saturates the T1 site at 1 equivalent of AccA

Chapter 5 established that the C-terminal of AccA does not have key role in metalating AniA *in vivo*. The *N. gonorrhoeae* ΔC-terminal *accA* mutant strain showed slight growth and NO_2^- consumption defects during Cu starvation. We are, therefore, interested in whether a ΔC-terminal AccA protein impacts Cu-transfer to AniA *in vitro*. The formation of the T1Cu binding site was monitored by plotting the absorbance at 600 and 460 nm following incubation of WT-AniA with different concentrations of Cu(II)-loaded ΔC-terminal AccA. Previous stoichiometry experiments using Cu(II) loaded ΔC-terminal AccA identified that it only bound one equivalent of Cu as Cu(II)-AccA (Table 4.3). The absorbance at 600 nm increased linearly over the course of 135 minutes then plateaued, regardless of the concentration of ΔC-terminal-AccA incubated with AniA (Figure 6.10ai). Interestingly, the absorbance at 460

nm plateaued after 120 minutes (Figure 6.10aii). Furthermore, the final absorbance at 600 and 460 nm when Cu was in excess was lower, after 180 minutes of AniA incubation with ΔC-terminal-AccA compared to WT AccA and the other AccA mutants (Figure 6.5a-Figure 6.10a). This suggests that the C-terminal tail may play a role in metalating the T1 site of AniA.

The endpoint of absorbance at 600 and 460 nm for each concentration of ΔC-terminal-AccA was plotted. The absorbance at both 600 and 460 nm increased linearly and plateaued at 1 equivalent of Cu(II)-loaded ΔC-terminal-AccA (Figure 6.10b). Each ΔC-terminal AccA protein was previously identified to contain one Cu atom. Therefore, the absorbance plateaued and the T1 site saturated at one equivalent of Cu(II) atoms per monomer of AniA. This means that the T2-AniA site was not metalated until after the T1 site had been saturated, suggesting that the C-terminal tail of AccA may have a role in loading the T2 site of AccA.

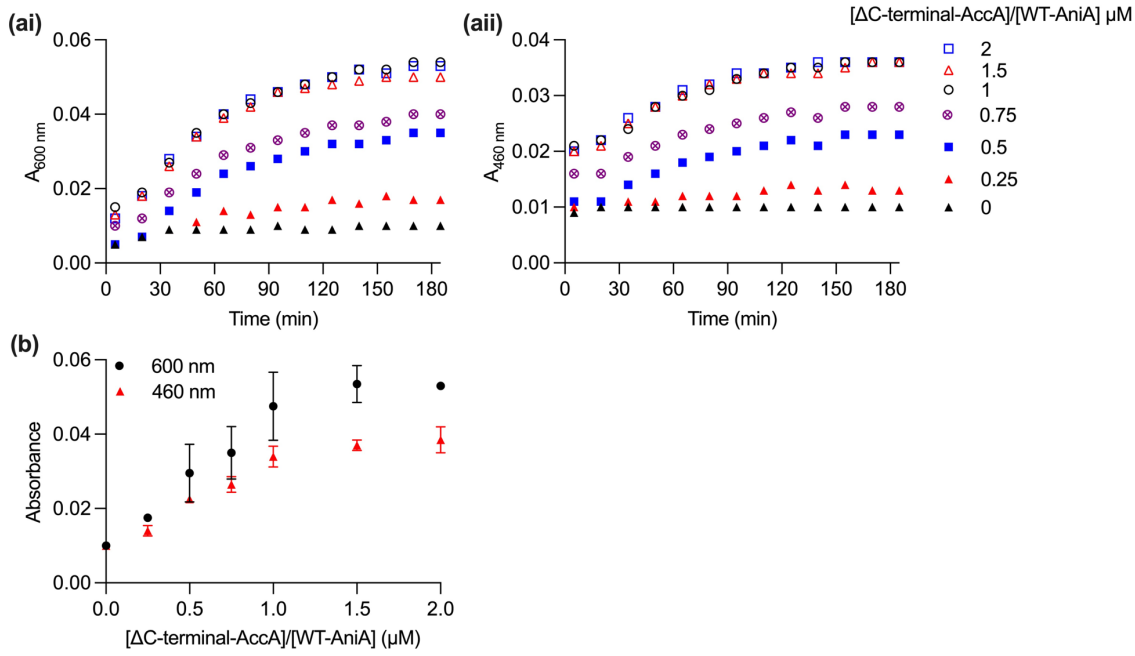

Figure 6.10: Cu-transfer from Cu(II)-ΔC-terminal AccA to AniA saturates the T1 Cu-binding site at 1 equivalent of protein in WT-AniA. (a) Cu-transfer to the T1Cu site of WT-AniA at different Cu(II)-ΔC-terminal AccA protein concentrations over time. Absorbance was measured at 600 nm **(ai)** and 460 **(aii)** in 5-minute intervals over 185 minutes of 70 μM WT-AniA in the presence of 0 (black triangle), 0.25 (red triangle), 0.5 (blue square), 0.75 (purple circle with cross), 1 (black open circle), 1.5 (red open triangle), and 2 (blue open square) equivalents of Cu(II)-ΔC-terminal AccA. Experiments were performed in duplicate but only one replicate shown. **(b)** Endpoint of Cu-transfer to the T1Cu site of WT AniA after incubation with different Cu(II)-ΔC-terminal AccA concentrations. Absorbance was measured at 600 nm (black circles) and 460 nm (red circles). Data points represent the mean of n = 2. Error bars represent standard deviation.

6.4.5 The rate of Cu-transfer to AniA is slower from a ΔC-terminal-AccA protein than from WT-AccA

We have established that WT-AccA, ΔCu primary-AccA, ΔCu tract-AccA, and ΔC-terminal-AccA proteins were all able to metalate the T1Cu site of AniA *in vitro*. However, metalation by the ΔC-terminal-AccA protein resulted in an AniA protein that was less blue, observed spectroscopically as a reduced absorbance at 600 and 460 nm (Figure 6.11a). The initial rates of absorbance increase at 600 and 460 nm were also determined by calculating the slope of the curve until the curve started to plateau. Regardless of the AccA protein used in the experiment, the rates of absorbance increase, and thus the rates of T1Cu loading, all seemed to saturate at 1 molar equivalent of AccA per AniA monomer (Figure 6.11b). However, the initial rates of T1Cu loading appeared to be overall slower using the ΔC-terminal-AccA protein, compared to experiments using WT-, ΔCu primary-, and ΔCu tract-AccA proteins (Figure 6.11b). Thus, it appears that loading of the T1Cu site in AniA, at least *in vitro*, is impaired by deletion of the His/Met-rich C-terminal domain of AccA.

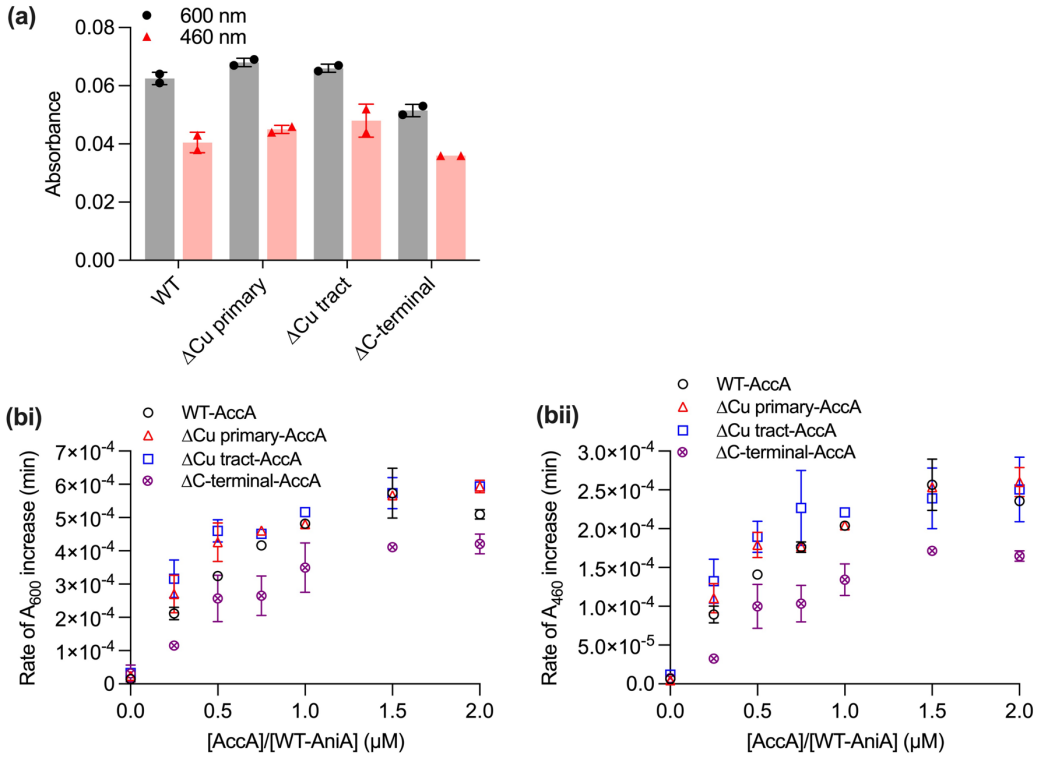

Figure 6.11: The rate of Cu-transfer to AniA. (a) Final absorbance of Cu-transfer from AccA proteins to AniA. The rate of Cu-transfer from different concentration of AccA proteins to AniA was determined using the initial linear slope of increasing absorbance at 600 nm **(bi)** and 460 **(bii)** in 5-minute intervals of 70 μM WT-AniA in the presence of increasing concentrations of WT AccA (black circles), ΔCu primary AccA (red triangles), ΔCu tract AccA (blue squares), and ΔC-terminal AccA (purple circles with cross). Data points represent the mean of n = 2. Error bars represent standard deviation.

6.5 Cu-binding to AniA induces trimerisation

As previously discussed, the *apo*-form of AniA, and indeed other CuNIRs, have not been extensively studied. AniA, and many other CuNIR proteins, are known to be homotrimers.[26,27,114] However, the X-ray crystal structure of AniA shows that the T2Cu centre is located at the monomer interface and is coordinated by residues from two monomers: H139 and H174 from one monomer, and H329 from a second monomer. [111] We therefore present two models of how Cu is incorporated into AniA: either AniA forms a trimer as an *apo*-protein and then Cu is loaded into the T2Cu site of the trimer; or the *apo*-protein exists as a monomer and the addition of Cu into the T2Cu site promotes trimerisation.

To distinguish between these possibilities, the oligomerisation states of AniA in the *apo*- (Cu free) and *holo*- (Cu-loaded) forms were investigated using analytical size exclusion

chromatography (SEC). *Apo*-WT-AniA eluted from the column as one major peak, centred at 17.04 mL (Figure 6.12a). There was a relatively minor tail at 15.86 mL, suggesting the presence of a mixture of oligomerisation states. Comparison of both peaks with the elution of protein standards from the same column suggested that they correspond to a protein size of approximately 55 kDa for the major peak and 114 kDa for the minor tail (Figure 6.12a). The molecular weight of AniA is 35 kDa as a monomer (105 kDa as a trimer), confirmed by ESI-MS analysis of the full-length protein. It is likely that the major peak contains the monomeric form of AniA, while the minor tail contains the trimeric form or higher molecular weight aggregates. The Cu-loaded or *holo*-WT-AniA eluted as a single major peak centred at 16.14 mL, corresponding to a protein size of 96 kDa. This is consistent with the expected trimeric form of AniA. Therefore, loading with Cu induced a clear change in the oligomeric state of AniA, likely from a monomer to a trimer, suggesting that trimerisation is Cu-dependent.

To further examine the role of the T1Cu and T2Cu ligands in trimer formation by AniA, we repeated the analytical SEC experiment using the ΔT1-AniA and ΔT2-AniA mutant proteins. The *apo*-forms of both mutant AniA proteins eluted from the column at 17.27 mL for ΔT1-AniA and 17.23 mL for ΔT2-AniA, suggesting that both *apo*-proteins are monomeric (Figure 6.12b-c). Like the WT-AniA protein, the chromatograms of both proteins also showed the minor tail centred at approximately 16 mL, likely corresponding to a trimer. Interestingly, unlike *holo*-WT-AniA, the *holo*-forms of ΔT1-AniA and ΔT2-AniA proteins eluted as a mixture of the monomeric and trimeric species at approximately 17.3 mL and 16.2 mL, respectively (Figure 6.12b-c). In both cases, the monomeric peak at 17.3 mL was the major peak. This result suggests that deletion of either the T1Cu or T2Cu binding site impairs the ability of the AniA protein to trimerise. Therefore, trimer formation is likely dependent upon Cu loading into both the T1Cu and the T2Cu sites.

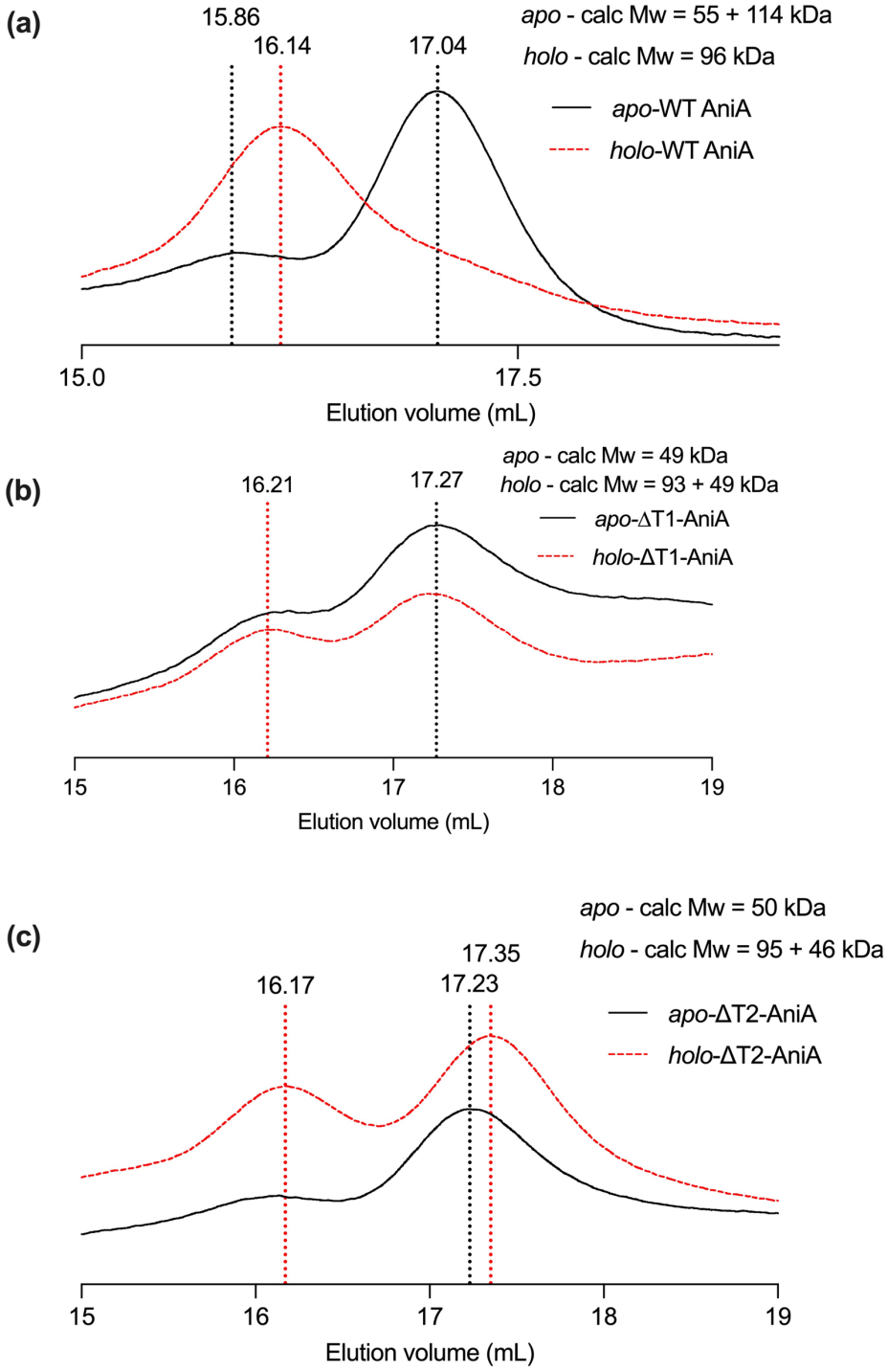

Figure 6.12: Cu binding to AniA influences oligomerisation. Analytical size exclusion chromatography of *apo*- (black line), and *holo*- (red dashed line) of WT- **(a)**, ΔT1- **(b)**, and ΔT2- **(c)** AniA proteins. *Holo*-AniA was incubated with excess Cu O/N at room temperature. Protein (100 µL of 30 µM) was injected onto an ÄKTA Pure and was ran through a Superose 6 10.300 GL column. Protein was eluted in 1.2 column volumes of elution buffer. Experiments were performed in duplicate but only one replicate shown.

6.5.1 *Apo*-AniA exists in a mixed oligomerisation state that is stabilised upon AccA binding

The analytical SEC data suggested that the *apo*-WT-AniA exists in a mixture of oligomerisation states. To probe this mixture at a higher resolution, mass photometry was employed. This technique confirmed that *apo*-WT-AniA in solution exists as a mixture of oligomers. The dominant peak corresponded to a calculated molecular weight of 49 kDa, which likely represents the monomeric form of the protein (Figure 6.13ai). Additional peaks corresponding to 79, 106, 147, and 180 kDa likely represent higher order oligomers or aggregates, presumably the dimeric, trimeric, tetrameric, and pentameric proteins (Figure 6.13ai).

When mass photometry was repeated using *holo*-WT-AniA protein, a single peak corresponding to a calculated molecular weight of 107 kDa was detected (Figure 6.13aii). This result confirmed that the *holo*-WT-AniA protein exists as a trimer, as would be expected from the X-ray crystal structure of this protein (Figure 6.12aii). Therefore, Cu loading into AniA again induced a change in the oligomeric state of WT-AniA from a mixture of monomer and higher order aggregates to a trimer (Figure 6.12aiii).

Previous work by Jen *et al.* (2015) showed direct interaction between both *apo*- and *holo*-AniA and AniA using surface plasmon resonance.[120] However, this did not capture the oligomerisation state of AniA, or any changes of this state. We were, therefore, interested to determine if interaction between AccA and AniA also leads to an oligomerisation state, which may contribute to understanding how AccA loads AniA with Cu.

Excess AccA was added to the *apo*-AniA protein immediately before the entire mixture was loaded onto the mass photometer. Regardless of the specific form of AccA and its Cu occupancy, addition of AccA led to the formation of a single major peak at 41 kDa for *apo*-AccA, 55 kDa for Cu(I)Cu(II)-AccA, or 61 kDa for Cu(II)Cu(II)-AccA (Figure 6.13bi-iii). It is difficult to identify these peaks with confidence at this stage. They may correspond to WT-AniA monomer alone, an AniA-AccA pair, or higher-order AniA-AccA aggregates. AccA alone is too small to be detected by the mass photometer. Nevertheless, addition of AccA

clearly suppressed the formation of the higher order oligomers or aggregates of WT-AniA, and stabilised only one major oligomeric form, which is certainly smaller than a trimer. It should be noted that because AccA was added immediately prior to data collection, there would not be significant amounts of Cu loading from AccA to WT-AniA. In the future, these experiments would be repeated to confirm that the results are reproducible. Furthermore, measuring the same sample over a time course of Cu loading via mass photometry would confirm the hypothesis that Cu loading to AniA induces trimerisation. Additionally, repeating these experiments using the mutant AccA and AniA proteins would further elucidate the role of oligomerisation in the metalation of AniA.

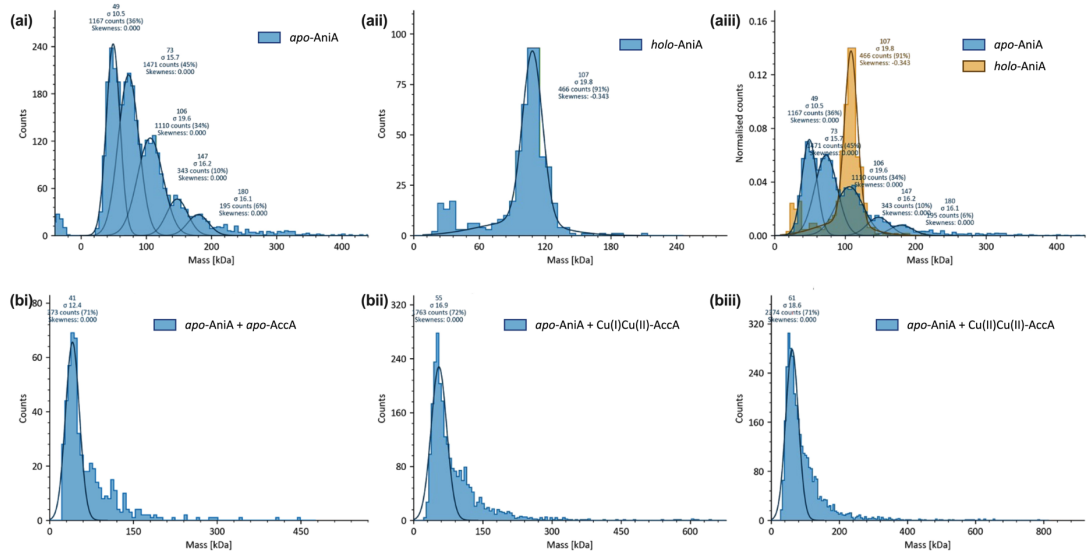

Figure 6.13: *Apo*-AniA exists in a mixed oligomerised state which is stabilised by AniA. (a) Refeyn mass photometry of *apo*-AniA **(ai)**, *holo*-AniA **(aii)** AniA and a comparison between *apo*- (blue) and *holo*- (orange) AniA **(aiii)**. *Holo*-AniA was incubated with excess Cu O/N at room temperature. **(b)** Refeyn mass photometry of a mixture of *apo*-AniA and *apo*-AccA **(bi)**, *apo*-AniA and Cu(I)Cu(II)-AccA **(bii)** and *apo*-AniA and Cu(II)Cu(II)-AccA **(biii)**. Cu-loaded AccA was incubated with Cu for 15 minutes and buffer exchanged using a PD-10 desalting column.

6.6 Discussion

This thesis has identified that AccA binds Cu with high affinity and has an important role in activating AniA *in vivo*. We were therefore, interested to determine the role of AccA in metalating AniA *in vitro* to further elucidate the role of AccA as a cupro-chaperone in *N. gonorrhoeae.*

6.6.1 AccA metalates AniA *in vitro,* but Cu loading is slow

We have demonstrated that AccA is able to metalate AniA which confirmed our hypothesis that AccA is a Cu metallochaperone for AniA. However, there was some unexpected features to metal loading. Although we would expect a metallochaperone to increase the rate of Cu loading, we observed metal loading with AccA to be slower than loading with free Cu.[54] This may be explained by the lack of a buffer for Cu in these experiments. Aqueous 'free' Cu is extremely high-energy and Cu would readily flow down a thermodynamic gradient into the low energy high-affinity Cu binding sites of AniA (Figure 6.14). Meanwhile, Cu bound to AccA is lower in energy than aqueous Cu. AniA remains thermodynamically downstream of AccA, however, the energy barrier for Cu-transfer is higher from AccA to AniA compared to that from aqueous ('free') Cu to AniA (Figure 6.14a). The Cu in mutants of AccA that weaken the affinity for Cu, i.e. the ΔCu primary or ΔCu tract mutant, is higher energy than the Cu in the WT AccA. This explains why AniA is still metalated by these mutants, as Cu would still flow down a thermodynamic gradient to the low energy sites in AniA (Figure 6.14b). To more accurately mimic the conditions in the cell *in vitro,* an artificial buffer can be created. Whilst the components that make up the periplasmic Cu buffer still remain unknown, the artificial buffer should contain molecules that are known to bind Cu. The experiments in this chapter were performed using Cu(II) which exhibits preferred coordination to the imidazole nitrogen found in His, over thiol and thioester groups such as those found in Cys or Met.[144] Furthermore, the role of L-His in buffering Ni *in vivo* has been established.[145] We therefore could use L-His as an artificial Cu buffer to further investigate Cu-transfer to AniA. We hypothesise that the buffered Cu would not transfer directly to AniA, and AccA would be required in a stepwise transfer of Cu from the buffer to AniA (Figure 6.14c).

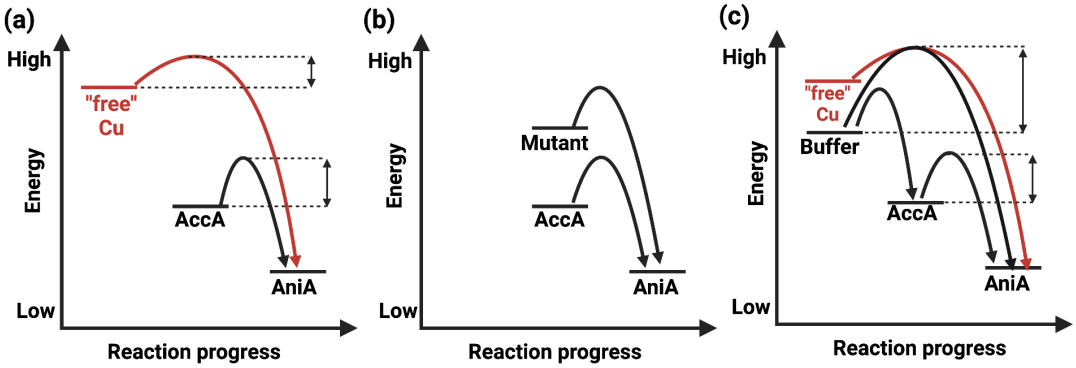

Figure 6.14: Thermodynamic model of Cu-transfer to AniA. (a) Transfer of Cu from aqueous solution 'free' Cu is thermodynamically more favourable than transfer from AccA *in vitro*. Dotted lines represent the energy barrier which must be overcome to permit Cu-transfer. **(b)** Cu bound to AccA has a higher energy than AniA. Weakening Cu binding of AccA increases the energy of the Cu meaning it will still be transferred. **(c)** An artificial buffer such as L-His may more accurately demonstrate Cu loading AniA in the cell. Buffered Cu exists at a lower energy than aqueous Cu, therefore, the energy barrier of direct transfer to AniA is greater than a stepwise transfer to AccA, followed by AniA.

6.6.2 Both Cu sites of AccA are required to metalate one monomer of AniA, but the C-terminal tail is required for T2Cu metalation

Experiments in this chapter identified that one molecule of AccA metalates one monomer of AniA. As AccA binds two Cu atoms, in the Cu primary and C-terminal sites, this suggests that both metal ions are transferred. This contrasts with earlier *in vivo* studies which showed that the C-terminal tail of AccA was not required to activate AniA unless Cu starvation was achieved. Analysis of Cu-transfer from mutant AccA proteins may explain this difference in the importance of the C-terminal tail in AniA metalation. The ΔC-terminal AccA protein only bound one equivalent of Cu, however, the T1Cu site of AniA was saturated at equal equivalents of AccA and AniA monomer. This suggests that Cu is loaded exclusively into the T1Cu site rather than the T2Cu site. Unfortunately, total metal content in AniA was not measured after incubation with AccA, so we cannot know if the T2Cu site is metalated by the end of experiments. However, we assume that the T2Cu site was fully metalated upon incubation with excess AccA. After the T1Cu sites are saturated by Cu from the primary AccA site, excess may then be used to metalate the T2Cu site when the C-terminal tail is missing. We have established that the media used for *in vivo* analysis is Cu sufficient, therefore the ΔC-terminal AccA protein could acquire Cu from the periplasmic buffer, transfer

Cu to the T1Cu site of AniA, and repeat this process to metalate the T2Cu site. However, during Cu starvation and decreased availability of periplasmic Cu, some AniA may be metalated at the T1Cu site only. To confirm this hypothesis, we could repeat the transfer experiments from WT and ΔCu-terminal AccA proteins to AniA, separate the two proteins *via* chromatography and measure the total Cu content in AniA. We would expect the AniA loaded with WT AccA to be fully metalated, but the AniA loaded by ΔC-terminal to have only half of its metal sites occupied.

Additionally, the conditions under which these experiments were performed do accurately reflect *in vivo* cellular conditions. Due to the spectral properties of the T1Cu site, Cu-transfer could only be visualised using Cu(II). However, as AniA is only active during periods of O_2-limitation, Cu would be bound to AccA as Cu(I).[128] This could be mimicked *in vitro* with Cu(I) loaded AccA, however, we could not measure Cu-transfer directly as the Cu(I)-loaded T1Cu site is silent. Alternatively, we could separate the proteins at the endpoint of the experiment and measure Cu occupancy of AniA by ICP-MS.

6.6.3 Cu loading to AniA induces trimerisation

As there has been little research on how NirK proteins acquire their nutrient Cu, structural studies of NirK proteins have always been in the metalated form. Therefore, it is assumed that NirK proteins are always trimeric. This is observed through the crystal structures of the proteins that show them as trimers, including the gonococcal AniA protein.[114,118] However, this thesis identified that *apo*-AniA exists in a mixed oligomerisation state, predominantly in the monomeric form, and Cu-loading induced trimerisation. An in-depth analysis of the literature identified a single source where Cu occupancy of AniA, and other NirK proteins, has altered the oligomerisation state. In an unpublished PhD thesis (J Cardinale, 2000), addition of molecules that can chelate Cu, dithiodiethylcarbamic acid (DDC) and dithiothreitol (DDT), induced monomerisation of trimeric AniA which was visualised using Western Blotting.[146] This suggests that Cu occupancy impacts both stability and oligomerisation of AniA. This may be explained by the T2Cu site of AniA, and NirK, located at the monomer interface.[147] Cu binding to the T2Cu site may bring the two monomers together and enforce the protein-protein interactions required for oligomerisation. Additionally, Cu-transfer

experiments from either ‘free’ aqueous Cu or from AccA were slow. This may be because the role of AccA is to first stabilise AniA as a monomer, observed in mass photometry experiments, then to provide Cu to induce trimerisation. This hypothesis is supported by results generated using ΔT2-AniA protein, which indicated that Cu loading to the T1Cu site in this mutant is much faster compared to WT-AniA. Therefore, the rate-limiting step is trimerisation of AniA, rather than direct Cu-transfer.

Cu-induced trimerisation of AniA may explain why the C-terminal of AccA is required to metalate the T2Cu site *in vitro.* The C-terminal tail of AccA is flexible, therefore, ligand-exchange to the amino acid residues at the monomer interface of AniA may be favourable. Additionally, initial mass photometry experiments showed that AccA, with or without Cu, induces monomerisation of AniA. The C-terminal tail may insert itself at this monomer interface functioning to separate monomers that are not metalated and have oligomerised due to weak hydrophobic protein-protein interactions.[148] Insertion of Cu from the C-terminal tail to one monomer would promote binding of the second monomer which stabilises the trimer. Repeating mass photometry experiments with the ΔC-terminal AccA protein would confirm this model.

Chapter 7: Conclusions and future work

7.1 Conclusions

This thesis has investigated the role of the metallochaperone AccA in metalating the Cu-containing nitrite reductase AniA in the Gram-negative bacterium *Neisseria gonorrhoeae.* We have established that AccA binds both Cu(I) and Cu(II). The conserved PCu_AC motif of $HX_nMX_{21/22}HXM$, named Cu primary, and consisting of the amino acid residues H69, M80, H103, and M105, was confirmed to be the Cu(I) binding site and bound Cu with femtomolar affinity. The C-terminal tail of AccA was confirmed to be the Cu(II) binding site, and bound Cu with picomolar affinity. We confirmed that the Cu primary site of AccA was required for metalation and activation of AniA *in vivo*, but the C-terminal tail had only a minor involvement during Cu starvation. Further analysis of direct Cu-transfer identified that both Cu sites of AccA were required to metalate AniA *in vitro*, with the C-terminal tail involved with T2Cu-site metalation. Subsequent investigation of the AniA protein by analytical size exclusion chromatography and mass photometry confirmed that *apo*-AniA exists in a mixed oligomerisation state, but predominantly as a monomer, which differed from existing literature. AccA stabilised AniA as a monomer and *holo*-AniA existed as a trimer.

We, therefore, suggest the following model of metalation of AniA by AccA. First, AccA acquires Cu from the periplasmic buffer at both the Cu primary and C-terminal sites. AccA then associates with AniA, the C-terminal tail of AccA disrupts oligomerisation of *apo*-protein, and inserts Cu into both T1- and T2Cu sites. Insertion of Cu then induces trimerisation of AniA (Figure 7.1).

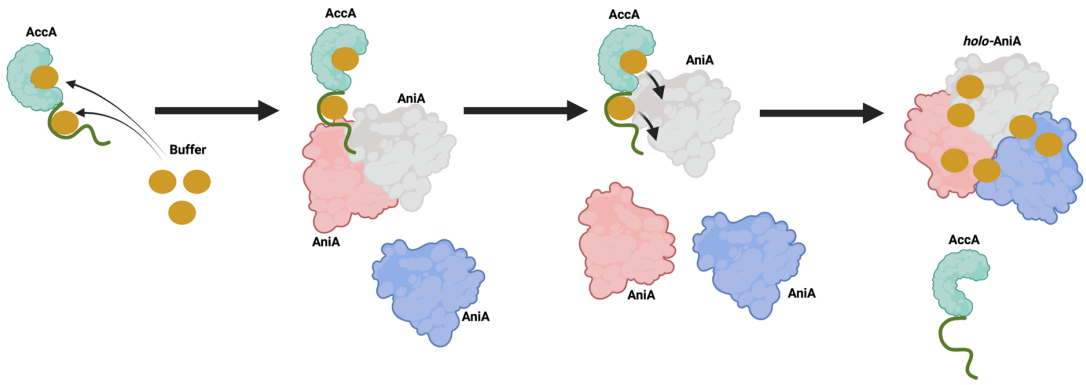

Figure 7.1: Model of Cu insertion into AniA from AccA. 1. AccA acquires Cu from periplasmic buffer in both Cu primary and C-terminal tail Cu sites. 2. AccA associates with AniA and induces monomerization of *apo*-protein. 3. Cu-transfer from AccA to AniA. 4. Process repeats until AniA is formed.

7.2 Future work

7.2.1 Confirming the role of the Cu tract in stabilising the Cu primary site of AccA

We have established that the Cu tract of AccA is required to stabilise the Cu primary site of AccA. Mutating the amino acid residues in the Cu tract weakened the affinity for Cu(I) of the Cu primary site from -16.7 M to -14.3 M. However, as discussed in Chapter 4, the calculated affinity of the ΔCu tract mutant for Cu(I) may be incorrect as it lies between the affinity of the probes (BCA and BCS) used. We would, therefore, like to confirm the Cu(I) affinity for the ΔCu tract AccA protein by modifying the experiment to alter ΔCu tract concentration instead of Cu concentration in competition assays. By confirming the Cu(I) affinity, we will be able to further analyse why the defect in the ΔCu tract-*accA* mutant strain is milder than the single Cu primary mutants despite the similar calculated affinities. We can then individually mutate the amino acids that we identified as a potential tract (Met36, His71, Met78, and Met107), to identify the extent of each residue in stabilising the Cu primary site. We predict that His71 or Met107 may play a role in second sphere coordination of the Cu primary site of AccA, due to the proximity of these residues to the Cu centre. If a weakened affinity for Cu(I) were to be identified in either of these mutants, determining the structure of this mutant may provide an insight into its interaction with the Cu primary site.

7.2.2 AccA to AniA Cu-transfer

There is much that remains unanswered regarding metalated of AniA by AccA. All *in vitro* Cu-transfer reactions from AccA to AniA in this thesis were performed with Cu(II). However, AccA would encounter and bind Cu(I) *in vivo*. These experiments would idealy be replicated using AccA that has been incubated with Cu(I) with an additional step to analyse the final Cu occupancy of AniA. Additionally, in the experiments that were performed, we did not confirm that the T2Cu site of AniA was filled. It may be possible to establish this through visualisation of the T2 Cu site using electron paramagnetic resonance (EPR). Furthermore, investigation of Cu-transfer from AccA to both ΔT1- and ΔT2-AniA proteins would further elucidate the role of AccA in metalating AniA. An artificial buffer to mimic the Cu availability in the host, such as L-His or Cys, could provide an insight into the thermodynamic gradient in metalation of AniA. Loading AniA with aqueous 'free' Cu was quicker than direct transfer of Cu from AccA. An artificial buffer would, therefore, more accurately mimic the condition *in vivo* where AniA could not acquire Cu from the buffer until it was saturated.

7.2.3 Investigating oligomerisation of AniA

The mechanisms underpinning stabilising of AniA as a monomer by AniA remains unknown. We hypothesise that the C-terminal tail plays a role in this. Additionally, mass photometry experiments in this thesis were only performed once, due to limitations in access to equipment. We, therefore, want to first repeat the mass photometry experiments of *apo*- and *holo*- AniA to confirm that the *apo*- protein exists in a mixed oligomerisation state, but that the *holo*-AniA protein is a stable trimer. We would then add both *apo*- and *holo*-AccA to *apo*-AniA. Previously, stabilisation of the monomer was immediate. We could measure the same samples at timed intervals, to observe metal loading of AniA from *holo*-AccA but not from *apo*-AccA. This may allow visualisation of trimer formation and in turn, metal transfer in real time. We predict that the C-terminal tail of AccA is involved in stabilising AniA as a monomer. Repeating mass photometry experiments using AccA mutant proteins may further elucidate these interactions.

7.2.3 AccA and AniA interaction

This thesis has confirmed that AccA and AniA interact with each other, although does not identify the site of this interaction. It would, therefore, be insightful to trap the two proteins and co-crystalise them to generate structures. This could be achieved in two ways; by increasing the affinity of AccA for Cu, or weaken the affinity of AniA for Cu. However, this assumes that protein dissociation occurs upon Cu-transfer from AccA to AniA. It would be interesting to mutate the amino acid residues of the T2Cu site, to abolish the cross-monomer Cu binding. This could be achieved by creating either a H139A/H174A double mutant or a H329A single mutant. If the C-terminal of AccA does interact with the T2Cu site of AniA, these two mutants may identify which residue(s) of AniA are involved in the interaction. These mutants may make co-crystalising the two proteins easier as this would weaken the affinity AniA has for Cu.

References

1. Andreini, C., Bertini, I., Cavallaro, G., Holliday, G. L. & Thornton, J. M. Metal ions in biological catalysis: from enzyme databases to general principles. *JBIC J. Biol. Inorg. Chem.* **13**, 1205–1218 (2008).
2. Lee, M. S., Gippert, G. P., Soman, K. V., Case, D. A. & Wright, P. E. Three-dimensional solution structure of a single zinc finger DNA-binding domain. *Science* **245**, 635–637 (1989).
3. Bird, A. *et al.* Mapping the DNA Binding Domain of the Zap1 zinc-responsive transcriptional activator . *J. Biol. Chem.* **275**, 16160–16166 (2000).
4. Riordan, J. F. The Role of Metals in Enzyme Activity. *Ann Clin Lab Sci.* **7**, 119-129 (1977).
5. Ali, Md. E. *et al.* The iron–sulfur core in Rieske proteins is not symmetric. *JBIC J. Biol. Inorg. Chem.* **19**, 1287–1293 (2014).
6. Mock, W. L., Freeman, D. J. & Aksamawati, M. Fluxionate Lewis acidity of the Zn2+ ion in carboxypeptidase A. *Biochem. J.* **289**, 185–193 (1993).
7. Williams, R. J. P. The biochemistry of zinc. *Polyhedron* **6**, 61–69 (1987).
8. Yamashita, M. M., Wesson, L., Eisenman, G. & Eisenberg, D. Where metal ions bind in proteins. *Proc. Natl. Acad. Sci.* **87**, 5648–5652 (1990).
9. Gooding, J. J., Hibbert, D. B. & Yang, W. Electrochemical metal ion sensors. Exploiting amino acids and peptides as recognition elements. *Sensors* **1**, 75–90 (2001).
10. Karlin, S. & Zhu, Z. Y. Characterizations of diverse residue clusters in protein three-dimensional structures. *Proc. Natl. Acad. Sci.* **93**, 8344–8349 (1996).
11. Nagy, P. Kinetics and Mechanisms of thiol–disulfide exchange covering direct substitution and thiol oxidation-mediated pathways. *Antioxid. Redox Signal.* **18**, 1623–1641 (2013).
12. Winterbourn, C. C. & Hampton, M. B. Thiol chemistry and specificity in redox signaling. *Free Radic. Biol. Med.* **45**, 549–561 (2008).
13. Davis, A. V. & O'Halloran, T. V. A place for thioether chemistry in cellular copper ion recognition and trafficking. *Nat. Chem. Biol.* **4**, 148–151 (2008).

14. Sundberg, R. J. & Martin, R. B. Interactions of histidine and other imidazole derivatives with transition metal ions in chemical and biological systems. *Chem. Rev.* **74**, 471–517 (1974).
15. Dudev, T. & Lim, C. Effect of Carboxylate-Binding Mode on Metal Binding/Selectivity and Function in Proteins. *Acc. Chem. Res.* **40**, 85–93 (2007).
16. Sigel, H. & Martin, R. B. Coordinating properties of the amide bond. Stability and structure of metal ion complexes of peptides and related ligands. *Chem. Rev.* **82**, 385–426 (1982).
17. Irving, H. & Williams, R. J. P. Order of stability of metal complexes. *Nature* **162**, 746–747 (1948).
18. Boal, A. K. & Rosenzweig, A. C. Structural biology of copper trafficking. *Chem. Rev.* **109**, 4760–4779 (2009).
19. Decker, H. & Terwilliger, N. Cops and robbers: putative evolution of copper oxygen-binding proteins. *J. Exp. Biol.* **203**, 1777–1782 (2000).
20. Holland, P. L. & Tolman, W. B. A Structural model of the Type 1 copper protein active site: N2S(thiolate)S(thioether) ligation in a Cu(II) complex. *J. Am. Chem. Soc.* **122**, 6331–6332 (2000).
21. Arcos-López, T., Schuth, N. & Quintanar, L. The Type 1 Blue Copper Site: From Electron Transfer to Biological Function. *Met. Ions Life Sci.* **20**, 51–90 (2020).
22. Gray, H. B., Malmström, B. G. & Williams, R. J. P. Copper coordination in blue proteins. *JBIC J. Biol. Inorg. Chem.* **5**, 551–559 (2000).
23. MacPherson, I. S. & Murphy, M. E. P. Type-2 copper-containing enzymes. *Cell. Mol. Life Sci.* **64**, 2887–2899 (2007).
24. Rompel, A. *et al.* Spectroscopic and exafs studies on catechol oxidases with dinuclear copper centers of type 3: Evidence for μ-η2:η2-peroxo-intermediates during the reaction with catechol. *J. Inorg. Biochem.* **59**, 715 (1995).
25. Roberts, S. A. *et al.* A labile regulatory copper ion lies near the T1 copper site in the multicopper oxidase CueO *. *J. Biol. Chem.* **278**, 31958–31963 (2003).

26. Dodd, F. E., Hasnain, S. S., Abraham, Z. H. L., Eady, R. R. & Smith, B. E. Structures of a blue-copper nitrite reductase and its substrate-bound complex. *Acta Crystallogr. Sect. D* **53**, 406–418 (1997).

27. Dodd, F. E., Van Beeumen, J., Eady, R. R. & Hasnain, S. S. X-ray structure of a blue-copper nitrite reductase in two crystal forms. The nature of the copper sites, mode of substrate binding and recognition by redox partner. *J. Mol. Biol.* **282**, 369–382 (1998).

28. Scott, R. A. Functional significance of cytochrome c oxidase structure. *Structure* **3**, 981–986 (1995).

29. Gorelsky, S. I., Ghosh, S. & Solomon, E. I. Mechanism of N2O reduction by the μ4-S tetranuclear CuZ cluster of nitrous oxide reductase. *J. Am. Chem. Soc.* **128**, 278–290 (2006).

30. Pomowski, A. *et. al.* N2O binding at a [4Cu:2S] copper–sulphur cluster in nitrous oxide reductase. *Nature.* **477**, 234–237 (2011).

31. Müller, M. & Azzi, A. Cytochrome c oxidase metal centers: location and function. *J. Bioenerg. Biomembr.* **23**, 291–302 (1991).

32. Pham, A. N., Xing, G., Miller, C. J. & Waite, T. D. Fenton-like copper redox chemistry revisited: Hydrogen peroxide and superoxide mediation of copper-catalyzed oxidant production. *J. Catal.* **301**, 54–64 (2013).

33. Wardman, P. & Candeias, L. P. Fenton chemistry: an introduction. *Radiat. Res.* **145**, 523–531 (1996).

34. Toyokuni, S. Reactive oxygen species-induced molecular damage and its application in pathology. *Pathol. Int.* **49**, 91–102 (1999).

35. Macomber, L., Imlay, J. The iron-sulfur clusters of dehydratases are primary intracellular targets of copper toxicity. *PNAS*. **106**, 8344–8339 (2009).

36. Cabiscol Català, E., Tamarit Sumalla, J. & Ros Salvador, J. Oxidative stress in bacteria and protein damage by reactive oxygen species. *Int Microbiol.* **3**, 3–8 (2000).

37. Stringfellow, H. M., Jones, M. R., Green, M. C., Wilson, A. K. & Francisco, J. S. Selectivity in ROS-induced peptide backbone bond cleavage. *J. Phys. Chem. A* **118**, 11399–11404 (2014).

38. Hemnani, T. & Parihar, M. S. Reactive oxygen species and oxidative DNA damage. *Indian J Physiol Pharmacol.* **42**, 440–452 (1998).

39. Yu, T.-W. & Anderson, D. Reactive oxygen species-induced DNA damage and its modification: A chemical investigation. *Mutat. Res. Mol. Mech. Mutagen.* **379**, 201–210 (1997).

40. Imlay, J. A. Iron-sulphur clusters and the problem with oxygen. *Mol. Microbiol.* **59**, 1073–1082 (2006).

41. Winterbourn, C. C. Toxicity of iron and hydrogen peroxide: the Fenton reaction. *Toxicol. Lett.* **82–83**, 969–974 (1995).

42. Macomber, L., Rensing, C. & Imlay, J. A. Intracellular copper does not catalyze the formation of oxidative DNA damage in *Escherichia coli*. *J. Bacteriol.* **189**, 1616–1626 (2007).

43. Zuily, L. *et al.* Copper induces protein aggregation, a toxic process compensated by molecular chaperones. *mBio* **13**, e03251-21 (2022).

44. Robison, A. T. R. *et al.* Analysis of copper-induced protein precipitation across the *E. coli* proteome. *Metallomics* **15**, mfac098 (2023).

45. Linder, M. C. & Hazegh-Azam, M. Copper biochemistry and molecular biology. *Am. J. Clin. Nutr.* **63**, 797S-811S (1996).

46. Foster, A. W., Osman, D. & Robinson, N. J. Metal preferences and metallation. *J. Biol. Chem.* **289**, 28095–28103 (2014)

47. Imlay, J. The mismetallation of enzymes during oxidative stress. *J. Biol. Chem.* **289**, 28121–28128 (2014).

48. Waldron, K. J. *et al.* Structure and metal loading of a soluble periplasm cuproprotein. *J. Biol. Chem.* **285**, 32504–32511 (2010).

49. Foster, A. W. *et al.* A tight tuneable range for Ni(II)-sensing and -buffering in cells. *Nat. Chem. Biol.* **13**, 409–414 (2017).

50. Osman, D. *et al.* Bacterial sensors define intracellular free energies for correct enzyme metalation. *Nat. Chem. Biol.* **15**, 241–249 (2019).

51. Stewart, L. J. *et al.* Role of glutathione in buffering excess intracellular copper in *Streptococcus pyogenes*. *mBio*. **11**, e02804–02820 (2020).

52. Braymer, J. J. & Giedroc, D. P. Recent developments in copper and zinc homeostasis in bacterial pathogens. *Curr. Opin. Chem. Biol.* **19**, 59–66 (2014).

53. Waldron, K. J. & Robinson, N. J. How do bacterial cells ensure that metalloproteins get the correct metal? *Nat. Rev. Microbiol.* **7**, 25–35 (2009).

54. Stewart, L. J. *et al.* Handling of nutrient copper in the bacterial envelope. *Metallomics* **11**, 50–63 (2019).

55. Tottey, S. *et al.* Protein-folding location can regulate manganese-binding versus copper- or zinc-binding. *Nature* **455**, 1138–1142 (2008).

56. Bird, A. J. Metallosensors, the ups and downs of gene regulation. *Adv. Microb. Physiol.* **53**, 231–267 (2008).

57. Caballero, H. R., Campanello, G. C. & Giedroc, D. P. Metalloregulatory proteins: metal selectivity and allosteric switching. *Biophys. Chem.* **156**, 103–114 (2011).

58. Brown, N. L., Stoyanov, J. V., Kidd, S. P. & Hobman, J. L. The MerR family of transcriptional regulators. *FEMS Microbiol. Rev.* **27**, 145–163 (2003).

59. Sameach, H. *et al.* Structural and dynamics characterization of the MerR family metalloregulator CueR in its eepression and activation states. *Struct. Lond. Engl. 1993* **25**, 988-996.e3 (2017).

60. Changela, A. *et al.* Molecular basis of metal-ion selectivity and zeptomolar sensitivity by CueR. *Science* **301**, 1383–1387 (2003).

61. Outten, F. W., Huffman, D. L., Hale, J. A. & O'Halloran, T. V. The independent cue and cus systems confer copper tolerance during aerobic and anaerobic growth in *Escherichia coli*. *J. Biol. Chem.* **276**, 30670–30677 (2001).

62. Yamamoto, K. & Ishihama, A. Transcriptional response of *Escherichia coli* to external copper. *Mol. Microbiol.* **56**, 215–227 (2005).

63. Munson, G. P., Lam, D. L., Outten, F. W. & O'Halloran, T. V. Identification of a copper-responsive two-component system on the chromosome of *Escherichia coli* K-12. *J. Bacteriol.* **182**, 5864–5871 (2000).

64. Andrei, A. *et al.* Cu homeostasis in bacteria: the ins and outs. *Membranes* **10**, 242 (2020).

65. Glauninger, H. *et al.* Metal-dependent allosteric activation and inhibition on the same molecular scaffold: the copper sensor CopY from *Streptococcus pneumoniae*. *Chem. Sci.* **9**, 105–118 (2018).

66. Corbett, D. *et al.* The combined actions of the copper-responsive repressor CsoR and copper-metallochaperone CopZ modulate CopA-mediated copper efflux in the intracellular pathogen Listeria monocytogenes. *Mol. Microbiol.* **81**, 457–472 (2011).

67. Padilla-Benavides, T., George Thompson, A. M., McEvoy, M. M. & Argüello, J. M. Mechanism of ATPase-mediated Cu+ export and delivery to periplasmic chaperones. *J. Biol. Chem.* **289**, 20492–20501 (2014).

68. Völlmecke, C., Drees, S. L., Reimann, J., Albers, S.-V. & Lübben, M. The ATPases CopA and CopB both contribute to copper resistance of the thermoacidophilic archaeon *Sulfolobus solfataricus*. *Microbiol. Read. Engl.* **158**, 1622–1633 (2012).

69. Argüello, J. M., Raimunda, D. & Padilla-Benavides, T. Mechanisms of copper homeostasis in bacteria. *Front. Cell. Infect. Microbiol.* **3**, 73 (2013).

70. Wijekoon, C. J. K. *et al.* Copper ATPase CopA from *Escherichia coli*: quantitative correlation between ATPase activity and vectorial copper transport. *J. Am. Chem. Soc.* **139**, 4266–4269 (2017).

71. Andrei, A. *et al.* The CopA2-Type P1B-Type ATPase CcoI serves as central hub for *cbb3*-Type cytochrome oxidase biogenesis. *Front. Microbiol.* **12**, 712465 (2021).

72. Coombs, J. M. & Barkay, T. New findings on evolution of metal homeostasis genes: evidence from comparative genome analysis of bacteria and archaea. *Appl. Environ. Microbiol.* **71**, 7083–7091 (2005).

73. González-Guerrero, M., Raimunda, D., Cheng, X. & Argüello, J. M. Distinct functional roles of homologous Cu+ efflux ATPases in Pseudomonas aeruginosa. *Mol. Microbiol.* **78**, 1246–1258 (2010).

74. Long, F. *et al.* Structure and mechanism of the tripartite CusCBA heavy-metal efflux complex. *Philos. Trans. R. Soc. B Biol. Sci.* **367**, 1047–1058 (2012).

75. Hernández-Montes, G., Argüello, J. M. & Valderrama, B. Evolution and diversity of periplasmic proteins involved in copper homeostasis in gamma proteobacteria. *BMC Microbiol.* **12**, 249 (2012).

76. Li, P. *et al.* PcoB is a defense outer membrane protein that facilitates cellular uptake of copper. *Protein Sci. Publ. Protein Soc.* **31**, e4364 (2022).

77. Kenney, G. E. & Rosenzweig, A. C. Chalkophores. *Annu. Rev. Biochem.* **87**, 645–676 (2018).

78. Rensing, C. & Grass, G. *Escherichia coli* mechanisms of copper homeostasis in a changing environment. *FEMS Microbiol. Rev.* **27**, 197–213 (2003).

79. Koh, E.-I. & Henderson, J. P. Microbial copper-binding siderophores at the host-pathogen interface. *J. Biol. Chem.* **290**, 18967–18974 (2015).

80. Lear, L., Hesse, E., Buckling, A. & Vos, M. Copper selects for siderophore-mediated virulence in *Pseudomonas aeruginosa. BMC Microbiol.* **22**, 303 (2022).

81. Grass, G. & Rensing, C. CueO is a multi-copper oxidase that confers copper tolerance in Escherichia coli. *Biochem. Biophys. Res. Commun.* **286**, 902–908 (2001).

82. Djoko, K. Y., Xiao, Z. & Wedd, A. G. Copper resistance in *E. coli*: the multicopper oxidase PcoA catalyzes oxidation of copper(I) in Cu(I)Cu(II)-PcoC. *Chembiochem Eur. J. Chem. Biol.* **9**, 1579–1582 (2008).

83. Vita, N. *et al.* Bacterial cytosolic proteins with a high capacity for Cu(I) that protect against copper toxicity. *Sci. Rep.* **6**, 39065 (2016).

84. Dennison, C., David, S. & Lee, J. Bacterial copper storage proteins. *J. Biol. Chem.* **293**, 4616–4627 (2018).

85. Rosenzweig, A. C. Metallochaperones: bind and deliver. *Chem. Biol.* **9**, 673–677 (2002).

86. Capdevila, D. A., Edmonds, K. A. & Giedroc, D. P. Metallochaperones and metalloregulation in bacteria. *Essays Biochem.* **61**, 177–200 (2017).

87. Abriata, L. A. *et al.* Mechanism of CuA assembly. *Nat. Chem. Biol.* **4**, 599–601 (2008).

88. Schimo, S. *et al.* Cytochrome c oxidase biogenesis and metallochaperone interactions: steps in the assembly pathway of a bacterial complex. *PLoS One.* **12**, e0170037 (2017).

89. Trasnea, P. I. *et al.* A copper relay system involving two periplasmic chaperones drives cbb3-type cytochrome c oxidase biogenesis in *Rhodobacter capsulatus. ACS Chem. Biol.* **13**, 1388–1397 (2018).

90. Trasnea, P. I. *et al.* Cooperation between two periplasmic copper chaperones is required for full activity of the cbb3-type cytochrome c oxidase and copper homeostasis in *Rhodobacter capsulatus*. *Mol. Microbiol.* **100**, 345–361 (2016).
91. Nittis, T., George, G. & Winge, D. Yeast Sco1, a protein essential for cytochrome c oxidase function is a Cu(I)-binding protein. *J. Biol. Chem.* **276**, 42520–6 (2001).
92. Maghool, S., Ryan, M. T. & Maher, M. J. What role does COA6 play in cytochrome c oxidase biogenesis: a metallochaperone or thiol oxidoreductase, or both? *Int. J. Mol. Sci.* **21**, 6983 (2020).
93. Hannappel, A. *et al.* Bacterial model systems for cytochrome c oxidase biogenesis. *Indian. J. Chem.* (2011).
94. Thompson, A. K., Gray, J., Liu, A. & Hosler, J. P. The roles of Rhodobacter sphaeroides copper chaperones PCuAC and Sco (PrrC) in the assembly of the copper centers of the aa3-type and the cbb3-type cytochrome c oxidases. *Biochim. Biophys. Acta BBA - Bioenerg.* **1817**, 955–964 (2012).
95. Osman, D. *et al.* Copper homeostasis in *Salmonella* is atypical and copper-CueP is a major periplasmic metal complex. *J. Biol. Chem.* **285**, 25259–25268 (2010).
96. Multhaup, G., Strausak, D., Bissig, K.-D. & Solioz, M. Interaction of the CopZ copper chaperone with the CopA copper ATPase of *Enterococcus hirae* assessed by surface plasmon resonance. *Biochem. Biophys. Res. Commun.* **288**, 172–177 (2001).
97. Cobine, P. A. *et al.* Copper transfer from the Cu(I) chaperone, CopZ, to the repressor, Zn(II)CopY: metal coordination environments and protein interactions. *Biochemistry.* **41**, 5822–5829 (2002).
98. Meydan, S. *et al.* Programmed ribosomal frameshifting generates a copper transporter and a copper chaperone from the same gene. *Mol. Cell* **65**, 207–219 (2017).
99. Hearnshaw, S. *et al.* A tetranuclear Cu(I) cluster in the metallochaperone protein CopZ. *Biochemistry.* **48**, 9324–9326 (2009).
100. Singleton, C., Hearnshaw, S., Zhou, L., Le Brun, N. E. & Hemmings, A. M. Mechanistic insights into Cu(I) cluster transfer between the chaperone CopZ and its cognate Cu(I)-transporting P-type ATPase, CopA. *Biochem. J.* **424**, 347–356 (2009).

101. Mealman, T. D. *et al.* N-terminal region of CusB is sufficient for metal binding and metal transfer with the metallochaperone CusF. *Biochemistry* **51**, 6767–6775 (2012).

102. Mealman, T. D. *et al.* Interactions between CusF and CusB identified by NMR spectroscopy and chemical cross-linking coupled to mass spectrometry. *Biochemistry* **50**, 2559–2566 (2011).

103. Djoko, K. Y. *et al.* Phenotypic characterization of a copA mutant of *Neisseria gonorrhoeae* identifies a link between copper and nitrosative stress. *Infect. Immun.* **80**, 1065–1071 (2012).

104. Kidd, S. P., Potter, A. J., Apicella, M. A., Jennings, M. P. & McEwan, A. G. NmlR of *Neisseria gonorrhoeae*: a novel redox responsive transcription factor from the MerR family. *Mol. Microbiol.* **57**, 1676–1689 (2005).

105. Deeudom, M., Koomey, M. & Moir, J. W. B. Roles of c-type cytochromes in respiration in *Neisseria meningitidis. Microbiol. Read. Engl.* **154**, 2857–2864 (2008).

106. Pitcher, R. S. & Watmough, N. J. The bacterial cytochrome cbb3 oxidases. *Biochim. Biophys. Acta BBA - Bioenerg.* **1655**, 388–399 (2004).

107. Buschmann, S. *et al.* The structure of cbb3 cytochrome oxidase provides insights into proton pumping. *Science* **329**, 327–330 (2010).

108. Seib, K. L. *et al.* Defenses against Oxidative Stress in *Neisseria gonorrhoeae*: a System Tailored for a Challenging Environment. *Microbiol. Mol. Biol. Rev.* **70**, 344–361 (2006).

109. Nóbrega, C. S. *et al.* The solution structure of the soluble form of the lipid-modified azurin from *Neisseria gonorrhoeae*, the electron donor of cytochrome c peroxidase. *Biochim. Biophys. Acta BBA - Bioenerg.* **1857**, 169–176 (2016).

110. Miller, K. E. Diagnosis and treatment of *Neisseria gonorrhoeae* infections. *Am. Fam. Physician* **73**, 1779–1784 (2006).

111. Tavares, P., Pereira, A. S., Moura, J. J. G. & Moura, I. Metalloenzymes of the denitrification pathway. *J. Inorg. Biochem.* **100**, 2087–2100 (2006).

112. Overton, T. W. *et al.* Coordinated regulation of the *Neisseria gonorrhoeae*-truncated denitrification pathway by the nitric oxide-sensitive repressor, NsrR, and nitrite-insensitive NarQ-NarP. *J. Biol. Chem.* **281**, 33115–33126 (2006).

113. Mellies, J., Jose, J. & Meyer, T. F. The *Neisseria gonorrhoeae* gene aniA encodes an inducible nitrite reductase. *Mol. Gen. Genet. MGG* **256**, 525–532 (1997).

114. Boulanger, M. J. & Murphy, M. E. P. Crystal structure of the soluble domain of the major anaerobically induced outer membrane protein (AniA) from pathogenic *Neisseria:* a new class of copper-containing nitrite reductases11Edited by D. Rees. *J. Mol. Biol.* **315**, 1111–1127 (2002).

115. Hopper, A., Tovell, N. & Cole, J. A physiologically significant role in nitrite reduction of the CcoP subunit of the cytochrome oxidase cbb3 from *Neisseria gonorrhoeae*. *FEMS Microbiol. Lett.* **301**, 232–240 (2009).

116. Hopper, A. C., Li, Y. & Cole, J. A. A critical role for the *cccA* gene product, cytochrome c_2, in diverting electrons from aerobic respiration to denitrification in *Neisseria gonorrhoeae. J. Bacteriol.* **195**, 2518–2529 (2013).

117. Baarda, B. I., Zielke, R. A., Jerse, A. E. & Sikora, A. E. Lipid-modified azurin of *Neisseria gonorrhoeae* is not surface exposed and does not interact with the nitrite reductase AniA. *Front. Microbiol.* **9**, 2915 (2018).

118. Sikora, A. E. *et al.* Peptide inhibitors targeting the *Neisseria gonorrhoeae* pivotal anaerobic respiration factor AniA. *Antimicrob. Agents. Chemother.* **61**, e00186-217 (2017).

119. Vik, A. *et al.* Broad spectrum O-linked protein glycosylation in the human pathogen Neisseria gonorrhoeae. *PNAS.* **106**, 4447–4452 (2009).

120. Jen, F. E. C. *et al.* A genetic screen reveals a periplasmic copper chaperone required for nitrite reductase activity in pathogenic *Neisseria*. *FASEB. J.* **29**, 3828–3838 (2015).

121. Householder, T. C. *et al.* Gonococcal nitric oxide reductase Is encoded by a single gene, norB, which Is required for anaerobic growth and is induced by nitric oxide. *Infect Immun.* **68**, 5241–5246 (2000).

122. Chacón, K. N. & Blackburn, N. J. Stable Cu(II) and Cu(I) mononuclear intermediates in the assembly of the CuA center of *Thermus thermophilus* cytochrome oxidase. *J. Am. Chem. Soc.* **134**, 16401–16412 (2012).

123. Fisher, O. S. *et al.* PCuAC domains from methane-oxidizing bacteria use a histidine brace to bind copper. *J. Biol. Chem.* **294**, 16351–16363 (2019).

124. Dillard, J. P. Genetic manipulation of *Neisseria gonorrhoeae. Curr. Protoc. Microbiol.* **0 4**, Unit4A.2 (2011).

125. Canonica, F. *et al.* Structural basis and mechanism for metallochaperone-assisted assembly of the CuA center in cytochrome oxidase. *Sci. Adv.* **5**, eaaw8478 (2019).

126. Hanage, W. P., Fraser, C. & Spratt, B. G. Fuzzy species among recombinogenic bacteria. *BMC Biol.* **3**, 6 (2005).

127. Stefanelli, P. *et al.* Molecular characterization of nitrite reductase gene (aniA) and gene product in *Neisseria meningitidis* isolates: Is aniA essential for meningococcal survival? *IUBMB Life* **60**, 629–636 (2008).

128. Whitehead, R. N. *et al.* The small FNR regulon of *Neisseria gonorrhoeae*: comparison with the larger Escherichia coli FNR regulon and interaction with the NarQ-NarP regulon. *BMC Genomics* **8**, 35 (2007).

129. Schneewind, O. & Missiakas, D. Sec-secretion and sortase-mediated anchoring of proteins in Gram-postive bacteria. *Biochim. Biophys. Acta* **1843**, 1687–1697 (2014).

130. Young, T. R. & Xiao, Z. Principles and practice of determining metal–protein affinities. *Biochem. J.* **478**, 1085–1116 (2021).

131. Young, T. R. *et al.* A set of robust fluorescent peptide probes for quantification of Cu(II) binding affinities in the micromolar to femtomolar range. *Metallomics.* **7**, 567–578 (2015).

132. Roosen-Runge, F., Heck, B. S., Zhang, F., Kohlbacher, O. & Schreiber, F. Interplay of pH and binding of multivalent metal ions: charge inversion and reentrant condensation in protein solutions. *J. Phys. Chem. B* **117**, 5777–5787 (2013).

133. Dudev, T., Lin, Dudev, M. & Lim, C. First−second shell interactions in metal binding sites in proteins: a PDB survey and DFT/CDM calculations. *J. Am. Chem. Soc.* **125**, 3168–3180 (2003).

134. Canonica, F., Hennecke, H. & Glockshuber, R. Biochemical pathway for the biosynthesis of the CuA center in bacterial cytochrome c oxidase. *FEBS Lett.* **593**, 2977–2989 (2019).

135. Kundu, S., Kim, W. Y., Bertke, J. A. & Warren, T. H. Copper(II) activation of nitrite: nitrosation of nucleophiles and generation of NO by thiols. *J. Am. Chem. Soc.* **139**, 1045–1048 (2017).

136. Giovannoni, G., Land, J. M., Keir, G., Thompson, E. J. & Heales, S. J. R. Adaptation of the nitrate reductase and Griess reaction methods for the measurement of serum nitrate plus nitrite levels. *Ann. Clin. Biochem.* **34**, 193–198 (1997).

137. Rensing, C. *et al.* CopA: an *Escherichia coli* Cu(I)-translocating P-type ATPase. *PNAS.* **97**, 652–656 (2000).

138. Djoko, K. Y. & McEwan, A. G. Antimicrobial action of copper is amplified via inhibition of heme biosynthesis. *ACS Chem. Biol.* **8**, 2217–2223 (2013).

139. Li, Y. *et al.* Organization of the electron transfer chain to oxygen in the obligate human pathogen *Neisseria gonorrhoeae*: roles for cytochromes c4 and c5, but not cytochrome c2, in oxygen reduction. *J. Bacteriol.* **192**, 2395–406 (2010).

140. Foster, A. W., Young, T. R., Chivers, P. T. & Robinson, N. J. Protein metalation in biology. *Curr. Opin. Chem. Biol.* **66**, 102095 (2022).

141. Branch, A. H., Stoudenmire, J. L., Seib, K. L. & Cornelissen, C. N. Acclimation to nutritional immunity and metal intoxication requires zinc, manganese, and copper homeostasis in the pathogenic *Neisseriae*. *Front. Cell. Infect. Microbiol.* **12**, 909888 (2022).

142. Rydén, L. & Björk, I. Reinvestigation of some physicochemical and chemical properties of human ceruloplasmin (ferroxidase). *Biochemistry* **15**, 3411–3417 (1976).

143. Green, E. R. & Mecsas, J. Bacterial Secretion Systems – An overview. *Microbiol. Spectr.* **4** (2016).

144. Festa, R. A. & Thiele, D. J. Copper: an Essential Metal in Biology. *Curr. Biol. CB* **21**, R877–R883 (2011).

145. Brawley, H. N. & Lindahl, P. A. direct detection of the labile nickel pool in *Escherichia coli*: new perspectives on labile metal pools. *J. Am. Chem. Soc.* **143**, 18571–18580 (2021).

146. Cardinale, J. A. Structural and functional analysis of AniA, the major anaerobically induced outer membrane protein of *Neisseria gonorrhoeae*. *ProQuest*. 84–86 (2000)

147. Sasaki, D. *et al.* Structures of substrate- and product-bound forms of a multi-domain copper nitrite reductase shed light on the role of domain tethering in protein complexes. *IUCrJ* **7**, 557–565 (2020).

148. Li, X. & Zou, H. A molecular dynamics and quantum mechanical investigation of intermolecular interaction and electron-transfer mechanism between copper-containing nitrite reductase and redox partner pseudoazurin. *Phys. Chem. Chem. Phys.* **25**, 7783–7793 (2023).